Anion Coordination induced Supramolecular Self-assemblies of Hydrogen bonding Tripodal Scaffolds: From Charge-assisted Complexation to Neutral Molecular Capsules

A Dissertation Submitted in Partial Fulfillment for the Degree of

Doctor of Philosophy

Sandeep Kumar Dey

(Roll No. 07612222)

Supervisor: Dr. Gopal Das

Department of Chemistry

Indian Institute of Technology Guwahati

July – 2012

Dedicated to my Parents

INDIAN INSTITUTE OF TECHNOLOGY GUWAHATI

Department of Chemistry

STATEMENT

I do hereby declare that the matter embodied in this thesis is the result of investigations carried out by me in the Department of Chemistry, Indian Institute of Technology Guwahati, India, under the guidance of Dr. Gopal Das, Associate Professor, Department of Chemistry, Indian Institute of Technology Guwahati, India.

In keeping with the general practice of reporting scientific observations, due acknowledgements have been made wherever this work is based on the findings of other investigators.

2nd July, 2012 **Sandeep Kumar Dey**

IIT Guwahati

INDIAN INSTITUTE OF TECHNOLOGY GUWAHATI

Department of Chemistry

CERTIFICATE

This is to certify that Mr. Sandeep Kumar Dey has been working under my supervision since January, 2008 as a regular registered Ph. D. student. His thesis entitled **"Anion Coordination Induced Supramolecular Self-assemblies of Hydrogen Bonding Tripodal Scaffolds: From Charge-assisted Complexation to Neutral Molecular Capsules"** is an authentic record of the results obtained from the research work carried out under my supervision in the Department of Chemistry, Indian Institute of Technology Guwahati, Assam, India. I am forwarding his thesis to submit for the award of degree of Doctor of Philosophy, from this institute. I hereby certify that he has fulfilled all the requirements, according to the rules of this institute regarding the investigations embodied in his thesis and this work has not been submitted elsewhere for a degree.

Dr. Gopal Das
(Thesis Supervisor)
Associate Professor
Department of Chemistry
IIT Guwahati
Assam - 781039, India

Acknowledgement

This opportunity to extend my gratitude should commence with my parents and family, whose love and inspiration has always been strength for me. Their eternal blessing and constant support has guided me this far and positively, this will take me far forward in future to achieve the success they dreamt of. Besides, no words would suffice to express my feelings for Nilima, my wife, whose love and care have so luxuriously continued to enrich my life. She has always been there to support and encourage me even in frustrating and difficult times of my life, for which I wish to submit my hearty thanks to her.

I wish to express my sincere gratitude towards my PhD supervisor Dr. Gopal Das and doctoral committee members, Dr. Biplab Mandal, Dr. Subhradip Ghosh, Dr. Boomishankar and Dr. C. K. Jana for their advice and suggestions. I would also like to thank ex-Head Prof. A.T. Khan, present-Head Prof. A. Chattopadhya, scientific officer Mr. Babulal Das and other technical and non-technical staff members of the Department of Chemistry, IIT Guwahati for providing me with the necessary facilities whenever required.

I take this opportunity to thank my Lab members and friends, Ballav Da, Dr. Harjyoti, Avijit Da, Bedo Da, Bimlesh Da, Arghya, Jiban, Chirantan, Nazi Da, Romen, Abhijit, Barun and Arunava for their co-operation in my research work, without which it would not been easy to complete the PhD thesis. It was great to work and spend times with these interesting human beings and I will always cherish the memories of their jokes, laughter and humor throughout my life. Most of these people have a positive approach towards life and I wish them success in every aspects of their life.

Finally, I would like to pay my sincere thanks of appreciation to my school teacher Mr. Debdulal Das, who has been an idol of motivation and inspiration for my academic career. Some friends whom I don't want to exclude from the list are Sukumar, Rana, Raju, Ram, Sanjib, Tapash, Gopesh, Heiylung, Jacob, Pandav, Uttam, Partha, Ching and Shambhu whose friendship had enrich my life and we often spend some good time whenever together.

Still many names are missing whose contribution and help is worth mentioning.

Sandeep

Synopsis

The contents of this thesis entitled **"Anion Coordination Induced Supramolecular Self-assemblies of Hydrogen Bonding Tripodal Scaffolds: From Charge-assisted Complexation to Neutral Molecular Capsules"** have been divided into six chapters based on the results of experimental work performed during the research period.

Chapter 1: Self-assembly and anion coordination chemistry of tripodal scaffolds

This chapter provides a brief introduction on 'supramolecular host-guest chemistry' with special reference to self-assembly and anion coordination chemistry of some hydrogen bonding tripodal scaffolds. Cavitands and capsules are fascinating associates of the receptor family, where the confined interior space or cavity formed by self-assembly of the monomeric unit through noncovalent interactions has been employed for various technological and biomedical applications. When two or more identical subunits are geometrically and functionally complementary with one another, they may self-assemble to form a super molecule. Structural features of the cavity or crystal void such as, shape, size or electronic properties, determine the usefulness of the super-structure. Flexible podand receptors with appended hydrogen bonding functions can efficiently be employed as building blocks for the construction of self-assembled super-structure.

Furthermore, inspired by the recognition tools exploited by Nature, anion coordination chemistry has emerged into a prominent and active field of research within the realm of ''supramolecular chemistry'' with new synthetic hosts capable of recognizing anions with environmental and biomedical relevance. Since the beginning of anion receptor chemistry, acyclic podand receptors functionalized with amide, pyrrole/indole and urea/thiourea groups have widely been employed for anion binding and encryption. Whereas, the binding of anionic guests within pre-organized macrocyclic systems are relatively straightforward to understand but the binding processes of flexible podand receptors remain more elusive. Multi-armed receptors with appended hydrogen bonding functions have been shown to coordinate with targeted anionic species *via* formation of capsular or pseudo-capsular assemblies. These capsular assemblies have shown a number of interesting properties e.g. encapsulation of anion–water clusters, capturing aerial carbon dioxide as carbonate, selective salt extraction from water and transmembrane anion transportation.

Synopsis

Chapter 2: Experimental methods and characterization

In this chapter, a detailed report of the various reagents used in the synthesis of tripodal receptors, $\mathbf{L_1}$-$\mathbf{L_5}$, their synthetic procedures, crystallization details and specifications of instruments/equipments employed in the characterization of synthesized receptors and their various complexes with anions are presented.

Chapter 3: Anion/Solvent induced conformational adaptation in tripodal podands

This chapter focuses on two *N*-bridged tripodal ether receptors, $\mathbf{L_1}$ (tris[2-(*p*-nitrophenoxy)ethyl]amine) and $\mathbf{L_2}$ (tris[2-(*p*-methylphenoxy)ethyl]amine), that have shown a distinct behaviour on their self-assembly and binding ability upon complexation with various anions. An understanding of the conformational adaptation associated with flexible $\mathbf{L_1}$ and $\mathbf{L_2}$ has been made in terms of X-ray diffraction analyses of single-crystals, obtained under different growth conditions. $\mathbf{L_1}$ can reproducibly be crystallized in three different polymorphic forms by the judicious choice of solvents or solvent mixtures whereas, $\mathbf{L_2}$ crystallized in a highly symmetric bowl shaped C_3v conformation irrespective of solvent of crystallization. Furthermore, the structural aspects of conformational adaptability associated with protonated $\mathbf{L_1}$ and $\mathbf{L_2}$, in presence of different counter anions has been investigated in detail along with the solution-state evidence of structural differences. Anion binding with protonated $\mathbf{L_1}$ is attributable entirely to the electrostatic $(N–H)^+\bullet\bullet\bullet A^-$ interactions where the hydrogen of bridgehead nitrogen is *exo*-oriented and thereby, interacts with anion in an open conformation *via* strong electrostatic effects in association with several weak C-H$\cdots A^-$ hydrogen bonds involving multiple receptor cations. In contrast, protonation of $\mathbf{L_2}$ in presence of inorganic anions results in conformational locking of the tripodal scaffold by intramolecular $(N–H)^+\bullet\bullet\bullet$O(ether) trifurcated hydrogen bond formation due to *endo*-orientation of the bridgehead hydrogen. Whereas, use of organic anions as template leads to *exo*-orientation of the apical proton and thereby, results into conformational opening of the receptor side arms due to electrostatic $(N–H)^+\bullet\bullet\bullet A^-$ and π-stacking interactions with the aromatic anions. Thus, receptors $\mathbf{L_1}$ and $\mathbf{L_2}$ are the examples of simple tripodal scaffolds that adapt its conformation to respond to the demands of specific anion(s) or solvent of crystallization. Moreover, the receptor molecules can provide an excellent case of understanding weak C–H hydrogen bonds in stabilizing the anion complexes.

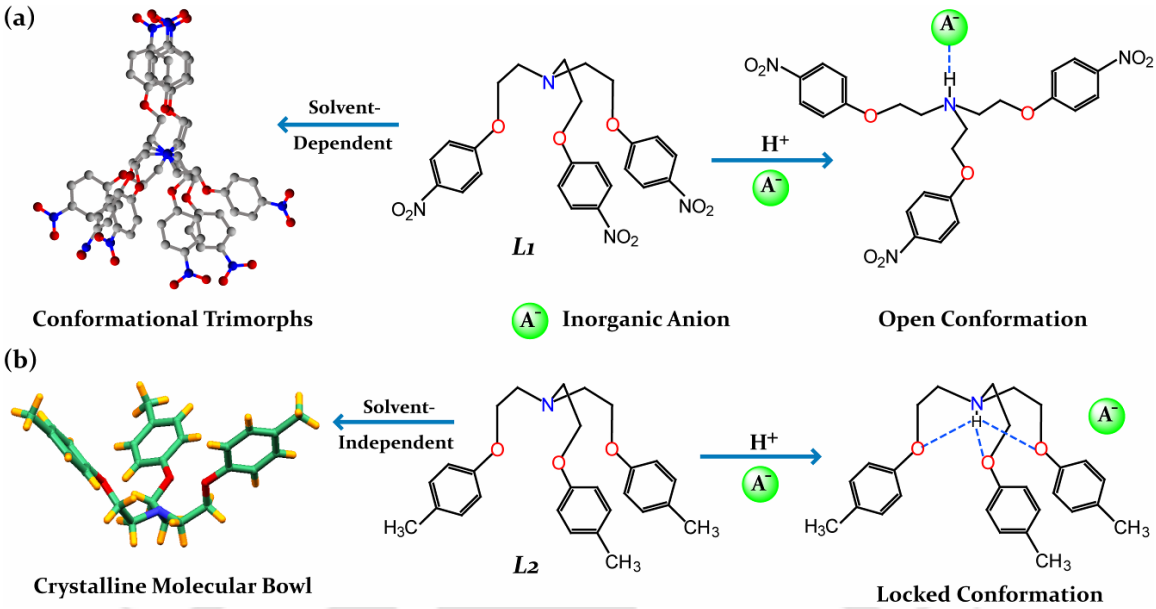

Scheme 1 A comprehensive representation of the research work included in this chapter.

Chapter 4: A fluoride selective chromogenic tris(amide) receptor

This chapter describes a π–acidic tris(amide) receptor, **L_3** (tris[2-(3,5-dinitrobenzamide)ethyl]amine) which behaves as a selective chemosensor for F^- ion by encapsulation of the anion within the receptor cavity in polar aprotic solvents exhibiting solvatochromism and solvatomorphism. The highly ordered hydrogen bonding cavity of **L_3** can give rise to colorimetric changes as the peripheral dinitrophenyl functions being a part of the tris(amide) receptor facilitate an anion—π charge-transfer (CT) interaction upon selective recognition of anion. The fluoride recognition chemistry is immediately detected in solution by a dramatic increase in solubility of the receptor in polar aprotic solvents with a concomitant optical signalling from colourless to orange/purple upon addition of TBAF and confirmed by UV/Vis spectroscopy. Both X-ray structure determination and NMR spectroscopy establish the participation of amide –NH and aromatic –CH protons in recognition of F^- within the receptor cavity. The selectivity and inherent anion–π CT character of **L_3** in response to F^- was further confirmed by comparison to a control receptor, **CL_3** (ethyl ester of carboxy-dinitrobenzene) that cannot differentiate F^- from other basic anions, such as AcO^- and $H_2PO_4^-$, producing optical signal from colourless to blue irrespective of solvent choice and polarity indicating the worth of preorganized hydrogen bonding scaffold in **L_3** towards selective and solvatochromic F^- recognition.

Furthermore, in a proof-of-concept experiment, the high selectivity of **L₃** towards F^- has been efficiently employed in the transformation of charged anion complexes $[(H\mathbf{L_3})^+ \bullet A^-]$ into F^--bound pseudo-molecular capsule. ^{1}H NMR titration of a $[(H\mathbf{L_3})^+ \bullet A^-]$ ($A^- = Cl^-$ and HSO_4^-) complex with increasing equivalents of TBAF showed the in situ generation of F^--encapsulated complex after 5 equiv. addition of F^- ions.

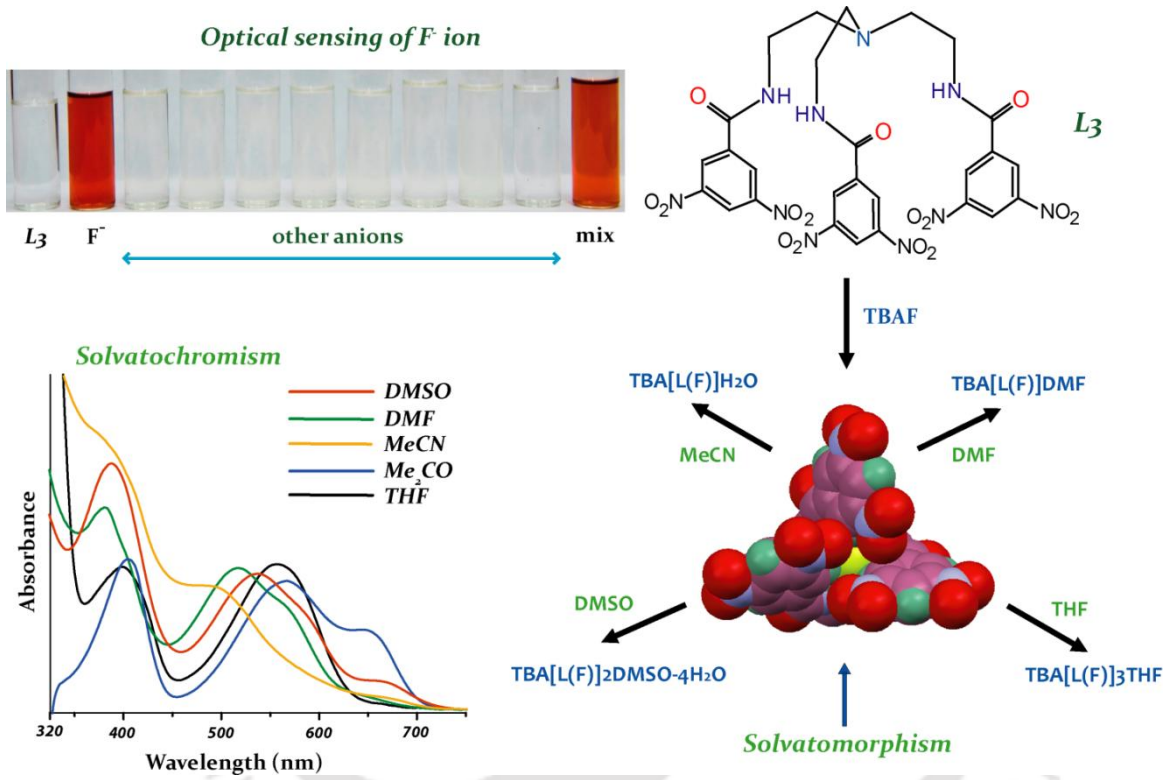

Scheme 2 A comprehensive representation of the research work included in this chapter.

Chapter 5: Efficient fixation of atmospheric CO_2 by a tris(urea) receptor

This chapter highlights the F^- and OH^- ion induced fixation atmospheric CO_2 as CO_3^{2-}-encapsulated molecular capsule of a tris(urea) receptor, **L₄** appended with electron-withdrawing *m*-nitrophenyl terminals [tris(2-aminoethyl)-(3-nitrophenyl)urea]. It is remarkable to note that almost quantitative yield of CO_3^{2-}-capsule (above 90% based on **L₄**) can reproducibly be obtained from the basic receptor-OH^- solution (1:1 mixture) after 3 days of exposure to an unmodified atmosphere (RT), which indeed indicates the high affinity of **L₄** toward aerial CO_2 fixation by encapsulation of the in situ generated CO_3^{2-} guest within a centrosymmetric dimeric assembly of the receptor *via* 14 hydrogen bonding interactions. Furthermore, a detailed solution-state studies involving ^{1}H NMR titration and 2D-NOESY

NMR experiments have been carried out in presence of various anions to validate the binding and encapsulation of anion within the receptor scaffold. In addition, the structural evidence for encapsulation of a deprotonated hydrogensulfate anion (SO_4^{2-}) within the centrosymmetric capsular assembly of the receptor *via* 12 N–H···O hydrogen bonds has also been reported.

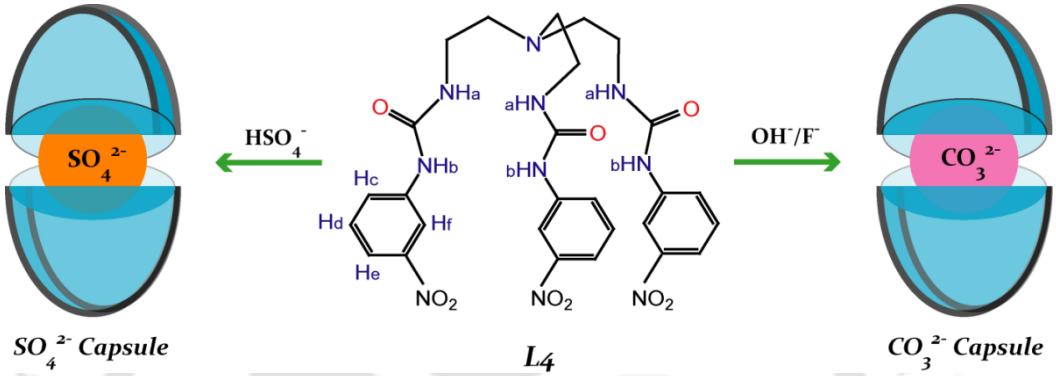

Scheme 3 A comprehensive representation of the research work included in this chapter.

Chapter 6: Selective inclusion of PO_4^{3-} within persistent dimeric capsules of a tris(thiourea) receptor

The highlight of this chapter is a π–acidic tris(thiourea) receptor, **L**$_5$ [tris(2-aminoethyl)-(4-nitrophenyl)thiourea] that can selectively encapsulate a PO_4^{3-} anion within the persistent and rigidified dimeric capsules of the receptor (2:1 host/guest), assembled by aromatic $\pi\cdots\pi$ stacking between the receptor side arms. **L**$_5$ in presence of excess TBA(H_2PO_4) has been found to encapsulate PO_4^{3-} *via* hydrogen bond activated deprotonation of bound $H_2PO_4^-$, as evident from the origin of a new set of signals in the ^{1}H NMR titration experiments. Notably, quaternary ammonium salts of PO_4^{3-}–encapsulated complex can reproducibly be obtained by a solution-state deprotonation of $[H\mathbf{L}_5]^+$ moieties and bound HPO_4^{2-} anion of complex $[2(H\mathbf{L}_5)^+\bullet HPO_4^{2-}]\bullet 3H_2O$ (2:1 receptor/anion), induced by the presence of large excess of basic anions such as HCO_3^-/CO_3^{2-}, CH_3COO^-, and F^-. Qualitative as well as quantitative ^{1}H and ^{31}P NMR experiments (DMSO-d_6) have been carried out in detail to demonstrate the selective and preferential inclusion of PO_4^{3-} by **L**$_5$ in solution-states. X-ray structures and ^{31}P NMR studies carried out on the isolated crystals of phosphate complexes provide evidences of binding discrepancy of inorganic phosphates with protonated and neutral form of the receptor. Furthermore, extensive studies have been carried out with other anions of different sizes and dimensions in solid-state and solution as well. Notably, crystallization of **L**$_5$ in

presence of quaternary ammonium salts of F^-, HCO_3^- and HSO_4^- resulted in solvent (MeCN/DMSO) sealed F^- encapsulated pseudo-molecular capsule, CO_3^{2-} encapsulated molecular capsule and cation (TBA) sealed SO_4^{2-} encapsulated pseudo-molecular capsule, respectively.

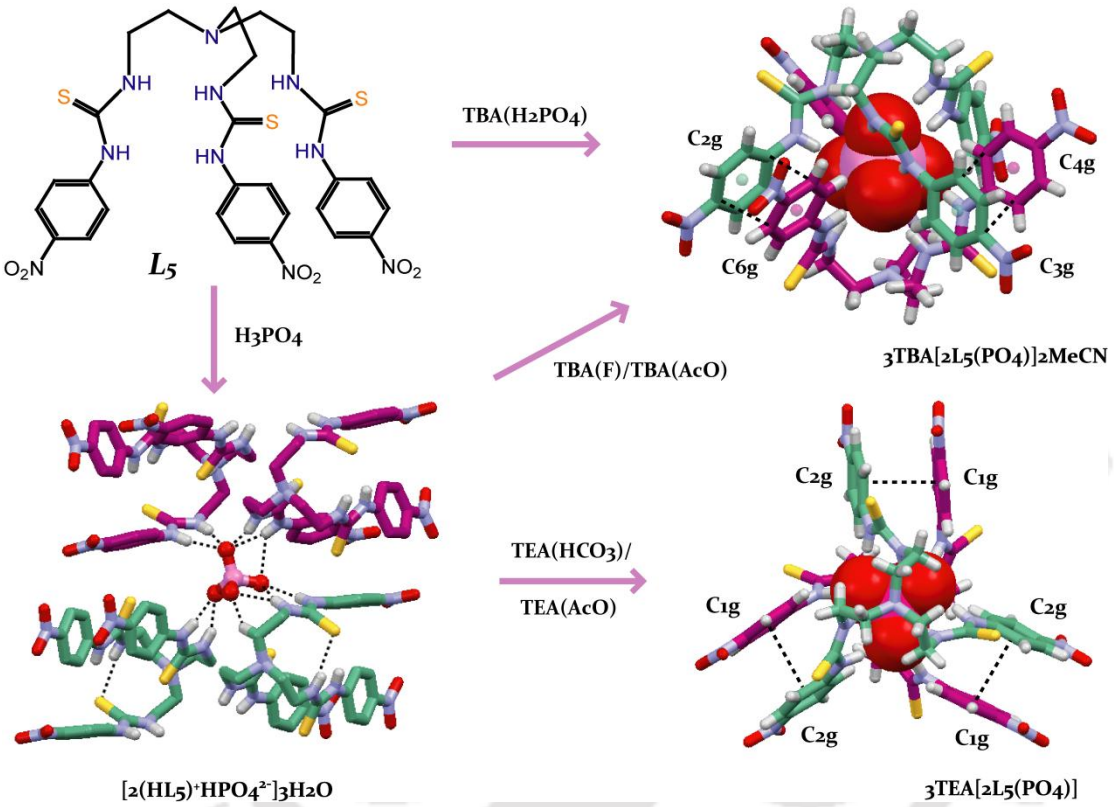

Scheme 4 A comprehensive representation of the research work included in this chapter.

At the end of the thesis an overall conclusion of the research work and a brief discussion about the future perspective and further research scope in the area of molecular self-assembly and anion receptor chemistry with special focus on anion induced molecular capsules are presented.

Contents

Contents

Contents

Contents

Chapter 1

Self-assembly and Anion Coordination Chemistry of Tripodal Scaffolds

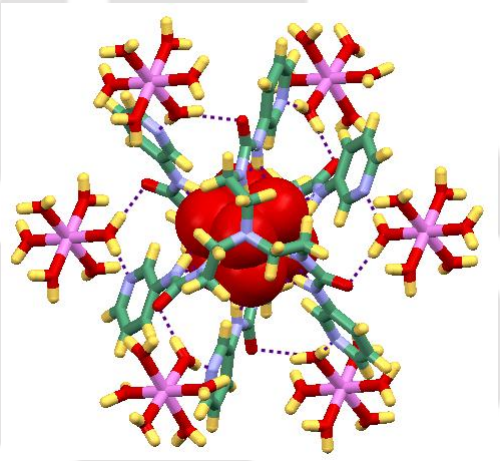

1.1 Supramolecular chemistry: An introduction

Supramolecular chemistry has been defined by one of its leading proponents, Jean-Marie Lehn, who won the Nobel Prize for his work in the area in 1987, as the 'chemistry of molecular assemblies and of the intermolecular interactions'. Other definitions include phrases such as 'chemistry beyond the molecule' and 'chemistry of the noncovalent bond'. While traditional chemistry focuses on the covalent bond and coordinative bond formation, supramolecular chemistry examines the weaker and reversible noncovalent interactions between molecules such as hydrogen bonding, ion-ion and ion-dipole interactions, cation–π and anion–π interactions, π–π interactions, Van-der Waals forces, and hydrophobic effects.[1] Important concepts that have been demonstrated by supramolecular chemistry include molecular self-assembly, host-guest chemistry, mechanically-interlocked molecular architectures, foldamers, dendrimers and molecular electronic devices.[1] As it is practised today, supramolecular chemistry is one of the most vigorous and fast growing fields of chemical endeavour. Supramolecular chemistry deals with subtle interactions, and consequently control over the processes involved can require great precision.

A hydrogen bond may be regarded as a specific kind of dipole-dipole interaction in which a hydrogen atom attached to an electronegative atom (or electron withdrawing group) is attracted to a neighbouring dipole on an adjacent molecule or functional group. Because of its relatively strong (4–120 kJ mol^{-1}) and highly directional nature, hydrogen bonding has been described as the 'master key interaction in supramolecular chemistry'.[1] Typical examples include, the formation of carboxylic acid dimer and base pairing in DNA by hydrogen bonding (Scheme 1.1). Hydrogen bonding is perhaps the most important discriminating cohesive force in directing the crystallization and self-assembly of organic molecules.[2] Self-assembly is the process by which molecules adopt a defined arrangement by virtue of rotations about single bonds (intramolecular torsions) and intermolecular hydrogen bonding. Self-assembly is highly precise, self-controlling and self-repairing since equilibrium-controlled processes are implicated.[3]

Hydrogen bonds come in a bewildering range of lengths, strengths and geometries. A single, strong hydrogen bond per molecule may be sufficient to determine the solid-state structure and exert a marked influence in the solution and gas phases. Weaker hydrogen bonds play a role in structure stabilization and can be significant when large number of them act in concert. Recent interest has also focused on apparent and feeble hydrogen bonding interactions involving hydrogen atoms attached to carbon, rather than electronegative atoms such as nitrogen and oxygen (electronegativities: C 2.55, N 3.04, O 3.44 and H 2.20).

In supramolecular host-guest chemistry, the host is commonly referred to a large molecule or aggregate such as an enzyme or synthetic cyclic and acyclic compounds possessing a sizeable central hole or cavity.[1] The guest may be an ionic species (cation/anion), a neutral molecule or a more sophisticated molecule such as a hormone, pheromone or neurotransmitter. The thermodynamic stability of a supramolecular host-guest complex may be enhanced by operation of a chelate effect or macrocyclic effect. The macrocyclic effect makes cyclic hosts such as corands (e.g. crown ethers) up to a factor of 10^4 times more stable than closely related acyclic podands with the same type of binding sites. Furthermore, in order to bind, a host molecule must have binding sites that are of the correct electronic character (polarity, hydrogen bond donor/acceptor ability, hardness or softness etc.) to complement the guest. If a host molecule does not undergo a significant conformational change upon guest binding, it is said to be preorganized. Host preorganization is a key concept because it represents a major enhancement in the overall free energy of guest complexation.[4]

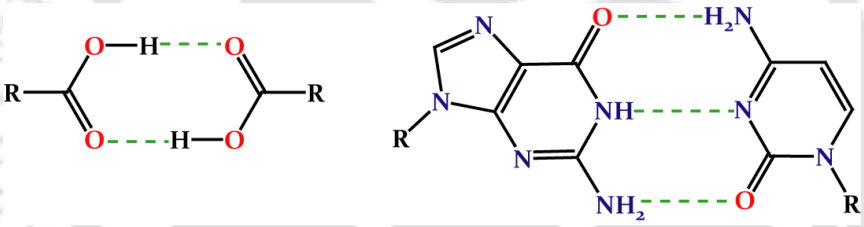

Scheme 1.1 A hydrogen bonded carboxylic acid dimer and base pairing in DNA (Guanine–Cytosine) by hydrogen bonding.

The objective of the Thesis is to explore the molecular self-assembly and anion coordination chemistry of some newly synthesized *N*-bridged tripodal receptors bearing terminal aryl functions, which assist in effective anion binding and recognition.

1.2 Anion receptor chemistry

Unlike transition-metal coordination, the binding of anions with synthetic receptors falls into the realm of 'supramolecular chemistry'.[5] Anion receptor chemistry has attracted growing attention in supramolecular chemistry due to the essential roles that anions play in biology, medicine, catalysis, and environmental science.[6] Binding affinities between anions and their hosts are mostly attributed to hydrogen-bonding and/or electrostatic interactions, with the former being the more influential in promoting selective binding through topological complementarity. As Moyer and Bonnesen et al. has pointed out, it is important to understand the factors influencing anion recognition in the traditional analytical sense, where simple physical properties such as size, charge and hydrophilicity tend to govern selective

exchange of one anion over another. They introduced the term *bias* for this type of phenomenon and deduce that truly selective anion receptors must involve some elements of strategic design, including appropriately positioned hydrogen bond coordination sites.[7] The introduction of multiple hydrogen bonding sites along with the resulting topological considerations in anion receptors leads to the concept of double valence for anions as well as for transition-metal ions. For anions, however, the primary valence is the negative charge on the anion and the secondary valence is provided by hydrogen bonds to the anion.[8] Bowman-James et al. has categorized the binding of anions based on their coordination numbers which is helpful in defining the notions of complementarity for a given anion and can aid to the design of optimal anion-binding host structures.[9]

The most effective way to bind anions consist in taking advantage of their negative charge and accordingly, ammonium and quaternary ammonium receptors have been the principal receptor of choice since, they ensure an adequate electrostatic attraction reinforced by hydrogen bond contacts with the coordinated anions.[10] However, pyrrole, indole, amide and urea/thiourea functions have been the subject of intensive investigations for its performance in the construction of neutral anion receptors *via* favourable hydrogen bonding interactions.[11] However, if the -NH protons are acidic enough, in particular when an electron-withdrawing substituent is introduced into the receptor molecule, deprotonation may occur in the presence of a highly basic anion, such as fluoride and acetate.[12] Wide structural modifications on the hydrogen bonding scaffold have been attempted to increase the acidity of the -NH protons by introducing electron-withdrawing substituents, e.g., $-NO_2$ and $-CF_3$ *via* the mediation of a π-system and to form a preorganized binding cleft or cavity using a rigid (calixarene or polynorbornane) or flexible structural skeleton that leads to a binding environment with size and shape complementary for a given anion. Recently, Custelcean et al. has reviewed the structural role of anions in crystal engineering since anions play diverse roles in the formation of crystals.[13] Besides conventional $N–H\cdots A^-$ hydrogen bonding, theoretical calculations on electrostatic anion–π interactions have been complemented by mounting experimental evidences for their existence in the solid state and in solution.[14] However, true examples of anion–π interactions in crystals remain extremely rare because of the competition with $C–H\cdots A^-$ hydrogen bonds, which tend to prevail.[15] Another competitor is the weak σ interaction involving a small amount of charge transfer from the anion to an arene system, which is geometrically characterized by the anion being situated above the periphery rather than the centre of the arene. More recently, a new type of noncovalent interaction involving an electrophilic halogen atom (halocarbon) and a high electron density centre (like anion), has been established both experimentally and theoretically.[16] Halogen

bonds are highly directional (∠D-X—A close to linear), in many respects behave like hydrogen bonds.

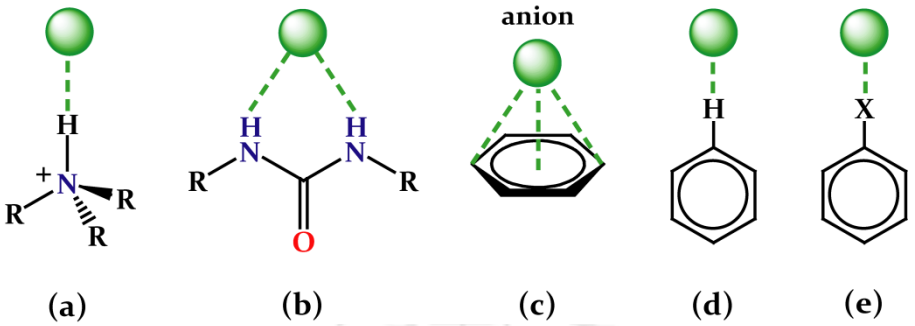

Scheme 1.2 Anion binding by different types of noncovalent interactions; (a) electrostatic N–H···A$^-$ interaction by an ammonium cation; (b) complementary N–H···A$^-$ interaction by a urea function; (c) anion–π interaction; (d) C–H···A$^-$ interaction by an aryl function and (e) C–X···A$^-$ halogen bonding by a halocarbon (X = F$^-$, Cl$^-$, Br$^-$, I$^-$).

Since the beginning of anion coordination chemistry, tris(2-aminoethyl)amine-based acyclic and macrocyclic tripodal scaffolds bearing –NH functions have widely been employed for anion binding and encryption featuring receptor cavities.[17] Whereas, the binding of anionic guests within pre-organized macrocyclic systems are relatively straightforward to understand but the binding processes of flexible podand receptors remain more elusive. Acyclic podand receptors with multi armed hydrogen bonding functionality have been shown to coordinate with targeted anionic species via formation of capsular or pseudo-capsular assemblies. Nature utilizes the principle of encapsulation for purposes such as the protection of fragile structures and compartmentalization of functions.[18] One of the most fascinating features of molecular capsules is their ability to create a distinct microenvironment that isolates the encapsulated guest from the bulk of solvent media and thereby, leads to the phenomenon of molecular/ion-sorting when possible formation of different capsules are present in the same solution. When two podand molecules with interior anion binding elements create a dimeric capsular assembly, there is a possibility to satisfy the higher coordination numbers required for the binding of multi-charged oxyanions and hydrated anions. These capsular assemblies have shown a number of interesting properties e.g. encapsulation of anion–water clusters, capturing aerial carbon dioxide as carbonate, selective salt extraction from water etc.[17b]

Thus, given my interest in the field of anion receptor chemistry, a major portion of the Thesis describes the anion-coordination induced capsular and pseudo-capsular assembly formation in hydrogen bonding tripodal scaffolds with special reference to the selective and/or preferential recognition of a specific anion over other competitive anions.

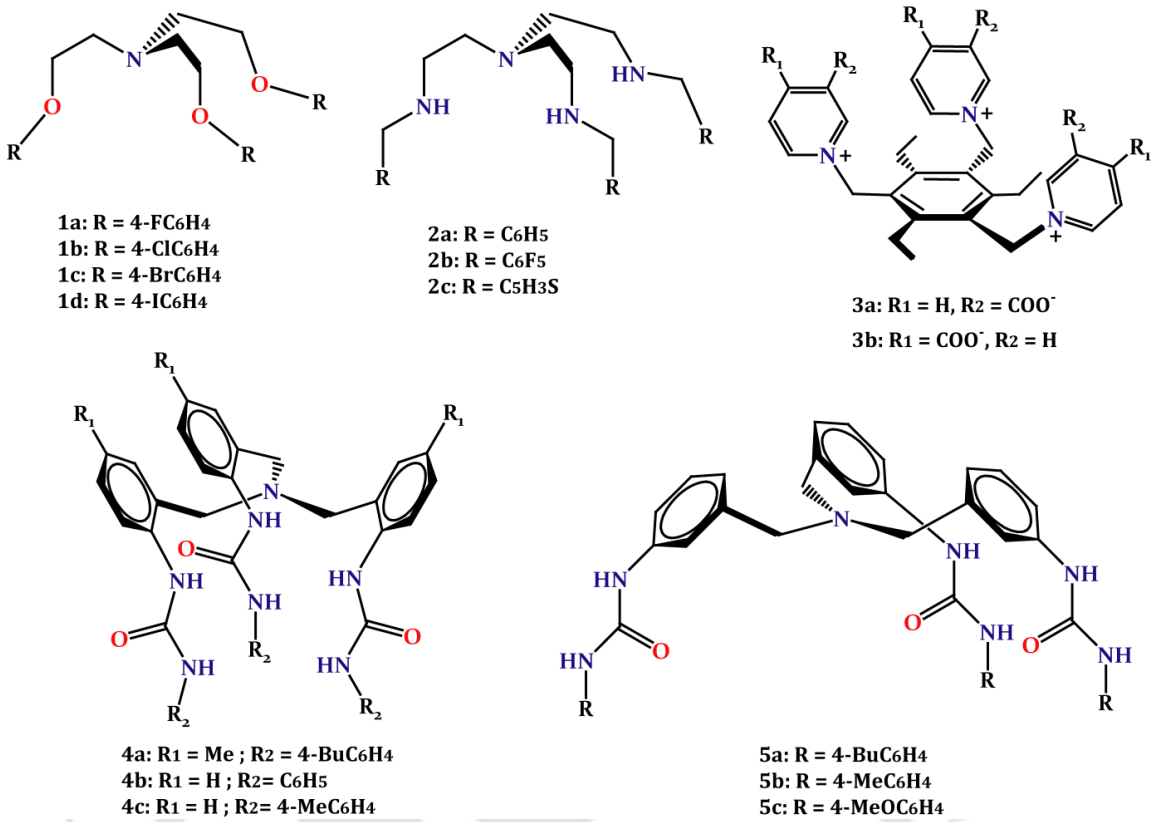

Scheme 1.3 Various *N*-bridged and arene-bridged tripodal receptors studied as self-assemblers.

1.3 Molecular self-assembly of tripodal scaffolds

Self-assembly of small molecules into well-defined architectures is one of the fundamental topics in supramolecular chemistry. A key feature of self-assembly is its high degree of convergence that gives rise to fascinating and complex structures from very simple building blocks.[19] When two or more identical subunits are geometrically and functionally complementary, they may self-assemble to form a super molecule. Podands, cavitands and capsules are interesting members of the receptor family, where the confined interior space or cavity formed by self-assembly of the monomeric unit through noncovalent interactions has been employed for various applications.[20] Structural features of the cavity such as, shape, size or electronic properties, determine the usefulness of the super-structure. Modules integrating self-assembling capsules are generally based on conformationally restricted systems such as, calixarenes, resorcinarenes and glycoluril, in order to minimize entropy losses.[21] However, flexible podand receptors with appended hydrogen bonding functions can also be employed as efficient building blocks for the construction of self-assembling capsules.[22]

As a representative example of this class, the halide functionality dependent formation of molecular capsule in tripodal ether receptor, **1c** (Scheme 1.3) is noteworthy.[23] Receptors **1a**, **1b**, and **1d** crystallized in rhombohedral symmetry with C_3 symmetry axis passing through

the bridgehead nitrogen and formed hemicarcerands through self-assembly in the solid-state. The crystal packing of receptor **1a** showed that the molecules are stabilized through weak intermolecular C-H···O-(ether) interactions. In receptor **1b**, the molecules are stabilized through C-H···Cl and C-H···π interactions. And in receptor **1d**, the molecules are stabilized through aliphatic and aromatic C-H···π interactions (Figure 1.1). In all three receptors, each tripodal unit is surrounded by six other units occupying a chair conformation with a distance of 11.06, 13.32, and 12.85 Å between the bridgehead nitrogen atoms (N···N) in the crystal structures of **1a**, **1b**, and **1d**, respectively (Figure 1.1).

However, in crystal structure of receptor **1c**, two tripodal units self-assemble to form a molecular capsule (**1c•1c**) *via* intermolecular C-H···π and C-H···Br interactions. Two units of **1c** are flipped inward toward each other in a staggered conformation [*d*(N···N) = 4.17 Å] and held together *via* aromatic C-H···π interactions, to generate a dimeric capsule with an interior cavity (Figure 1.1d). Like receptors **1a**, **1b**, and **1d**, each tripodal unit of **1c** is hexagonally surrounded by six other molecules forming a chair conformation and the overall crystal packing is governed by C-H···Br, C-H···π, and π···π interactions to form a highly symmetrical organic solid. The molecular capsule is stable in MeCN solution as confirmed by the ESI-MS spectrum (*m*/*z* 1228.86) and ^{1}H NMR spectrum. The ^{1}H NMR spectrum recorded after 10 h of dissolving the crystals of (**1c•1c**) in CD_3CN suggested that, equilibrium was established between the capsular form and the monomeric form with a dissociation constant of ~ 8.8 M^{-1} at 293 K (Figure 1.1e).

Tripodal amine receptors are also interesting member of the podand family, which can self-assemble into symmetric organic solid (Scheme 1.3). As a representative example, receptor **2b** that crystallized in trigonal system possesses a preorganized C_3 symmetric tripodal cleft suitable for guest encapsulation.[24] Examining the non-covalent interactions revealed that, each tripodal unit is hexagonally surrounded by six other molecules (in the same plane), where each pentafluorophenyl ring is intermolecularly connected with two other pentafluorophenyl moieties of two neighbouring molecules *via* C-F···F-C interactions with a distance of 2.65 Å (Figure 1.1f). Crystal packing diagram showed the formation of a honeycomb like cavity, which could be due to the highly symmetrical arrangement of **2b** in the solid-state. Survey of crystal structures on arene-based tripodal receptors revealed their inherent tendency to crystallize in a bowl shaped conformation. As a representative example, the zwitterionic receptor **3a** (Scheme 1.3) crystallized with all three arms oriented in the same direction and encapsulates multiple lattice water molecules within the capsular assembly of two water-bridged receptor units (Figure 1.1g).[25] Whereas, the *meta*-isomer **3a**

can readily be isolated as a free zwitterion, the *para*-isomer **3b** proved to be extremely difficult to obtain in a guest-free form.

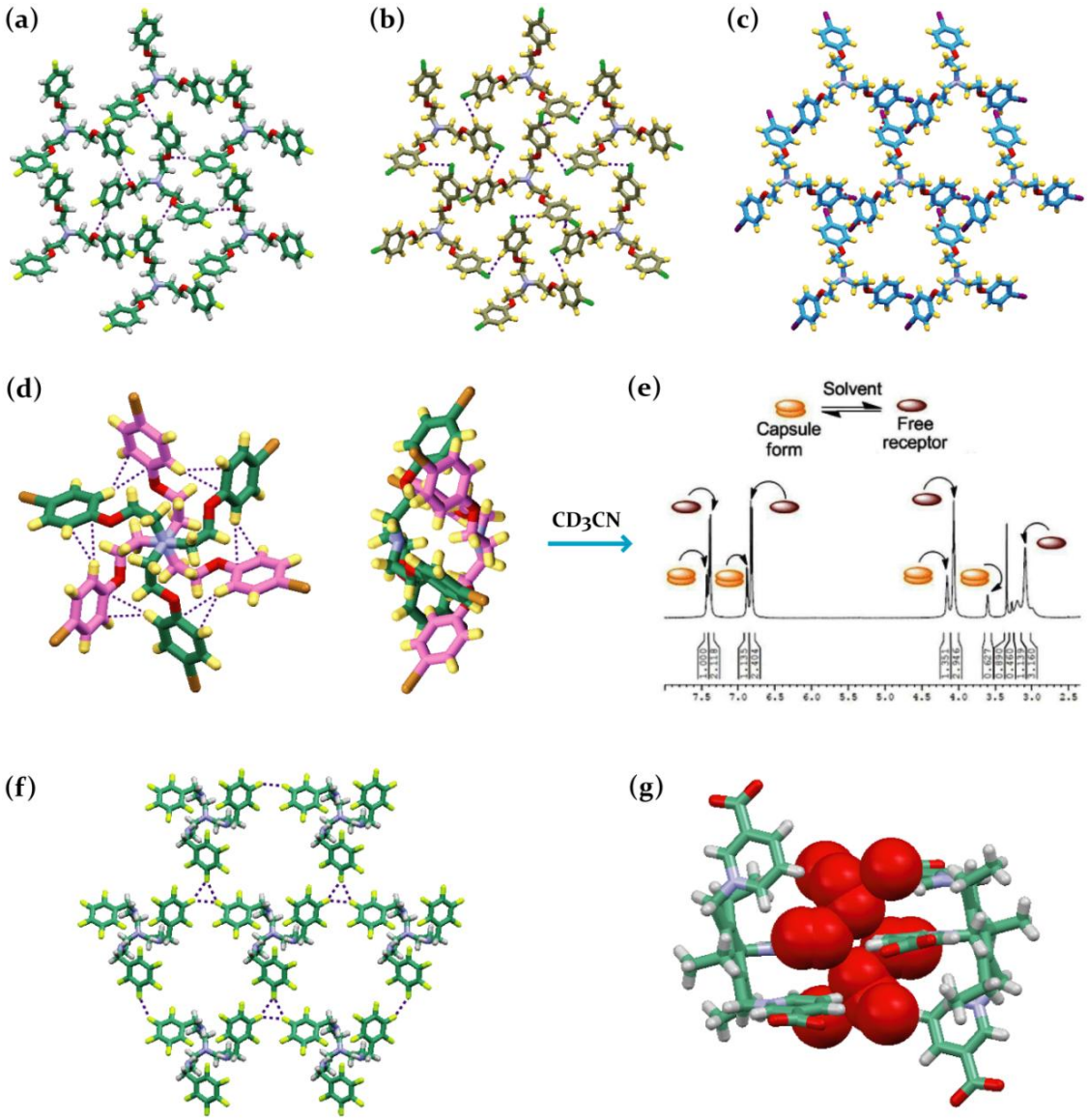

Figure 1.1 Self-assembly of tripodal ether receptors **1a** (a), **1b** (b) and **1d** (c) into symmetric hemicarcerands; (d) Self-assembled molecular capsule of receptor **1c** (front view and lateral view); (e) ^{1}H NMR spectrum (400 MHz) of the molecular capsule (**1c•1c**), recorded after 10 h of dissolving crystals in CD_3CN; (f) Self-assembly of tripodal amine receptor **2b** into highly symmetrical organic solid, and (g) Self-assembly of tripodal zwittreionic receptor **3a** into hydrated molecular capsule.

In their pioneering work, Alajarin, Steed and Pastor et al. has efficiently employed tris(ureidobenzyl)amine scaffolds (Scheme 1.3) as flexible bricks for the construction of self-assembled molecular capsules.[22] The advantages of these flexible self-assemblers is that they can adapt their conformation in order to maximize intermolecular interactions and self-assemble *via* complementary N-H···O=C hydrogen bonding interactions between the secondary urea groups of two tripodal units. Structural elucidation of triureas **4a** and **4b**

revealed the formation of dimeric capsular assembly in which two monomers of **4a** and **4b** interact by intercalation of their arms, through a belt of six hydrogen bonded urea functions. The dimers were formed by two enantiomeric tripods turned 60° with respect to each other resulting in S_6 symmetry for the dimeric capsule (Figure 1.2). The formation of these dimeric superstructures may be considered as a chiral self-discrimination process since one enantiomer module recognizes its mirror image. Furthermore, the dimeric structures (**4a•4a**) and (**4b•4b**) exist as solvent free capsules which may be explained taking into account that six of the twelve hydrogen atoms attached to the $(ArCH_2)_3N$ fragments almost fill the relatively small cavity (Figure 1.3a).

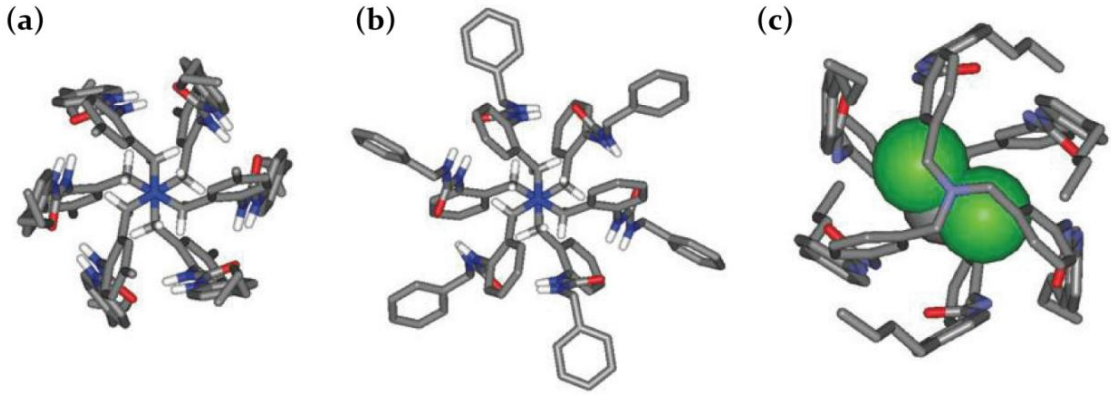

Figure 1.2 (a) Dimeric capsular structure of receptor **4a**; (b) Dimeric capsular structure of receptor **4b**, and (c) Dimeric capsular structure of receptor **5a**, encapsulating a CH_2Cl_2 molecule.

The pattern of ^{1}H NMR signals in DMSO-d_6 (a competitive solvent with hydrogen bonding), is consistent with averaged C_3v symmetry characteristic of the monomers. However, two sets of signals emerged in $CDCl_3$ corresponding to two species of different symmetry (Figure 1.3a). This fact was interpreted as mixtures of two species in equilibrium: more symmetric (C_3v) monomeric **4**, and less symmetric (S_6) dimeric (**4•4**). The appearance of two sets of signals indicates that the dimerization-disassembly rate is slow on the NMR time scale. Notably, the ratio of the two species is highly dependent on the identity of R^2. Thus, when R^2 = Aryl, the spectra display the signals of the less symmetric set almost exclusively. Finally, ESI-MS experiments provide further evidence for the dimerization process (**4•4**), displaying the molecular ions for the protonated dimeric species in the corresponding spectra measured in $CHCl_3$. The equilibrium between **4** and (**4•4**) could be shifted to the dimeric species by decreasing the temperature or increasing the concentration. Thus, tris(2-ureidobenzyl)amines **4a–c** have been established as good self-assemblers in the solid-state and solution. However, the cavity is not large enough to accommodate a guest molecule.

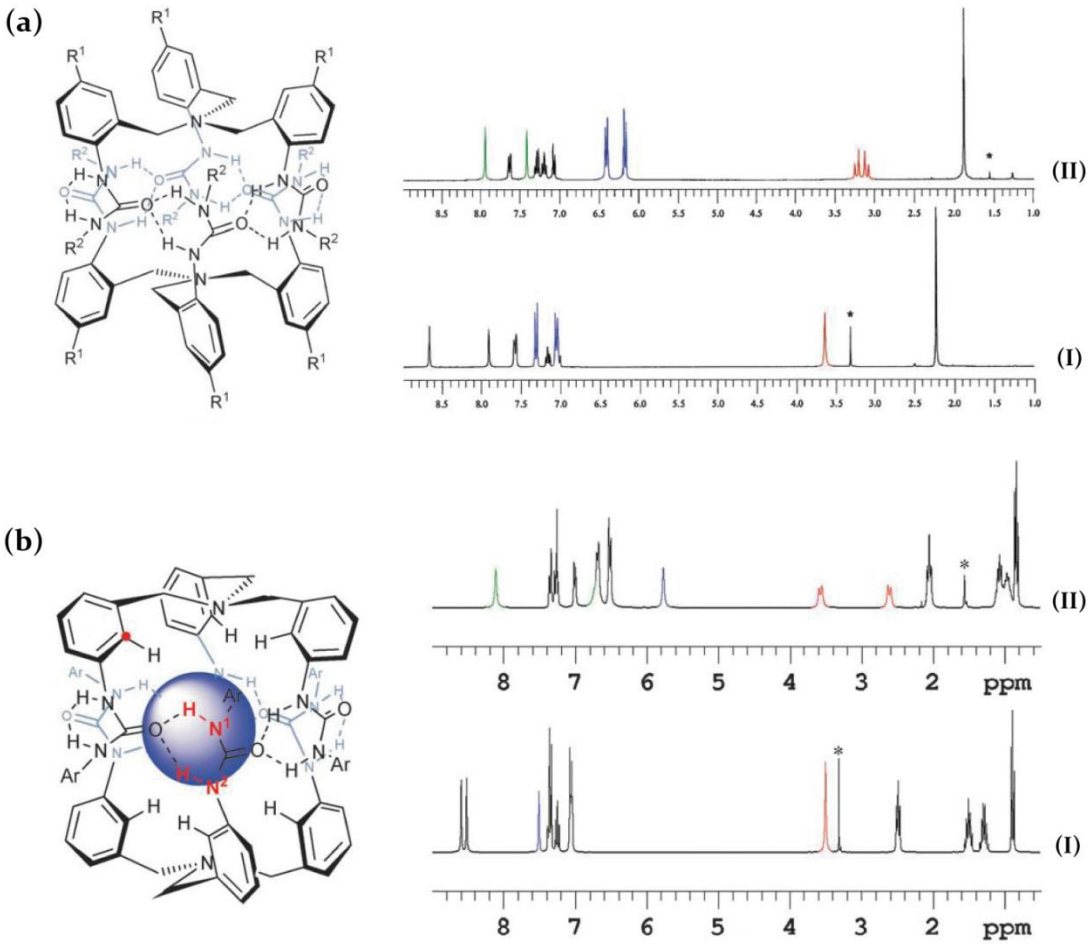

Figure 1.3 (a) Schematic representation showing the belt of hydrogen bonded urea functions in the dimeric structure of receptors **4a-c**, and ^{1}H NMR spectra (300 MHz) of **4c** (I) in DMSO-d_6 and (II) in $CDCl_3$ at 296 K (* represents signal for residual water); (b) Schematic representation showing the belt of hydrogen bonded urea functions in the dimeric structure of receptors **5a-c**, and ^{1}H NMR spectra (300 MHz) of **5a** (I) in DMSO-d_6 and (II) in $CDCl_3$ at 296 K (* represents signal for residual water).

The closely related tris(3-ureidobenzyl)amines **5a–c** share all the structural and functional features necessary for self-assembly with their 2-substituted counterparts **4a-c**, but they formed dimeric capsules with larger internal cavities. Single-crystal X-ray analysis of **2a** revealed the formation of a dimeric capsule filled with a CH_2Cl_2 molecule and encircled by the belt of six hydrogen bonded urea functions (Figure 1.2c). The arrangement of interdigitated arms leads to a cavity of markedly larger dimensions than those of (**4a•4a**), since for (**5a•5a**) the methylene protons of the $(ArCH_2)_3N$ fragment point outside. ^{1}H NMR spectroscopy and ESI-MS again support the persistence of dimeric aggregates (**5•5**) in non-competitive solvents. In contrast to (**4•4**), the association of (**5•5**) is so strong that the observation of the monomeric form is not possible. In regard to the symmetry criteria, the spectra of triureas **5** in $CDCl_3$ display the resonances due to the methylene protons of the $(ArCH_2)_3N$ as two doublets, which is consistent with a frozen conformation of the

tribenzylamine skeleton in a propeller arrangement (Figure 1.3b). In contrast, averaged C_3v symmetries were observed in DMSO-d_6 corresponding to the monomeric form.

However, structural survey of tren-based amide, urea and thiourea receptors (Scheme 1.4) revealed the formation of intramolecular N-H···X=C (X = O/S) hydrogen bond between the receptor side arms that disrupt the adoption of a C_3v symmetric conformation (Annexure 1) in them and the overall packing of the crystals are primarily governed by intermolecular N-H···X interactions with the neighbouring receptor molecules or with included solvent molecules. The intramolecular interactions, while potentially blocking the cavity, can also provide a preorganization effect, resulting in an effective clawlike topology for incorporating guest species.

1.4 Anion coordination chemistry of tripodal scaffolds

Although Nature exemplify how proteins can selectively and efficiently bind anions by weak intermolecular forces, the development of novel artificial receptors for the selective recognition of anions still remains a challenging task, with hydrogen bonds being fundamental in determining binding selectivity *via* topological complementarity. Anions generally have very high solvation energies that must be compensated by the host for effective anion recognition and complexation. Among the numerous design choices, trigonal receptors have been especially of interest because of their potential for binding molecules with C_3 rotation axes, such as nitrate, phosphate, and sulfate. The binding ability of trigonal anion receptors varies with the attached functionality to the tripodal unit, since functional groups modify the hydrogen bonding capability.

1.4.1 Tripodal amine receptors

Tren-based tripodal amine receptors have been shown to coordinate with anions of different dimensionality in its triprotonated form. In this section, we take into account of three such tripodal amine receptors, **2a-c** (Scheme 1.3) bearing peripheral aromatic functions to discuss the structural aspects of anion binding in their protonated forms. Bowman-James et al., in her work on receptor **2a** showed that the ligand in its triprotonated state binds a Br^- anion in the C_2v-like cleft as observed from the X-ray structure analysis of complex $[(H_3\mathbf{2a})(Br^-)_3]$.[26] Two of the receptor side arms are pointed in the same direction and binds a Br^- anion in between the cleft *via* N-H···Br^- interactions, whereas, the other two Br^- ions lie outside of the receptor cleft (Figure 1.4a). In the crystal structure of the phosphate complex, $[(H_3\mathbf{2a})(H_2PO_4^-)_3]\bullet H_3PO_4$ four phosphate species are associated with the triprotonated receptor, and have been assigned as three $H_2PO_4^-$ counter anions located between each receptor side arms (Annexure 1), and an additional H_3PO_4 molecule situated above the quasi-

planar tripod with the three arms pointing outward in a trigonal-planar-like arrangement (Figure 1.4b).[26]

A more interesting example of anion binding by a tripodal amine receptor has been demonstrated by Ghosh et al. by introducing a pentafluorophenyl unit as the aryl terminal to the tripodal scaffold (receptor **2b**).[24] Structural elucidation of the isostructural halide (F^-, Cl^- and Br^-) complexes, $[(H_3\mathbf{2b})(X^-)_3]$ showed binding and encapsulation of a halide anion within the C_3v-symmetric cavity of triprotonated **2b** *via* three N-H···X^- interactions (Figure 1.4c). In the case of complex $[(H_3\mathbf{2b})(OTs^-)_3]$, tetrahedral *p*-toluenesulphonate anion is partially engulfed within the protonated receptor cavity *via* N-H···O interactions (Figure 1.4d). Interestingly, in the mixed anion complex $[(H_3\mathbf{2b})_2(SiF_6^{2-})(BF_4^-)_4]CH_3OH{\bullet}H_2O$, octahedral hexafluorosilicate anion is encapsulated within the dimeric capsular assembly of two inversion symmetric $(H_3\mathbf{2b})^{3+}$ units by a number of N-H···F hydrogen bonds (Figure 1.4e). The potentiometric titration experiments in a methanol/water (1:1 v/v) binary solvent system showed high affinity of the receptor toward more basic fluoride and acetate anions, with a lesser affinity for other inorganic anions.

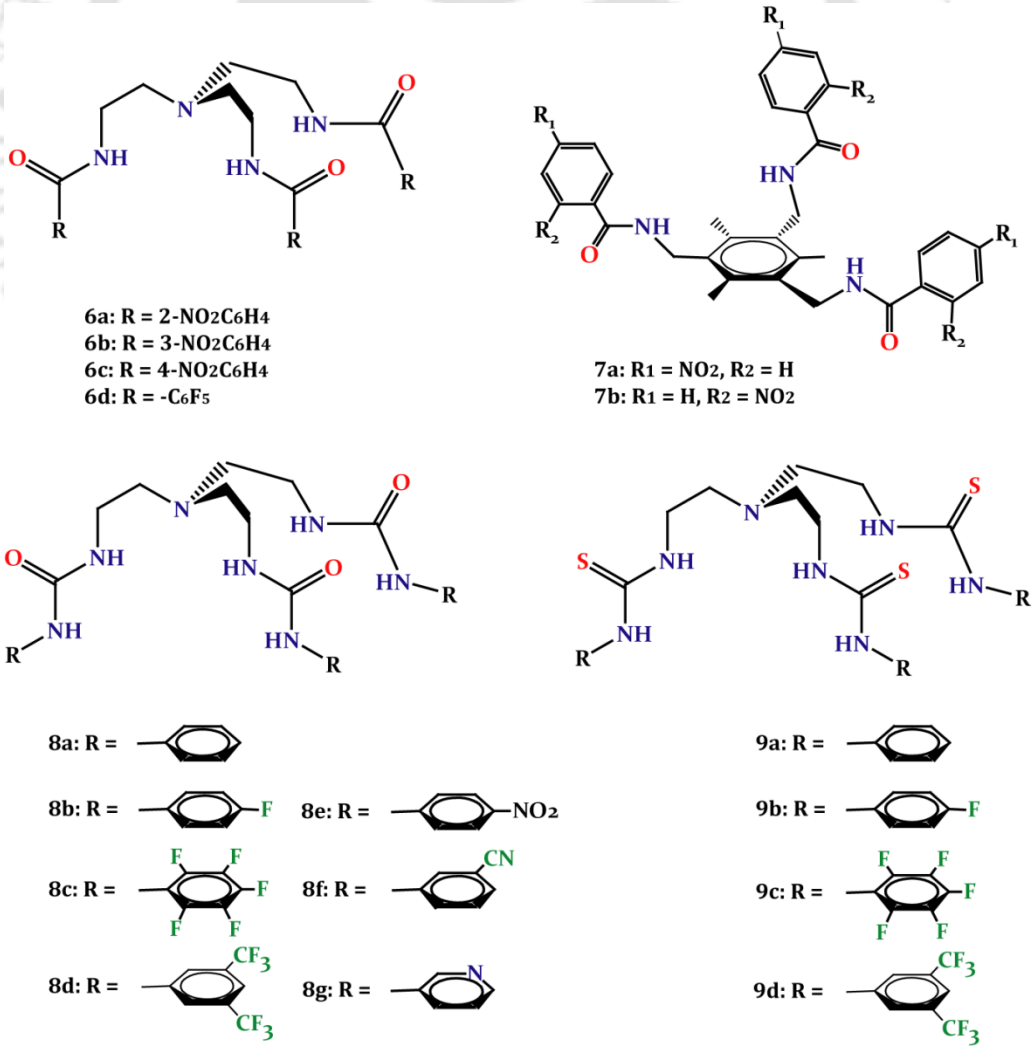

Scheme 1.4 Various *N*-bridged and *arene*-bridged tripodal anion receptors.

Hossain et al. has recently showed that, functionalization of the tripodal amine scaffold with a thiophene terminal (receptor **2c**) results in encapsulation of a nitrate anion in a selective orientation, forming a C_3 symmetric complex, $[(H_3\mathbf{2c})(NO_3^-)_3]$.[27] The anion is coordinated to three protonated secondary amines with six N-H···O hydrogen bonds in a plane perpendicular to the principal rotation axis passing through the bridgehead nitrogen of the protonated receptor and the nitrogen of the encapsulated nitrate (Figure 1.4f). On the other hand, in the structure of the iodide complex $[(H_3\mathbf{2c})(I^-)_3]$, an iodide anion is bound above the quasi-planar tripod with the three arms pointing outward in a trigonal-planar-like arrangement (Figure 1.4g). ^{1}H NMR titration studies showed that the triprotonated receptor forms a 1:1 complex with nitrate yielding a binding constant of K = 315 M^{-1} in chloroform and showing a moderate selectivity over halides. Thus, the attached aryl terminals in the receptor designing could play an important role towards the formation of different microenvironment for anion binding and encapsulation.

1.4.2 Tripodal amide receptors

Anion binding properties of tris(amide) receptors **6a–d** (Scheme 1.4) with electron withdrawing aryl substituents have been extensively studied by Ghosh et al. in solution as well as in solid state. Solution state anion binding experiments of nitrophenyl functionalized receptors **6a–c** showed the preferential binding of halides over oxyanions (Annexure 1). Substantial changes in chemical shifts were observed for the amide protons (–NH) and aromatic protons (–CH) with F^- and Cl^- in cases of **6b** and **6c**, and exclusively with F^- in case of **6a**, indicating the participation of –NH and –CH protons in the solution state anion binding events.[28] X-ray crystallography results showed that, anion binding with the protonated receptor is attributable entirely to N-H···A^- and C-H···A^- interactions in all the isolated complexes and in none of the cases anion encapsulation inside the receptor cavity was observed.[29] However, the pentafluorophenyl-based tris(amide) receptor **6d** has been found to encapsulate a monohydrated F^- anion [TBA(**6d**·F^-H_2O)] and a naked Cl^- anion [TBA(**6d**·Cl^-)] within the receptor cavity when crystallized in presence of TBAF and TBACl from individual aqueous solutions of **6d**.[30] In the crystal structure of complex [TBA(**3d**·F^-H_2O)], the F^- anion is bound in a distorted tetrahedral fashion *via* three amide N-H···F^- hydrogen bonds and a O-H···F^- hydrogen bond donated from the encapsulated water molecule (Figure 1.5a). Furthermore, the oxygen of the encapsulated water is in strong lp···π interaction with the pentafluorophenyl rings resulting in ditopic recognition of F^- and H_2O inside the small cavity of **6d** (Figure 1.5a). Whereas, monotopic recognition of Cl^- was observed in complex [TBA(**6d**·Cl^-)] where the Cl^- anion is in strong hydrogen bonding interaction with the three amide protons (Annexure 1).

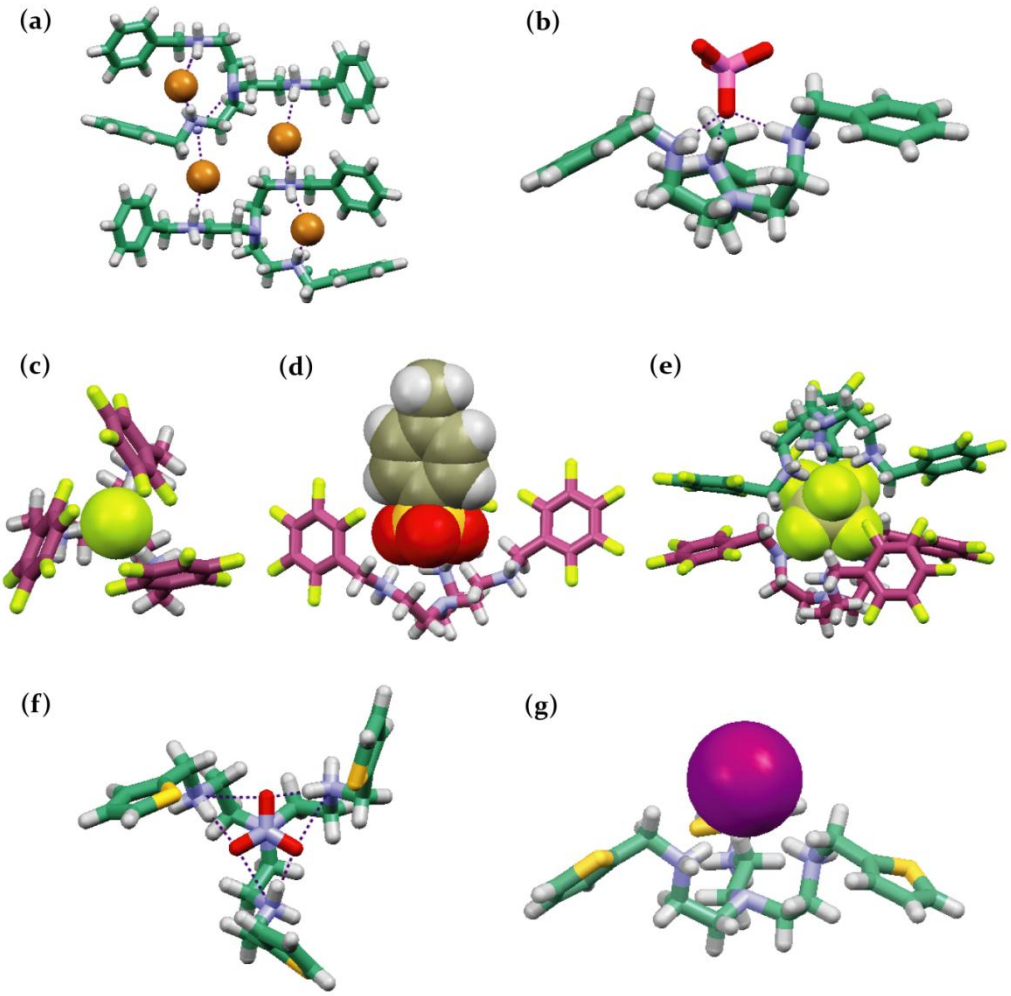

Figure 1.4 X-ray structures showing, (a) Br^- binding by protonated **2a** in complex $[(H_3\mathbf{2a})(Br^-)_3]$; (b) Binding of a H_3PO_4 molecule by protonated **2a** in complex $[(H_3\mathbf{2a})(H_2PO_4^-)_3]\bullet H_3PO_4$; (c) Binding and encapsulation of a F^- anion by protonated **2b** in complex $[(H_3\mathbf{2b})(F^-)_3]$; (d) Binding and pseudo-encapsulation of a p-toluene sulfonate anion by protonated **2b** in complex $[(H_3\mathbf{2b})(OTs^-)_3]$; (e) Binding and pseudo-encapsulation of the SiF_6^- anion by two units of protonated **2b** in complex $[(H_3\mathbf{2b})_2(SiF_6^{2-})(BF_4^-)_4]CH_3OH\bullet H_2O$; (f) Binding and encapsulation of a NO_3^- anion within the C_3 cavity of protonated **2c** in complex $[(H_3\mathbf{2c})(NO_3^-)_3]$, and (g) Binding of a I^- anion above the C_3 plane of protonated **2c** in complex $[(H_3\mathbf{2c})(I^-)_3]$.

In contrast to the *N*-bridged amide receptors, an arene-based tripodal amide receptor with electron withdrawing *p*-nitrophenyl terminals, **7a** showed encapsulation of hydrated anions like $[(F^-)_2(H_2O)_6]$, $[(Cl^-)_2(H_2O)_4]$ and $[(AcO^-)_2(H_2O)_4]$ inside the staggered dimeric capsular assembly of the receptor (Figure 1.5), when crystallized in presence of excess quaternary ammonium salts of the respective anion in moist dioxane media.[31] Although **7a** demonstrates the formation of capsular assembly upon anion or hydrated anion complexation, its positional isomer with electron withdrawing *o*-nitrophenyl terminals, **7b** showed selective dimeric capsule formation templated by the fluoride–water cluster, $[(F^-)_2(H_2O)_6]$, and non-capsular aggregation with other anions such as chloride, acetate and nitrate anions (Figure 1.5).[32] Thus, simple alteration of the $-NO_2$ group substitution in the receptor design resulted

in a marked difference in the aggregation properties of **7a** and **7b** upon complexation of anions and hydrated anionic guest species.

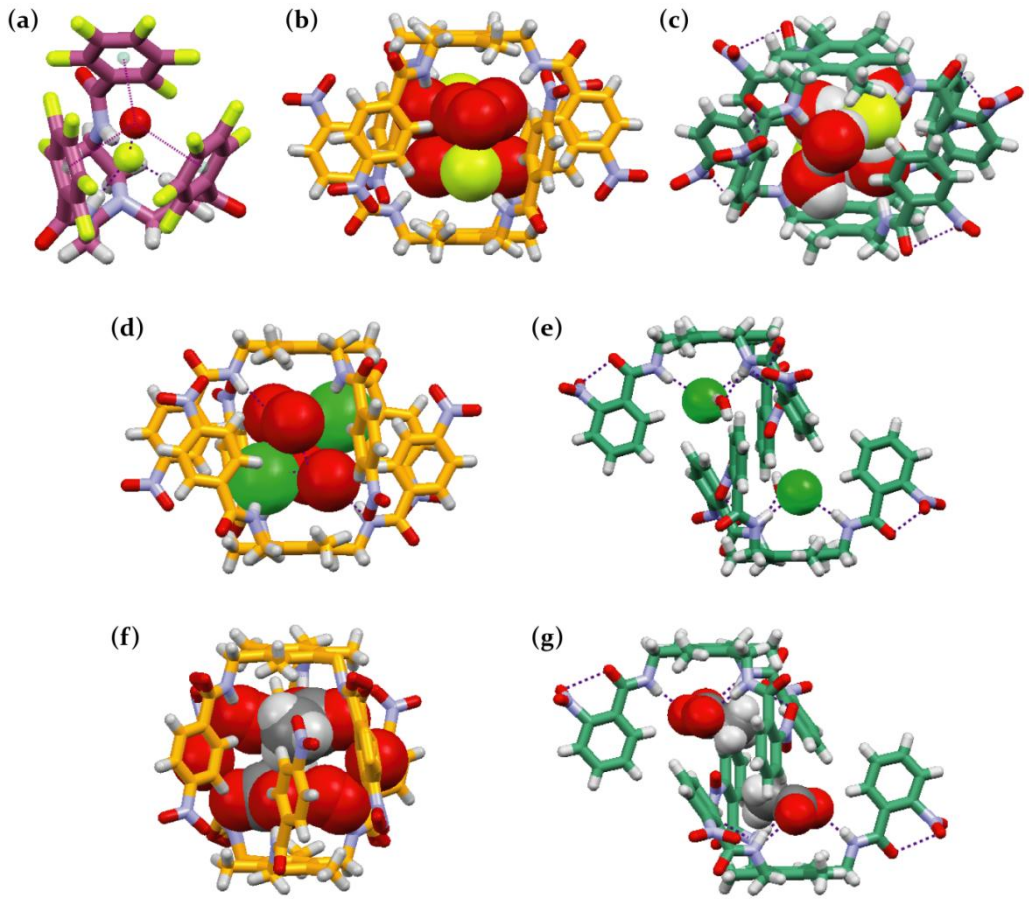

Figure 1.5 X-ray structures showing, (a) encapsulation of a monohydrated F anion by receptor **6d**; (b) encapsulation of $[(F^-)_2(H_2O)_6]$ adduct within the dimeric assembly of **7a**; (c) encapsulation of $[(F^-)_2(H_2O)_6]$ adduct within the dimeric assembly of **7b**; (d) encapsulation of $[(Cl^-)_2(H_2O)_4]$ adduct within the dimeric assembly of **7a**; (e) non-capsular aggregation of **7b** upon Cl^- binding; (f) encapsulation of $[(AcO^-)_2(H_2O)_4]$ adduct within the dimeric assembly of **7a**, and non-capsular aggregation of **7b** upon AcO^- binding.

1.4.3 Tripodal urea and thiourea receptors

Since the pioneering work of Wilcox[33] and Hamilton[34] that showed urea moieties can act as appropriate binding sites for anions, in particular oxoanions, a variety of acyclic and cyclic receptors containing urea and thiourea subunits have been developed and applied for anion complexation and sensing over the past years. In particular, urea and thiourea functions can establish two directional hydrogen bonds with the planar anions (e.g., AcO^- and HCO_3^-) or chelate a spherical anion (e.g., halides). Thiourea is a much stronger acid than urea (pK_A = 21.1 and 26.9, respectively in DMSO), thus it is expected that thiourea containing receptors establish stronger hydrogen bond interactions and form more stable complexes with anions than their urea containing counterparts.[35] Furthermore, survey of tripodal anion receptors

showed the dominant utility of urea and thiourea functionality over other classes of hydrogen bond donors.

Anion binding properties of tripodal urea and thiourea receptors **8a** and **9a** were studied using ^{1}H-NMR experiments.[36] In both the cases, a 1:1 complex stoichiometry was suggested upon binding of a dihydrogen phosphate anion *via* six hydrogen bonds inside the tripodal cavity. However, based on the experimental results, Gale et al. has recently suggested that the thiourea receptor **9a** is capable of both chloride/nitrate antiport and more significantly of transporting the more hydrophilic bicarbonate anion *via* a chloride/bicarbonate antiport mechanism than its urea analogue **8a**.[37] The crystal structures of the carbonate complex of **9a** revealed that two receptor molecules are oriented in a face-to-face fashion and encapsulates a carbonate anion in the centre *via* twelve strong hydrogen bonding interaction.[37] The same author has recently prepared a series of fluorinated tripodal anion receptors containing urea and thiourea groups including **8b-d** and **9b-d** (Scheme 1.4) and studied their anion complexation and transport properties.[38] ^{1}H NMR titration and single crystal X-ray diffraction revealed the ability of the fluorinated receptors to bind different anions with varying affinities in a 1:1 or 2:1 stoichiometry in solution and in the solid state. However, attempted crystallization of a bicarbonate complex of thiourea receptor **9c** failed, presumably because bicarbonate functioned as a Brønsted base and deprotonated one of the thiourea –NH groups instead of forming an anion complex. Thus, the crystal structure obtained was that of a dimer of deprotonated **9c**, stabilized by intermolecular hydrogen bonds between the remaining –NH functions and the sulphur atom of the deprotonated thiourea group (Figure 1.6a). Interestingly, the carbonate complex of the urea receptor **8c** (analogue of **9c**) has been obtained in quantitative yield as air stable crystals, from an equimolar mixture of the receptor-hydroxide solution.[39] The source of CO_3^{2-} in the system is from the atmospheric CO_2 that has been efficiently fixed by the OH^- ions added to the receptor solution in DMSO. Structural elucidation revealed that a CO_3^{2-} anion is encapsulated within the dimeric cage structure of two **8c** molecules by as much as 16 hydrogen bonds from the six urea groups (Figure 1.6b). The ^{1}H NMR titration data gave the best fit for a 1:2 stoichiometry of guest to host with an overall association constant of log K = 4.04, which supported the solution state existence of capsular assembly as observed in the solid state structure. Similar to **9a**, crystallization of urea **8d** in presence of excess TEA(HCO_3^-) yielded CO_3^{2-} encapsulated molecular capsules stabilized by several N-H···O hydrogen bonding interactions.[38]

The tetrabutylammonium sulfate complex of **9b**, showed the binding and encapsulation of a disordered SO_4^{2-} anion within a dimeric cage structure of the receptor by making 14 N-H···O hydrogen bonds to the anion. An identical mode of disordered sulfate binding (2:1 host-

guest, Figure 1.6d) within the cage of two inversion-symmetric molecules of receptor **8c** has previously been reported by Ghosh et al.[40] On the other hand, crystal structure of the sulfate complex of thiourea **9c** showed a 1:1 stoichiometry as observed in solution. Six strong hydrogen bonds between the sulfate oxygen atoms and the thiourea –NH functions are responsible for the complex formation. Additionally, one of the TBA counter ions is held in close contact with the encapsulated sulfate anion *via* three C-H···O interactions donated from the CH_2 groups adjacent to the positively charged nitrogen in TBA cation (Figure 1.6e). Furthermore, Das et al. has shown the crystallographic evidence of sulfate encapsulation by the urea receptor **8e** in a 1:1 stoichiometry.[41] Structural analysis showed that, all three urea functions are involved in N-H···O hydrogen bonding with a sulfate anion which is further hydrogen bonded to three water molecules resulting in a nine coordination number for the encapsulated sulfate. The concurrent interactions of three lattice water molecules with two encapsulated sulfate anions by O···H-O-H···O hydrogen bonds generates a rugby ball shaped sulfate–water–sulfate adduct held inside a pseudo dimeric assembly of receptor **8e** (Figure 1.6f). The binding constant values calculated from the UV/Vis titration experiments revealed the preferential binding of SO_4^{2-} and $H_2PO_4^-$ over other oxyanions in an acetonitrile/water mixture (95/5, v/v) solution.

Structural analysis of the crystals of the dihydrogen phosphate complexes of **8c** and **9c** showed that a $H_2PO_4^-$ anion is bound inside the tripodal cleft by seven hydrogen bonding interactions. Additionally, the encapsulated $H_2PO_4^-$ is hydrogen bonded with another $H_2PO_4^-$ to form a centrosymmetric dimer, with non-intercalated arms between the two tripodal receptor units (Figure 1.7a). The solution state binding of $H_2PO_4^-$ and HPO_4^{2-} with urea **8c** has also been demonstrated by the ^{31}P-NMR spectroscopy in DMSO-d_6.[42] On the other hand, the complexes formed by **9b** and **9d** with TBA(H_2PO_4) showed the deprotonation of bound $H_2PO_4^-$ anion as observed in solution during ^{1}H NMR titrations and crystallized as 2:1 receptor-HPO_4^{2-} complexes in the presence of excess TBA(H_2PO_4). In both the structures, a HPO_4^{2-} anion is bound inside the dimeric capsular assembly of the receptor by 14 hydrogen bonds to the six thiourea functions (Figure 1.7b).

The tetrabutylammonium chloride complexes of receptors **8b**, **9b**, and **9c** crystallized as 1:1 complexes, reflecting the stoichiometry observed in solution. In all three complexes, a chloride anion is bound within the tripodal cavity by six N-H···Cl^- hydrogen bonds, one from each NH group (Figure 1.7c). Similarly, binding of fluoride within the tripodal cavity is also governed by six N-H···F^- hydrogen bonds (Figure 1.7d), as observed in the crystal structure of fluoride complex of **8c**. The solution state binding of F^- with **8c** was also clearly shown by the ^{19}F-NMR spectrum in DMSO-d_6.[40]

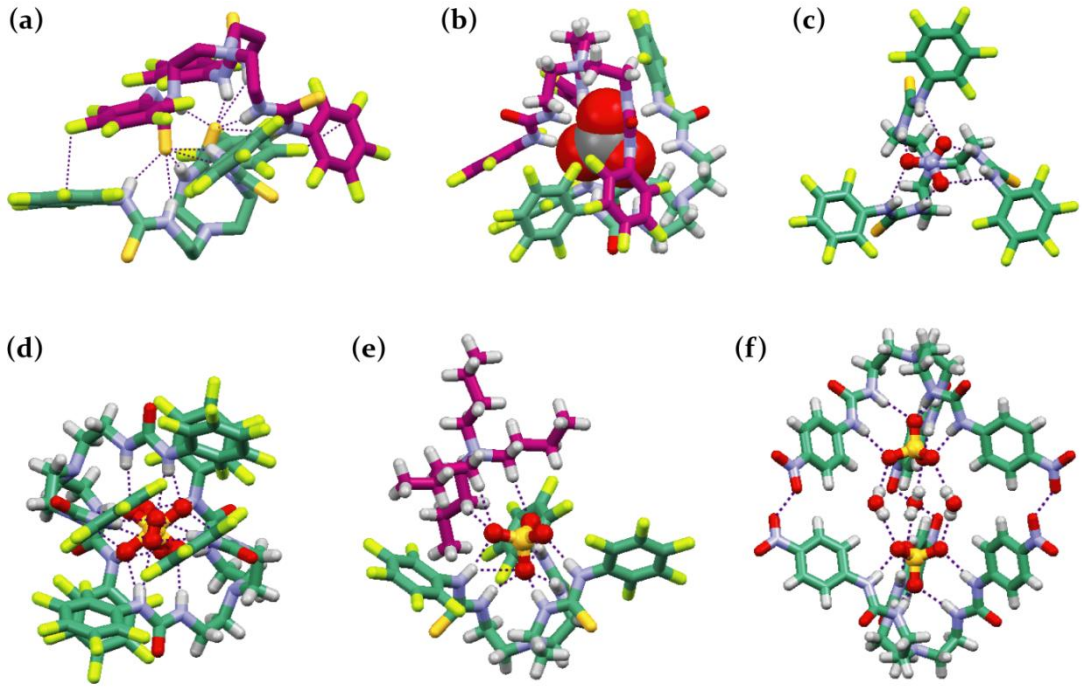

Figure 1.6 X-ray structures showing, (a) the dimeric interaction between two deprotonated **9c** (obtained in presence of CO_3^{2-}); (b) CO_3^{2-}–encapsulated dimeric capsule of **8c** (obtained in presence of OH^-); (c) NO_3^-–encapsulation within the C_3 symmetric cavity of **9c**; (d) SO_4^{2-}–encapsulated dimeric capsule of **8c**; (e) TBA cation-sealed SO_4^{2-}–encapsulated receptor **9c**, and (f)encapsulation of a SO_4^{2-}–$(H_2O)_3$–SO_4^{2-}adduct within a pseudo-dimeric capsular assembly of receptor **8e**.

It is however, interesting to note that functionalization of **8a** with metal-coordinating *m*–CN groups afforded the receptor **8f** that has been utilized by Custelcean et al. for the selective separation of SO_4^{2-} over other anions *via* the formation of a selective MOF (Metal–Organic Framework).[43] Complexation of **8f** with 0.5 equivalents of Ag_2SO_4 in water/acetone yielded a coordination polymer with the composition $[Ag_2(\mathbf{8f})_2(SO_4)](acetone)1.5(H_2O)_{3.7}$, as indicated by elemental analysis and single-crystal X-ray diffraction. Both molecular modelling (MMFF94) and crystal structure analyses showed that SO_4^{2-} is coordinated to two molecules of **8f** with twelve hydrogen bonds from the six urea groups. Additionally, two receptor molecules that encapsulate a SO_4^{2-} anion are held together by CN–Ag and C=O–Ag coordinative bonds to form a molecular cage (Figure 1.8a). Attempts to crystallize **8f** with other soluble silver salts having anions of different geometry and basicity such as $AgBF_4$, $AgNO_3$, $AgMeSO_3$ and $AgMeCO_2$ failed to produce coordination polymers and yielded crystals of the free ligand only. Similarly, crystallization of **8f** in presence of $(Me_4N)_2SO_4$ was also unsuccessful which indicated that silver coordination and MOF formation are critical in stabilizing the sulfate encapsulated dimeric capsule.

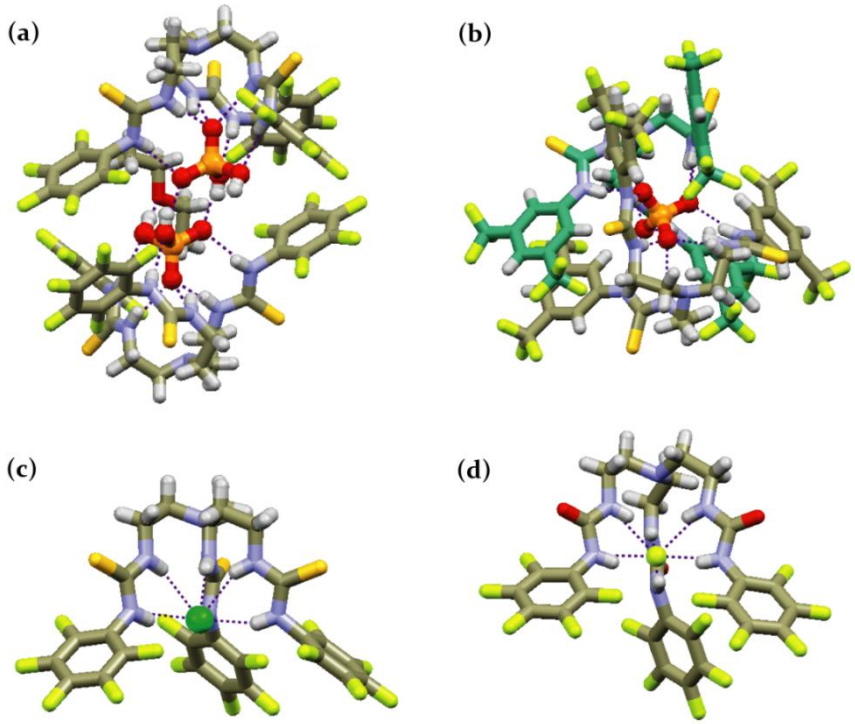

Figure 1.7 X-ray structures showing, (a) encapsulation of hydrogen bonded $H_2PO_4^-$ dimer within a pseudo-dimeric capsular assembly of receptor **9c**; (b) encapsulation of a deprotonated dihydrogenphosphate (HPO_4^{2-}) within a dimeric capsular assembly of receptor **9d**; (c) Cl^- encapsulation within the receptor cavity of **9c**, and (d) F^- encapsulation within the receptor cavity of **8c**.

Based on similar ideas, Custelcean et al. and Wu et al. have independently prepared the urea receptor **8g**, for the effective binding and separation of SO_4^{2-} by the formation of crystalline capsules.[44] Crystallization of **8g** with various metal sulphates such as $MnSO_4$, $ZnSO_4$, $CdSO_4$, $CoSO_4$ and $MgSO_4$ in 1:1 H_2O/MeOH media yielded crystals suitable for X-ray crystallography analysis with the composition $[MSO_4(\mathbf{8g})_2(H_2O)_6]$. In all the structures, a SO_4^{2-} anion is encapsulated within the dimeric cage of the receptor **8g** *via* twelve N–H···O hydrogen bonds from the six urea groups. Furthermore, the SO_4^{2-}encapsulated receptor molecules are held together by six O–H···N-(pyridine) and six O–H···O-(C=O) hydrogen-bonding bridges with the water molecules coordinated to the metal centre (coordinated to six water molecules) (Figure 1.8b). The necessity of a dication/dianion pair for the formation of the crystalline capsule and the selective separation of SO_4^{2-} from the solution containing excess NO_3^- was also established. Magnesium salts of various dianions like SO_3^{2-}, CO_3^{2-} and SeO_4^{2-} also formed crystalline frameworks of similar geometrical parameters and showed anion recognition inside the dimeric capsule with **8g**. The competition experiments of **8g** with these anions established the following anion selectivity order: $SO_4^{2-} > SeO_4^{2-} > CO_3^{2-} > SO_3^{2-}$ which is different from both the Hofmeister bias and anion basicity scale whereas the trend was in agreement with the lattice energy calculations on the crystal structures.

Custelcean et al. has further investigated the fundamental factors controlling the anion selectivity of **8g** by solution and solid state thermodynamic measurements and anion competition experiments in water.[45]

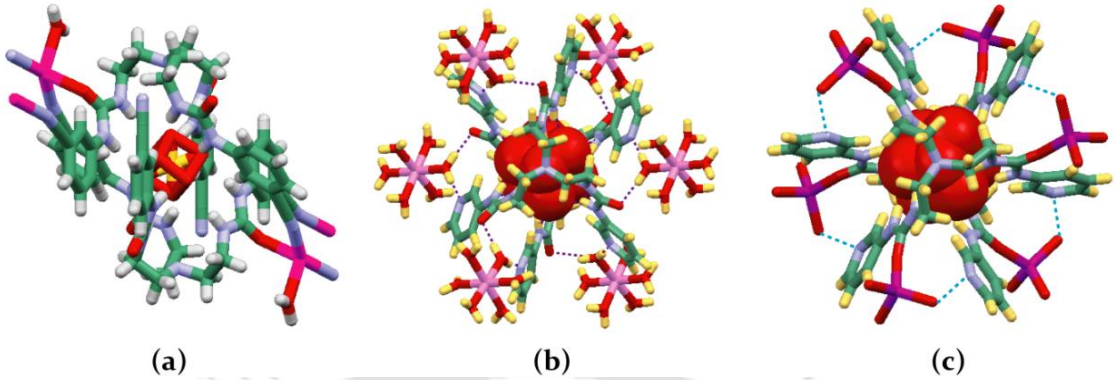

Figure 1.8 X-ray structures showing, (a) SO_4^{2-}–encapsulated rigid dimeric cage in complex $[Ag_2(\mathbf{8f})_2(SO_4)](acetone)1.5(H_2O)_{3.7}$ stabilized by Ag^+ coordination; (b) SO_4^{2-}–encapsulated rigid dimeric cage in complex $[MgSO_4(\mathbf{8g})_2(H_2O)_6]$, stabilized by multiple hydrogen bonded water bridges, and (c) SO_4^{2-}–encapsulated rigid dimeric cage in complex $[Li_2SO_4(\mathbf{8g})_2(H_2O)_2]$, stabilized by Li^+ coordination and hydrogen bonded water bridges.

Crystallization of **8g** in the presence of Li_2SO_4, from H_2O/MeOH solutions afforded crystals with the composition $[Li_2SO_4(\mathbf{8g})_2(H_2O)_2]$, as determined by single-crystal X-ray diffraction and elemental analysis.[46] Structural elucidation revealed the formation of S_6-symmetrical capsules containing two molecules of the receptor held together by 6 H_2O–Li^+ units through Li···O(urea) coordinative bonds and O–H···N-(pyridine) hydrogen bonding bridges with the water molecules coordinated to the metal centre (Figure 1.8c). Although, the sulfate coordination within the capsular assembly has been found to be similar with the crystalline complex $[MgSO_4(\mathbf{8g})_2(H_2O)_6]$, there are some subtle but significant differences. First, $[Li_2SO_4(\mathbf{8g})_2(H_2O)_2]$ has higher symmetry (S_6) compared with $[MgSO_4(\mathbf{8g})_2(H_2O)_6]$ (*i*) and second, the size of $[Li_2SO_4(\mathbf{8g})_2(H_2O)_2]$ capsule is significantly smaller, with a distance between the tertiary N atoms of the two **8g** units of 9.17 Å, which is 0.48 Å shorter than the corresponding distance in $[MgSO_4(\mathbf{8g})_2(H_2O)_6]$. Li salts of SeO_4^{2-} and SO_3^{2-} were found to form crystalline complexes that are isomorphous with $[Li_2SO_4(\mathbf{8g})_2(H_2O)_2]$, as determined by single-crystal X-ray crystallography. Competitive crystallization of **8g** (2 equivalents) with 1 equiv. of Li_2SO_4 and one equivalent of each SO_3^{2-}, CO_3^{2-} and SeO_4^{2-} (added as Na salt) in H_2O/MeOH mixture, established the shape recognition of SO_4^{2-} against SO_3^{2-} and CO_3^{2-}, and size recognition against SeO_4^{2-}.

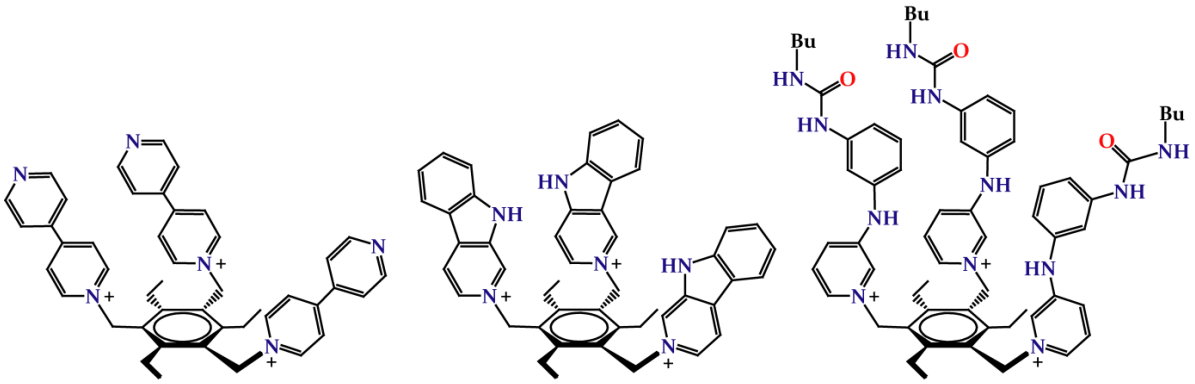

10 **11** **12**

Scheme 1.5 Some pyridinium-functionalized tripodal receptors on a benzene platform.

1.4.4 Pyridinium-functionalized tripodal receptors

One of the long held aims of anion receptor chemistry has been to selectively recognize anions in water. A highly effective strategy that has been used to improve the anion binding efficiency in highly competitive solvent systems such as water has involved the use of zwitterionic receptors. Steed et al. has demonstrated the bromide ion induced dimeric capsule formation from the water soluble zwitterionic tripodal receptor **3b**.[25] The receptor is neutral and does not have any hydrogen bond donor elements. However, it stabilizes the anion inside a dimeric capsular assembly *via* electrostatic and C–H···Br^- interactions. The crystal structure of Na[(**3b**)$_2$Br]13H_2O uncovered an outstanding 2:1 (host : Br^-) self-assembled capsule in which a bromide ion is encapsulated by two units of zwitterionic receptor **3b** in water (Figure 1.9a). Acidification of **3a** with excess HPF_6 in water resulted in the precipitation of complex with the composition [H**3a**·PF_6·2H_2O]. Structural analysis revealed the noncapsular aggregation of the receptor moieties as an infinite 1D ribbon *via* COO^-···HOOC hydrogen bonds with the acidic –COOH proton is shared almost equally between the two carboxylate groups and the PF_6^- anion is situated between a pair of pyridinium groups engaging in anion–π interactions (Annexure 1).

In contrast to the bromide-encapsulated complex of **3b**, the hydrated bromide salt of receptor **10** (Scheme 1.5) with the composition [**10**(Br^-)$_3$]4H_2O·2C_2H_5OH, showed a deformation of the host conformation from the ideal C_3v symmetry in which **10** acts as a second sphere ligand for a hydrated bromide anion *via* C–H···Br^- interactions (Figure 1.9b).[47] Treatment of [**10**(Br^-)$_3$] with NH_4PF_6 in water resulted in the immediate precipitation of the solvent free hexafluorophosphate salt of receptor **10**. Recrystallization from water-acetonitrile media yielded an acetonitrile solvate of compound [**10**(PF_6^-)$_3$] in the chiral hexagonal space group $P6_3$, suggesting the adoption of a threefold-symmetric conformation, in contrast to the bromide salt. The adoption of this chiral conformation is apparently a direct consequence of

the encapsulation a PF_6^- anion within the molecular cavity *via* multiple C–H···F interactions and the twisting of the bipyridyl moieties necessary to avoid unfavourable steric interactions between the meta-pyridyl protons (Figure 1.9c).

Based on the nature of anion binding elements used, Fabbrizzi et al. have combined the charged pyridinium functions along with the hydrogen bond donating pyrrolic subunit in receptor **11** (Scheme 1.5) for the binding of anions.[48] Crystal structure of the nitrate-encapsulated complex [**11**(NO_3)]$(PF_6)_2(C_2H_5O)_2$, showed that two of the three receptor side arms are almost coplanar and the pyrrolic –NH protons are hydrogen bonded to the encapsulated nitrate anion by N–H···O interactions, while the third arm is hydrogen bonded with a lattice diethylether by N–H···O interaction. Two such units intercalate among themselves to form a nitrate encapsulated dimeric capsule (Figure 1.9d). Interestingly, the crystal structure of the bromide-encapsulated complex [(**11**$)_2$(Br)(H_2O)]$(PF_6)_3(CH_3CN)_2$, showed that one half of the molecular capsule accommodates the water molecule within a single receptor unit and the other half accommodated the bromide ion *via* strong N–H···O hydrogen bonding interactions (Figure 1.9e).

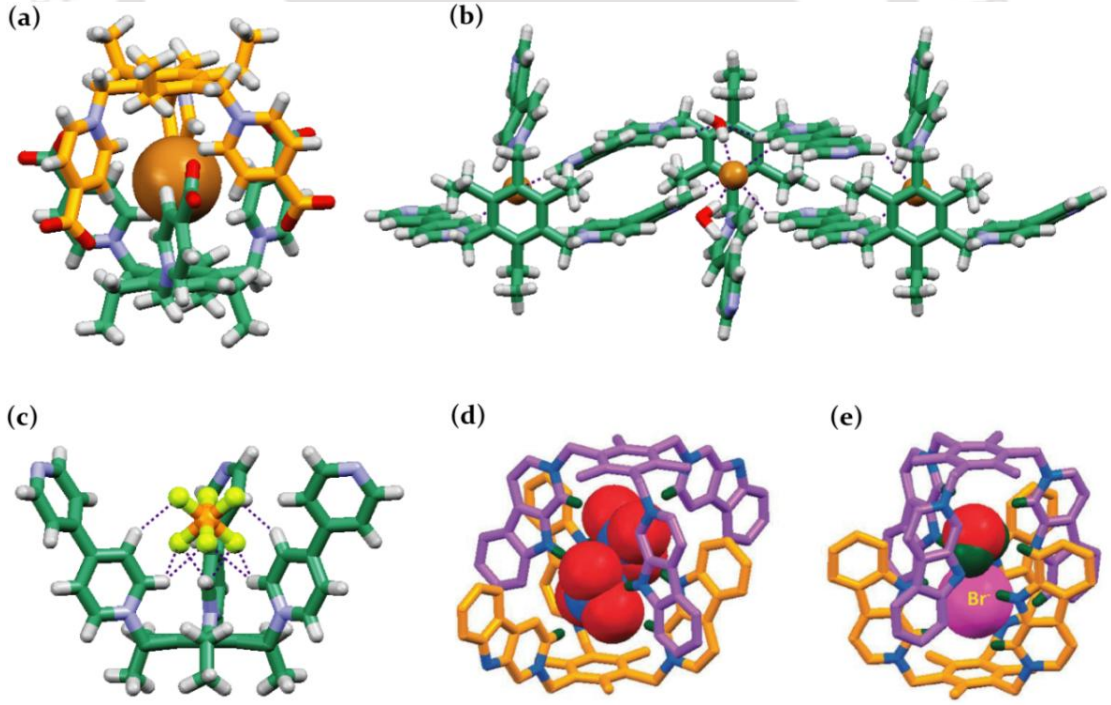

Figure 1.9 X-ray structures showing, (a) Br^- ion induced dimeric capsule of **3a**; (b) non-capsular aggregation of **10** upon binding of hydrated Br^- ions; (c) binding of a PF_6^- anion within the C_3 symmetric cavity of **10**, and (d) encapsulation of two nitrate anions within the dimeric capsular assembly of **11** in complex [**11**(NO_3)]$(PF_6)_2(C_2H_5O)_2$ and (e) encapsulation of a hydrated Br^- anion within the dimeric capsular assembly of **11** in complex [(**11**$)_2$(Br)(H_2O)]$(PF_6)_3(CH_3CN)_2$ (Note: the receptor unit encapsulating the water molecule is doubly deprotonated).

Steed et al. have described the role of intramolecular hydrogen bonding between the remote functional groups in increasing the preorganization of an anion-binding within the receptor cavity of **12** (Scheme 1.5).[49] In his work, the author has formulated a new strategy for the conformational control and increasing preorganization in flexible anion hosts. The possibility of the dimerization of two molecules of **12** by the hydrogen bonded belt of six urea groups was ruled out by the observation of ESI-MS and ^{1}H NMR dilution experiments. The DFT model of the 3-up conformer of **12** revealed the trigonal prismatic hydrogen bonded arrangement around the Cl^- anion comprising of three N–H···Cl^- and three pyridinium C–H···Cl^- interactions whereas the peripheral urea motifs are zipped together to form a unimolecular capsule upon chloride recognition (Annexure 1).

1.5 Concluding remarks

In general, tripodal scaffolds with appropriately positioned hydrogen bonding groups can display exceptional self-assembling abilities. Notably, the functionalization of the tribenzylamine skeleton with one ureido group in every arm of the tripod leads to hydrogen bonded dimeric associations in solution and in the solid state. Furthermore, the tertiary amino group can be employed as a pH switch for the dimeric assembly-disassembly process. In anion receptor chemistry, tris(2-aminoethyl)amine based tripodal urea/thiourea receptors have shown their high potential towards anion assisted capsule and pseudo-capsule formation. Higher coordination number of oxyanions like sulfate, phosphates and carbonate assist in dimeric capsular assembly formation while halides tend to form unimolecular capsules. On the other hand tripodal amide receptors on a benzene platform have shown their interest for recognition of hydrated anions, especially hydrated fluoride, *via* capsular assembly formation. Thus, a crucial task for going towards technological applications is the construction of molecular capsules for the recognition of hydrated anions rather than naked anions could be of better approach to target anions in natural environment. Capsular assemblies create a microenvironment with higher number of hydrogen bonding interaction sites that dictate the selectivity as well as assist to overcome the higher hydration energies of the anions. The recognition and binding of anions in molecular capsules is definitely a field which can expand considerably and bring immense advances in specialised applications such as: (a) removal and extraction of fluoride and other toxic anionic species from drinking water, (b) utilizing the binding and selectivity of the molecular capsules towards anionic species for the drug delivery applications, and (c) utilizing the molecular capsules as molecular reactors by stabilizing the anionic reactive intermediates inside the nanocavity.

References

1. J. W. Steed and J. L. Atwood, *Supramolecular chemistry*, John Wiley and Sons, Ltd; 1997.
2. T. Steiner, Hydrogen Bond in the Solid State. *Angew. Chem., Int. Ed*., 2002, **41**, 48.
3. (a) D. S. Lawrence, T. Jiang and M. Levett, *Chem. Rev*., 1995, **95**, 2229; (b) L. M. Greig and D. Philp, *Chem. Soc. Rev*., 2001, **30**, 287.
4. D. J. Cram, *Angew. Chem., Int. Ed*., 1986, **25**, 1039.
5. A. Bianchi, K. Bowman-James and E. Garcia-Espana, *Supramolecular Chemistry of Anions*, Wiley-VCH, New York, 1997.
6. J. L. Sessler, P. A. Gale and W. S. Cho, *Anion Receptor Chemistry*, The Royal Society of Chemistry, Cambridge, UK, 2006.
7. Moyer, B. A.; Bonnesen, P. V. *Physical factors in anion separations, In Supramolecular Chemistry of Anions*; Wiley-VCH: New York, 1997; chapter 1.
8. D. J. Mercer and S. J. Loeb, *Chem. Soc. Rev*., 2010, **39**, 3612.
9. K. Bowman-James, *Acc. Chem. Res*., 2005, **38**, 671.
10. (a) H. -J. Schneider and A. K. Yatsimirsky, *Chem. Soc. Rev*., 2008, **37**, 263; (b) E. Garcia-Espana, P. Diaz, J. M. Llinares and A. Bianchi, *Coord. Chem. Rev*., 2006, **250**, 2952; (c) S. O. Kang, M. A. Hossain and K. Bowman-James, *Coord. Chem. Rev*., 2006, **250**, 3038.
11. (a) P. A. Gale, *Chem. Commun*., 2008, 4525; (b) C. Caltagirone and P. A. Gale, *Chem. Soc. Rev*., 2009, **38**, 520; (c) P. A. Gale, *Acc. Chem. Res*., 2006**, 39**, 465; (d) A-F. Li, J-H. Wang, F. Wang and Y-B. Jiang, *Chem. Soc. Rev*., 2010, **39**, 3729.
12. (a) T. Gunnlaugsson, P. E. Kruger, P. Jensen, F. M. Pfeffer and G. M. Hussey, *Tetrahedron Lett*., 2003, **44**, 8909; (b) S. Camiolo, P. A. Gale, M. B. Hursthouse and M. E. Light, *Org. Biomol. Chem*., 2003, **1**, 741; (c) V. Amendola, D. Esteban-Gomez, L. Fabbrizzi and M. Licchelli, *Acc. Chem. Res*., 2006, **39**, 343.
13. R. Custelcean, *Chem. Soc. Rev.*, 2010, **39**, 3675.
14. (a) B. L. Schottel, H. T. Chifotides and K. R. Dunbar, *Chem. Soc. Rev*., 2008, **37**, 68; (b) H. T. Chifotides, B. L. Schottel and K. R. Dunbar, *Angew. Chem., Int. Ed.*, 2010, **49**, 7202.
15. (a) B. P. Hay and V. S. Bryantsev, *Chem. Commun*., 2008, 2417; (b) B. P. Hay and R. Custelcean, *Cryst. Growth Des*., 2009, **9**, 2539.
16. G. Cavallo, P. Metrangolo, T. Pilati, G. Resnati, M. Sansoteraa and G. Terraneo, *Chem. Soc. Rev.*, 2010, **39**, 3772.
17. (a) P. Ballester, *Chem. Soc. Rev.*, 2010, **39**, 3810; (b) M. Arunachalam and P. Ghosh, *Chem. Commun*., 2011,**47**, 8477.
18. (a) C. J. Avers, *Molecular Cell Biology.*, Addison-Wesley: Reading, 1986; (b) J. L. Atwood and A. Szumna, *J. Am. Chem. Soc*., 2002, **124**, 10646; (c) J. Rebek Jr., *Acc. Chem. Res.* 1999, **32**, 278.
19. (a) J. -M. Lehn, *Proc. Natl. Acad. Sci*., 2002, **99**, 4763; (b) L. R. MacGillivray and J. L. Atwood, *Angew. Chem., Int. Ed.*, 1999, **38**, 1018.
20. (a) T. Heinz, D. M. Rudkevich and J. Rebek, Jr., *Nature*, 1998, **394**, 764; (b) J. Rebek, Jr., *J. Am. Chem. Soc.*, 2002, **124**, 12074.
21. (a) J. Rebek Jr., *Chem. Commun*., 2000, 637; (b) L. R. MacGillivray and J. L. Atwood, Nature, 1997, **389**, 469; (c) J. M. Rivera, T. Martin and J. Rebek Jr., *J. Am. Chem. Soc*., 2001, **123**, 5213; (d) T. Szabo, G. Hilmersson and J. Rebek Jr., *J. Am. Chem. Soc*., 1998, **120**, 6193; (e) R. M. Grotzfeld, N. Branda and J. Rebek Jr., *Science*, 1996, **271**, 487.
22. M. Alajarin, R-A. Orenes, J. W. Steed and A. Pastor, *Chem. Commun*., 2010, **46**, 1394.
23. A. S. Singh, B-Y. Chen, Y-S. Wen, C. Tsai and S-S. Sun, *Org. Lett.*, 2009, **11**, 1867.
24. P. Bose, I. Ravikumar, and P. Ghosh, *Inorg. Chem*., 2011, **50**, 10693.
25. A. L. Cresswell, M-O. M. Piepenbrock and J. W. Steed, *Chem. Commun*., 2010, **46**, 2787.
26. M. A. Hossain, J. A. Liljegren, D. Powell and K. Bowman-James, *Inorg. Chem*., 2004, **43**, 3751.

27. M. Isiklan, M. A. Saeed, A. Pramanik, B. M. Wong, F. R. Fronczek, and M. A. Hossain, *Cryst. Growth Des*., 2011, **11**, 959.
28. I. Ravikumar, P. S. Lakshminarayanan and P. Ghosh, *Inorg. Chim. Acta*., 2010, doi:10.1016/j.ica.2010.02.030
29. P.S. Lakshminarayanan, E. Suresh and P. Ghosh, *Inorg. Chem*., 2006, **45**, 4372.
30. I. Ravikumar, Subrata Saha and Pradyut Ghosh, *Chem. Commun*., 2010, DOI: 10.1039/c0cc03469j
31. M. Arunachalam and P. Ghosh, *Inorg. Chem*., 2010, **49**, 943.
32. M. Arunachalam and P. Ghosh, *Chem. Commun*., 2009, 5389.
33. P. J. Smith, M. V. Reddington and C. S. Wilcox, *Tetrahedron Lett*., 1992, **33**, 6085.
34. E. Fan, S. A. Van Arman, S. Kincaid and A. D. Hamilton, *J. Am. Chem. Soc*., 1993, **115**, 369.
35. F. G. Bordwell, *Acc. Chem. Res*., 1988, 21, 456.
36. C. Raposo, M. Almaraz, M. Martin, V. Weinrich, M. L. Mussons, V. Alcazar, M. C. Caballero and J. R. Moran, *Chem. Lett*., 1995, 759.
37. N. Busschaert, P. A. Gale, C. J. E. Haynes, M. E. Light, S. J. Moore, C. C. Tong, J. T. Davis and W. A. Harrell, Jr., *Chem. Commun*., 2010, **46**, 6252.
38. N. Busschaert, M. Wenzel, M. E. Light, P. Iglesias-Hernandez, R. Perez-Tomas and P. A. Gale, *J. Am. Chem. Soc*., 2011, **133**, 14136.
39. I. Ravikumar and P. Ghosh, *Chem. Commun*., 2010, **46**, 1082.
40. I. Ravikumar, P. S. Lakshminarayanan, M. Arunachalam, E. Suresh and P. Ghosh, *Dalton Trans*., 2009, 4160.
41. D. A. Jose, D. K. Kumar, B. Ganguly and A. Das, *Inorg. Chem*., 2007, **46**, 5817.
42. B. Akhuli, I. Ravikumar, and P. Ghosh, *Chemical Science*, 2012, **3**, 1522.
43. R. Custelcean, B. A. Moyer and B. P. Hay, *Chem. Commun*., 2005, 5971.
44. (a) R. Custelcean, P. Remy, P. V. Bonnesen, D.-e. Jiang and B. A. Moyer, *Angew. Chem., Int. Ed*., 2008, **47**, 1866; (b) B. Wu, J. Liang, J. Yang, C. Jia, X. -J. Yang, H. Zhang, N. Tang and C. Janiak, *Chem. Commun*., 2008, 1762.
45. R. Custelcean, A. Bock and B. A. Moyer, *J. Am. Chem. Soc*., 2010, **132**, 7177.
46. R. Custelcean and P. Remy, *Cryst. Growth Des*., 2009, **9**, 1985.
47. W. J. Belcher, M. Fabre, T. Farhan and J. W. Steed, *Org. Biomol. Chem*., 2006, **4**, 781.
48. V. Amendola, M. Boiocchi, L. Fabbrizzi and A. Palchetti, *Chem.–Eur. J*., 2005, **11**, 5648.
49. D. R. Turner, M. J. Paterson and J. W. Steed, *Chem. Commun*., 2008, 1395.

Chapter 2

Experimental methods and Characterization

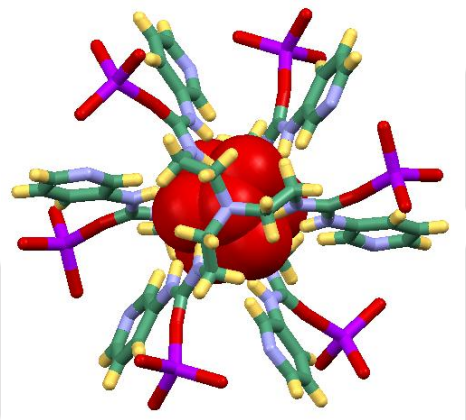

In this chapter, a detailed report of the various reagents used in the synthesis of tripodal receptors, **L_1-L_5** (Scheme 2.1), their synthetic procedures, crystallization details and specifications of instruments/equipments employed in the characterization of synthesized receptors and their various complexes with anions are presented.

2.1 Materials

All reagents and solvents were obtained from commercial sources and used as received without further purification. Tris(2-aminoethyl)amine (tren), 3,5-dinitrobenzoyl chloride, 3-nitrophenylisocyanate and 4-nitrophenylisothiocyanate were purchased from Sigma-Aldrich (U.S.A) whereas, 4-nitrophenol, 4-cresol, triethanolamine and thionyl chloride were purchased from Merck chemicals (India). All quaternary ammonium salts were purchased from Sigma-Aldrich (U.S.A) whereas, inorganic and organic acids such as, HCl, HBr, HNO_3, $HClO_4$, H_2SO_4, H_3PO_4, CF_3COOH, picric acid and pyromellitic acid were obtained either from Merck or LOBA chemicals (India). Deuterated solvents such as, $CDCl_3$ and CD_3CN were purchased from Sigma-Aldrich (U.S.A) whereas DMSO-d_6 was purchased from Merck chemicals (India) and used as received. Solvents for synthesis and crystallization experiments were purchased either from Merck or LOBA chemicals (India) and dried using standard procedures, wherever mentioned in the synthetic procedures.

2.2 Experimental methods

^{1}H NMR and 2D NOESY NMR spectra were recorded on a Varian FT-400 MHz instrument and chemical shifts were recorded in parts per million (ppm) on the scale using tetramethylsilane (TMS) or residual solvent peak as a reference and ^{13}C spectra were obtained at 100 MHz at 298 K. FT-IR spectra were recorded on a Perkin-Elmer-Spectrum One FT-IR spectrometer with KBr disks in the range 4000-450 cm^{-1}. Powder X-ray diffraction patterns of dried crystalline powder were recorded using a Bruker-D8 Advance X-ray diffractometer with Cu-$K\alpha$ radiation at λ = 0.15418 nm. Thermal analysis (TGA and DSC) of dried samples was performed using an SDTA 851-E TGA thermal analyser (*Mettler Toledo*) with a heating rate of 5-10^{o}C/min in a N_2 atmosphere. The absorption spectra were recorded on a Perkin-Elmer Lambda-25/35 UV-Visible spectrophotometer with a quartz cuvette.

Association constants (log *K*) of anions with **L_3, L_4** and **L_5** were obtained by ^{1}H NMR titrations of the receptor with tetraethyl ammonium (TEA) or tetrabutyl ammonium (TBA) salts of anions in DMSO-d_6 at 298 K. The initial concentration of the receptor solution was 5 mM/10 mM. Aliquots of anions were added from the stock solutions up to 1:10 host-guest

stoichiometry. The residual solvent peak in DMSO-d_6 (2.50 ppm) was used as an internal reference, and each titration was performed with at least 15 measurements.

Following equation was used to determine the association constant (K) values.

$$\Delta\delta = \{([A]_0 + [\mathbf{L}]_0 + 1/K) +/- (([A]_0 + [\mathbf{L}]_0 + 1/K)^2 - 4[\mathbf{L}]_0[A]_0)^{1/2}\}\Delta\delta_{max}/2[\mathbf{L}]_0$$

Where, **L** = receptor and A = anion. An error limit in log *K* was less that 15%.

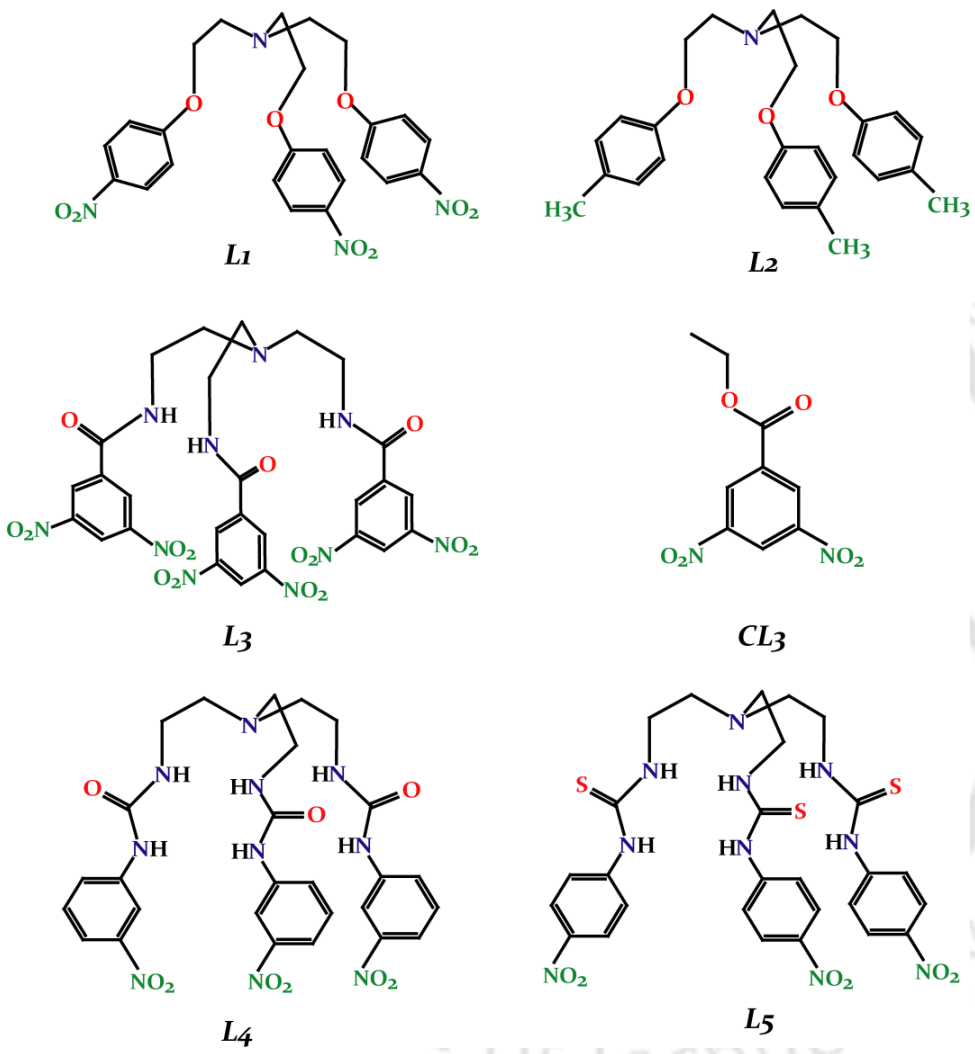

Scheme 2.1 Molecular structures of tripodal receptors, $\mathbf{L_1}$-$\mathbf{L_5}$ and control receptor $\mathbf{CL_3}$.

2.3 Single crystal X-ray crystallography

In each case, a crystal of suitable size was selected from the mother liquor and immersed in silicone oil, and it was mounted on the tip of a glass fiber and cemented using epoxy resin. The intensity data were collected using a Bruker SMART APEX-II CCD diffractometer, equipped with a fine focus 1.75 kW sealed tube Mo-K_α radiation (λ = 0.71073 Å) at 298(3) K, with increasing ω (width of 0.3° per frame) at a scan speed of 5 s/ frame. The SMART software was used for data acquisition. Data integration and reduction were undertaken with

SAINT and XPREP software.[1] Multi-scan empirical absorption corrections were applied to the data using the program SADABS.[2] Structures were solved by direct methods using SHELXS-97[3] and refined with full-matrix least-squares on F^2 using SHELXL-97.[4] All non-hydrogen atoms were refined anisotropically and hydrogen atoms attached to all carbon atoms were geometrically fixed and the positional and temperature factors are refined isotropically. However, in some cases the tetraalkylammonium cation(s) and/or solvent molecules were treated isotropically due to heavy disorder. Hydrogen atoms attached with the amide, urea and thiourea nitrogen atoms were located from electron Fourier map and refined isotropically. Usually, temperature factors of hydrogen atoms attached to carbon atoms are refined by restraints -1.2 or -1.5 U_{iso} (C), although the isotropic free refinement is also acceptable. Structural illustrations have been drawn with MERCURY-2.3.[5] for Windows. Parameters for data collection and crystallographic refinement details of receptor **L_1-L_5** and their various anion complexes are summarized in the respective chapters.

2.4 Synthesis and characterization of receptors, L_1- L_5

2.4.1 Tris[2-(*p*-nitrophenoxy)ethyl]amine, L_1

To a solution of *p*-nitrophenol (5 g, 36 mmol) in *n*-propanol (30 mL) crushed NaOH (1.77 g, 43 mmol) was added at once, and the solution was stirred at room temperature for about an hour. To the resulting suspension, tris(2-chloroethyl)amine hydrochloride[6] (2.88 g, 12 mmol) was added and the mixture was refluxed for 8 hours followed by removal of the solvents under reduced pressure and addition of 20 mL of cold water. The expected product was extracted with 3 x 30 mL of $CHCl_3$. The organic layer was washed several times with water and dried over anhydrous Na_2SO_4 and solvents were removed under reduced pressure. The crude product was purified by column chromatography with 75% ethyl acetate (in petroleum ether) as the eluent or by recrystallization in ethanol. The desired compound was a pale yellow crystalline solid. Yield: 65%; m.p. 110°C.

^{1}H-NMR (400 MHz, $CDCl_3$): δ = 3.09 (t, 6H, -NCH_2), 4.20 (t, 6H, -OCH_2), 7.08 (d, 6H, ArH), 8.13 (d, 6H, ArH); ^{13}C-NMR (100 MHz, DMSO-d_6) δ 52.97 (×3C, -NCH_2), 63.37 (×3C, -OCH_2), 115.35 (×3C, ArC), 125.88 (×6C, ArC), 141.36 (×3C, ArC), 162.67 (×6C, ArC); FT-IR (υ cm^{-1}): 1348 (*sym.*, NO_2), 1545 (*asym.*, NO_2), 1598 (C=C).

2.4.2 Tris[2-(*p*-methylphenoxy)ethyl]amine, L_2

To a solution of *p*-cresol (5 g, 46 mmol) in ethanol (30 mL) crushed NaOH (2.27 g, 55 mmol) was added, and the solution was stirred at room temperature for about an hour. To the resulting suspension, tris(2-chloroethyl)amine hydrochloride[6] (3.71 g, 15 mmol) was added

at once, and the mixture was refluxed for 8 hours followed by removal of the solvents under reduced pressure and addition of 20 mL of cold water. The expected product was extracted from this mixture, with 3 x 20 mL of $CHCl_3$. The organic layer was washed several times with water and dried over anhydrous Na_2SO_4 and solvents were removed under reduced pressure. The crude product was purified by column chromatography using ethyl acetate and hexane (1:9) or by recrystallization in methanol. The desired compound was a white crystalline solid. Yield: 78%; m.p. 65°C.

^{1}H-NMR (400 MHz, $CDCl_3$) δ 2.29 (s, 9H, -CH_3), 3.13 (t, 6H, -NCH_2), 4.07 (t, 6H, -OCH_2), 6.80 (d, 6H, ArH), 7.07 (d, 6H, ArH); ^{13}C-NMR (100 MHz, $CDCl_3$): δ 20.64 (×3C, -CH_3), 54.59 (×3C, -NCH_2), 66.98 (×3C, -OCH_2), 114.58 (×3C, ArC), 130.04 (×6C, ArC), 156.81 (×6C, ArC); FT-IR (υ cm^{-1}): 1236 (C-O), 1609 (C=C), 2923 (C-H).

2.4.3 Tris[2-(3,5-dinitrobenzamide)ethyl]amine, L_3

Reaction of tris(2-aminoethyl)amine, (tren) with 3,5-dinitrobenzoyl chloride in a 1:3 molar ratio at room temperature yielded the tris(amide) receptor, **L_3** in quantitative yield. 0.292 g of tris(2-aminoethyl)amine (2 mmol) was dissolved in 30 mL of dry chloroform ($CHCl_3$) in a 100 mL round bottomed flask and 0.708 g (7.0 mmol) of dry triethylamine (Et_3N) was added to the reaction mixture. Then, 1.380 g of 3,5-dinitrobenzoyl chloride (6 mmol) was added in portions to the reaction mixture over a period of 1 hour with constant stirring at room temperature. After the addition was complete, a pale brown precipitate formed and the reaction mixture was allowed to stir overnight at room temperature. The precipitate thus obtained was filtered and washed several times with (3 x 30 mL) water, a couple of times with (2 x 10) mL of methanol and finally with diethyl ether to get the desired product. The brown product thus collected was dried in air and characterized by NMR, FT-IR, ESI-MS and single crystal X-ray diffraction analyses. Yield: 75%; m.p. 252°C.

^{1}H NMR (DMSO-d_6, 400 MHz) δ (ppm) 2.84 (s, 6H, NCH_2), 3.48 (d, 6H, CONH-CH_2), 8.88 (d, 3H, *p*-ArH), 8.91 (s, 6H, *o*-ArH), 9.15 (s, 3H, amide–NH); ^{13}C NMR (100 MHz, DMSO-d_6): δ 45.73 (×3C, -NCH_2), 53.08 (×3C, CONH-CH_2), 120.58 (×3C, ArC), 127.35 (×6C, ArC), 137.06 (×3C, ArC), 148.01 (×6C, ArC), 162.20 (×3C, C=O); ESI-mass: 729.15 [M+1]; FT-IR (υ cm^{-1}): 1346 (NO_2 *sym.*), 1540 (NO_2 *asym.*), 1670 (C=O), 3428 (N-H).

2.4.4 Ethyl-3,5-dinitrobenzoate, CL_3

Ethyl ester of carboxy-dinitrobenzene was prepared by esterification of 3,5-dinitrobenzoic acid in ethanol with catalytic amount of concentrated H_2SO_4, at 80°C for 12 hours under reflux. After overnight reflux, ethanol was removed under reduced pressure and the desired

product was extracted from the mixture with 3 x 20 mL of $CHCl_3$. The organic layer was washed several times with water and dried over anhydrous Na_2SO_4. Removal of solvents under reduced pressure yielded white crystalline solid of **CL_3** and characterized by NMR and FT-IR analyses. Yield: 54%.

^{1}H-NMR (400 MHz, $CDCl_3$) δ 1.37 (t, 3H, -CH_3), 4.41 (q, 2H, -CH_2), 9.04 (s, 2H, *o*-ArH), 9.09 (s, 1H, *p*-ArH); ^{13}C NMR (100 MHz, $CDCl_3$): δ 14.18 (×1C, -CH_3), 62.97 (×1C, -CH_2), 122.26 (×1C, ArC), 129.38 (×1C, ArC), 134.07 (×1C, ArC), 148.58 (×1C, ArC), 162.46 (×1C, C=O); FT-IR (υ cm^{-1}): 1338 (NO_2 *sym.*), 1544 (NO_2 *asym.*), 1654 (C=O).

2.4.5 Tris(2-aminoethyl)-3-nitrophenylurea, L_4

Reaction of tris(2-aminoethyl)amine, (tren) with 3-nitrophenyl isocyanate in a 1:3 molar ratio at room temperature yielded the tris(urea) receptor, **L_4** in quantitative yield. 2.460 g (15 mmol) of 3-nitrophenyl isocyanate was dissolved in 30 mL of dry tetrahydrofuran (THF) in a 100 mL round bottomed flask and 0.730 ml (5 mmol) of tris(2-aminoethyl)amine (tren) dissolved in 10 ml of dry THF was added drop-wise (using a dropping funnel) over a period of 1 hour with constant stirring at room temperature. The resulting solution mixture was stirred overnight at room temperature when a pale yellow precipitate was formed. Then, the volume of the solvent (THF) was reduced to around 10 ml under *vacuum* and the obtained solid product was filtered off and washed with 10 ml of dichloromethane (DCM) a couple of times to remove the unreacted reagents. The pale yellow precipitate thus collected was dried in air and characterized by NMR, FT-IR, ESI-MS and single crystal X-ray diffraction analyses. Yield: 84%.

^{1}H NMR (DMSO-d_6, 400 MHz) δ (ppm) 2.64 (d, 6H, -NCH_2), 3.23 (d, 6H, -NCH_2CH_2), 6.31 (s, 3H, CH_2–NH), 7.41 (t, 3H, ArH), 7.59 (d, 3H, ArH), 7.66 (d, 3H, ArH), 8.44 (s, 3H, ArH), 9.07 (s, 3H, Ar–NH); ^{13}C NMR (100 MHz, DMSO-d_6): δ (ppm) 37.72 (×3C, -NCH_2), 53.78 (×3C, -NCH_2CH_2), 111.58 (×3C, ArC), 115.40 (×3C, ArC), 123.62 (×3C, ArC), 129.77 (×3C, ArC), 141.83 (×3C, ArC), 148.08 (×3C, ArC), 155.08 (×3C, C=O); ESI-mass: 639.249 [M+1]; FT-IR (υ cm^{-1}): 1245 (C-N), 1350 (NO_2 *sym.*), 1527 (NO_2 *asym.*), 1597 (C=C), 1655 (-C=O), 3328 (N-H).

2.4.6 Tris(2-aminoethyl)-4-nitrophenylthiourea, L_5

Reaction of tris(2-aminoethyl)amine, (tren) with 4-nitrophenyl isothiocyanate in a 1:3 molar ratio at room temperature yielded the tris(thiourea) receptor, **L_5** in quantitative yield. 2.70 gm (15 mmol) of 3-nitrophenyl isocyanate was dissolved in 30 mL of tetrahydrofuran (THF) in a 100 mL round bottomed flask and 0.73 ml (5 mmol) of tris(2-aminoethyl)amine (tren)

dissolved in 10 ml of dry THF was added drop-wise (using a dropping funnel) over a period of 1 hour with constant stirring at room temperature. After overnight stirring, solvents were removed under *vacuum* and the obtained solid product was washed with plenty of methanol to remove the unreacted reagents. Finally, the pale yellow solid thus collected was dried in air and characterized by NMR, FT-IR, ESI-MS and single crystal X-ray diffraction analyses. Yield: 82%.

^{1}H-NMR (400 MHz, DMSO-d_6) δ 2.81 (t, 6H, -NCH_2), 3.66 (s, 6H, -NCH_2CH_2), 7.78 (d, 6H, ArH), 8.13 (d, 6H, ArH), ~ 8.20 (s, 3H, -CH_2NH), ~ 10.20 (s, 3H, Ar-NH); ^{13}C NMR (100 MHz, DMSO-d_6): δ 41.90 (×3C, -NCH_2), 51.62 (×3C, -NCH_2CH_2), 120.38 (×6C, ArC), 124.52 (×6C, ArC), 141.78 (×3C, ArC), 146.25 (×3C, ArC), 179.95 (×3C, C=S); ESI-mass: 687.1639 [M+1]; FT-IR (υ cm^{-1}): 1334 (NO_2 *sym.*), 1510 (C=S), 2927 (C-H).

2.5 Synthesis and characterization of anion complexes of L_1–L_5

2.5.1 Complexes of receptor L_1

Anion complexes of protonated $\mathbf{L_1}$ (**1a**-**1e**), were obtained upon addition of a methanolic solution of the corresponding acids (1.2 equiv. of 37% HCl, 49% HBr, HNO_3, CF_3COOH and 70% $HClO_4$ respectively) to the individual solutions of $\mathbf{L_1}$ in methanol. After a constant stirring for half an hour a solid (white or pale yellow) precipitate was formed in each case, which was then filtered, washed with ether and dried under vacuum. Single crystals suitable for X-ray diffraction analysis were obtained from slow evaporation of CH_3OH–CH_3CN (1:1) binary mixture solution of the complexes at RT within 1-2 weeks. All complexes have been characterized by ^{1}H-NMR, FT-IR and single-crystal X-ray diffraction techniques.

Chloride complex, $[(H\mathbf{L_1})^+ \bullet Cl^-]$ (**1a**). Yield: 78% based on $\mathbf{L_1}$; ^{1}H-NMR (400 MHz, DMSO-d_6) δ 3.79 (s, 6H, -NCH_2), 4.54 (s, 6H, -OCH_2), 7.16 (d, 6H, ArH), 8.23 (d, 6H, ArH); FT-IR (υ cm^{-1}): 1351 (*sym.*, NO_2), 1536 (*asym*. NO_2), 1610 (C=C).

Bromide complex, $[(H\mathbf{L_1})^+ \bullet Br^-]$ (**1b**). Yield: 75% based on $\mathbf{L_1}$; ^{1}H-NMR (400 MHz, DMSO-d_6) δ 3.84 (s, 6H, -NCH_2), 4.56 (s, 6H, -OCH_2), 7.17 (d, 6H, ArH), 8.23 (d, 6H, ArH); FT-IR (υ cm^{-1}): 1363 (*sym.*, NO_2), 1550 (*asym*. NO_2), 1603 (C=C).

Nitrate complex, $[(H\mathbf{L_1})^+ \bullet NO_3^-]$ (**1c**). Yield: 68% based on $\mathbf{L_1}$; ^{1}H-NMR (400 MHz, DMSO-d_6) δ 3.84 (s, 6H, -NCH_2), 4.56 (s, 6H, -OCH_2), 7.17 (d, 6H, ArH), 8.23 (d, 6H, ArH); FT-IR (υ cm^{-1}): 1347 (*sym.*, NO_2), 1544 (*asym*. NO_2), 1595 (C=C).

Trifluoroacetate complex, $[(H\mathbf{L_1})^+ \bullet CF_3CO_2^-]$ (**1d**). Yield: 62% based on $\mathbf{L_1}$; ^{1}H-NMR (400 MHz, DMSO-d_6) δ 3.09 (s, 6H, NCH_2), 4.20 (s, 6H, OCH_2), 7.07 (d, 6H, ArH), 8.13 (d, 6H, ArH); FT-IR (υ cm^{-1}): 1341 (*sym.*, NO_2), 1552 (*asym*. NO_2), 1607 (C=C).

Perchlorate complex, $[(H\mathbf{L_1})^+ \bullet ClO_4^-]$ (**1e**). 60% based on $\mathbf{L_1}$; ^{1}H-NMR (400 MHz, DMSO-d_6) δ 3.84 (s, 6H, NCH_2), 4.56 (s, 6H, OCH_2), 7.16 (d, 6H, ArH), 8.22 (d, 6H, ArH); FT-IR (υ cm^{-1}): 1075 (Cl=O), 1336 (*sym.*, NO_2), 1549 (*asym.*, NO_2), 1598 (C=C).

2.5.2 Complexes of receptor $\mathbf{L_2}$

Anion complexes of protonated $\mathbf{L_2}$ (**2a-2d**), were isolated as white or yellow solids upon addition of a methanolic solution of the corresponding acids (1.2 equiv. of 37% HCl, 49% HBr, picric acid and pyromellitic acid respectively) to the individual solutions of $\mathbf{L_2}$ in methanol. After a constant stirring for about an hour a solid precipitate was formed which was then filtered, washed with ether and dried under vacuum. Colourless/yellow crystals suitable for single crystal X-ray analysis were grown by slow evaporation of CH_3OH–CH_3CN (1:1) binary solution mixture of the solids at room temperature within 1-2 weeks. All complexes have been characterized by ^{1}H-NMR, FT-IR and single-crystal X-ray diffraction techniques.

Perchlorate complex, $[(H\mathbf{L_2})^+ \bullet ClO_4^-]$ (**2a**). Yield: 94% based on $\mathbf{L_2}$; ^{1}H-NMR (400 MHz, DMSO-d_6) δ 2.24 (s, 9H, -CH_3), 3.78 (s, 6H, -NCH_2), 4.37 (t, 6H, -OCH_2), 6.85 (d, 6H, ArH), 7.11 (d, 6H, ArH); FT-IR (υ cm^{-1}): 1086 (Cl=O), 1241 (C-O), 1608 (C=C).

Bromide complex, $[(H\mathbf{L_2})^+ \bullet Br^-]2H_2O$ (**2b**). Yield: 68% based on $\mathbf{L_2}$; ^{1}H-NMR (400 MHz, DMSO-d_6) δ 2.22 (s, 9H, -CH_3), 3.74 (t, 6H, -NCH_2), 4.39 (t, 6H, -OCH_2), 6.83 (d, 6H, ArH), 7.08 (d, 6H, ArH); FT-IR (υ cm^{-1}): 1272 (C-O), 1609 (C=C).

Picrate complex, $[(H\mathbf{L_2})^+ \bullet PA^-]$ (**2c**). Yield: 75% based on $\mathbf{L_2}$; ^{1}H-NMR (400 MHz, DMSO-d_6) δ 2.22 (s, 9H, -CH_3), 3.78 (s, 6H, -NCH_2), 4.36 (t, 6H, -OCH_2), 6.83 (d, 6H, ArH), 7.09 (d, 6H, ArH), 8.58 (s, 2H, PA-H); FT-IR (υ cm^{-1}): 1233 (C-O), 1318 (NO_2), 1616 (C=C).

Pyromellitate complex, $[(H\mathbf{L_2})^+ \bullet PMA^-]$ (**2d**). Yield: 72% based on $\mathbf{L_2}$; ^{1}H-NMR (400 MHz, DMSO-d_6) δ 2.20 (s, 9H, -CH_3), 3.49 (s, 6H, -NCH_2), 4.22 (t, 6H, -OCH_2), 6.80 (d, 6H, ArH), 7.06 (d, 6H, ArH), 8.28 (s, 2H, PMA-H); FT-IR (υ cm^{-1}): 1251 (C-O), 1725 (C=O).

2.5.3 Complexes of receptor $\mathbf{L_3}$

Fluoride-encapsulated complex, TBA[$\mathbf{L_3}$(F)] (**3a**). Tetrabutylammonium (TBA) salt of fluoride-encapsulated complex, **3a** (solvates **I-IV**), were obtained as single crystals suitable for X-ray diffraction analysis by slow evaporation of a solution mixture of $\mathbf{L_3}$ charged with an excess TBAF (10 equiv.) in aprotic solvents *viz.* MeCN, DMF, THF and DMSO to yield the respective solvates with the composition TBA[$\mathbf{L_3}$(F)]H_2O (**3a-I**), TBA[$\mathbf{L_3}$(F)]DMF (**3a-II**), TBA[$\mathbf{L_3}$(F)]3THF (**3a-III**) and TBA[$\mathbf{L_3}$(F)]2DMSO·$4H_2O$ (**3a-IV**) respectively. Crystallization yield: ~ 40-50% based on $\mathbf{L_3}$ in each case.

^{1}H NMR, **3a-IV** (DMSO-d_6, 400 MHz) δ (ppm) 0.91 (t, 12H, TBA-CH_3), 1.30 (q, 8H, TBA-CH_2), 1.57 (t, 8H, TBA-CH_2), 2.60 (s, 6H, -NCH_2), 3.16 (t, 8H, TBA-N^+CH_2), 3.19 (s, 6H, CONH-CH2), 8.79 (s, 3H, *p*-ArH), 9.64 (s, 6H, *o*-ArH), 12.69 (s, 3H, amide–NH); ^{13}C NMR (DMSO-d_6, 100 MHz) δ (ppm) 13.76 (×4C, TBA-CH_3), 19.51 (×4C, TBA-CH_2), 23.40 (×4C, TBA-CH_2), 38.55 (×3C, -NCH_2), 53.89 (×3C, CONH-CH_2), 57.91 (×4C, TBA-N^+CH_2), 120.63 (×3C, ArC), 127.97 (×6C, ArC), 137.65 (×3C, ArC), 148.23 (×6C, ArC), 162.57 (×3C, C=O); FT-IR (ν, cm^{-1}) 1343 (*sym*. NO_2), 1538 (*asym*. NO_2), 1645 (C=O), 2962(C-H), ~ 3421 (broad, N-H).

KF complex, [$\mathbf{L_3}$•$KF(H_2O)_2$] (**3b**). Complex **3b** was prepared by adding an equivalent amount of potassium fluoride solution (in water) into a suspension of $\mathbf{L_3}$ in acetonitrile. After the addition of KF salt, the suspension was stirred for about an hour at 60^{o}C under reflux condition. The resulting solution thus obtained was filtered into a test tube and allowed to slowly evaporate at room temperature for crystallization. Red crystals of **3b** suitable for single crystal X-ray analysis were obtained within 10-12 days. Crystallization yield: 28-30% based on $\mathbf{L_3}$.

^{1}H NMR (DMSO-d_6, 400 MHz) δ (ppm) 2.70 (s, 6H, NCH_2), 8.83 (s, 3H, *p*-ArH), 9.19 (s, 6H, *o*-ArH). Due to the poor solubility of isolated crystals of **3b** in deuterated solvents like CD_3CN and DMSO-d_6, the ^{13}C NMR spectrum could not be recorded. FT-IR (ν, cm^{-1}) 1342 (*sym*. NO_2), 1537 (*asym*. NO_2), 1646 (C=O), 2921 (C-H), 3254 and 3354 (N-H).

Anion complexes of protonated $\mathbf{L_3}$ (**3c-3f**), were isolated as white solids upon addition of a methanolic solution of the corresponding acids (1.2 equiv. of 37% HCl, 49% HBr, 70% $HClO_4$ and conc. H_2SO_4 respectively) to the individual solutions of $\mathbf{L_3}$ in DMSO. After the addition of acid, the respective solutions were stirred for about 30 min and filtered in a test tube for crystallization. Slow evaporation of the filtrates at room temperature yielded colorless crystals suitable for X-ray crystallography analysis in each case within 1-2 weeks. All complexes have been characterized by ^{1}H-NMR, FT-IR and single-crystal X-ray diffraction techniques.

Chloride complex, [$(H\mathbf{L_3})^+$•Cl^-] (**3c**). Yield 68% based on $\mathbf{L_3}$; ^{1}H NMR (DMSO-d_6, 400 MHz) δ (ppm) 3.61 (s, 6H, NCH_2), 3.82 (s, 6H, CONH-CH_2), 8.91 (d, 3H, *p*-ArH), 8.94 (d, 6H, *o*-ArH), 9.66 (s, 3H, amide–NH), 10.57 (s, 1H, apical-NH); FT-IR (υ cm^{-1}): 1348 (*sym.*, NO_2), 1538 (*asym.*, NO_2), 1670 (C=O).

Bromide complex, [$(H\mathbf{L_3})^+$•Br^-]H_2O (**3d**). Yield: 62% based on $\mathbf{L_3}$; ^{1}H NMR (DMSO-d_6, 400 MHz) δ (ppm) 3.64 (s, 6H, NCH_2), 3.82 (s, 6H, CONH-CH_2), 8.90 (s, 6H, *o*-ArH), 8.92

(s, 3H, *p*-ArH), 9.57 (s, 3H, amide–NH), 9.62 (s, 1H, apical-NH); FT-IR (υ cm^{-1}): 1348 (*sym*., NO_2), 1538 (*asym*., NO_2), 1675 (C=O).

Perchlorate complex, $[(H\mathbf{L_3})^+ \bullet ClO_4^-]H_2O \cdot DMSO$ (**3e**). Yield: 66% based on $\mathbf{L_3}$; ^{1}H NMR (DMSO-d_6, 400 MHz) δ (ppm) 3.64 (s, 6H, -NCH_2), 3.82 (s, 6H, CONH-CH_2), 8.84 (s, 6H, *o*-ArH), 8.91 (s, 3H, *p*-ArH), 9.51 (s, 3H, amide–NH), 9.36 (s, 1H, apical-NH); FT-IR (υ cm^{-1}): 1080 (ClO_4^-), 1348 (*sym*., NO_2), 1538 (*asym*., NO_2), 1675 (C=O).

Hydrogensulfate complex, $[(H\mathbf{L_3})^+ \bullet HSO_4^-]DMSO$ (**3f**). Yield: 56% based on $\mathbf{L_3}$; ^{1}H NMR (DMSO-d_6, 400 MHz) δ (ppm) 3.63 (s, 6H, -NCH_2), 3.82 (s, 6H, CONH-CH2), 8.88 (s, 6H, *o*-ArH), 8.90 (s, 3H, *p*-ArH), 9.58 (s, 3H, amide–NH), 9.82 (s, 1H, apical-NH); FT-IR (υ cm^{-1}): 1188 (HSO_4^-), 1505 (*asym*., NO_2), 1590 (C=C).

2.5.4 Complexes of receptor $\mathbf{L_4}$

Carbonate-encapsulated complex, $2TBA[2\mathbf{L_4}(CO_3)]$ (**4a**). Tetrabutylammonium (TBA) salt of carbonate-encapsulated complex, **4a** was initially obtained by charging an excess (10 equiv.) of TBAF into a 5 mL DMSO solution of $\mathbf{L_4}$ (195 mg, 0.3 mmol). After the addition of F^- ions, the solution was stirred for about 15 min. at room temperature and filtered in a test tube for crystallization. Slow evaporation of the filtrate at room temperature yielded colourless crystals suitable for single crystal X-ray crystallography analysis within 8-10 days. Isolated yield of **4a** is 74 % after 10 days of exposure at RT.

Complex **4a** can also be obtained in a comparatively much higher yield simply by adding an equimolar quantity of TBA(OH) to a 5 ml DMSO solution of $\mathbf{L_4}$ (195 mg, 0.3 mmol), which upon slow evaporation at RT yielded air stable crystals of **4a** within a day or two. Isolated yield of **4a**: 92 % based on $\mathbf{L_4}$ after 3 days of exposure at RT.

^{1}H NMR (DMSO-d_6, 400 MHz) δ (ppm) 0.86 (t, 24H, TBA-CH_3), 1.25 (d, 16H, TBA-CH_2), 1.51 (s, 16H, TBA-CH_2), 2.52 (s, 12H, -NCH_2), 3.11 (s, 16H, TBA-N^+CH_2), 3.19 (s, 12H, -NCH_2CH_2), 7.18 (s, 6H, ArH), 7.49 (d, 6H, ArH), 7.59 (d, 6H, ArH), 8.27 (s, 6H, ArH), 10.50 (s, 6H, Ar–NH); ^{13}C NMR (100 MHz, DMSO-d_6): δ (ppm) 13.43 (×8C, TBA-CH_3), 19.22 (×8C, TBA-CH_2), 23.08 (×8C, TBA-CH_2), 36.75 (×6C, -NCH_2), 53.41 (×6C, -NCH_2CH_2), 57.59 (×8C, TBA-N^+CH_2), 111.25 (×6C, ArC), 114.75 (×6C, ArC), 123.33 (×6C, ArC), 129.05 (×6C, ArC), 142.16 (×6C, ArC), 147.59 (×6C, ArC), 155.13 (×6C, -C=O), 171.98 (CO_3^{2-}); FT-IR (υ cm^{-1}): 885 (CO_3^{2-}), 1238 (C-N), 1343 (NO_2 *sym*.), 1523 (NO_2 *asym*.), 1606 (C=C), 1699 (-C=O), 3390 (N-H).

Sulfate-encapsulated complex, $2TBA[2\mathbf{L_4}(SO_4)]$ (**4b**). Tetrabutylammonium (TBA) salt of sulfate-encapsulated complex, **4b** was obtained by adding an excess (10 equiv.) of

TBA(HSO_4) into a 5 mL DMSO solution of **L_4** (195 mg, 0.3 mmol). After the addition of bisulfate ions, the solution was stirred for about 30 min. at 60^oC and filtered in a test tube for crystallization. Slow evaporation of the filtrate at room temperature yielded colourless crystals suitable for single crystal X-ray crystallography analysis within 15 days of exposure to unmodified atmosphere. Isolated yield of **4b**: 58 % based on **L_4** after 15 days of exposure at RT.

^{1}H NMR (DMSO-d_6, 400 MHz) δ (ppm) 0.88 (t, 24H, TBA-CH_3), 1.26 (q, 16H, TBA-CH_2), 1.52 (s, 16H, TBA-CH_2), 2.49 (s, 12H, -NCH_2), 3.12 (t, 16H, TBA-N^+CH_2), 3.21 (s, 12H, -NCH_2CH_2), 7.10 (t, 6H, ArH), 7.33 (s, 6H, CH_2–NH), 7.44 (d, 6H, ArH), 7.57 (d, 6H, ArH), 8.24 (s, 6H, ArH), 9.58 (s, 6H, Ar–NH); ^{13}C NMR (100 MHz, DMSO-d_6): δ (ppm) 13.50 (×8C, TBA-CH_3), 19.25 (×8C, TBA-CH_2), 23.10 (×8C, TBA-CH_2), 37.08 (×6C, -NCH_2), 54.34 (×6C, -NCH_2CH_2), 57.59 (×8C, TBA-N^+CH_2), 111.39 (×6C, ArC), 114.82 (×6C, ArC), 123.35 (×6C, ArC), 128.93 (×6C, ArC), 141.99 (×6C, ArC), 147.65 (×6C, ArC), 154.92 (×6C, -C=O). FT-IR (υ cm^{-1}): 1089 (SO_4^{2-}), 1232 (C-N), 1351 (NO_2 *sym.*), 1524 (NO_2 *asym.*), 1600 (C=C), 1695 (-C=O), 3340 (N-H).

2.5.5 Complexes of receptor L_5

Hydrogenphosphate complex, [2(H**L_5**)$^+$•HPO_4^{2-}]•3H_2O (**5a**). Hydrogenphosphate complex of protonated **L_5**, **5a** was obtained by adding 0.5 mL of 49% orthophosphoric acid (H_3PO_4) to a 15 mL acetonitrile suspension of **L_5** (200 mg, 0.3 mmol). After the addition of acid, the suspension was stirred for about an hour at room temperature when a clear solution was formed. The resulting solution was filtered in a test tube and allowed to slowly evaporate at room temperature, which yielded colorless crystals suitable for X-ray crystallography analysis within 8-10 days. Yield of **5a**: 62% based on **L_5**.

^{1}H-NMR (400 MHz, DMSO-d_6) δ 2.92 (s, 6H, -NCH_2), 3.71 (s, 6H, -NCH_2CH_2), 7.82 (d, 6H, ArH), 8.12 (d, 6H, ArH), 8.37 (s, 3H, -CH_2NH), 10.53 (s, 3H, Ar-NH); ^{31}P-NMR (400 MHz, DMSO-d_6) δ 0.555 ppm; FT-IR (KBr, υ cm^{-1}): 1010 (P–O$^-$), 1269 (P=O), 1333 (NO_2, *sym*), 1504 (C=S), 1565 (NO_2, *asym*), 3325 (N–H).

Phosphate-encapsulated complex, 3TBA[2**L_5**(PO_4)]•2MeCN (**5b-I**). Tetrabutylammonium (TBA) salt of phosphate-encapsulated complex, **5b-I** was initially obtained by charging an excess (10 equiv) of TBA(H_2PO_4) into a 10 mL MeCN suspension of **L_5** (200 mg, 0.3 mmol). After the addition of $H_2PO_4^-$ ions, the solution was stirred for about 30 min at room temperature and filtered in a test tube for crystallization. Slow evaporation of the filtrate at

room temperature yielded yellow crystals of **5b-I** within 8-10 days. Isolated yield of **5b-I**: 36% based on $\mathbf{L_5}$, after 12 days of exposure at RT.

Complex **5b-I** can be obtained in a considerably higher yield by adding an excess quantity (10 equiv.) of tetrabutylammonium fluoride/acetate into a 10 ml MeCN solution of **5a** (200 mg, 0.14 mmol). After the addition of F^- or $CH_3CO_2^-$ ions, the individual solutions were stirred for about 15 min and filtered in a test tube for crystallization. Slow evaporation of the filtrate at room temperature yielded pale yellow crystals of **5b-I** in bulk amount within a week. The crystals thus obtained was isolated by decantation/filtration and dried at room temperature before characterization. Isolated yield of **5b-I**: 74 % based on **5a**, after 10 days of exposure at RT. The isolated complex has been characterized by ^{1}H NMR, ^{31}P NMR, FT-IR spectroscopy and powder X-ray diffraction patterns (PXRD) to determine the homogeneity of the formed complex obtained by two different methods.

^{1}H-NMR (400 MHz, DMSO-d_6) δ 0.928-0.966 (t, -CH_3, TBA), 1.285-1.358 (q, -CH_2, TBA), 1.559-1.577 (t, -CH_2, TBA), 3.046-3.087 (t, -NCH_2, TBA), 1.933-1.959 (q, CH_3CN), 2.703 (s, 12H, -NCH_2), 3.507 (s, 12H, -NCH_2CH_2), 7.746-7.807 (q, ArH), 11.935 (s, 6H, CH_2-NH), 12.998 (s, 6H, Ar-NH); ^{13}C NMR (100 MHz, DMSO-d_6): δ (ppm) 13.85 (×12C, TBA-CH_3), 20.37 (×12C, TBA-CH_2), 24.35 (×12C, TBA-CH_2), 44.30 (×6C, -NCH_2), 56.65 (×6C, -NCH_2CH_2), 59.37 (×12C, TBA-N^+CH_2), 121.17 (×12C, ArC), 124.33 (×12C, ArC), 141.82 (×6C, ArC), 149.85 (×6C, ArC), 181.73 (×6C, C=S); ^{31}P-NMR (400 MHz, DMSO-d_6) δ 10.171 ppm; FT-IR (KBr, υ cm^{-1}): 1015 (P–O^-), 1273 (P=O), 1329 (NO_2, *sym.*), 1504 (C=S), 1562 (NO_2, *asym.*), 2961 (C–H, TBA^+), 3474 (N–H).

Phosphate-encapsulated complex, 3TEA[2$\mathbf{L_5}$(PO_4)] (**5b-II**). Tetraethylammonium (TEA) salt of phosphate-encapsulated complex, **5b-II** was obtained as single crystals suitable for X-ray diffraction (XRD) analysis by charging an excess (10 equiv.) of TEA acetate and bicarbonate into separate solutions of **5a** (200 mg, 0.14 mmol) dissolved in 10 mL of MeCN. After the addition of acetate/bicarbonate ions, the individual solutions were stirred for about 15 min and filtered in a test tube for crystallization. Slow evaporation of the filtrate at room temperature yielded pale yellow crystals of **5b-II** in bulk amount within a week. The crystals thus obtained was isolated by decantation/filtration and dried at room temperature by pressing between filter papers before characterization. Isolated yield of **5b-II**: 78 % based on **5a**, after 10 days of exposure at RT. The isolated complex has been characterized by ^{1}H NMR, ^{31}P NMR, FT-IR spectroscopy and powder X-ray diffraction patterns (PXRD) to determine the homogeneity of the formed complex obtained from the individual solutions of **5a** in presence of excess acetate and bicarbonate ions.

^{1}H-NMR (400 MHz, DMSO-d_6) δ 1.077-1.105 (t, -CH_3, TEA), 2.460 (s, 6H, -NCH_2), 2.605 (s, 6H, -NCH_2CH_2), 3.100-3.154 (q, N^+-CH_2, TEA), 7.642-7.697 (t, 12H, ArH), 11.750 (s, 3H, CH_2-NH), 12.845 (s, 3H, Ar-NH); ^{13}C NMR (100 MHz, DMSO-d_6): δ (ppm) 7.98 (×12C, TEA-CH_3), 44.57 (×6C, -NCH_2), 53.38 (×6C, -NCH_2CH_2), 56.87 (×12C, TEA-N^+CH_2), 121.45 (×12C, ArC), 124.62 (×12C, ArC), 142.13 (×6C, ArC), 150.06 (×6C, ArC), 182.01 (×6C, C=S); ^{31}P-NMR (400 MHz, DMSO-d_6) δ 10.157 ppm; FT-IR (KBr, υ cm^{-1}): 1015 (P–O^-), 1274 (P=O), 1325 (NO_2, *sym.*), 1498 (C=S), 1567 (NO_2, *asym.*), 2804 (C–H, TBA^+), 3430 (N–H).

Carbonate-encapsulated complex, 2TEA[2$\mathbf{L_5}$(CO_3)] (**5c**). Tetraethylammonium (TEA) salt of carbonate-encapsulated complex, **5c** was obtained by adding an excess (10 equiv.) of TEA(HCO_3) into a 5 mL DMSO solution of $\mathbf{L_5}$ (200 mg, 0.3 mmol). After the addition of HCO_3^- ions, the solution was stirred for about 15 min and allowed to slowly evaporate for crystallization, which after 18-20 days of exposure to unmodified atmosphere yielded pale yellow crystals suitable for single-crystal XRD analysis. Yield of **5c**: 42 % based on $\mathbf{L_5}$.
^{1}H-NMR (400 MHz, DMSO-d_6) δ 1.078-1.109 (t, -CH_3, TEA), 2.461 (s, 6H, -NCH_2), 2.629 (s, 6H, -NCH_2CH_2), 3.105-3.159 (q, N^+-CH_2, TEA), 7.762-7.778 (d, 6H, ArH), 7.880-7.902 (d, 6H, ArH); ^{13}C NMR (100 MHz, DMSO-d_6): δ (ppm) 7.10 (×8C, TEA-CH_3), 41.69 (×6C, -NCH_2), 51.97 (×6C, -NCH_2CH_2), 51.51 (×8C, TEA-N^+CH_2), 120.41 (×12C, ArC), 123.93 (×12C, ArC), 141.25 (×6C, ArC), 147.18 (×6C, ArC), 179.89 (×6C, C=S); FT-IR (KBr, υ cm^{-1}): 1330 (NO_2, *sym.*), 1505 (C=S), 1564 (NO_2, *asym.*), 2927 (C–H, TBA^+), 3276 (N–H).

Sulfate-encapsulated complex, 2TBA[$\mathbf{L_5}$(SO_4)] (**5d**). Tetrabutylammonium (TBA) salt of sulfate-encapsulated complex, **5d** was obtained by adding an excess (10 equiv.) of TBA(HSO_4) into a 5 mL DMSO solution of $\mathbf{L_5}$ (200 mg, 0.3 mmol). After the addition of HSO_4^- ions, the solution was stirred for about 15 min and allowed to slowly evaporate for crystallization, which after 18-20 days of exposure to unmodified atmosphere yielded pale yellow crystals suitable for single-crystal XRD analysis. Yield of **5d**: 28% based on $\mathbf{L_5}$.
^{1}H-NMR (400 MHz, DMSO-d_6) δ 0.931-0.967 (t, -CH_3, TBA), 1.303-1.376 (q, -CH_2, TBA), 1.538-1.577 (t, -CH_2, TBA), 2.628 (s, -NCH_2), 3.042-3.084 (t, -NCH_2, TBA), 3.600 (s, 6H, -NCH_2CH_2), 7.969-7.992 (d, 6H, ArH), 8.129-8.152 (d, 6H, ArH), 9.907 (s, 3H, -CH_2NH), 11.677 (s, 3H, Ar-NH); FT-IR (KBr, υ cm^{-1}): 1109 (SO_4^{2-}), 1329 (NO_2, *sym.*), 1510 (C=S), 1560 (NO_2, *asym.*), 2960 (C–H, TBA^+), 3449 (N–H).

Fluoride-encapsulated complexes, TBA[$\mathbf{L_5}$(F)]•2DMSO (**5e-I**) and TBA[L(F)]•MeCN (**5e-II**). Dimethylsulfoxide (DMSO) and acetonitrile (MeCN) solvates of fluoride-encapsulated

complex, **5e-I** and **5e-II** were obtained by adding an excess (10 equiv.) of TBAF into the individual solutions of $\mathbf{L_5}$ in DMSO and MeCN respectively (200 mg, 0.3 mmol). After the addition of F^- ions, the solutions were stirred for about 15 min and allowed to slowly evaporate for crystallization, which after 10 days of exposure to unmodified atmosphere yielded pale yellow crystals suitable for single crystal XRD analysis. Yield: 40-45 % based on $\mathbf{L_5}$.

^{1}H-NMR of **5e-I** (400 MHz, DMSO-d_6) δ 0.915-0.951 (t, -CH_3, TBA), 1.282-1.335 (q, -CH_2, TBA), 1.563 (s, -CH_2, TBA), 3.131-3.171 (t, -NCH_2, TBA), 2.707 (s, 6H, -NCH_2), 3.613 (s, 6H, -NCH_2CH_2), 7.947-7.968 (d, 6H, ArH), 8.090-8.112 (d, 6H, ArH), 9.035 (s, 3H, -CH_2NH), 11.915 (s, 3H, Ar-NH); ^{13}C NMR (100 MHz, DMSO-d_6): δ 13.03 (×4C, TBA-CH_3), 19.57 (×4C, TBA-CH_2), 23.54 (×4C, TBA-CH_2), 40.91 (×3C, -NCH_2), 51.24 (×3C, -NCH_2CH_2), 58.59 (×4C, TBA-NCH_2), 120.05 (×6C, ArC), 124.42 (×6C, ArC), 139.44 (×3C, ArC), 151.24 (×3C, ArC), 180.99 (×3C, C=S). ^{19}F-NMR (400 MHz, DMSO-d_6) δ -123.737 ppm; FT-IR (KBr, υ cm^{-1}): 1329 (NO_2, *sym.*), 1506 (C=S), 1541 (NO_2, *asym.*), 1599 (C=O, DMSO), 2960 (C–H, TBA^+), 3276 (N–H).

Chloride complex, $[(H\mathbf{L_5})^+ \bullet Cl^-] \bullet DMF$ (**5f**). Chloride complex of protonated $\mathbf{L_5}$, **5f** was obtained by adding 0.5 mL of 37% hydrochloric acid (HCl) to a 5 mL dimethylformamide (DMF) solution of $\mathbf{L_5}$ (200 mg, 0.3 mmol). After the addition of HCl, the solution was stirred for about 30 min and was allowed to slowly evaporate at room temperature, which yielded colorless crystals suitable for XRD analysis within a week. Yield: 65 % based on $\mathbf{L_5}$.

^{1}H-NMR (400 MHz, DMSO-d_6) δ 3.461 (s, -NCH_2 and H_2O), 4.002 (s, 6H, -NCH_2CH_2), 7.88 (d, 6H, ArH), 8.17 (d, 6H, ArH), 8.65 (s, 3H, -CH_2NH), 10.84 (s, 3H, Ar-NH); FT-IR (KBr, υ cm^{-1}): 1335 (NO_2, *sym.*), 1504 (C=S), 1544 (NO_2, *asym.*), 3276 (N–H).

References

1. *SMART, SAINT and XPREP*; *Siemens Analytical X-ray Instruments Inc.*: Madison, WI, 1995.
2. G. M. Sheldrick, SADABS: *Software for Empirical Absorption Correction*; University of Gottingen, Institute fur Anorganische Chemieder Universitat: Tammanstrasse 4, D-3400, Gottingen, Germany, 1999-2003.
3. G.M. Sheldrick, *SHELXS-97*; University of Gottingen: Germany, 1997.
4. G. M. Sheldrick, *SHELXL-97*: *Program for Crystal Structure Refinement*; University of Gottingen, Gottingen, Germany, 1997.
5. Mercury 2.3, Supplied with Cambridge Structural Database; CCDC, Cambridge, U.K., 2007.
6. K. Ward, Jr. *J. Am. Chem. Soc.*, 1935, **57**, 914.

Chapter 3

Anion/Solvent Induced Conformational Adaptation in Tripodal Podands

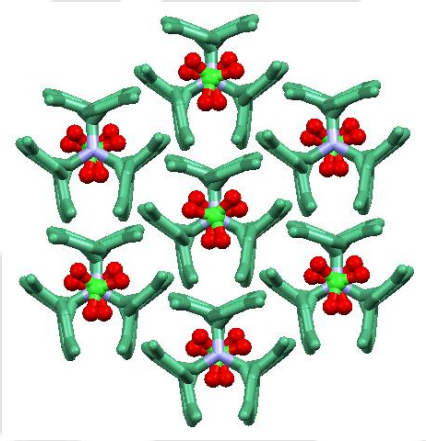

3.1 Background and Focus of the Chapter

The design and synthesis of new materials with desired physiochemical properties have been of recent interest, and this involves the generation and study of structural motifs in crystals, which are essentially guided by precise topological control through the manipulation of weak intermolecular interactions.[1] There are a rich variety of intermolecular interactions that serve as tools in engineering such molecular assemblies.[2] However, the control of crystal and network structures in a predictable manner still remains an elusive task because of the delicate balance and competition between directional noncovalent interactions, such as hydrogen bonds, and nondirectional noncovalent interactions, such as electrostatic and van der Waals (dispersive) forces. The effect of solvent of crystallization, an important parameter influencing nucleation, continues to be the subject of investigations.[3] Since the physicochemical properties of a compound can differ critically from one form to another, inducing and controlling a specific polymorph by the judicious choice of solvent(s) is of utmost importance, particularly in the context of synthesis of drugs and pharmaceuticals.[4] The energies of intramolecular torsions and intermolecular noncovalent interactions lie in the same range (0.5-10 kcal/mol) and therefore, there is an immediate possibility that conformationally flexible systems are prone to polymorphism which can further be affected by crystallization conditions.[5] However, regardless of their intrinsic conformational flexibility tripodal compounds have not received any attention in the context of polymorphism.

Furthermore, when anions are an integral part of supramolecular aggregates, it is expected that if the templating anion is changed/exchanged with other anions, it should in principle be possible to reorient or rupture the self-assembled architectures.[6] The use of anionic templates for the construction of superstructures has become an attractive strategy in recent years.[7] Template-directed processes that are anion specific can lead us to the challenging development of new selective systems with industrial, ecological, and biomedical applications.[8] The most effective way to bind anions consist in taking advantage of their negative charge. And accordingly, ammonium/polyammonium receptors are of primary choice, since they ensure an adequate electrostatic attraction reinforced by hydrogen-bond contacts with the coordinated anions.[9] Furthermore, hydrogen bonds formed by anions with –CH donors are weaker and more difficult to control as compared to –NH and –OH bonds. Although not typically considered to be significant donors, there is increasing evidence that -CH groups can actively take part in hydrogen bonding and lead to enhanced anion-binding affinity.[10]

The focus of this chapter will be anion and solvent induced conformational changes in two tripodal ether receptors, **L_1** and **L_2**. An understanding of the conformational adaptation associated with flexible **L_1** and **L_2** has been made in terms of X-ray diffraction analyses of single-crystals, obtained under different growth (crystallization) conditions. Furthermore, the structural aspects of conformational adaptation associated with protonated **L_1** and **L_2**, in presence of different counter anions has been investigated in detail along with the solution-state evidence of structural differences. Scheme 3.1 shows a comprehensive representation of the research work included in this chapter.

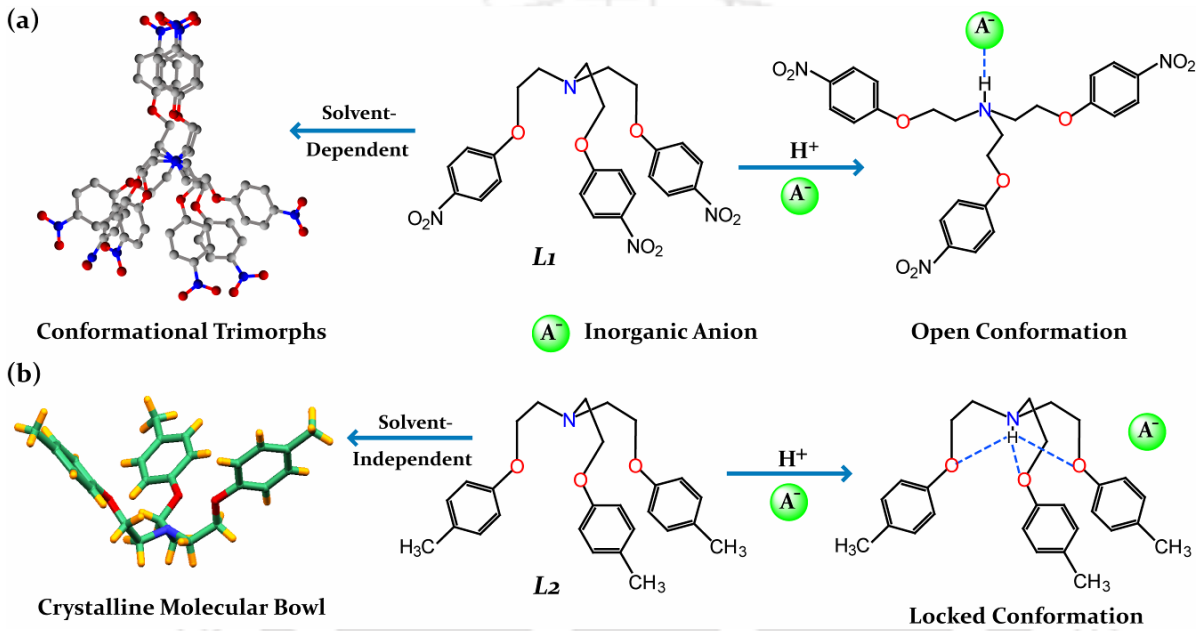

Scheme 3.1 (a) Solvent induced conformational polymorphism in **L_1** and anion binding of cationic **L_1** by strong electrostatic $(N–H)^{+}\cdots A^{-}$ interaction due to an extended conformation; (b) Solvent-independent formation of crystalline molecular bowl of **L_2** and conformational locking of the tripodal side arms in cationic **L_2** by strong electrostatic $(N–H)^{+}\cdots O$ interactions, in presence of inorganic anions.

3.2 Conformational polymorphism in receptor L_1

Solvent-induced conformational polymorphism of podand **L_1** arises from (i) the intrinsic conformational flexibility of the molecule, (ii) the correlation between the hydrogen bond donor ability of the alkyl/aryl groups and the hydrogen bond acceptor ability of the nitro oxygen atoms, and (iii) the nature of crystallization solvents. An understanding of the structural features associated with polymorphism in **L_1** has been made in terms of morphology, single-crystal X-ray structure, powder X-ray diffraction (PXRD), and differential scanning calorimetric (DSC) measurements. The crystallographic data and refinement details of polymorphs **I**, **II**, and **III** are given in Table 3.1. Crystal structure analyses revealed that, the conformational differences in three polymorphic forms result

principally from the bridge-head amino torsion τ_{amino} (C-N_{amino}-C-C) and τ_{ether} (N_{amino}-C-C-O_{ether}) relative to the *p*-nitrophenol fragment (Figure 3.1). There is no intramolecular hydrogen bonding between the tripodal side arms of polymorphs **I** and **III** whereas polymorph **II** displays an intramolecular edge-to-face (C-H···π) interaction between the phenyl rings of two proximal arms. The supramolecular self-assembly in three polymorphs are primarily guided by the control of methylene C-H···N dimeric interaction in form **I**, C-H···π and π···π interactions in form **II**, and C-H···π interactions in form **III** that differentiate the overall packing in the three forms. The three polymorphs display different hydrogen bonding network structures, constructed from an array of several intermolecular C-H···O-(nitro) interactions.

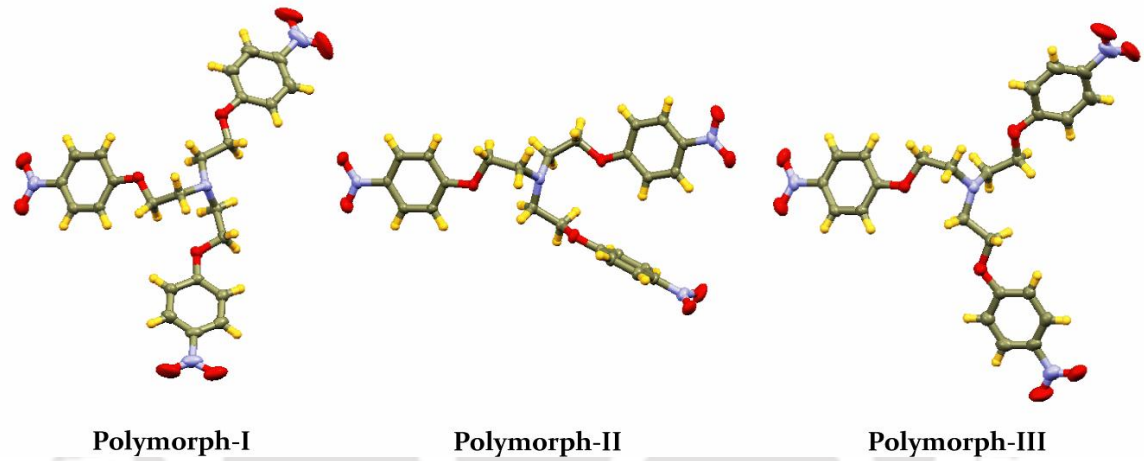

Figure 3.1 X-ray structures of polymorphs **I**, **II** and **III** (thermal ellipsoid plot with 30% probability) of receptor $\mathbf{L_1}$ obtained under different growth conditions.

3.2.1 Crystal structure of polymorph-I

This form crystallizes in the triclinic space group *P*–1 with Z=2. The torsions involving N_{amino}-C-C-O_{ether} (τ_{ether}) are in the folded conformation for two arms composed of the ethereal oxygen O1 and O4 and is in the extended conformation for the third arm composed of the ethereal oxygen O7 (Table 3.2). Structural elucidation revealed that, the two tripodal molecules of a unit cell are oriented in a face-to-face fashion with a strong dimeric association between the apical nitrogen (N1) and methylene hydrogen C10H(B) of either unit (N1···C10 = 3.704 Å , ∠C10-H(B)···N1 = 175^o), resulting in a six-member hydrogen bonded ring formation *via* complementary C-H···N interactions (Figure 3.2a). Furthermore, the dimeric units are self-assembled *via* intermolecular C-H···O-(nitro) interactions formed between the alkyl protons and one or both the oxygen atoms from each nitro group, generating a 3D sheet-structure in form **I** when viewed along the crystallographic a-axis (Figure 3.2b). The nitro oxygen atoms (O3, O5, O6, O8, and O9) act as acceptors in

intermolecular C-H···O hydrogen bonding with a donor-to-acceptor (C···O) distances ranging from 3.135 to 3.557 Å and C-H···O angles from 119° to 167° (Annexure 3).

3.2.2 Crystal structure of polymorph-II

This form crystallizes in the monoclinic space group $P2_1/n$ with Z=4. The torsions involving N_{amino}-C-C-O_{ether} (τ_{ether}) are all in the folded conformation, and the torsion values differ significantly from the other two forms (Table 3.2). Unlike form **I**, there is an intramolecular edge-to-face (C-H···π) interaction between an aryl proton C20H and the phenyl ring C2g involving carbon atoms C11-C16 (C20···C2g = 4.018 Å, ∠C20-H···C2g = 152°). Short contact analyses revealed that, the tripodal units are self-assembled *via* π···π stacking and intermolecular C-H···π and C-H···O-(nitro) interactions between the alkyl protons and one or both the oxygen from two nitro groups involving nitrogen N3 and N4 (Annexure 3). In addition, there are intermolecular nitro–nitro electrostatic interactions involving all three nitro groups (N2···O5 = 3.018 Å and N4···O2 = 2.873 Å). The phenyl ring C1g (centroid: C3-C8) of a tripodal unit is in π–stacking interaction with the phenyl ring C3g (centroid: C19-C24) of an adjacent unit (C1g···C3g = 3.734 Å), which are further cross-linked *via* several C-H···π and C-H···O-(nitro) interactions resulting in a three-dimensional hydrogen bonded network in form **II** (Figure 3.2c and 3.2d).

3.2.3 Crystal structure of polymorph-III

This form crystallizes in the orthorhombic space group *P*na2(1) with Z=4. The torsions involving N_{amino}-C-C-O_{ether} (τ_{ether}) are distinctly different from form **II** but similar to **I** with respect to the third-arm composed of the ethereal oxygen O7. However, the difference could be observed in the torsions (τ_{ether}) of other two arms composed of the ethereal oxygen O1 and O4 which are in the folded conformation and showing a change of 5.89° and 13.22°, respectively *w.r.t.* form **I** (Table 3.2). Unlike forms **I** and **II**, the tripodal units in **III** are self-assembled by weak C-H···π and C-H···O-(nitro) interactions formed between the alkyl hydrogen atoms and an oxygen atom from each nitro group. It is interesting to note that, a methylene proton C18H(B) from a tripodal unit is involved in intermolecular C-H···π interaction with the phenyl ring C3g (centroid: C19-C24) of an adjacent unit, each of which are further involved in a C-H···π interaction between the aromatic proton C8H and the phenyl ring C1g (centroid: C3-C8) of adjacent tripodal units, generating a brick-wall kind of structure along the crystallographic c-axis (C18···C3g = 4.058 Å, ∠C18-H(B)···C3g = 151° and C8···C1g = 4.056 Å, ∠C8-H···C1g = 151°) (Figure 3.2e). However, the overall packing of the crystal (Figure 3.2f) is additionally governed by several intermolecular C-H···O-(nitro) interactions with a donor-to-acceptor (C···O) distances ranging from 3.221 to 3.399 Å and C-H···O angles from 120° to 147° (Annexure 3).

Table 3.1 Crystallographic data and refinement details of crystal structures of **L_1** and **L_2**.

Crystallographic parameters	**L_1**			**L_2**
	Polymorph-**I**	Polymorph-**II**	Polymorph-**III**	
Formula	$C_{24}H_{24}N_4O_9$	$C_{24}H_{24}N_4O_9$	$C_{24}H_{24}N_4O_9$	$C_{27}H_{33}NO_3$
Fw	512.47	512.47	512.47	419.54
Crystal System	Triclinic	Monoclinic	Orthorhombic	Rhombohedral
Space group	*P*–1	$P2_1/n$	*Pna*2(1)	*R*3*c*
a(Å)	9.252(2)	10.5408(6)	23.1068(15)	20.4711(17)
b(Å)	11.950(3)	19.9111(12)	23.107	20.4711(17)
c(Å)	12.445(3)	11.8327(8)	4.6074(4)	9.5827(14)
α(°)	73.244(14)	90.00	90.00	90.00
β(°)	8.589(14)	105.594(3)	90.00	90.00
γ(°)	70.475(14)	90.00	90.00	120.00
V (Å^3)	1233.9(5)	2392.0(3)	2460.0(3)	3477.8(7)
Z	2	4	4	6
Dx (g cm^{-3})	1.379	1.429	1.386	1.202
μ (mm^{-1})	0.107	0.109	0.108	0.077
F(000)	536	1072	1072	1356
T(°K)	298(2)	298(2)	298(2)	298(2)
θ *max.*	28.32	28.38	28.40	28.46
Total reflections	20329	28611	33549	13751
Independent reflections	5904	5786	5963	1907
Observed reflections	2884	3323	4803	1278
Parameters refined (N_{par})	334	334	335	95
R_1, $I > 2\sigma(I)$	0.0459	0.0427	0.0522	0.0547
wR_2 (all data)	0.1318	0.1178	0.1348	0.1295
GOF (F^2)	1.016	0.954	0.921	1.043

3.2.4 Phase behaviours of polymorphs

Polymorphs **I** and **II** are quite stable at room temperature, but form **III** has been observed to undergo a solid to solid phase transition to form **I** at room temperature on storage over a period of about one month or so, which was confirmed by powder X-ray diffraction (PXRD) and differential scanning calorimetric (DSC) analyses of the samples. This simple observation argues strongly for the metastable nature of form **III**. More quantitative evidence for the stability of polymorphs **I** and **II** and metastability of **III** were obtained from DSC analyses of the isolated crystals of the three polymorphs (Figure 3.3).

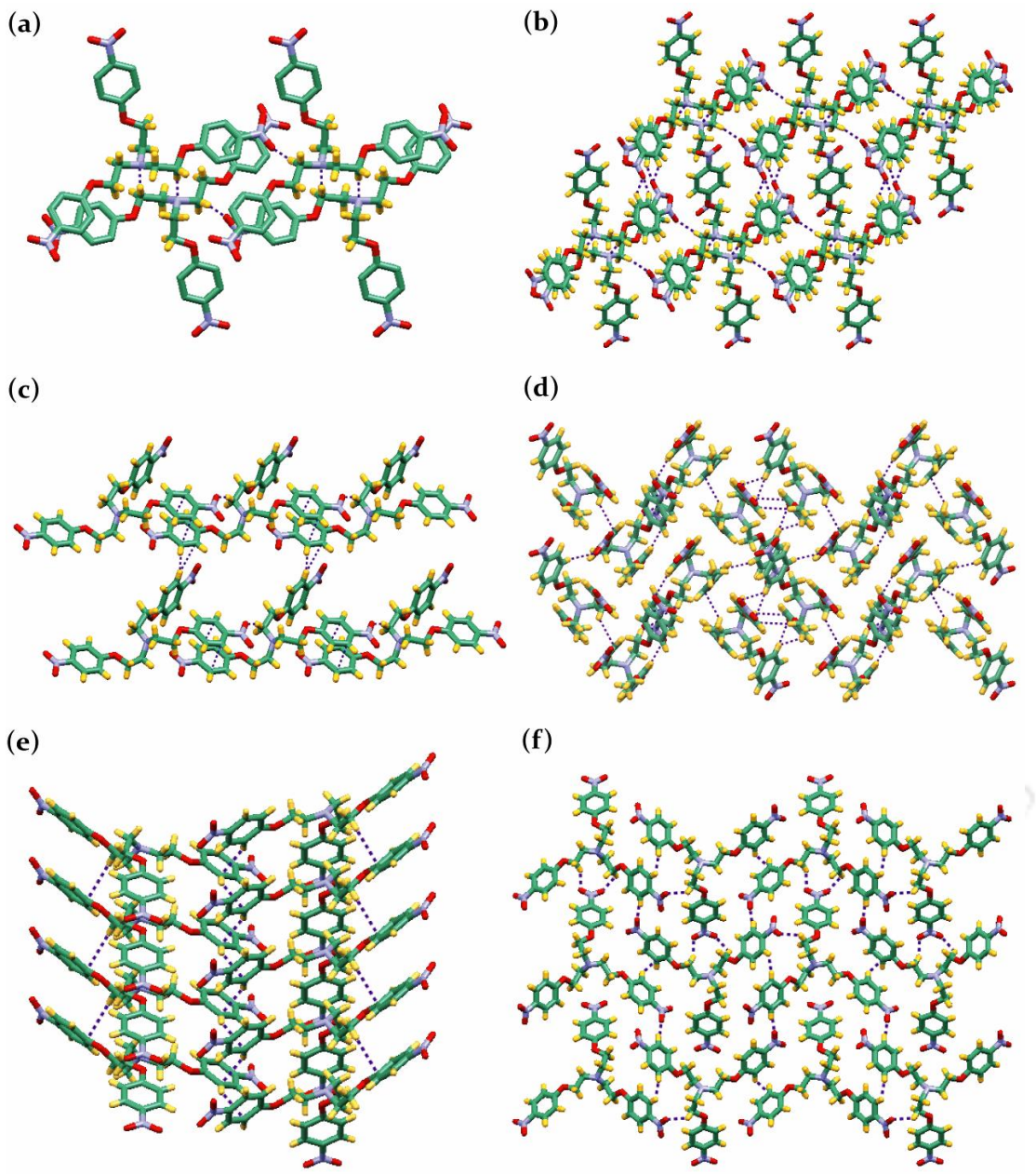

Figure 3.2 (a) Aliphatic C-H···N dimeric interaction between two molecules in polymorph-**I**; (b) Crystal packing diagram of polymorph **I**, as viewed down the a-axis; (c) Intermolecular C-H···π and π-stacking interactions in polymorph-**II**, along the c-axis; (d) Crystal packing diagram of polymorph **II**, as viewed down the b-axis; (e) Intermolecular C-H···π interactions in polymorph-**III**, along the c-axis; (d) Crystal packing diagram of polymorph **III**, as viewed down the b-axis.

Form **I** showed only one endothermic peak at 109°C corresponding to melting of the polymorph with an onset temperature of 104°C, and no phase transition was detected. Form **II** displayed a melting endotherm at 106.5°C with an onset temperature near 98°C; the DSC trace is otherwise featureless. Unlike **I** and **II**, form **III** showed two endothermic peaks, the first peak at 105°C with an onset temperature of 100°C appears to be a solid-to-solid phase transition to a more stable form **I** while the second endotherm at 109°C (onset temp. 106°C) coincides with the melting of form **I**. The melting endotherms of **I** and **II** differ by 2.5°C and

also showed differences in the breadth of melting ranges. Form **II** has a comparatively broader range of melting (~15^{o}C) than form **I** (~10^{o}C), also suggesting the fact that **II** has a slightly lower melting point than **I**. Thus, from the DSC analyses, it can be concluded that transformation of form **III** to a more stable form **I** is kinetically very facile, as transformation can also be observed at room temperature and the transition is most likely to be monotropic. Furthermore, enthalpies of formation of the polymorphs calculated from the DSC data were found to be -398, -474, and -120 kJ mol^{-1} for **I**, **II**, and **III**, respectively. As all of the DSC samples were cooled to ambient temperature after heating, no thermal event was observed during cooling, indicating super cooled liquids were likely formed.

Furthermore, the PXRD patterns of each polymorphic form collected at room temperature, confirm that they represent different crystalline phases (Figure 3.3). The differences in position and intensity of the diffraction peaks indicate different geometrical orientation of $\mathbf{L_1}$ in the three forms. These differences in bulk crystalline properties are in agreement with the difference in their crystal structures. Comparison with the simulated patterns of each form based on the single crystal structure determination suggests that, each crystallization batch was most likely of one single polymorph and not a mixture of multiple polymorphs. Although no significant differences were observed in the mid-IR region, notable changes could be observed in the far-IR and fingerprint regions of the different polymorphs that arise presumably from their structural differences and different hydrogen bonding arrangements (Annexure 3).

Table 3.2 Molecular conformation: Relevant torsion angles in polymorphs **I**, **II** and **III.**

Torsion	Atoms list	Polymorph-**I**	Polymorph-**II**	Polymorph-**III**
τ_{ether}	N1-C1-C2-O1	-75.86(2)	65.82(2)	-69.96(2)
	N1-C9-C10-O4	79.04(2)	75.36(1)	65.77(3)
	N1-C17-C18-O7	-168.72(1)	70.33(1)	-169.08(2)
τ_{amino}	C1-N1-C9-C10	-56.66(2)	-142.52(1)	64.88(3)
	C1-N1-C17-C18	159.22(1)	87.99(1)	79.45(2)
	C9-N1-C1-C2	-57.88(2)	-71.56(2)	97.81(2)
	C9-N1-C17-C18	-71.7(2)	-131.00(1)	-145.26(2)
	C17-N1-C1-C2	69.58(2)	68.78(2)	-126.58(2)
	C17-N1-C9-C10	175.70(1)	77.45(2)	-70.13(3)

3.2.5 Crystal growth and habit of polymorphs

The morphology of the crystal is another important manifestation besides the crystal structure (Annexure 3). Polarity of the solvents is one of the most important factors that may affect the habit of the growing crystal. Compound $\mathbf{L_1}$ is a polar molecule with a tertiary nitrogen atom and three active nitro groups, the presence of which facilitate the formation of several intermolecular noncovalent interactions among the tripodal units or possibly with solvent molecules, thus further affecting the habit of the crystals. Polymorph **I** was obtained individually from an acetonitrile (MeCN) or a dimethyl sulfoxide (DMSO) solution of $\mathbf{L_1}$, as thin yellow blocks upon slow evaporation at room temperature (RT). The homogeneity of the crystals formed was confirmed by examining the PXRD patterns of each crystallization batch and also comparison with the simulated pattern based on the single crystal structure data. Slow evaporation of a saturated solution of $\mathbf{L_1}$ in a 3:1 binary solvent mixture of ethanol and acetic acid yielded high quality rhomboid shaped crystals of polymorph **II**. Polymorph **III** was obtained upon slow evaporation of a saturated solution of $\mathbf{L_1}$ in a 3:1 binary solvent mixture of DMSO and acetic acid, which has reproducibly afforded thin light yellow needles of **III**. It is worth mentioning that crystallization from absolute ethanol yielded both blocky and rhomboid shape crystals of form **I** and **II**, respectively, with proportionally greater quantities of **II**. Exclusive crystallization of **I** from aprotic solvents (acetonitrile/DMSO), and concomitant crystallization of polymorphs **I** and **II** from ethanol guided us to carry out the crystallization experiment in a highly protic ethanol/acetic acid medium which yielded exclusively form **II**. In spite of our repeated efforts, we were unable to obtain single crystals of $\mathbf{L_1}$ suitable for X-ray analysis from low boiling solvents such as chloroform, ethyl acetate, tetrahydrofuran (THF) and methanol, and always ended up having powders which were found to contain a mixture of **I** and **II** when analyzed by PXRD. The crystallization experiments in different solvents showed that polymorphism in $\mathbf{L_1}$ are essentially guided by the nature of the solvent.

3.3 Crystal structure of receptor $\mathbf{L_2}$

Podand $\mathbf{L_2}$ crystallizes in a highly symmetric bowl-shape conformation with rhombohedral space group R_3c where a *C3v*-axis of symmetry can pass through the bridgehead nitrogen atom (Figure 3.4a). The torsion involving N_{amino}-C-C-O_{ether} (τ_{ether}) with an ideal value of 89.70° (~ 90°) implies that the tripodal arms are oriented neither in a folded nor in an open conformation with an average distance of 5.037 Å between the identical ethereal oxygen atoms. Crystal packing motif of $\mathbf{L_2}$ shows that the structure is stabilized by weak intermolecular C–H···π interactions forming hemicarcerand through self-assembly in the

solid state. Each tripodal unit is surrounded by six other molecules which occupy a chair conformation with a distance measuring 13.43 Å between the apical nitrogen atoms of two adjacent tripodal units. Each arm of a tripodal molecule is linked with its neighbouring unit by aromatic C–H···π interactions involving the hydrogen atom C5H and electron-π cloud of the phenyl rings (C5···Cg = 3.648 Å; ∠C5-H···Cg = 165°) generating a highly symmetrical 2D sheet like network (Figure 3.4b). It is important to mention that, irrespective of solvent of crystallization (protic or aprotic) and intrinsic conformational flexibility of the molecule, **L_2** crystallizes exclusively in this symmetric bowl conformation and does not exhibit solvent induced conformational polymorphism like **L_1**.

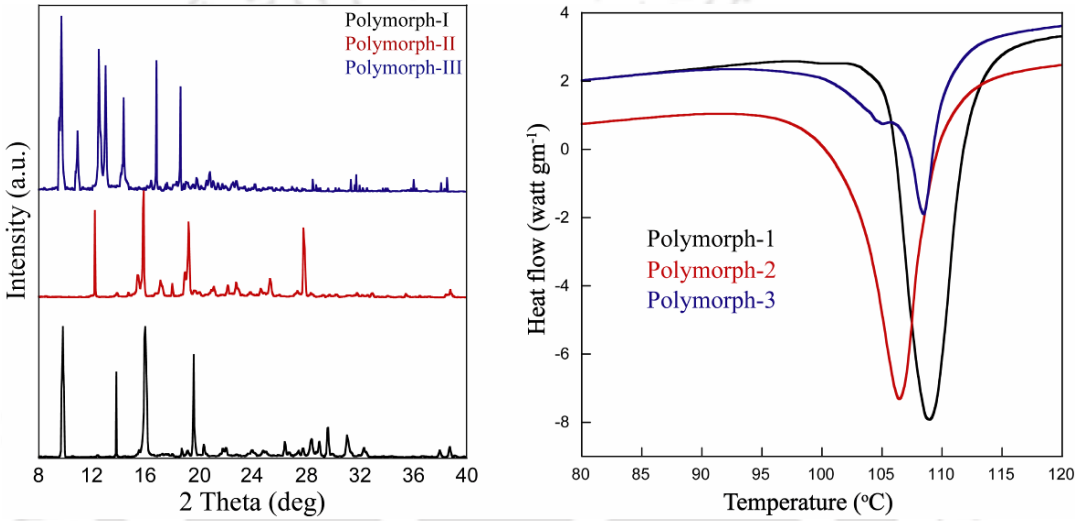

Figure 3.3: Experimental powder X-ray diffraction patterns (PXRD) and DSC thermographs of polymorphs **I**, **II**, and **III** of **L_1**.

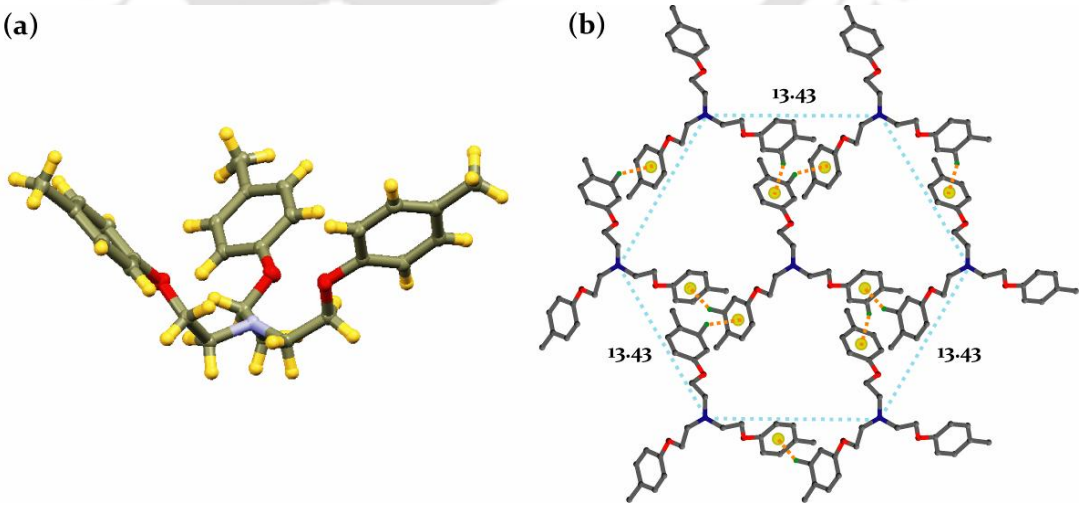

Figure 3.4 (a) X-ray structure of receptor **L_2** (thermal ellipsoid plot with 30% probability); (b) Highly symmetric crystal packing in **L_2** showing the hexagonal arrangement of tripodal units, occupying a cyclohexane conformation via intermolecular C–H···π interactions.

Table 3.3 Crystallographic data and refinement details of anion complexes of $\mathbf{L_1}$ (**1a-1e**).

Parameters	**1a**	**1b**	**1c**	**1d**	**1e**
Formula	$C_{24}H_{25}ClN_4O_9$	$C_{24}H_{25}BrN_4O_9$	$C_{24}H_{25}N_5O_{12}$	$C_{26}H_{25}F_3N_4O_{11}$	$C_{24}H_{25}ClN_4O_{13}$
Fw	548.93	593.38	575.49	626.50	612.93
Crystal System	Triclinic	Triclinic	Monoclinic	Triclinic	Monoclinic
Space group	*P*–1	*P*–1	$P2_1/n$	*P*–1	$P2_1/c$
a(Å)	7.475(6)	7.6818(6)	15.2304(7)	6.8340(9)	11.9923(5)
b(Å)	13.365(10)	13.3835(11)	8.9608(4)	12.5542(11)	12.5750(6)
c(Å)	13.784(10)	13.8995(12)	20.0560(10)	16.8656(18)	18.0740(8)
α(°)	98.90(3)	99.08(1)	90.00	99.533(5)	90.00
β(°)	102.77(3)	103.12(5)	101.073(3)	94.301(6)	103.045(2)
γ(°)	105.84(3)	106.33(3)	90.00	99.636(7)	90.00
V(Å^3)	1257.6(17)	1297.45(4)	2686.2(2)	1399.0(3)	2655.3(2)
Z	2	2	4	2	4
Dx (g cm^{-3})	1.450	1.532	1.421	1.485	1.531
μ (mm^{-1})	0.213	1.644	0.116	0.129	0.221
F (000)	572	608	1200	648	1272
T (°K)	298(2)	298(2)	298(2)	298(2)	298(2)
θ *max.*	22.56	28.34	28.27	28.37	28.39
Total reflns.	8173	10614	22545	10145	38561
Ind. reflns.	3172	6469	6659	7010	6585
Obs. reflns.	2570	6386	6185	6711	5805
N_{par}	348	356	375	402	384
R_1, $I > 2\sigma(I)$	0.0518	0.0344	0.0611	0.0688	0.0460
wR_2(all data)	0.1240	0.0928	0.1162	0.1081	0.0969
GOF (F^2)	0.810	1.026	1.018	0.931	0.999

3.4 Structural aspects of anion binding with protonated $\mathbf{L_1}$

The structural aspects of binding of different inorganic anions with the protonated receptor $\mathbf{L_1}$ have been examined crystallographically. Anion binding with protonated $\mathbf{L_1}$ is attributable entirely to the $(N–H)^+\cdots A^-$ and several C-H$\cdots A^-$ interactions involving multiple receptor cations where hydrogen of the protonated bridgehead nitrogen is *exo*-oriented and thereby, interacts with an anion *via* strong electrostatic effects. Protonation at the bridgehead nitrogen and presence of peripheral π–acidic functions render the aliphatic and aromatic protons of the receptor sufficiently acidic, for their active participation in weak C-H$\cdots A^-$ and intermolecular C-H$\cdots$O-(nitro) interactions. Although, charge neutralisation in the crystals and conventional hydrogen bonds are the main driving forces in the formation of all

supramolecular complexes, yet the weak C-H hydrogen bonds provide added stabilization to the complexes and thus, satisfy the geometrical necessity of the protonated receptor by providing a favourable electrostatic environment around the anion. Colourless crystals suitable for single-crystal X-ray analysis were obtained by slow evaporation of CH_3OH–CH_3CN binary solution mixtures of the isolated anion complexes (**1a-1e**) at room temperature. Parameters for data collection and crystallographic refinement details of anion complexes **1a-1e** are summarized in Table 3.3.

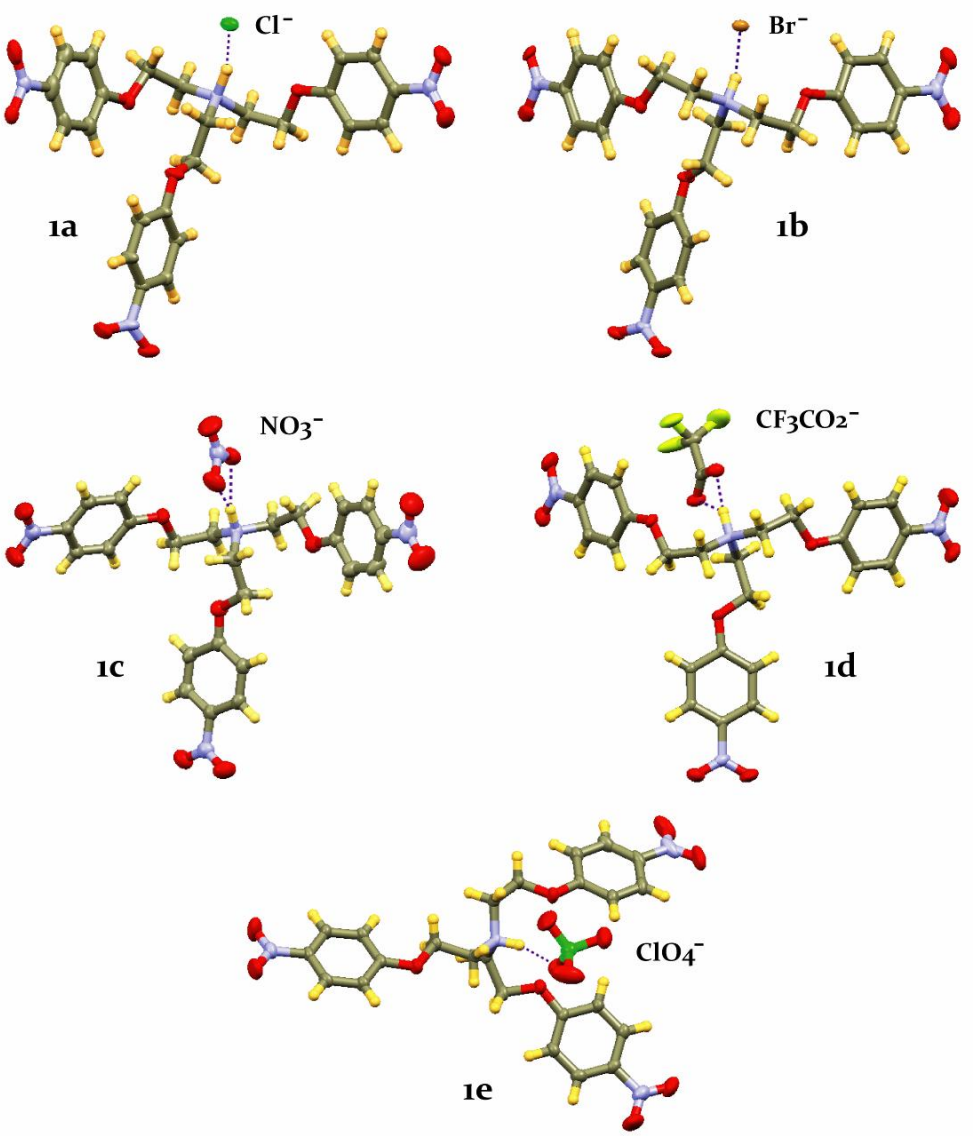

Figure 3.5 X-ray structures of anion complexes (**1a-1e**) of receptor $\mathbf{L_1}$ (thermal ellipsoid plot with 30% probability) depicting the electrostatic $(N–H)^+\cdots A^-$ interaction in each complex.

3.4.1 Chloride complex $[(HL_1)^+ \bullet Cl^-]$, (1a)

Complex **1a** crystallizes in triclinic system with *P*–1 space group. Structural elucidation revealed that, the binding of a chloride anion is governed by an electrostatic $(N–H)^+\cdots Cl^-$

interaction (N1···Cl^- = 3.013 Å) and six C–H···Cl^- contacts operating with an average hydrogen bond distance of 3.690 Å (Table 3.5). A methylene proton C18H(A) subsequent to the protonated bridgehead nitrogen is C-H bonded to Cl^- and two neighbouring receptor cations provide five other C–H···Cl^- contacts to the anion involving hydrogen atoms C2H(B), C9H(B) and C4H of one unit and, C9H(A) and C17H(A) from the other coordinating unit (Figure 3.6a). The crystal packing motif viewed down the b-axis shows bilayer assembly of receptor cations, organized *via* several C–H···O-(nitro) and π-stacking interactions where, chloride ions are sandwiched between the adjacent bilayers parallel along a-axis (Annexure 3).

3.4.2 Bromide complex $[(HL_1)^+ \bullet Br^-]$, (**1b**)

Complex **1b** crystallizes in triclinic system with *P*–1 space group. Identical to **1a**, there are six C–H···Br^- contacts from three encircling receptor cations operating with an average hydrogen bond distance of 3.786 Å (Table 3.5), in addition to the electrostatic (N–H)$^+$···Br^- interaction (N1···Br^- = 3.194 Å). A methylene hydrogen C18H(B) subsequent to the protonated apical nitrogen is C–H bonded to Br^- while aliphatic protons C1H(A), C17H(B), C1H(B), C10H(A) and aryl hydrogen C12H from two adjacent receptor cations are making contacts with the anion *via* weak C–H···Br^- interactions (Figure 3.6b). The crystal packing diagram viewed down the b-axis shows that the receptor cations beautifully pack in a bilayer array, assembled *via* multiple C–H···O-(nitro) and π···π interactions whereas multiple C–H···Br^- interactions stitches the adjacent bilayers along crystallographic a-axis (Annexure 3). An unusual seven-coordination in halide complexes (**1a** and **1b**) suggests that, the interactions with the C–H donors are too weak to impose a definite coordination structure around the halides, and instead the C-H groups on the flexible arms of the receptor embrace the anion so as to provide a favourable electrostatic environment around them.

3.4.3 Nitrate complex $[(HL_1)^+ \bullet NO_3^-]$, (**1c**)

Complex **1c** crystallizes in monoclinic system with P_21/n space group. Crystal structure elucidation revealed the formation of bifurcated (N–H)$^+$···A^- interaction between the hydrogen of protonated bridgehead nitrogen and nitrate oxygen atoms O10 and O11 (N1···O10 = 2.894 Å and N1···O11 = 2.881 Å). Additionally, each nitrate anion is in interaction with two adjacent receptor cations *via* four C–H···O contacts operating with an average hydrogen bond distance of 3.272 Å (Table 3.5). Two methylene protons C17H(A) and C18H(A) from the same receptor cation provides two C–H···O contacts to nitrate oxygen O11 while O10 and O12 accepts C–H···O bonds from the other coordinating cation involving hydrogen atoms C21H and C1H(A) respectively (Figure 3.6c). The packing diagram viewed down the a-axis clearly shows that the cationic array of receptor molecules are assembled *via*

multiple C–H···O-(nitro) interactions and the anions are entrapped between the cationic arrays in a zigzag fashion along b-axis (Annexure 3).

3.4.4 Trifluoroacetate complex $[(H\mathbf{L_1})^+ \bullet CF_3CO_2^-]$, (**1d**)

Complex **1d** crystallizes in triclinic system with *P*–1 space group. Structural analysis showed that, a $CF_3CO_2^-$ anion is coordinated to five receptor cations by a nine-point attachment involving oxygen and fluorine atoms of the anion. Similar to the nitrate complex (**1c**), the hydrogen of protonated bridgehead nitrogen is involved in bifurcated $(N–H)^+ \cdots A^-$ interaction with oxygen atoms O10 and O11 of the anion (N1···O10 = 3.248 Å, and N1···O11 = 2.742 Å) and a methylene hydrogen C9H(B) from the same receptor cation is hydrogen bonded to O10 *via* weak C–H···O interaction. Furthermore, four adjacent receptor cations that encircle an anion provide six other C–H contacts on the $CF_3CO_2^-$ anion with an average hydrogen bond distance of 3.304 Å (Table 3.5). Methylene hydrogen C1H(A) and C2H(B) from two different receptor cations are involved in bifurcated $C–H \cdots A^-$ interaction with O10, F2 and O11, F3, respectively, whereas aryl hydrogen C7H and C4H from two other units provide C–H contacts to F1 and F2, respectively (Figure 3.6d). It is interesting to note that, two arms of a receptor cation are projected in one direction to form a cleft shaped cavity and two such units intercalate to form a dimeric assembly encapsulating two $CF_3CO_2^-$ ions within the dimeric cleft (Annexure 3). The crystal packing diagram viewed down the b-axis, shows that the receptor cations beautifully pack in a bilayer array *via* multiple C–H···O-(nitro) and π-stacking interactions and the $CF_3CO_2^-$ ions are entrapped between the adjacent bilayers along a-axis (Annexure 3).

3.4.5 Perchlorate complex $[(H\mathbf{L_1})^+ \bullet ClO_4^-]$, (**1e**)

Complex **1e** crystallizes in monoclinic system with P_21/c space group. Similar to the halide complexes (**1a** and **1b**), there exist a strong $(N–H)^+ \cdots A^-$ interaction (N1···O12 = 2.974 Å) and a weak $C–H \cdots A^-$ interaction formed between an aryl proton C15H of the same receptor cation and perchlorate oxygen O13. In addition, two adjacent receptor cations provide four more C–H···O contacts on the perchlorate anion with an average hydrogen bond distance of 3.288 Å (Table 3.5). Perchlorate oxygen O10 and O12 are hydrogen bonded to a methylene proton C1H(A) whereas, O11 and O13 are in interaction with aromatic protons C23H and C12H of two different receptor cations (Figure 3.6e). The receptor cations are inter-linked among themselves *via* multiple C–H···O-(nitro) interactions and results in the formation of a zipper-like assembly when viewed down the crystallographic a-axis with the anions being arranged in a zigzag fashion stitching the adjacent cationic arrays by $C–H \cdots A^-$ interactions (Annexure 3).

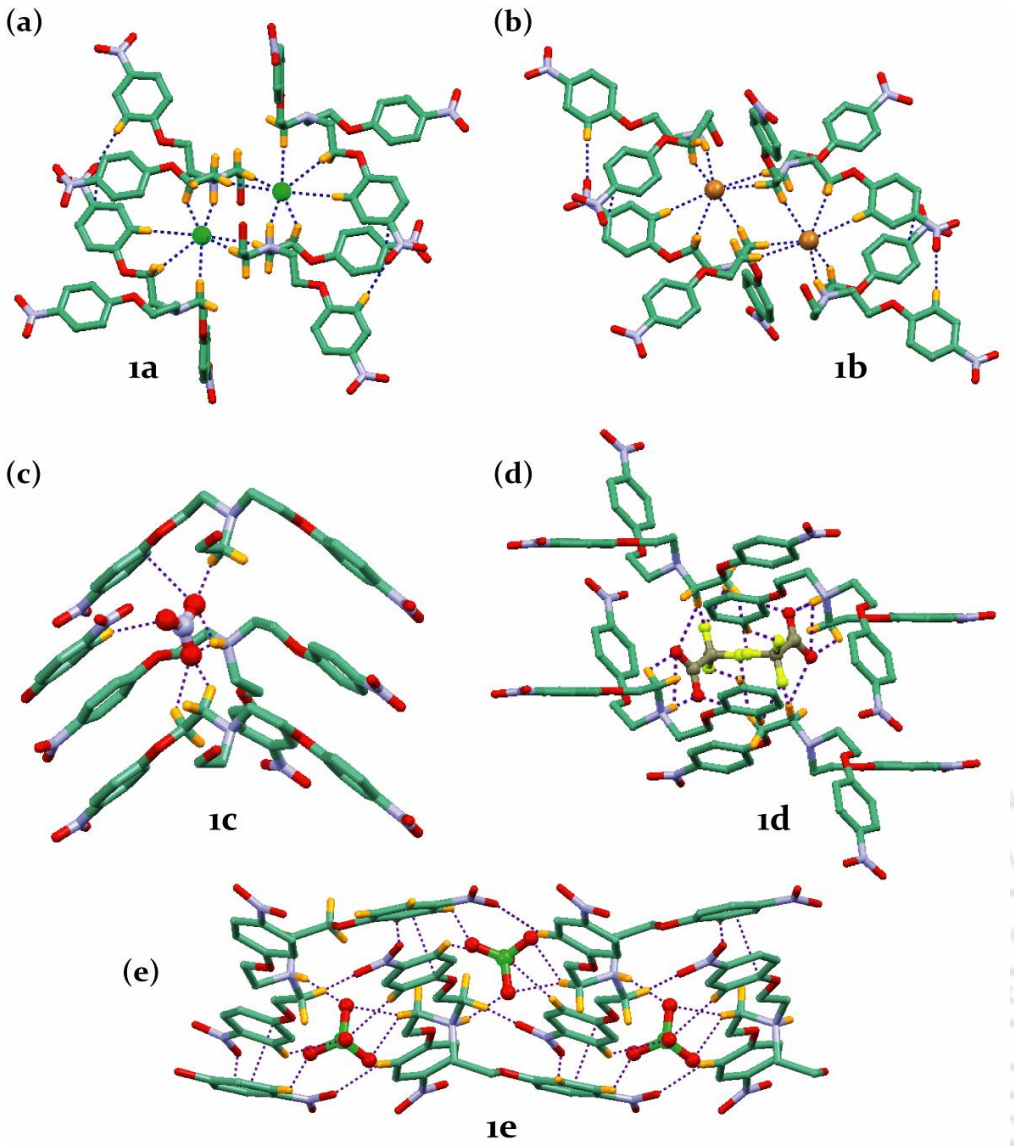

Figure 3.6 (a) Seven-point coordination of Cl^- anion in **1a**; (b) Seven-point coordination of Br^- anion in **1b**; (c) Six-point coordination of NO_3^- anion in **1c**; (d) Nine-point coordination of $CF_3CO_2^-$ anion in **1d**; (e) Six-point coordination of ClO_4^- anion in **1e.**

3.5 Structural aspects of anion binding with protonated L_2

Structural information obtained from single-crystal X-ray analyses of the anion complexes provide insight into the anion induced conformational adaptation of the flexible podand molecule, that respond to the demand of specific anion(s). Complexation of anions by protonated $\mathbf{L_2}$ is primarily governed by electrostatic interaction and multiple C-H···A^- hydrogen bonds that provide added stability to the complexes in association with intermolecular C–H···π and/or π···π interactions. Unlike receptor $\mathbf{L_1}$, protonation of $\mathbf{L_2}$ in presence of inorganic anions result in conformational locking of the tripodal pseudocavity by strong $(N–H)^+$···O-(ether) trifurcated hydrogen bond formation due to *endo*-orientation of the apical proton. Whereas, protonation in presence of organic anions leads to *exo*-orientation of the apical proton and thereby, results in conformational opening of the receptor side arms *via*

formation of $(N–H)^{+}\cdots A^{-}$ and π-stacking interactions with the aromatic organic anions. Colourless/yellow crystals suitable for single-crystal X-ray diffraction analysis were obtained by slow evaporation of $CH_3OH–CH_3CN$ binary solution mixtures of the isolated anion complexes (**2a-2d**) at room temperature. Parameters for data collection and crystallographic refinement details of anion complexes **2a-2d** are summarized in Table 3.4.

Table 3.4: Crystallographic data and refinement details of anion complexes of $\mathbf{L_2}$ (**2a-2d**).

Parameters	**2a**	**2b**	**2c**	**2d**
Formula	$C_{27}H_{34}ClNO_7$	$C_{27}H_{38}BrNO_5$	$C_{33}H_{36}N_4O_{10}$	$C_{37}H_{39}NO_{11}$
Fw	520.00	536.48	648.66	673.69
Crystal System	Rhombohedral	Monoclinic	Triclinic	Monoclinic
Space group	*R*3*c*	*C*2/*c*	*P*–1	$P2_1/c$
a(Å)	12.5863(1)	43.2178(12)	10.0888(3)	13.4682(13)
b(Å)	12.5863(1)	7.6050(2)	12.3654(4)	13.6433(13)
c(Å)	28.7108(5)	17.6312(4)	13.7716(4)	20.291(2)
$\alpha(^o)$	90.00	90.00	81.260(2)	90.00
$\beta(^o)$	90.00	105.385(3)	76.965(2)	104.935(3)
$\gamma(^o)$	120.00	90.00	83.641(1)	90.00
$V(Å^3)$	3938.87(8)	5587.2(3)	1649.10(9)	3602.5(6)
Z	6	8	2	4
$Dx(g\ cm^{-3})$	1.315	1.276	1.306	1.242
$\mu(mm^{-1})$	0.191	1.506	0.098	0.092
F(000)	1656	2256	684	1424
T(^{o}K)	298(2)	298(2)	298(2)	298(2)
θ max.	28.28	28.34	28.35	26.80
Total reflections	17213	43040	18236	16599
Ind. reflections	2175	6964	7968	7600
Obs. reflections	985	6598	7776	7498
N_{par}	113	330	432	453
$R_1, I > 2\sigma(I)$	0.0326	0.0352	0.0529	0.0615
wR_2 (all data)	0.0906	0.1094	0.1646	0.1611
GOF (F^2)	0.956	0.941	0.924	0.937

3.5.1 Perchlorate complex $[(H\mathbf{L_2})^{+}\bullet ClO_4^{-}]$, (**2a**)

Complex **2a** crystallizes in rhombohedral system with centrosymmetric space group *R*3c. Structural elucidation revealed that, the hydrogen of protonated bridgehead nitrogen is *endo*-oriented with respect to the tripodal side arms and is involved in intramolecular $(N–H)^{+}\cdots O$

hydrogen bonding with the three identical ethereal oxygen atoms (N1···O1 = 2.781 Å and ∠N1-H···O1 = 114°) (Figure 3.7a). As a result of trifurcated hydrogen bond formation, each tripodal side arm is now oriented in a folded conformation which is reflected in the torsion value of 63.30° (mean value) involving atoms N_{amino}–C–C–O_{ether} (τ_{ether}). Furthermore, distance between the ethereal oxygen atoms reduces to 3.667 Å, dropping the size of the tripodal cavity by 1.37 Å when compared to the structure of $\mathbf{L_2}$. Thus, intramolecular (N–H)$^+$···O hydrogen bond formation locks up the *C3v* cavity well known for anion binding and encryption.

Identical to $\mathbf{L_2}$, each receptor cation is surrounded by six other units occupying a chair conformation but with a distance measuring 12.01 Å between the apical nitrogen atoms of two adjacent cations involved in the cyclohexane class of chair conformation (Figure 3.7b). A considerable decrease of 1.42 Å in the cyclohexane ring size is possibly, due to the immediate outcome of conformational locking of the podand cavity which allows a closer approach of tripodal units in the crystals of **2a**. The protonated receptor does not have any kind of noncovalent interactions with the perchlorate anion. However, each arm of a receptor cation is linked with two neighbouring units by an aliphatic C–H···π (C1···Cg = 3.981 Å) interaction and a C–H···O interaction formed between a methyl proton and an ethereal oxygen of adjacent cation (C9···O1 = 3.467 Å). Expansion of **2a** through hydrogen bonds results in a highly symmetrical 3D organic solid (Figure 3.7b).

3.5.2 Bromide complex $[(HL_2)^+ \bullet Br^-]2H_2O$, (**2b**)

Complex **2b** crystallizes in monoclinic system with centrosymmetric space group *C*2/c. Identical to **2a**, the hydrogen of protonated bridgehead nitrogen is *endo*-oriented and forms trifurcated (N–H)$^+$···O hydrogen bonds to the ethereal oxygen atoms with an average distance of 2.758 Å (mean ∠N1-H···O = 114°). The tripodal arms are all oriented in a folded conformation (τ_{ether} = 60.14°, mean value) with an average distance of 3.569 Å between the ethereal oxygen atoms. Short contact analysis revealed that, the binding of bromide in **2b** is primarily governed by three C–H···Br^- and three O–H···Br^- interactions provided by three encircling receptor cations and lattice water molecules O4 and O5 (Figure 3.7c). The methylene protons C10H(B), C20H(A) and C19H(B) from individual receptor cation is C–H bonded to Br^- with an average hydrogen bond distance of 3.823 Å (Table 3.5). Six-coordination to Br^- is finally satisfied by the hydrogen bonded lattice water molecules (O4···O5 = 2.870 Å), where three H_2O molecules [one H_2O(4) and two H_2O(5)] make contacts with each bromide anion *via* O–H···Br^- interactions through an average hydrogen bond distance of 3.375 Å (Table 3.5). The crystal packing diagram viewed down the c-axis

clearly shows that the receptor molecules beautifully pack in a hydrophobic bilayer assembly *via* C–H···π interactions (C7···C3g = 3.655 Å and C14···C3g = 3.922 Å), and bromide ions are entrapped between the adjacent bilayers in association with the lattice water molecules generating a hydrophilic chain parallel along the b-axis (Figure 3.7d).

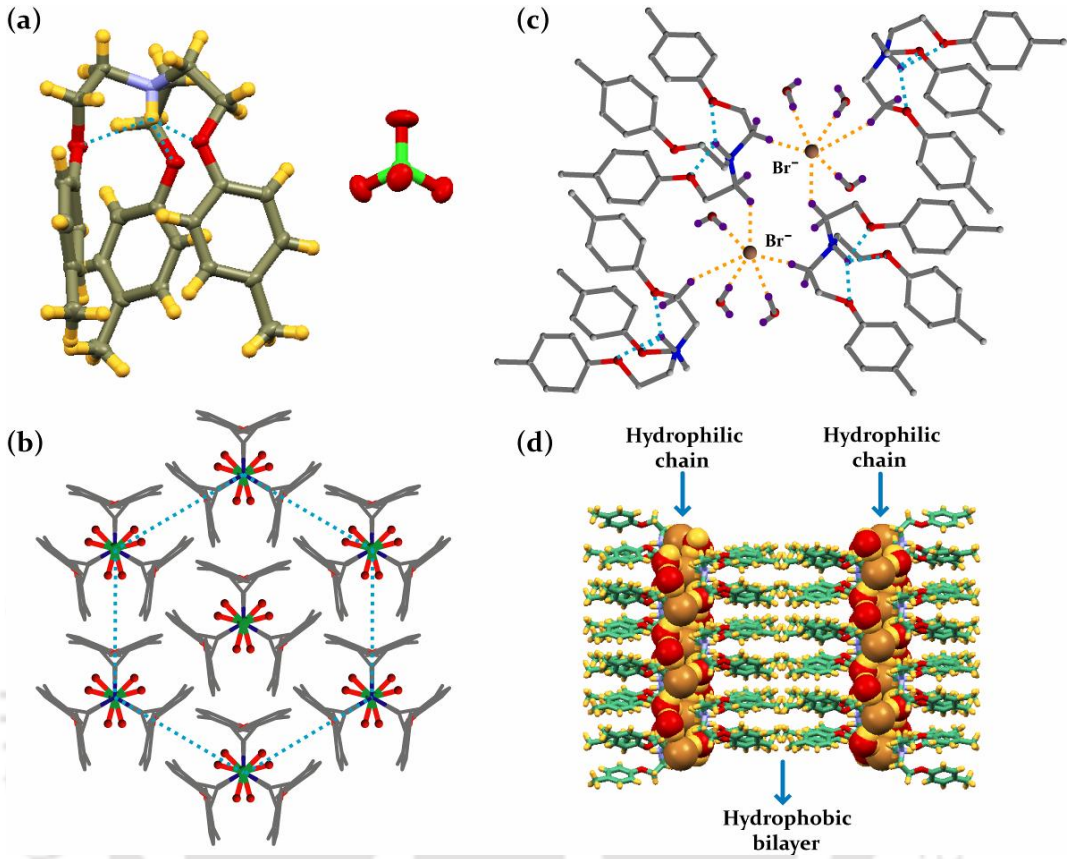

Figure 3.7 (a) X-ray structure of perchlorate complex **2a** (thermal ellipsoid plot with 30% probability), depicting the intramolecular $(N–H)^{+}\cdots$O-(ether) interactions; (b) Highly symmetric crystal packing in **2a** showing the hexagonal arrangement of tripodal units (in cyclohexane conformation); (c) Six-point coordination of Br^{-} anion in **2b**, along with intramolecular $(N–H)^{+}\cdots$ O-(ether) interactions; (d) Crystal packing diagram of **2b**, as viewed down the c-axis.

At this juncture we were interested to explore the role of organic anions in the system that affects the conformation of protonated $\mathbf{L_2}$ and we prepared complexes **2c** and **2d** by stirring a methanolic solution of $\mathbf{L_2}$ in presence of one equiv. of picric acid (PA) and pyromellitic acid (PMA) respectively.

3.5.3 Picrate complex $[(H\mathbf{L_2})^{+}\bullet PA^{-}]$, (**2c**)

Complex **2c** crystallizes in triclinic system with *P*–1 space group. Structural elucidation revealed that, the tripodal arms are oriented in three different directions with the hydrogen of protonated bridgehead nitrogen being *exo*-oriented and forms a strong intermolecular (N–

$H)^+\cdots A^-$ interaction with the phenolate oxygen O4 of picrate anion (N1···O4 = 2.713 Å). In addition, phenolate oxygen O4 is C–H hydrogen bonded to aliphatic protons C2H(A) and C11H(A) whereas nitro oxygen atoms O5 and O10 are in interaction with protons C13H and C19H(A) respectively, from the same receptor cation forming electrostatic $(N–H)^+\cdots A^-$ interaction (Figure 3.8a). Furthermore, four neighbouring receptor cations that encircle each picrate anion provide five more C–H···O contacts on the anion where, nitro oxygen O6 and O7 acts as bifurcated hydrogen bond acceptor by interacting with -CH protons C1H(A), C2H(A) and C5H, C19H(B), respectively and O9 is in interaction with the aryl proton C26H (Figure 3.8b). The crystal packing motif as viewed down the c-axis shows intermolecular π-stacking interaction between a phenyl ring (C2g) of each receptor cation and dimeric (π-stacked) picrate anion having an interacting distance of 3.839 Å.

3.5.4 Pyromellitate complex $[(HL_2)^+ \bullet PMA^-]$, (**2d**)

Complex **2d** crystallizes in monoclinic system with $P2_1/c$ space group. Structural elucidation revealed similar kind of conformational behaviour of the receptor cation as observed in picrate complex (**2c**). The tripodal arms being devoid of any intramolecular interactions are in an extended conformation and the *exo*-oriented hydrogen of protonated bridgehead nitrogen is involved in $(N–H)^+\cdots A^-$ interaction with the carboxylate oxygen O7 of pyromellitate anion (N1···O7 = 2.783 Å) (Figure 3.8c). Furthermore, carboxylate oxygen atoms O4, O7, O8 and O10 are making C–H···O contacts with alkyl hydrogen C19H(A), C5H, C1H(B) and C18H(A), respectively, from four different receptor cations encircling the anion, with an average hydrogen bond distance of 3.399 Å (Table 3.5). Identical to **2c**, **2d** retains the intermolecular π-stacking interaction between a phenyl ring (C2g) of receptor cation and electron π-cloud of the aromatic anion having an interaction distance of 3.931 Å (Figure 3.8d). Pyromellitate anions are interlinked among themselves via R_4^4 hydrogen bonded ring formation and thereby, generating 2D hydrogen bonded sheet structure along ab-plane of the crystal.

3.6 Rationalization on conformational aspects upon anion binding

From the crystal structure description of anion complexes **1a-1e**, it can be rationalized that, the presence of active nitro groups at the periphery of $\mathbf{L_1}$ assists in several intermolecular C–H···O-(nitro) hydrogen bond formation, which are primarily responsible for the flat and extended orientation of tripodal side arms along with *exo*-oriented apical hydrogen in anion complexes of protonated $\mathbf{L_1}$ (complexes **1a-1e**). However, the lack of conventional hydrogen bond acceptor groups (CN, NO_2, HSO_3 etc.) on the terminal aryl functions of $\mathbf{L_2}$, force the

receptor to attain a closed/folded conformation upon protonation in presence of inorganic anions (complexes **2a** and **2b**). Whereas, the existence of π–stacking interaction between a phenyl ring of protonated $\mathbf{L_2}$ and aromatic π–cloud of planar organic anion is probably responsible for conformational opening of the receptor side arms and *exo*-orientation of the apical hydrogen in complexes **2c** and **2d**.

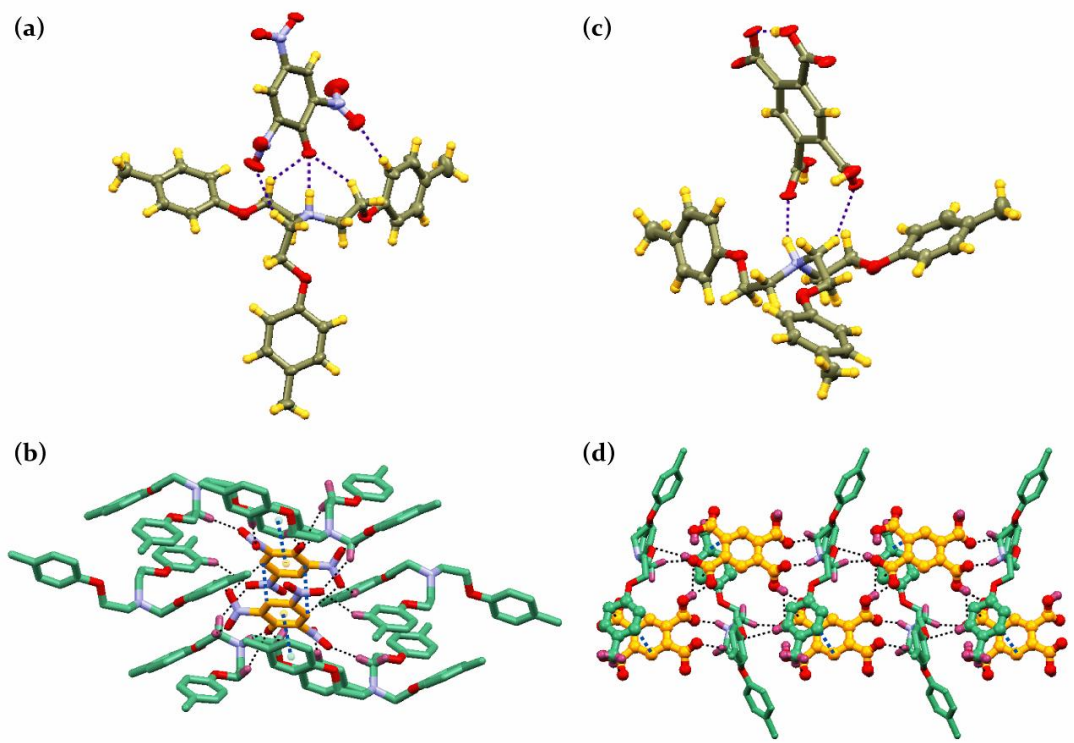

Figure 3.8 (a) X-ray structure of picrate complex **2c** (thermal ellipsoid plot with 30% probability), depicting the intermolecular $(N–H)^+\cdots A^-$ and $C–H\cdots A^-$ interactions; (b) Interactions of π–stacked dimeric picrate anion with multiple receptor cations via $C–H\cdots A^-$ and π···π interactions in complex **2c**; (c) X-ray structure of pyromellitate complex **2d** (thermal ellipsoid plot with 30% probability), depicting the intermolecular $(N–H)^+\cdots A^-$ and $C–H\cdots A^-$ interactions; (d) Interactions of pyromellitate anion with multiple receptor cations via $C–H\cdots A^-$ and π···π interactions in complex **2d**.

3.7 Solution-state evidence of anion binding

^{1}H NMR spectroscopy has been used to evaluate anion binding in the solution-state (DMSO-d_6; 298 K) and to correlate the structural and conformational changes of podand receptors upon protonation with a diverse range of anions. Considerable downfield shift of the aliphatic $–CH_2$ protons ($\Delta\delta$ = 0.30–0.70 ppm) in the ^{1}H NMR spectra of all anion complexes indicate the influence of protonation at the apical nitrogen on the neighbouring methylene protons. Since most of the $C–H\cdots A^-$ contacts are formed with the methylene protons subsequent to the ammonium ion, it can be argued that these donor atoms are simply in the way due to the close approach of negatively charged anions to the positively charged bridgehead nitrogen of protonated $\mathbf{L_1}$ and $\mathbf{L_2}$. Another argument is that, protonation at the

bridgehead nitrogen render the methylene $-CH_2$ protons sufficiently acidic for their active participation in anion binding *via* weak C–H···A^- interactions.

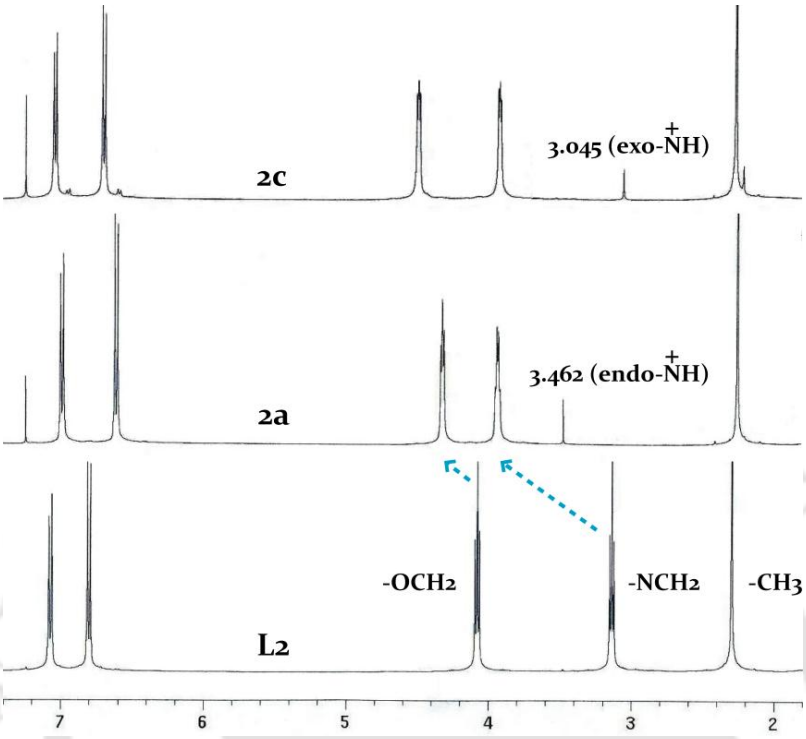

Figure 3.9 Comparison of the partial ^{1}H NMR spectra (in $CDCl_3$) of complexes **2a** and **2c** with receptor $\mathbf{L_2}$ demonstrating the occurrence of apical $(N–H)^+$ proton resonances at different δ values ($\Delta\delta$ = 0.417 ppm).

The excellent solubility of perchlorate and picrate complexes of $\mathbf{L_2}$ (complexes **2a** and **2c**) in $CHCl_3$ allowed us to perform ^{1}H NMR experiments in $CDCl_3$. Interestingly, the resonance for the *endo*-oriented hydrogen of protonated bridgehead nitrogen in **2a** occurs at δ = 3.462 ppm and in complex **2c**, where the hydrogen of protonated bridgehead nitrogen is *exo*-oriented resonates at δ = 3.045 ppm. The occurrence of bridgehead $(N–H)^+$ proton resonances at considerably different δ values ($\Delta\delta$ = 0.417 ppm) with notable changes in C–H proton resonances further account for the different conformational orientations of protonated $\mathbf{L_2}$ in presence of inorganic and organic anions in solution-state. In addition, spectral changes have also been observed for the aromatic protons, which indeed indicate a solution-state structural difference of the receptor side arms in presence of different set of anions. However, in DMSO-d_6 the resonances for apical $(N–H)^+$ proton could not be observed consistently.

3.8 Conclusion

In summary, we have structurally authenticated the solvent/anion induced conformational changes in two tripodal ether receptors, $\mathbf{L_1}$ and $\mathbf{L_2}$. From the crystal structure analyses and solution-state studies, it is evident that a mere variation of terminal aryl substitution results in significant conformational changes of the podand molecules induced by the presence of different anions or set of anions under identical growth condition. In short, the present findings provide evidence of solvent induced conformational polymorphism in $\mathbf{L_1}$ and inorganic anion assisted extended and open conformational adaptation by protonated $\mathbf{L_1}$ *via* $(N–H)^{+}\cdots A^{-}$ hydrogen bond formation. Whereas, receptor $\mathbf{L_2}$ represents the solvent independent formation of a crystalline molecular bowl, which upon protonation in presence of inorganic anions get conformationally locked/closed by trifurcated $(N–H)^{+}\cdots$O-(ether) hydrogen bond formation and planar organic anions force the protonated receptor molecule to become conformationally open *via* $(N–H)^{+}\cdots A^{-}$ and π–stacking interactions. Thus, receptors $\mathbf{L_1}$ and $\mathbf{L_2}$ are the examples of simple tripodal scaffolds that adapt its conformation to respond to the demands of specific anion(s) or solvent of crystallization. Detailed structural investigation of the anion complexes clearly demonstrates that, self-alignment and orientation of the receptor cation play a crucial role in making various supramolecular interactions possible in binding of anions of varied dimensionality. Moreover, the receptor molecules can provide an excellent case of understanding the C–H hydrogen bonds in its protonated and neutral form as well.

Table 3.5 Relevant hydrogen bond parameters in anion complexes of $\mathbf{L_1}$ and $\mathbf{L_2}$.

Complexes	D-H···A	*d*(H···A) (Å)	*d*(D···A) (Å)	∠(DHA) (°)
1a	N1-H···Cl1	1.95(4)	3.013(5)	160(3)
	C18-H(A)···Cl1	2.85(2)	3.633(6)	138(3)
	C2-H(B)···Cl1	2.82(2)	3.621(6)	140(3)
	C9-H(B)···Cl1	2.84(3)	3.684(6)	145(3)
	C4-H···Cl1	2.89(2)	3.821(6)	173(3)
	C9-H(A)···Cl1	2.66(2)	3.601(5)	162(3)
	C17-H(A)···Cl1	2.92(2)	3.780(5)	148(3)
1b	N1-H···Br1	2.32(4)	3.194(2)	158(1)
	C1-H(A)···Br1	2.81(9)	3.752(3)	161(1)
	C1-H(B)···Br1	2.87(7)	3.708(3)	145(1)
	C10-H(A)···Br1	2.94(1)	3.730(3)	138(1)
	C17-H(B)···Br1	2.99(9)	3.876(3)	152(2)
	C18-H(B)···Br1	2.95(1)	3.759(3)	141(2)
	C12-H···Br1	2.96(6)	3.894(2)	173(1)
1c	N1-H···O10	2.07(3)	2.894(4)	135(2)
	N1-H···O11	1.89(3)	2.881(4)	160(2)
	C1-H(A)···O10	2.28(3)	3.211(4)	160(2)
	C9-H(A)···O11	2.46(3)	3.184(4)	131(2)
	C10-H(A)···O11	2.47(3)	3.190(4)	130(2)
	C15-H···O12	2.61(3)	3.506(4)	161(3)
1d	N1-H···O10	2.60(3)	3.248(4)	120(2)
	N1-H···O11	1.71(3)	2.742(4)	174(3)
	C1-H(B)···F2	2.56(4)	3.487(5)	158(2)
	C1-H(B)···O10	2.43(3)	3.194(5)	134(2)
	C2-H(B)···F3	2.65(4)	3.529(5)	150(2)
	C2-H(B)···O11	2.68(2)	3.472(4)	138(2)
	C9-H(B)···O10	2.51(3)	3.055(4)	115(2)
	C4-H···F2	2.63(4)	3.086(6)	110(2)
	C7-H···F1	2.44(2)	3.306(4)	154(2)

1e	N1-H···O12	2.12(2)	2.974(3)	151(2)
	C1-H(A)···O10	2.43(2)	3.240(3)	140(1)
	C1-H(A)···O12	2.46(2)	3.385(3)	158(1)
	C12-H···O13	2.45(2)	3.266(3)	146(2)
	C15-H···O13	2.64(2)	3.302(3)	128(2)
	C23-H···O11	2.53(2)	3.250(3)	133(2)
2b	C10-H(B)···Br1	2.96(3)	3.816(3)	147(2)
	C19-H(B)···Br1	3.04(4)	3.815(4)	137(2)
	C20-H(A)···Br1	3.04(4)	3.839(3)	139(2)
	O4-H2···Br1	2.51(2)	3.396(3)	170(3)
	O5-H3···Br1	2.43(2)	3.322(3)	171(3)
	O5-H4···Br1	2.51(3)	3.408(3)	171(3)
2c	N1-H···O4	1.81(3)	2.713(3)	172(3)
	C2-H(A)···O4	2.65(2)	3.394(3)	133(1)
	C11-H(A)···O4	2.61(2)	3.386(4)	136(2)
	C13-H···O5	2.53(3)	3.455(5)	171(2)
	C19-H(A)···O10	2.37(3)	3.247(4)	148(1)
	C1-H(A)···O6	2.66(3)	3.263(4)	120(1)
	C2-H(A)···O6	2.67(3)	3.001(4)	100(1)
	C5-H···O7	2.52(2)	3.351(3)	148(2)
	C19-H(B)···O7	2.71(2)	3.476(3)	135(1)
	C26-H···O9	2.55(2)	3.435(3)	157(1)
	C22-H···C3g	3.53	4.179	128
2d	N1-H···O7	1.87(3)	2.783(3)	149(2)
	C5-H···O7	2.70(2)	3.594(4)	160(3)
	C18-H(A)···O10	2.55(3)	3.460(5)	156(2)
	C19-H(A)···O4	2.29(2)	3.210(4)	157(2)
	C1-H(B)···O8	2.46(2)	3.334(4)	149(2)
	O6-H···O4	2.67(2)	3.208(3)	124(2)
	O6-H···O5	1.71(2)	2.530(3)	176(2)
	O9-H···O10	2.71(2)	2.576(3)	071(2)

References

1. (a) A. P. Cote, A. I. Benin, N.W. Ockwig, M. O'Keeffe, A. J. Matzger, O. M. Yaghi, *Science*, 2005, **310**, 1166 ; (b) C. J. Kepert, D. Hesek, P. D. Beer, M. J. Rosseinsky, *Angew. Chem., Int. Ed.*, 1998, **37**, 3158; (c) T. Tanaka, T. Tasaki. Y. Aoyama, *J. Am. Chem. Soc*., 2002, **124**, 12453; (d) D. S. Lawrence, T. Jiang and M. Levett, *Chem. Rev*., 1995, **95**, 2229; (e) D. Philp and J. F. Stoddart, *Angew. Chem., Int. Ed*., 1996, **35**, 1154; (f) M. Fujita, A. Hori and B. Therrien, *Acc. Chem. Res*., 2005, **38**, 369.

2. (a) G. R. Desiraju, *Acc. Chem. Res*., 1996, **29**, 441; (b) G. R. Desiraju, *Acc. Chem. Res*., 2002, **35**, 565; (c) A. Nangia, *Acc. Chem. Res*., 2008, **41**, 595.

3. (a) T. Threlfall, *Org. Process Res. Dev*., 2000, **4**, 384; (b) R. K. R. Jetti, R. Boese, J. A. R. P. Sarma, L. S. Reddy, P. Vishweshwar and G. R. Desiraju, *Angew. Chem., Int. Ed*., 2003, **42**, 1963; (c) R. J. Davey, N. Blagden, S. Righini, S. Alison, M. J. Quayle and S. Fuller, *Cryst. Growth Des*., 2001, **1**, 59.

4. (a) J. Bernstein, *Polymorphism in Molecular Crystals*; Oxford University Press: Oxford, 2002; (b) S. R. Byrn, R. R. Pfeiffer and J. G. Stowell, *Solid-State Chemistry of Drugs*; SSCI: West Lafayette, IN, 1999; (c) R. J. Davey, *Chem. Commun*. 2003, 1463.

5. (a) C. Bilton, J. A. K. Howard, N. N. L. Madhavi, A. Nangia, G. R. Desiraju, F. H. Allen and C. C. Wilson, *Chem. Commun*., 1999, 1675; (b) V. S. S. Kumar, A. Addlagatta, A. Nangia, W. T. Robinson, C. K. Broder, R. Mondal, I. R. Evans, J. A. K. Howard and F. H. Allen, *Angew. Chem., Int. Ed*., 2002, **41**, 3848; (c) S. Chen, I. A. Guzei and L. Yu, *J. Am. Chem. Soc*., 2005, **127**, 9881.

6. M. Arunachalam and P. Ghosh, *Chem. Commun*., 2009, 3184.

7. (a) K. Uzarevic, I. Dilovic, D. Matkovic-Calogovic, D. Sisak and M. Cindric, *Angew. Chem., Int. Ed*., 2008, **47**, 7022; (b) M. D. Lankshear and P. D. Beer, *Acc. Chem. Res*., 2007, **40**, 657; (c) N. Gimeno and R. Vilar, *Coord. Chem. Rev*., 2006, **250**, 3161; (d) R. Vilar, *Angew. Chem., Int. Ed*., 2003, 42, 1460; (e) M. C. T. Fyfe, P. T. Glink, S. Menzer, J. F. Stoddart, A. J. P. White and D. J. Williams, *Angew. Chem., Int. Ed*., 1997, **36**, 2068;(f) D. Rais, J. Yau, D.M. P.Mingos, R. Vilar, A. J. P. White and D. J. Williams, *Angew. Chem., Int. Ed*., 2001, **40**, 3464.

8. (a) M. D. Best, S. L. Tobey and E. V. Anslyn, *Coord. Chem. Rev*., 2003, **240**, 3; (b) V. McKee, J. Nelson and R. M. Town, *Chem. Soc. Rev*., 2003, **32**, 309; (c) J. L. Sessler, S. Camiolo and P. A. Gale, *Coord. Chem. Rev*., 2003, **240**, 17; (d) J. M. Llinares, D. Powell and K. Bowman-James, *Coord. Chem. Rev*., 2003, **240**, 57; (e) K. Choi and A. D. Hamilton, *Coord. Chem. Rev*., 2003, **240**, 101.

9. K. Bowman-James, *Acc. Chem. Res*., 2005**, 38**, 671; (b) P. Ballester, *Chem. Soc. Rev*., 2010, **39**, 3810.

10. (a) K. J.Wallace, W. J. Belcher, D. R. Turner, K. F. Syed and J. W. Steed, *J. Am. Chem. Soc*., 2003, **125**, 9699; (b) C. A. Ilioudis, D. A. Tocher and J. W. Steed, *J. Am. Chem. Soc*., 2004, **126**, 12395; (c) J. Y. Kwon, Y. J. Jang, S. K. Kim, K.-H. Lee, J. S. Kim and J. Yoon, *J. Org. Chem*., 2004, **69**, 5155; (d) S. Ghosh, A. R. Choudhury, T. N. G. Row and U. Maitra, *Org. Lett*., 2005, **7**, 1441; (e) F. M. Raymo, M. D. Bartberger, K. N. Houk and J. F. Stoddart, *J. Am. Chem. Soc*., 2001, **123**, 9264; (f) Z. M. Loh, R. L. Wilson, D. A. Wild and E. J. Bieske, *J. Chem. Phys*., 2003, **119**, 9559.

11. S. K. Dey and G. Das, *Cryst. Growth Des*., 2010, **10**, 754.

12. S. K. Dey and G. Das, *CrystEngComm*, 2011, **13**, 269.

13. S. K. Dey and G. Das, *CrystEngComm*, 2011, **13**, 1664.

Chapter 4

A Fluoride Selective Chromogenic Tris(amide) receptor

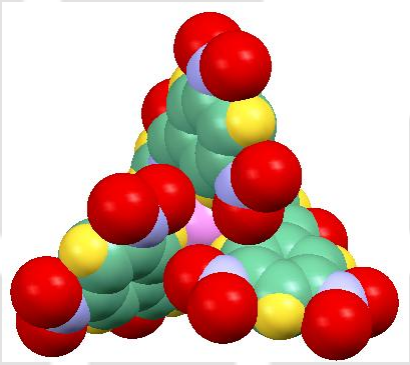

4.1 Background and Focus of the Chapter

The recent discovery of anion–π interaction, a noncovalent interaction between an anion and a π-acidic organic system with a strong positive quadrupole moment has added new dimensions to recognition, sensing, and transmembrane passage of anions.[1] Recently, Dunbar et al. reported chromogenic anion–π and charge transfer (CT) interactions involving halides ($Cl^- > Br^- > I^-$) and electron deficient aromatic rings in organic solvents[2] and Saha et al. reported the selective sensing of F^- by anion–π CT interactions involving the F^- ion and π-electron deficient NDI receptors.[3] Development of selective and sensitive chemosensors for F^- is important due to its diverse role in the medical and environmental sciences. A fluoride deficiency causes osteoporosis and poor dental health, whereas overexposure to F^- is blamed for fluorosis and osteosarcoma.[4] The EPA-recommended F^- level in drinking water is 1 ppm, and over 2 ppm is considered a health-risk.[5] Hydrogen bonded receptors rely either on adjacent chromophore units or deprotonation followed by electron delocalization to display a colorimetric response.[6] Therefore, they cannot differentiate F^- from other strongly basic anions, such as AcO^- and $H_2PO_4^-$.[7] In contrast, size-selective π–acidic hydrogen bonding scaffolds that exploit reversible anion–π CT interactions can be well employed to distinguish F^- from other basic anions.

This chapter deals with a π–acidic tris(amide) receptor, $\mathbf{L_3}$ (Scheme 4.1) which behaves as a selective chemosensor for F^- ion by strong anion–π CT interaction and thereby, exhibits solvatochromism in different aprotic solvents.[8] Interestingly, the receptor showed a distinct behaviour towards complexation of F^- anion when tetrabutylammonium fluoride (TBAF) and potassium fluoride (KF) salts were individually employed for recognition of F^- with $\mathbf{L_3}$. Single crystal X-ray diffraction analyses showed that an F^- anion is bound within the receptor cavity by strong N-H···F^- and C-H···F^- hydrogen bonds irrespective of solvent of crystallization, when TBAF was employed as an F^- source.[8] However, in presence of KF, the receptor is involved in side-cleft binding of a hydrated KF contact ion-pair governed by an amide N-H···F^-, an aryl C-H···F^- and a lp(F^-)···π interactions demonstrating a binding discrepancy of fluoride in quaternary ammonium and alkali salts by $\mathbf{L_3}$ in the solid-state.[9] The encapsulation of F^- using TBAF and side-cleft binding of KF can nicely be captured by following the changes in chemical shift of –NH and *ortho*-CH resonances of $\mathbf{L_3}$ in ^{1}H NMR experiments (DMSO-d_6) of the fluoride complexes and disappearance of through-space interaction between –NH and *ortho*-CH protons in 2D NOESY NMR experiments of 1:1 receptor-TBAF solution as compared to the free receptor.[9] The significance of the tripodal amide scaffold towards selective sensing of F^- was further established by synthesizing a control receptor, $\mathbf{CL_3}$ that cannot differentiate F^- from other basic anions, such as AcO^- and

$H_2PO_4^-$.[8] Furthermore, in a proof-of-concept experiment, the high selectivity of the receptor towards F^- recognition has been efficiently employed in the transformation of charged anion complexes $[(H\mathbf{L_3})^+ \bullet A^-$; where A^- = Cl^-, Br^-, ClO_4^- and $HSO_4^-]$ into F^-–bound pseudomolecular capsule of $\mathbf{L_3}$ in solution-states.[10] Scheme 4.1 shows a comprehensive representation of the research work included in this chapter.

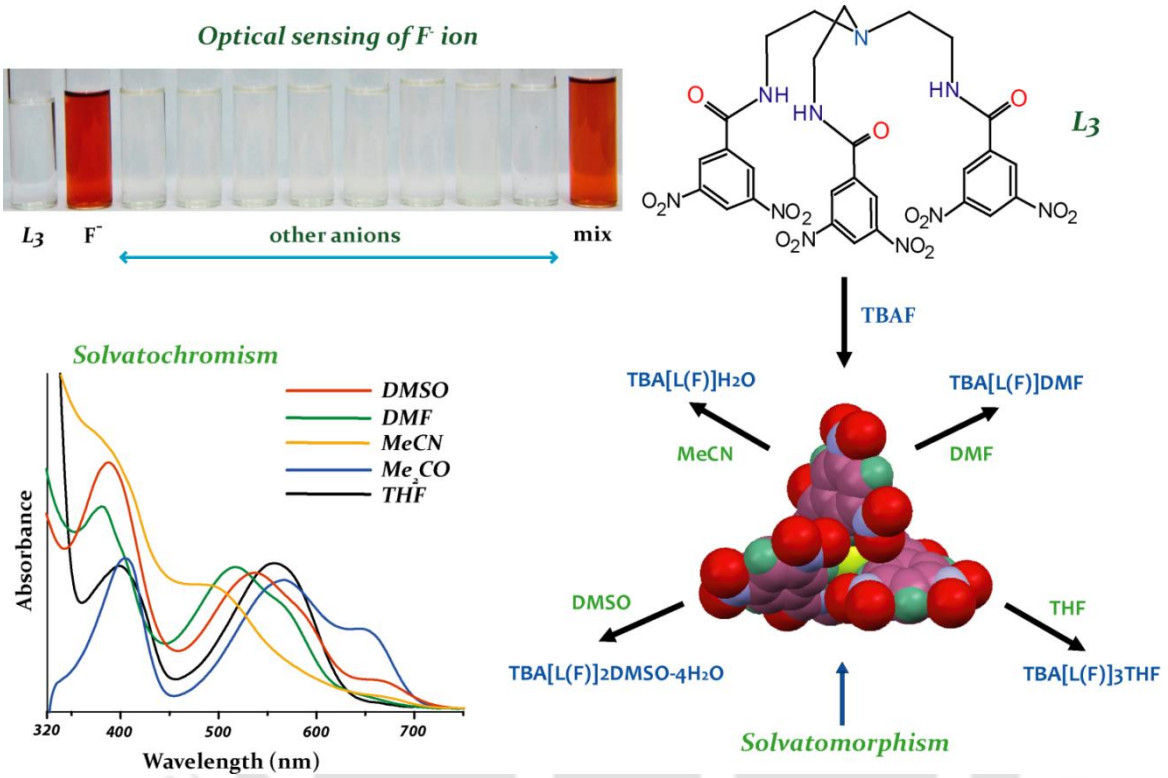

Scheme 4.1 Schematic representation depicting the selective optical sensing of F^- ion by receptor, $\mathbf{L_3}$ and solvatochromism (UV/Vis) and solvatomorphism exhibited upon recognition of F^- by $\mathbf{L_3}$.

4.2 Selective sensing of F^- by anion—π interaction

The fluoride recognition chemistry is immediately detected in solution by a dramatic increase in solubility of the receptor in polar aprotic solvents (DMSO, DMF, MeCN, acetone, THF and dioxane) with a concomitant optical signalling from colourless to orange/purple upon addition of excess TBAF to the suspension of $\mathbf{L_3}$. Whereas, addition of anions such as, $CH_3CO_2^-$ and $H_2PO_4^-$ having similar basicity to those of F^- do not induce any colorimetric response. The highly ordered hydrogen bonding scaffold give rise to the colorimetric changes as the π-acidic dinitrophenyl function being a part of the triamide receptor, can possibly induce an anion—π charge-transfer (CT) interaction upon selective recognition of fluoride anion. The selective recognition of F^- by $\mathbf{L_3}$ has been investigated in detail by UV/Vis spectroscopy. UV/Vis study suggests that $\mathbf{L_3}$ can selectively detect fluoride ion in the visible region of the spectrum (Figure 4.1), in a library of polar aprotic solvents.

Whereas **L₃** in absence or in presence of other anionic guests such as Cl^-, Br^-, I^-, AcO^-, NO_3^-, $H_2PO_4^-$, HSO_4^- and ClO_4^- shows no characteristic absorption in the visible region of the spectrum. Intense colorations with emergence of new bands in the optical spectral region can be attributed to strong anion—π CT interactions involving F^- ion and π-acidic dinitrophenyl functions of the triamide receptor. The CT absorptions also demonstrated a strong solvent dependence which can be visually marked and confirmed by optical spectroscopy (Figure 4.1b). However, the CT bands did not exhibit a linear correlation to solvent polarity probably due to the complexity of solute-solvent interactions where hydrogen bond accepting nature of the solvents plays a critical role.

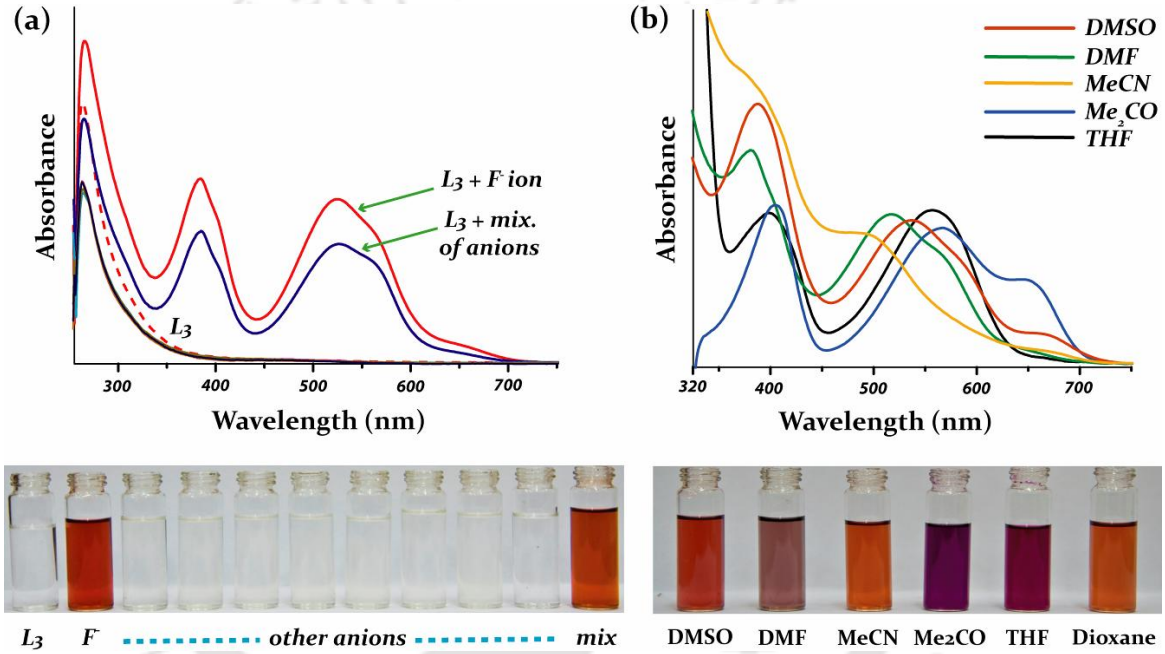

Figure 4.1 (a) Observed UV/Vis spectral changes and optical colour changes upon addition of TBA salts of various anions (excess) to the DMSO solutions of **L₃**; (b) UV/Vis spectra of **L₃** in various aprotic solvents upon addition of excess TBAF and the corresponding colour changes.

Upon increasing addition of a standard F^- solution (10 *m*M) to a solution of **L₃** (10 μM) in DMSO, three new absorption bands appear at λ_{max} = 388 (λ_1), 537 (λ_2) and 665 (λ_3) nm and grows with increasing F^- concentration (Figure 4.2a). UV/Vis titration of **L₃** with TBAF in acetone, exhibited a considerable bathochromic shift of 17 and 28 nm in the λ_1 and λ_2 absorptions (λ_1 = 405 nm and λ_2 = 565 nm), whereas a hypsochromic shift of 19 nm has been observed for λ_3 absorption (λ_3 = 646 nm) (Figure 4.2b). Similarly in THF, an appreciable bathochromic shift of 12 and 20 nm were observed for the λ_1 and λ_2 absorptions (λ_1 = 400 nm and λ_2 = 557 nm) (Figure 4.2c), indicative of an additional solute–solvent interaction that acted as a mechanism to stabilize the receptor-F^- complex more in acetone and THF relative to DMSO. However in DMF, titration curves showed a hypsochromic shift of 7 and 20 nm in

the λ_1 and λ_2 absorptions (λ_1 = 381 nm and λ_2 = 517 nm) (Figure 4.2d), suggestive of a minor interaction of the receptor-F^- complex with the DMF molecules compared to acetone, THF and DMSO. The shortest wavelength for λ_2 absorption was 498 nm recorded in MeCN and dioxane (Figure 4.2e and 4.2f) which exhibit identical spectral patterns, and the longest wavelength was 565 nm observed in acetone, indicating that the receptor-F^- complex is more stabilized in acetone followed by THF and DMSO among other aprotic solvents. The origin of multi-CT bands can possibly be explained due to the existence of electron-resonance between the lone pair electrons of F^- ion with two or more closely spaced unoccupied orbitals of the π-acidic receptor.

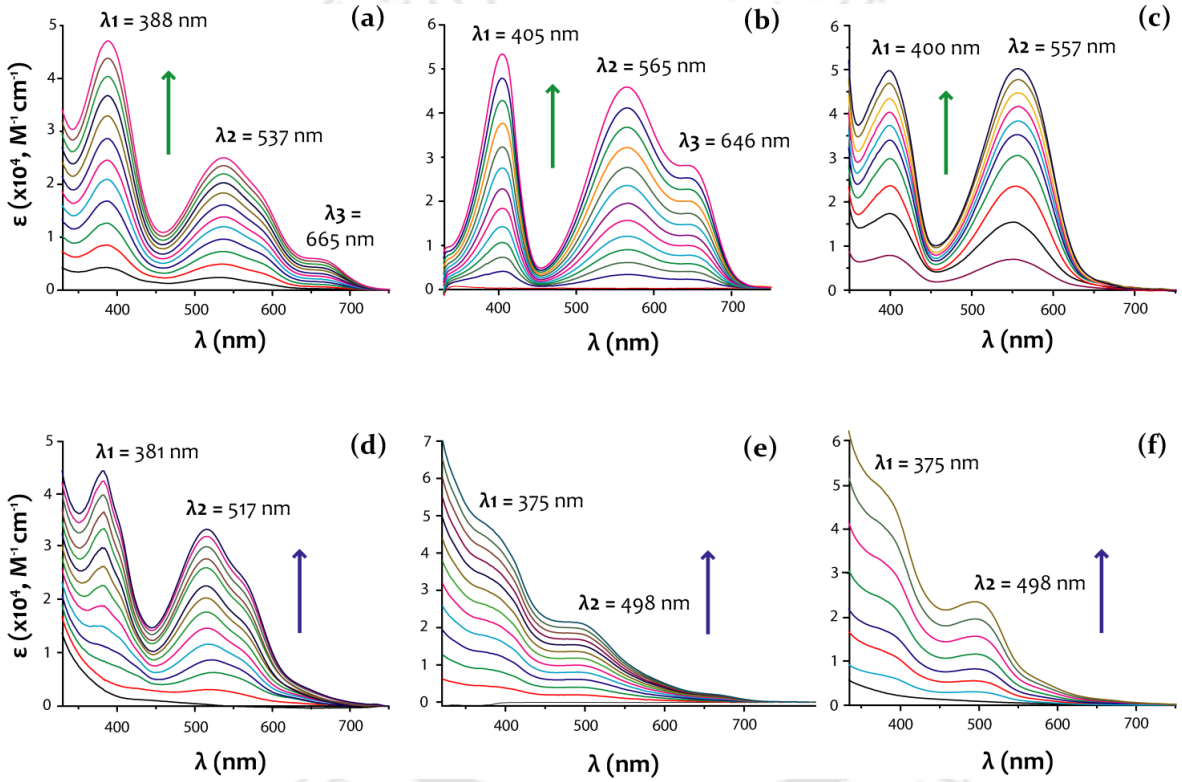

Figure 4.2 UV/Vis titration of $\mathbf{L_3}$ (10 μM) in various aprotic solvents upon addition of standard F^- solution (10 mM); (a) in DMSO, (b) in acetone, (c) in THF, (d) in DMF, (e) in MeCN and (f) in dioxane.

The selectivity and anion–π CT character of $\mathbf{L_3}$ in response to F^- was further confirmed by comparison to a control receptor, $\mathbf{CL_3}$ (ethyl ester of carboxy-dinitrobenzene) that cannot differentiate F^- from other basic anions, such as AcO^- and $H_2PO_4^-$, producing optical signal from colourless to blue irrespective of solvent choice and polarity indicating the worth of preorganized hydrogen bonding scaffold in $\mathbf{L_3}$ towards selective and solvatochromic F^- recognition (Figure 4.3). It is worth mentioning that, titration of $\mathbf{L_3}$ with TBAOH resulted in similar spectral behaviour as observed with F^-, further confirmed the existence of anion–π

CT interaction. Furthermore, progressive additions of protic solvent (such as methanol or water) resulted in gradual attenuation of the CT bands perhaps due to the capability of protic solvents to compete for F^- along with amide -NH functions and π-acidic arenes, disfavouring the formation of anion—π CT complexes in solution (Annexure 4). Thus, the nature of the chromophoric change can be attributed to strong F^-—π CT interaction wherein F^- is hydrogen bonded to the amide -NH functions and interacts significantly with the π-acidic aryl functions as confirmed by ^{1}H NMR spectroscopy**.**

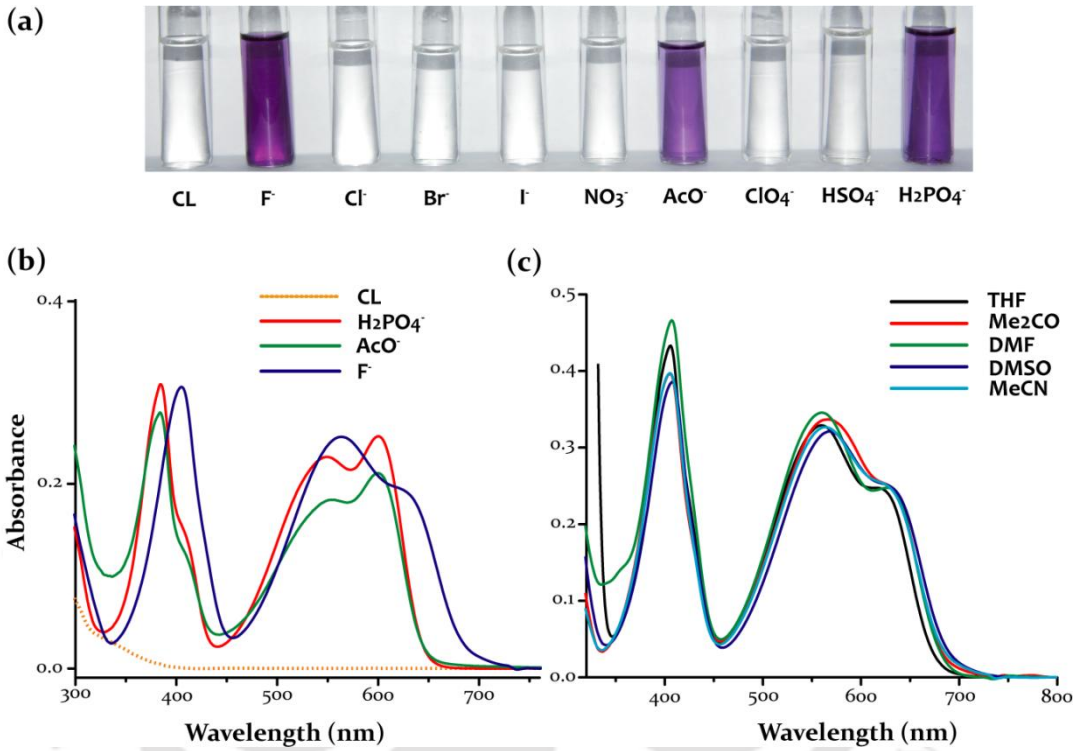

Figure 4.3 (a) Optical colour changes observed with the addition of excess anions to the acetonitrile solutions of $\mathbf{CL_3}$; (b) UV/Vis spectral changes of $\mathbf{CL_3}$ in acetonitrile solution upon addition of TBA salts of strongly basic anions such as, F^-, AcO^- and $H_2PO_4^-$; (c) No observable changes in λ_{max} values were recorded in the UV/Vis spectra of $\mathbf{CL_3}$ in various aprotic solvents upon addition of excess TBAF.

4.3 F^-–binding study by NMR spectroscopy

The selectivity of $\mathbf{L_3}$ towards fluoride was further confirmed by ^{1}H NMR experiments. In a qualitative experiment, addition of equivalent amount TBAF to a solution of $\mathbf{L_3}$ in DMSO-d_6, resulted in a significant downfield shift of -NH and *ortho*-CH resonances with a $\Delta\delta$ value of 3.55 and 0.72 ppm respectively (Annexure 4), indicative of a structural alteration of the receptor side arms that could influence both the -NH and *ortho*-CH protons to encapsulate F^- within the receptor cavity. The encapsulation of F^- in a 1:1 host/guest stoichiometry has been confirmed by quantitative ^{1}H NMR and 2D-NOESY NMR experiments in DMSO-d_6 (Figure

4.4). The ^{1}H NMR titration curve gives the best fit for 1:1 binding model for host to guest, in agreement with Job's plot analysis showing a maximum at 0.55 and an association constant (log *K*) value of > 7.0 (error limit ≤ 15%). ^{19}F NMR analysis of a 1:1 receptor-F^- solution in DMSO-d_6 showed an upfield shift of 1.726 ppm relative to the free fluoride resonance of TBAF, indicating the participation of the anion in hydrogen bonding with the receptor (Annexure 4). In 2D-NOESY NMR experiments, the free receptor molecule showed some strong NOE couplings between the amide –NH and aryl -CH protons (N-H···H-C) and between the identical set of –NH and aryl –CH protons (N-H···H-N and C-H···H-C) (Figure 4.4d). However, 2D-NOESY NMR analysis of an equivalent mixture receptor-F^- solution showed the absence of through-space N-H···H-C coupling and interactions between the identical set of –NH protons (N-H···H-N) become significantly weaker while C-H···H-C couplings persist (Figure 4.4e), indicating the binding and encapsulation of fluoride within the hydrogen bonding scaffold in a 1:1 host-guest stoichiometry. It is important to mention that unlike the solid-state structure (**L**$_3$•DMSO) the receptor exhibits C_3v symmetry in solution where the tripodal side arms are equivalent with each other and interacts significantly among the different sets of proton. Upon binding and encapsulation of fluoride by –NH and –CH hydrogen bonds, the interactions between the different sets of proton in **L**$_3$ get hindered for which they either found to be absent or become significantly weaker in presence of F^- (Scheme 4.2).

Interestingly, ^{1}H NMR titration of **CL**$_3$ showed a gradual upfield shift of the acidic aryl protons with increasing F^- concentration as prevalent in the CT complexes of tripodal nitro aromatics with halides (Annexure 4). Furthermore, excess addition of other halides and oxoanions to the individual receptor solutions in DMSO-d_6 showed no appreciable change in chemical shift values of the -NH and -CH resonances (Annexure 4), suggesting the non interacting nature or very weak interactions of other anions with **L**$_3$.

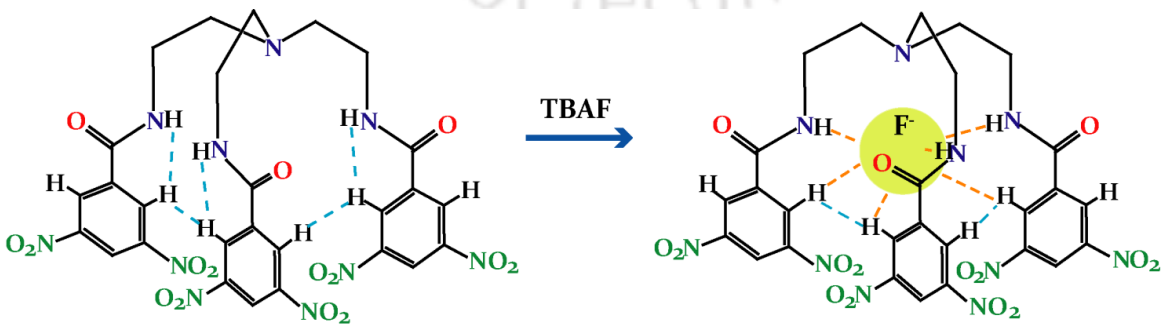

Scheme 4.2 Schematic representation depicting the through-space NOE couplings in **L**$_3$ and observed binding mode of **L**$_3$ with F^- in solution.

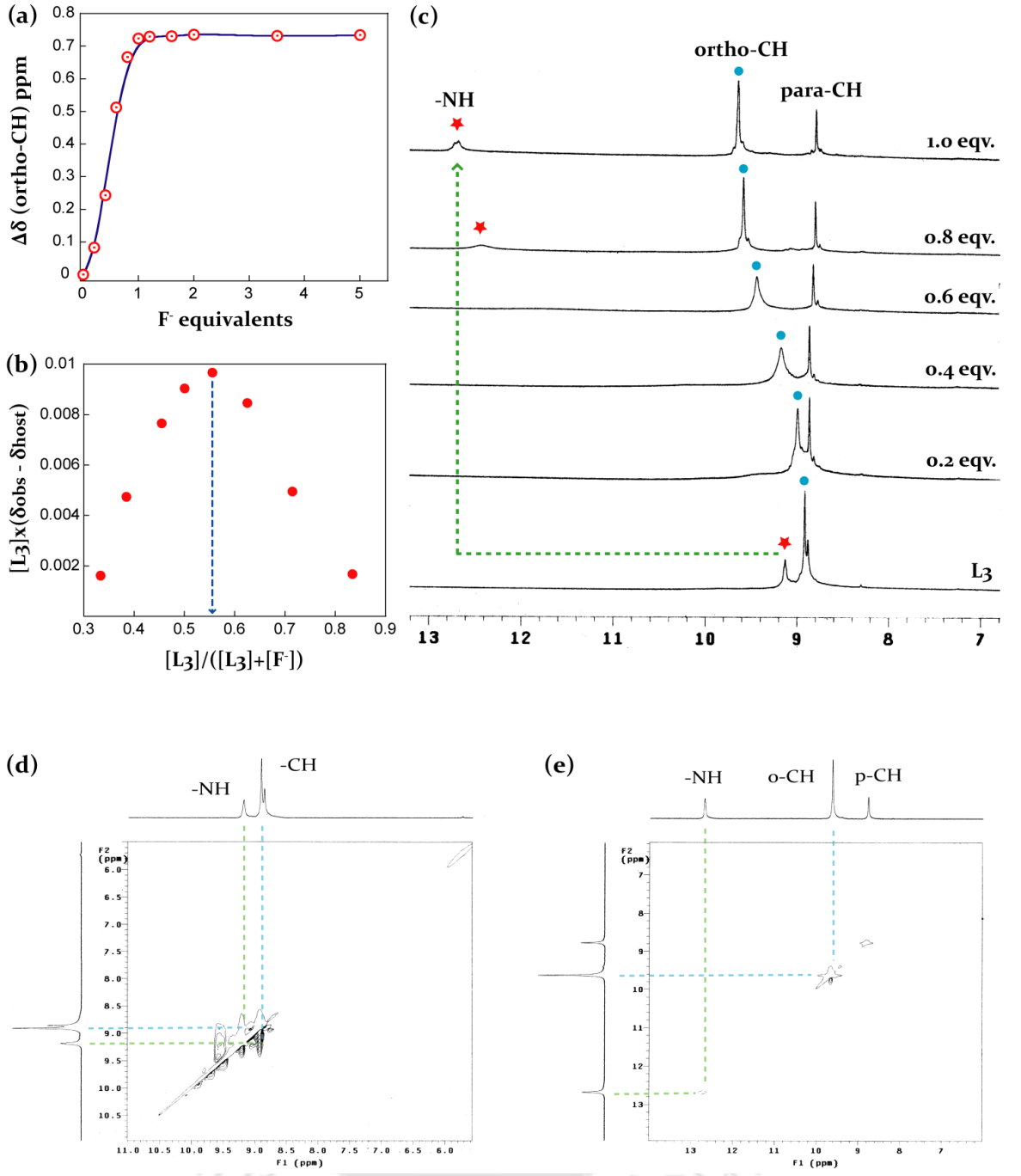

Figure 4.4 (a) Change in chemical shift of ortho–CH proton resonances of $\mathbf{L_3}$ (20 mM) upon titration with TBAF in DMSO-d_6 at 298 K; (b) Jobs plot showing 1:1 host to guest binding; (c) Partial ^{1}H NMR (aromatic region) spectra showing the titration of $\mathbf{L_3}$ with TBAF; (d) 2D NOESY NMR spectrum of $\mathbf{L_3}$ in DMSO-d_6. (e) 2D NOESY NMR spectrum of $\mathbf{L_3}$ in presence of F^- (1 equiv) in DMSO-d_6.

4.4 Crystal structure of receptor L_3, [L_3•DMSO]

Single crystals of $\mathbf{L_3}$ suitable for X-ray diffraction analysis were obtained from a DMSO solution, upon slow evaporation at room temperature. DMSO solvate of $\mathbf{L_3}$ [$\mathbf{L_3}$•DMSO] crystallizes in the triclinic space group *P*-1 with Z=2. Structural elucidation revealed that, the

combined effect of intramolecular hydrogen bonding and aromatic π···π stacking resist the open conformation of the receptor (Figure 4.5a). An amide hydrogen (N8H) and an aryl proton (C22H) from the same receptor side arm is intramolecularly hydrogen bonded to an amide oxygen O6 of another arm *via* N-H···O and C-H···O interactions respectively, [N8···O6 = 2.895(3) Å and C22···O6 = 3.194(3) Å] whereas the aryl function C1g (centroid: C4-C9) from the third receptor side arm is involved in aromatic π···π interaction with ring C2g (centroid: C13-C18) [C1g···C2g = 3.751(3) Å]. Intermolecular short contact analysis (D···A < 4.0 Å) of the structure further shows that, the DMSO oxygen (O16) is hydrogen bonded to an amide proton N5H [N5···O16 = 2.838(3) Å] and an aryl hydrogen C14H [C14···O16 = 3.244(3) Å] from the same flexible side arm of the receptor and also, interacts with the π-acidic aryl function C2g (centroid: C13-C18) of an adjacent receptor unit *via* lp···π interaction [O16···C2g = 3.535 Å]. Additionally, one of the methyl hydrogen C29H(A) of lattice DMSO is in interaction with the amide oxygen O1 [C29···O1 = 3.408(4) Å], resulting in an hydrogen bonded dimer formation with two DMSO and two molecules of **L_3** (Figure 4.5a).

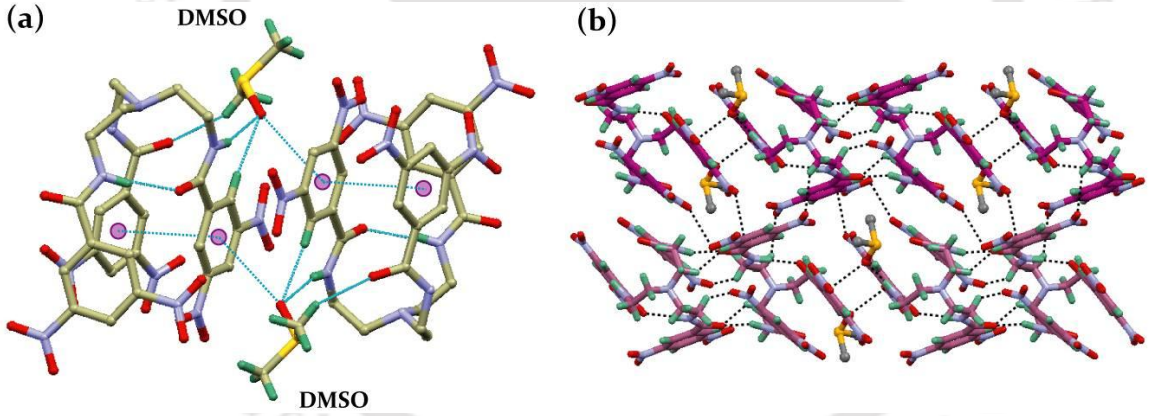

Figure 4.5 (a) X-ray structure of [**L_3**-DMSO] showing the intramolecular H-bonds between the receptor side arms and intermolecular interactions with the lattice solvent; (b) Crystal packing motif of [**L_3**-DMSO] as viewed down the *b*-axis, showing the hydrogen bonds and electron donor-acceptor interactions between two adjacent 1D chains of receptor molecules.

Each solvent-bridged dimer is in association with the adjacent dimeric unit *via* strong N-H···O hydrogen bond that involves interaction between the amide proton N2H with the amide oxygen O11 of two neighbouring dimers [N2···O11 = 2.869(3) Å]. The association between solvent-bridged dimers is further stabilized by two aliphatic C-H···O interactions in which the methylene protons C1H(A) and C20H(A) from two different arms of a receptor dimer (DMSO bridged) make contacts with the amide oxygen O11 and nitro oxygen O2 of another dimeric unit [C1···O11 = 3.429(2) Å and C20···O2 = 3.131(3) Å] resulting in a 1D

chain of oppositely oriented receptor units along c-axis (Figure 4.5b). However, the overall packing of the crystal is additionally governed by three aliphatic C-H···O-(nitro) interactions and n→π* (O:→C) interactions where lone pair of oxygen from nitro group is added to C=C or C=O double or partially double bonds, resulting in the formation of a 2D hydrogen bonded sheet like structure when viewed down the crystallographic b-axis (Figure 4.5b).

4.5 Solvatomorphism in F^-–encapsulated complex, TBA[L_3(F)]

Efforts were made to examine the solid-state binding of F^- with receptor **L_3**, following the solvatochromism of **L_3** towards selective recognition of F^- in the solution-state studies. Slow evaporation of individual solution mixtures of **L_3** and excess TBAF (10 equiv) in polar aprotic solvents *viz.* MeCN, DMF, THF and DMSO resulted in solvatomorphs of F^-–encapsulated complex (at room temperature) with the composition TBA[**L_3**(F)]•H_2O (**3a-I**), TBA[**L_3**(F)]•DMF (**3a-II**) TBA[**L_3**(F)]•3THF (**3a-III**) and TBA[**L_3**(F)]•2DMSO•$4H_2O$ (**3a-IV**) respectively, as single crystals suitable for X-ray diffraction analysis. Complexes **3a-I** and **3a-III** crystallized in monoclinic system with $P2_1/c$ space group whereas, **3a-II** and **3a-IV** crystallized in triclinic system with *P*-1 space group. The crystallographic data and refinement details of solvatomorphs **I-IV** are given in Table 4.1. In complexes **3a-III** and **3a-IV**, the lattice solvent molecules were found to be highly disordered and to gain a better insight into the nature of the solvents included in the crystal lattice; we have carried out thermo gravimetric analysis (TGA) of the isolated crystals. PLATON/SQUEEZE was performed to refine the host framework in **3a-III** along with the entrapped F^- ion and TBA cation and by excluding the disordered solvent (THF) electron densities. These calculations amount to 130 electrons per molecule and may be attributed to three disordered THF molecules, further supported by the TGA curve of the isolated crystals of **3a-III** (Annexure 4). TGA of **3a-III** showed a three step weight loss of 11.40% (–0.71 mg) for the three lattice THF molecules and TGA of **3a-IV** showed a weight loss of 15.72% (–1.51 mg) for the lattice solvent molecules close to the calculated value of 16.19%.

Structural analyses revealed that irrespective of solvent of crystallization, F^- is encapsulated within the receptor scaffold governed by six strong hydrogen bonds donated from the amide -NH protons and three aryl *ortho*-CH protons (Figure 4.6). The encapsulated F^- ion is hydrogen bonded to –NH functions with an average N···F^- distances of 2.706, 2.679, 2.705 and 2.708 Å in solvatomorphs **I-IV** respectively, whereas the coordinating *ortho*-CH protons interact with an average C···F^- distances of 2.998, 2.929, 2.998 and 2.993 Å in **I-IV** respectively, demonstrating the strong binding of F^- with **L_3** in the solid-state (Table 4.2). The active participation of the *ortho*-CH protons in F^- binding is primarily due to the

presence of electron withdrawing nitro functions in the aryl terminals of the receptor which render these protons considerably acidic towards forming strong C-H···F^- hydrogen bonds. Interestingly in **3a-II**, the encapsulated F^- interacts with two aryl functions *via* off-centre F^- ···π interactions with distances of 4.007 and 4.054 Å respectively (Figure 4.6b). Identical F^- ···π interaction has also been observed in **3a-IV**, where the encapsulated F^- interacts with an aryl function with a contact distance of 4.039 Å (Annexure 4). The FT-IR spectra of the complexes, **I-IV** show a considerable shift up to 20 cm^{-1} for the C=O frequency relative to free $\mathbf{L_3}$ due to the formation of strong N-H···F^- hydrogen bonds (Annexure 4).

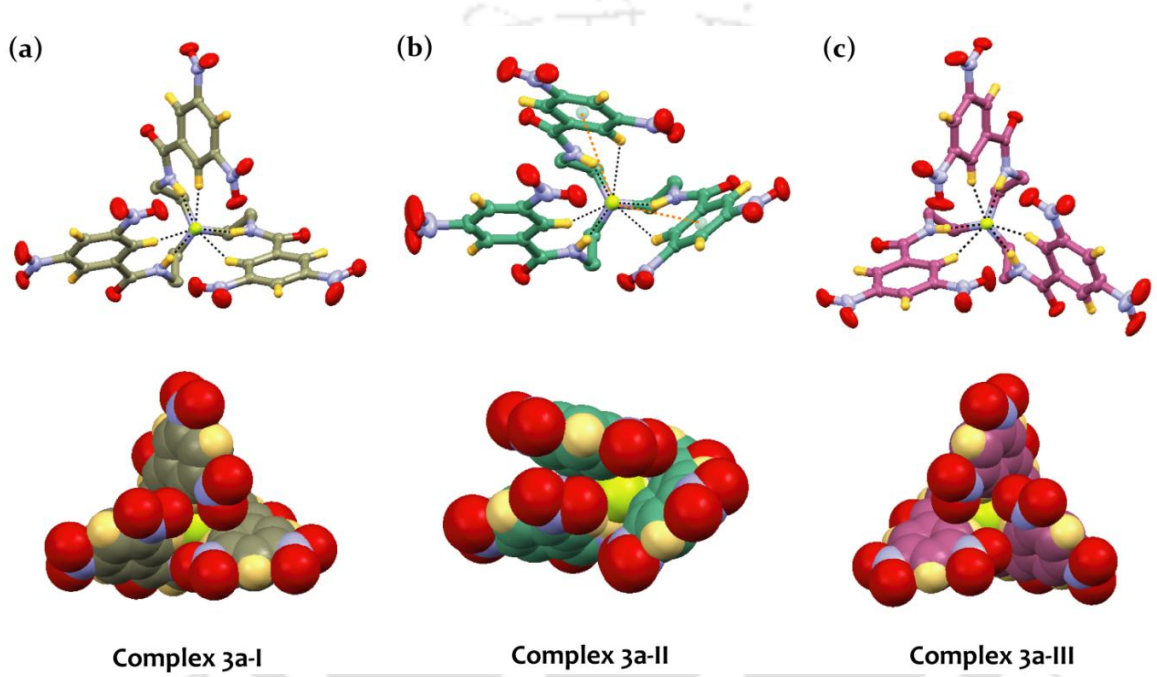

Figure 4.6 X-ray structures (thermal ellipsoid plot with 30% probability and space fill model) of solvatomorphs of F^-–encapsulated complex showing binding and encapsulation of F^- within the receptor cavity; (a) TBA[$\mathbf{L_3}$(F)]•H_2O (**3a-I**), (b) TBA[$\mathbf{L_3}$(F)]•DMF (**3a-II**), (c) TBA[$\mathbf{L_3}$(F)]•3THF (**3a-III**). TBA cation and solvent molecule(s) are omitted for clarity in each case.

Following the solvatomorphism of F^-–encapsulated complex, it can be vaguely argued that crystallization of a lattice water in complex **3a-I**, suggest weak interactions of the F^-–complex with MeCN and thereby, the shortest λ_{max} values for the CT absorptions were observed in MeCN. In contrast, crystallization of three THF molecules in the solvated complex **3a-III**, suggest significant interactions of the F^-–complex with THF and thereby, the longest λ_{max} values for the CT absorptions were observed in THF followed by DMSO, DMF and MeCN. Furthermore, the presence of one DMF and two DMSO molecules in the crystals of **3a-II** and **3a-IV**, respectively, indicates comparatively better interactions of the F^-–complex with the respective solvents and thereby, demonstrating a gradual bathochromic shift of the CT absorptions relative to MeCN.

Table 4.1 Crystallographic parameters and refinement details of solvated receptor [**L$_3$**·DMSO] and solvates of TBA[**L$_3$**(F)] complex (**3a**, **I-IV**).

Parameters	**L$_3$**·DMSO	**3a-I**	**3a-II**	**3a-III**	**3a-IV**
Formula	$C_{29}H_{30}N_{10}O_{16}S$	$C_{43}H_{60}FN_{11}O_{16}$	$C_{46}H_{67}FN_{12}O_{16}$	$C_{43}H_{60}FN_{11}O_{15}$	$C_{47}H_{72}FN_{11}O_{21}S_2$
Fw	806.70	1006.02	1063.12	990.02	1210.30
Cry. system	Triclinic	Monoclinic	Triclinic	Monoclinic	Triclinic
Space group	*P*-1	$P2_1/c$	*P*-1	$P2_1/c$	*P*-1
a/Å	11.2942(3)	16.129(3)	10.0759(3)	10.0293(9)	9.8296(6)
b/Å	12.4744(4)	15.781(2)	16.7929(6)	33.293(3)	19.1561(13)
c/Å	12.8671(4)	25.393(4)	16.8986(5)	19.4982(17)	19.1973(13)
α/^{o}	84.723(2)	90.00	79.197(2)	90.00	61.201(3)
β/^{o}	79.650(3)	127.592(9)	78.461(3)	90.382(6)	83.109(4)
γ/^{o}	88.404(2)	90.00	89.753(2)	90.00	89.652(4)
V/Å^3	1775.65(9)	5121.4(15)	2750.23(16)	6510.4(10)	3139.3(4)
Z	2	4	2	4	2
D_c/g cm^{-1}	1.509	1.305	1.284	1.010	1.280
μ (mm^{-1})	0.180	0.103	0.100	0.079	0.166
T/^{o}K	298(2)	298(2)	298(2)	298(2)	298(2)
θ max.	28.29	24.89	28.39	24.87	24.92
Total reflns	13679	35440	29276	73179	40060
Ind. reflns	8734	8854	13732	11177	10638
Obs. reflns	7605	7719	11770	9245	9471
N_{par}	520	644	683	635	748
R_1, $I > 2\sigma(I)$	0.0508	0.0603	0.0693	0.0814	0.0914
wR_2	0.1510	0.2034	0.1841	0.1952	0.1859
GOF (F^2)	0.911	1.008	1.011	1.018	1.011

4.6 Binding discrepancy of F$^-$ in complex [L$_3$•KF(H$_2$O)$_2$], (3b)

It is obvious that, receptors for anions such as fluoride should target the alkali metal salts rather than the quaternary ammonium salts because in nature, fluoride exists mostly as its Na/K salts (minerals such as villiaumite and carobbiite). Thus, attempts were made to obtain single crystals of alkali fluoride complexes of **L$_3$**, in order to explore the structural aspects of F$^-$-binding when NaF/KF is used as a source for complexation of F$^-$ with **L$_3$**. Single crystals of **3b** suitable for X-ray diffraction analysis was obtained from an equivalent solution mixture of KF (aqueous solution) added into an acetonitrile solution of **L$_3$**. However, efforts to obtain single crystals of NaF complex of **L$_3$** were not fruitful.

Crystal structure analysis of **3b** showed the formation of 1:1 stoichiometric complex, which crystallizes in triclinic space group *P*-1 with Z=2 (Table 4.3). Identical to (**L$_3$**•DMSO), the receptor unit is conformationally locked by intramolecular N-H···O, C-H···O and π···π interactions between the receptor side arms [N2···O6 = 2.904(3) Å, C9···O6 = 3.188(4) Å, C2g···C3g = 3.750 Å]. Complementary N-H···O and C-H···O hydrogen bonding between two arms of the receptor presumably assist one of the aryl functions of intramolecularly hydrogen bonded receptor side arms to be in closer proximity with the aryl function of third arm resulting in a significant π···π interaction (Figure 4.7a). Unlike the F^-–encapsulated complexes (**3a, I-IV**), K–F is bound as a contact ion-pair with **L$_3$** where K^+ is coordinated to two water molecules [K^+···F^- = 1.494(3) Å, K^+···O18 = 1.788(5) Å and K^+···O19 = 1.778(6) Å]. From the short contact analysis, it is evident that a hydrated KF contact ion-pair is hydrogen bonded to two adjacent receptor molecules *via* an amide N-H···F^-, an aryl C-H···F^- and a lp(F^-)···π interaction [N5···F1 = 2.841(4) Å; C14···F1 = 3.240(4) Å and F1···C2g = 3.527 Å] resulting in a dimeric association of the receptor molecules bridged by two coordinated KF(H_2O)$_2$ moieties (Figure 4.7a). Similar modes of interaction have previously been observed in (**L$_3$**•DMSO) involving the oxygen of DMSO in replace of F^- ion. Expansion through hydrogen bond shows that, two such dimeric units are further associated with each other by an amide N-H···O and an aliphatic C-H···O interactions [N8···O1 = 2.860(3) Å, C19···O1 = 3.432(4) Å, C19···O2 = 3.622(6) Å and C2···O13 = 3.134(6) Å] resulting in a 1D chain of inversely oriented receptor molecules in association with hydrogen bonded KF(H_2O)$_2$ moieties diagonally along *ac*-axis (Figure 4.7b). Furthermore, two such 1D chains are interlinked among themselves by multiple C-H···O-(nitro) and n→π* (O:→N/C) interactions which eventually governs the overall packing of the crystal (Figure 4.7c).

In the ^{1}H-NMR spectrum of isolated crystals of **3b** (DMSO-d_6), the amide –NH resonance could not be observed and the *ortho*-CH resonance showed a minor downfield shift of 0.28 ppm relative to the F^-–encapsulated complex which showed a huge downfield shift of 3.34 ppm and 0.70 ppm for –NH and *ortho*-CH resonances (Figure 4.8). Similar spectral changes have also been recorded in CD_3CN (Annexure 4), suggesting that KF can even compete and form hydrogen bonds with the receptor in solvents such as DMSO which is highly capable of interacting with **L$_3$**. However, in the attempted crystallization of **3b** from DMSO, the receptor molecule tend to get solvated with time which can be attributed to an additional C-H···O interaction between the lattice solvent and an amide oxygen of **L$_3$** in association with other noncovalent interactions. Overall, from the ^{1}H-NMR analyses, it is customary to claim that complexation of F^- involving three N-H···F^- and three C-H···F^- hydrogen bonds result in

a larger deshielding of the coordinating protons in F^-–encapsulated complex as compared to the KF complex which involves side-cleft binding of hydrated KF *via* participation of one N-H···F^-, one C-H···F^- and lp(F^-)···π interactions. Thus, a binding discrepancy of F^- has been observed in solid-state as well as in solution, when tetrabutylammonium fluoride (TBAF) and potassium fluoride (KF) salts were individually employed for the coordination of F^- anion by **L_3**.

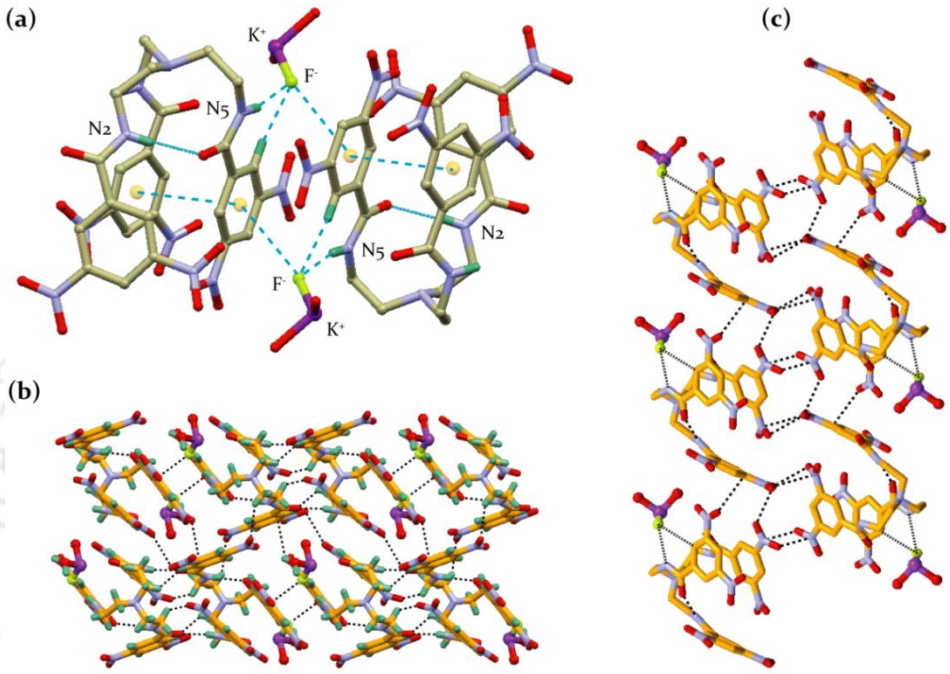

Figure 4.7 (a) X-ray structure of complex **3b** showing the intramolecular hydrogen bonding and interactions with the KF(H_2O)$_2$ adduct; (b) Crystal packing of **3b** as viewed down the *a*-axis showing the hydrogen bonding and electron donor-acceptor interactions between two adjacent 1D chains of receptor molecules; (c) View of the n→π* (O:→N/C) electron donor-acceptor interactions.

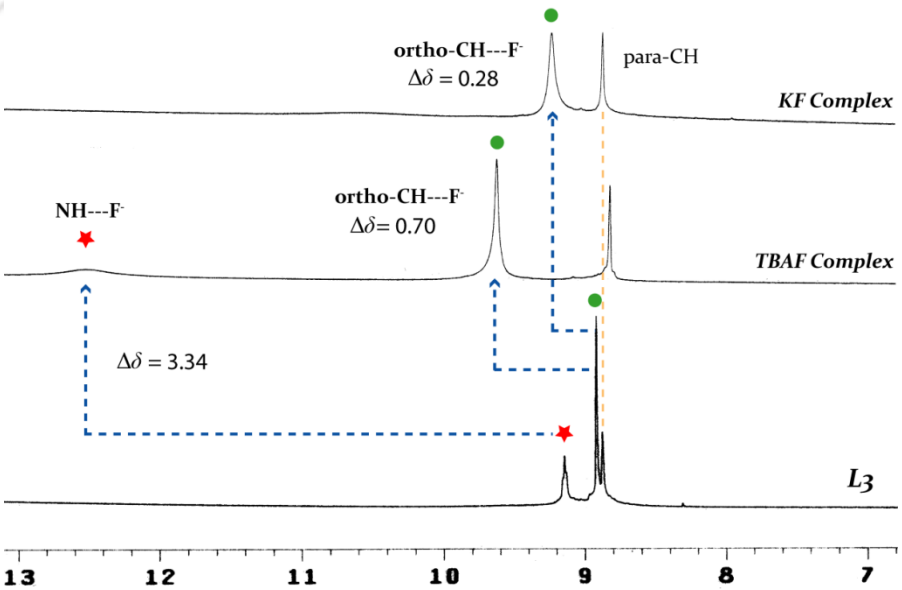

Figure 4.8 Comparison of the partial ^{1}H-NMR spectra (aromatic region) of **L_3** with an F^-–encapsulated complex, **3a** and KF complex, **3b** in DMSO-d_6 at 298 K.

Table 4.2 Hydrogen bonding of encapsulated F^- ion in solvates of TBA[**L**(F)] complex (**3a**, **I-IV**).

Solvates of TBA[**L**(F)]	D-H···F	*d*(H···F)/Å	*d*(D···F)/Å	∠D-H···F/°
3a-I	N2-H···F1	1.84(2)	2.683(4)	165(2)
TBA[**L**(F)]•H_2O	N5-H···F1	1.87(2)	2.718(3)	167(2)
	N8-H···F1	1.88(2)	2.718(3)	163(2)
	C9-H···F1	2.13(2)	3.012(3)	156(2)
	C18-H···F1	2.14(2)	2.970(4)	147(2)
	C27-H···F1	2.10(2)	3.012(4)	164(2)
3a-II	N2-H···F1	1.87(1)	2.674(3)	154(2)
TBA[**L**(F)]•DMF	N5-H···F1	1.83(2)	2.649(3)	156(2)
	N8-H···F1	1.95(1)	2.716(3)	147(2)
	C9-H···F1	2.25(2)	2.865(4)	122(2)
	C18-H···F1	2.18(1)	2.970(3)	142(2)
	C27-H···F1	2.38(1)	2.954(3)	119(2)
3a-III	N2-H···F1	1.82(2)	2.674(4)	169(2)
TBA[**L**(F)]•3THF	N5-H···F1	1.83(2)	2.687(4)	170(3)
	N8-H···F1	1.89(2)	2.755(4)	173(2)
	C9-H···F1	2.09(2)	2.984(5)	161(3)
	C18-H···F1	2.08(2)	2.985(5)	161(3)
	C27-H···F1	2.14(2)	3.027(5)	158(3)
3a-IV	N2-H···F1	1.85(2)	2.703(5)	170(3)
TBA[**L**(F)]•2DMSO·4H_2O	N5-H···F1	1.85(3)	2.696(5)	167(2)
	N8-H···F1	1.90(2)	2.726(3)	158(3)
	C5-H···F1	2.12(2)	3.027(5)	163(3)
	C14-H···F1	2.13(3)	3.025(5)	160(2)
	C23-H···F1	2.35(2)	2.929(4)	120(3)

4.7 Structural aspects of anion binding with protonated L_3

Four anion complexes of protonated $\mathbf{L_3}$ (**3c-3f**) were obtained as single-crystals suitable for X-ray diffraction analysis by slow evaporation of individual DMSO solutions of $\mathbf{L_3}$ in presence of different mineral acids (HCl, HBr, $HClO_4$ and H_2SO_4). Structural information obtained from XRD analysis of the isolated crystals provide insight into the proper binding topology of halides (Cl^- and Br^-) and oxyanions (ClO_4^- and HSO_4^-) with the protonated receptor molecule. Structural analyses revealed that, complexation of anion(s) are primarily governed by N-H···A^- and C-H···A^- interactions involving multiple receptor cations. In all four complexes, the receptor cavity is conformationally locked by intramolecular $(N–H)^+$···O hydrogen bonding formed between the *endo*-oriented hydrogen of protonated bridgehead

nitrogen and one of the amide oxygen of protonated receptor. In addition, the complexes are further stabilized by several intermolecular C-H···O-(nitro) hydrogen bonds, which induce rigidity to the formed cationic podand and serve as the foundation for crystallization of the desired complexes. The crystallographic data and refinement details of charged anion complexes **3c**-**3f** are given in Table 4.3.

4.7.1 Chloride complex $[(HL_3)^+ \bullet Cl^-]$, (3c)

Complex **3c** crystallizes in triclinic space group *P*-1 and the asymmetric unit contains two symmetry independent receptor cations ($Z' = 2$) and two chloride anions. In both the conformers (**C1** and **C2**), the *endo*-oriented proton of the apical amine is in strong intramolecular $(N–H)^+\cdots O$ hydrogen bonding with one of the amide oxygen of receptor cation [N1···O11 = 2.718(2), ∠N1-H···O11 = 151°(2) and N11···O21 = 2.774(4), ∠N11-H···O21 = 156°(2)]. Both the chloride ions, $Cl^-(1)$ and $Cl^-(2)$ are in interaction with two adjacent receptor cations of dissimilar conformations with a five-point attachment each (Figure 4.9a) *via* three N–H···Cl^- and two C–H···Cl^- interactions having an average donor-to-acceptor distance of 3.268 (N···Cl^-) and 3.589 Å (C···Cl^-) respectively (Table 4.4). Examination of the coordination environment of the anion revealed that the amide hydrogen N8H and aryl proton C23H of conformer **C1** are in coordination with $Cl^-(1)$ whereas the hydrogen atoms N2H, N5H and C5H are in interaction with $Cl^-(2)$. In a similar fashion, the amide hydrogen N12H, N18H and aryl proton C36H of the other conformer **C2** provides a three point coordination to $Cl^-(1)$ while N15H and C41H make interactions with $Cl^-(2)$ completing the five-point attachment on each chloride anion (Figure 4.9a).

4.7.2 Bromide complex $[(HL_3)^+ \bullet Br^-]H_2O$, (3d)

Complex **3d** crystallizes in monoclinic space group $P2_1/c$ and the asymmetric unit contains two symmetry independent receptor cations ($Z' = 2$) and two bromide anions with two lattice water molecules (O31 and O32) as solvent of crystallization. Identical to complex **3c**, intramolecular $(N–H)^+\cdots O$ hydrogen bonding involving the *endo*-oriented apical proton and an amide oxygen is also prevalent in both the conformers (**C1** and **C2**) of complex **3d** (N1···O6 = 2.903(4), ∠N1-H···O6 = 152°(4) and N11···O21 = 2.868(4), ∠N11-H···O21 = 147°(3)). Binding of bromide with adjacent receptor cations clearly showed that, bromide ions $Br^-(1)$ and $Br^-(2)$ are in interaction with two receptor cations of identical symmetry with a five-point attachment each. Two amide protons N12H, N18H and an aryl proton C32H from a receptor cation with conformation **C2,** provides a three-point coordination to $Br^-(1)$ whereas hydrogen atoms N15H and C41H of another receptor cation with identical conformation provides the other two contacts on $Br^-(1)$ (Figure 4.9b). However, in case of $Br^-(2)$, two adjacent receptor cations of conformation **C1** provide a four-point contact *via*

one N–H···Br^- and one C–H···Br^- interactions each, while the fifth coordination contact is provided by a lattice water molecule O31 (Figure 4.9c) which is in strong hydrogen bond interaction with the amide hydrogen N8H [N8···O31 = 2.952(7) Å and ∠N8-H···O31 = 171°(4)].

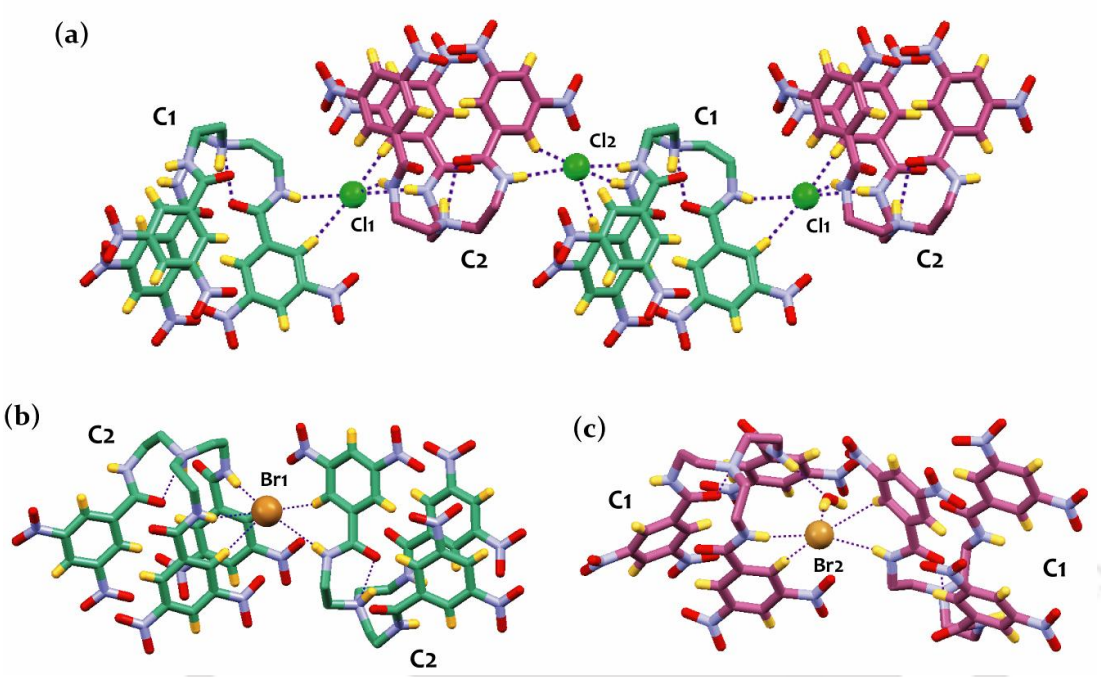

Figure 4.9 (a) X-ray structure of complex **3c** depicting the hydrogen bonding contacts on Cl^- ions, Cl^-(1) and Cl^-(2) with two symmetry independent receptor cations; (b) and (c) X-ray structure of complex **3d** is depicting the hydrogen bonding contacts on Br^- ions, Br^-(1) and Br^-(2) respectively with two symmetry identical receptor cations. Symmetry independent receptor cations are shown in different colours.

4.7.3 Perchlorate complex $[(HL_3)^+ \bullet ClO_4^-]H_2O \bullet DMSO$, (3e)

Complex **3e** crystallizes in triclinic space group *P*-1 with one disordered DMSO and a water molecule as solvent of crystallization. In addition to electrostatic $(N–H)^+$···O hydrogen bonding [N1···O1 = 2.742(5); ∠N1-H···O1 = 168°(3)], there exists an intramolecular N–H···O hydrogen bond between an amide hydrogen N5H and an amide oxygen O11 [N5···O11 = 2.984(4); ∠N5-H···O11 = 167°(4)] from two different arms of a receptor cation. Hydrogen bonding contacts on ClO_4^- showed a six-point coordination of the anion provided by two adjacent receptor cations and lattice DMSO which is hydrogen bonded to the lattice water molecule (Figure 4.10a). Perchlorate oxygen O17 is engaged in a trifurcated hydrogen bonding contact with the amide hydrogen N2H and two methylene protons C2H(A) and C1H(B) from the two coordinating receptor cations, whereas O18 is involved bifurcated interaction with the same amide hydrogen N2H and aryl proton C5H of a receptor cation.

The six-point coordination on ClO_4^- anion is finally satisfied by a weak C-H···O interaction between perchlorate oxygen O16 and a methyl hydrogen C28H(A) of lattice DMSO.

4.7.4 Hydrogensulfate complex $[(HL_3)^+ \bullet HSO_4^-]$DMSO, (3f)

Complex **3f** crystallizes in monoclinic space group *Cc* with one disordered DMSO molecule as solvent of crystallization. Due to disorder, it was not possible to locate the hydrogen of the monovalent sulfate anion (HSO_4^-) in order to unambiguously determine the degree of protonation and charge upon the anion. However, structural elucidation revealed the 1:1 stoichiometric salt formation confirming the HSO_4^- complex of protonated $\mathbf{L_3}$. Similar to the halide complexes, intramolecular $(N–H)^+\cdots O$ hydrogen bonding is also prevalent in complex **3f** [N1···O6 = 2.816(5); ∠N1-H···O6 = 154°(4)]. Hydrogen bonding contacts on HSO_4^- showed a seven-point coordination of the anion provided by three adjacent receptor cations and lattice DMSO (Figure 4.10b). Sulfate oxygen O16 behaves as a trifurcated hydrogen bond acceptor by interacting with the amide proton N2H and two aryl protons C9H and C23H from two coordinating receptor cations whereas O18 is involved in bifurcated interaction with the amide hydrogen N2H and methylene proton C1H(B) of the same receptor cation. Finally, O17 interacts with the amide hydrogen N5H of a third coordinating receptor cation and methyl hydrogen C28H(C) of lattice DMSO completing the seventh coordination contacts on HSO_4^-.

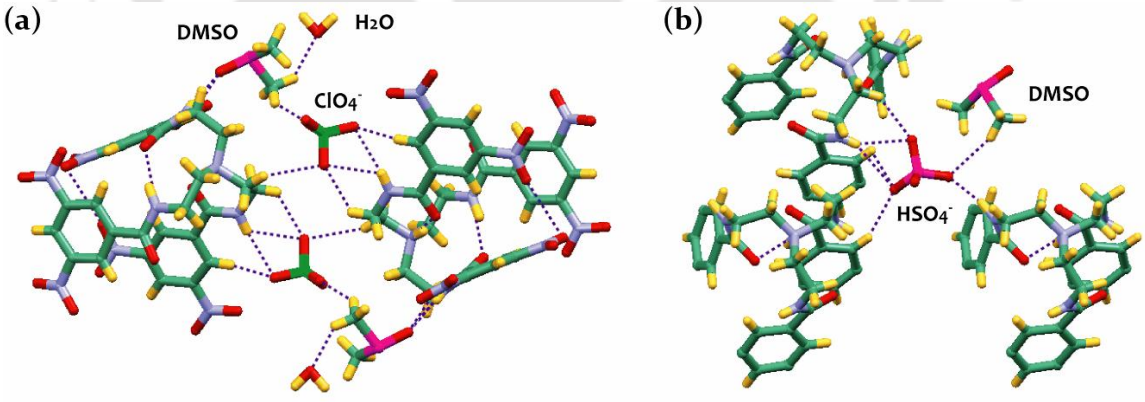

Figure 4.10 (a) X-ray structure of complex **3e** depicting the hydrogen bonding contacts on ClO_4^- ion with two receptor cations and lattice DMSO; (b) X-ray structure of complex **3f** is depicting the hydrogen bonding contacts on HSO_4^- ion with three receptor cations and lattice DMSO.

4.8 Transformation of charged anion complexes into F^-–encapsulated complex

In a proof-of-concept experiment performed, the high selectivity of $\mathbf{L_3}$ towards recognition of F^- has been efficiently employed in the transformation of charged anion complexes (**3c** and **3f**) into F^-–encapsulated complex, by charging an excess of F^- ions to the individual solutions of **3c** and **3f** in DMSO. Upon addition of excess F^- ions, the colourless solutions of

3c and **3f** becomes deeply coloured, indicating a solution-state transformation of the charged anion complexes into F^-–encapsulated neutral complex by a solution-state deprotonation of the protonated receptor molecules induced by the presence of basic F^- ions. Furthermore, room temperature evaporation of the solution mixtures yielded yellow crystals of F^-–encapsulated complex, which were confirmed by ^{1}H NMR and ^{19}F NMR (DMSO-d_6) of the isolated crystals.

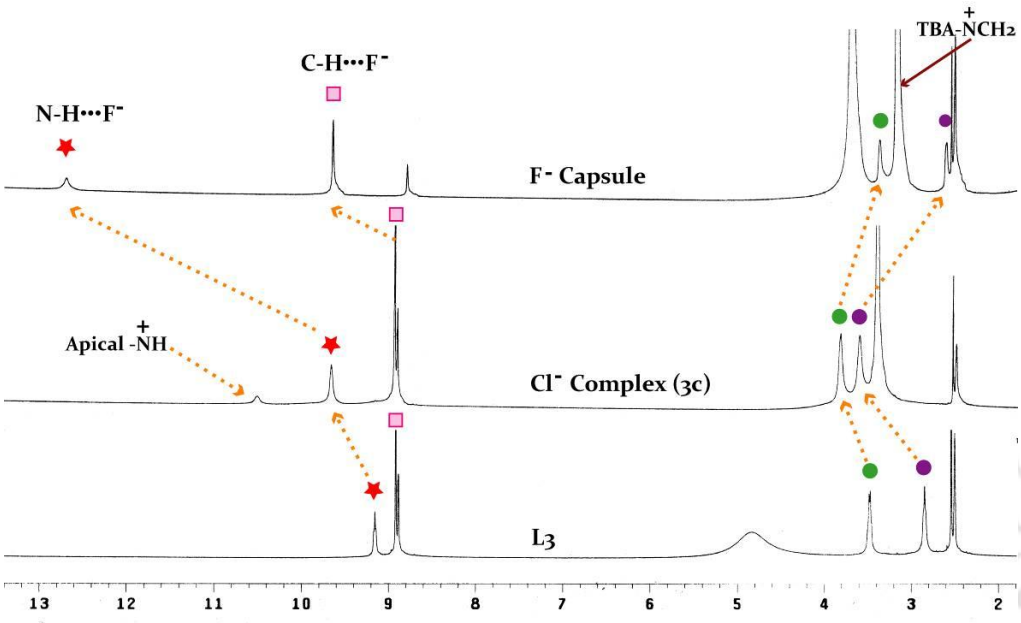

Figure 4.11 Partial ^{1}H-NMR spectra showing the formation of F^-–encapsulated complex upon addition of 5 equivalents of TBAF to a DMSO-d_6 solution of complex **3c**, which is compared with the free receptor, $\mathbf{L_3}$ (DMSO-d_6).

To further explore the transformation process, we have performed ^{1}H-NMR titration experiments of complexes **3c** and **3f** with increasing equivalents of TBAF in DMSO-d_6 (Figures 4.11 and 4.12). Appreciable downfield shift of the aliphatic -NCH_2 protons ($\Delta\delta$ ppm: 0.77 in **3c**, 0.80 in **3d**, 0.81 in **3e** and 0.79 in **3f** *w.r.t.* $\mathbf{L_3}$) in the ^{1}H-NMR spectra of the charged anion complexes **3c**-**3f** indicate the influence of protonation at the apical nitrogen on the neighbouring methylene protons. Furthermore, observable downfield shift of the amide –NH protons ($\Delta\delta$ ppm: 0.51 in **3c**, 0.42 in **3d**, 0.37 in **3e** and 0.43 in **3f** *w.r.t.* $\mathbf{L_3}$) indicate interactions of the respective anion with the amide functions of protonated $\mathbf{L_3}$ as observed in the solid-state structures of **3c**-**3f**. In the quantitative ^{1}H-NMR titration experiments, addition of one equiv. of F^- to a solution **3c** or **3f**, resulted in a considerable upfield shift of the aliphatic -NCH_2 proton resonances with $\Delta\delta$ values of 0.85 and 0.87 ppm for **3c** and **3f** respectively, and noticeable upfield shift of the amide –NH resonance indicated in situ formation of the charge neutral receptor $\mathbf{L_3}$ in solution (Figure 4.12). In addition, the signal for the apical proton (protonated apical nitrogen) which resonates at 10.52 and 9.80 ppm in

3c and **3f** respectively disappear upon addition of F^-, further confirmed the in situ generation of neutral $\mathbf{L_3}$. With second equiv. of F^- addition, the amide –NH signal disappeared whereas the signal for *ortho*-CH protons gets broadened and experience a slight downfield shift, which could be due to binding induced broadening of signals upon recognition of F^- (Figure 4.12). Further addition of F^- ions (upto five equiv.) resulted in gradual and appreciable downfield shift of *ortho*-CH proton resonances ($\Delta\delta$ = 0.68 ppm in case of **3c** and $\Delta\delta$ = 0.70 ppm in case of **3f**) with reappearance of –NH signal at four equiv. of F^- ($\Delta\delta$ = 2.95 ppm in case of **3c** and $\Delta\delta$ = 2.84 ppm in case of **3f**), indicating the formation of F^-–encapsulated complex. The final spectrum thus obtained at five equiv. of F^- addition, matches perfectly with the ^{1}H-NMR spectrum of the isolated crystals of F^-–encapsulated complex (Figures 4.11 and 4.12).

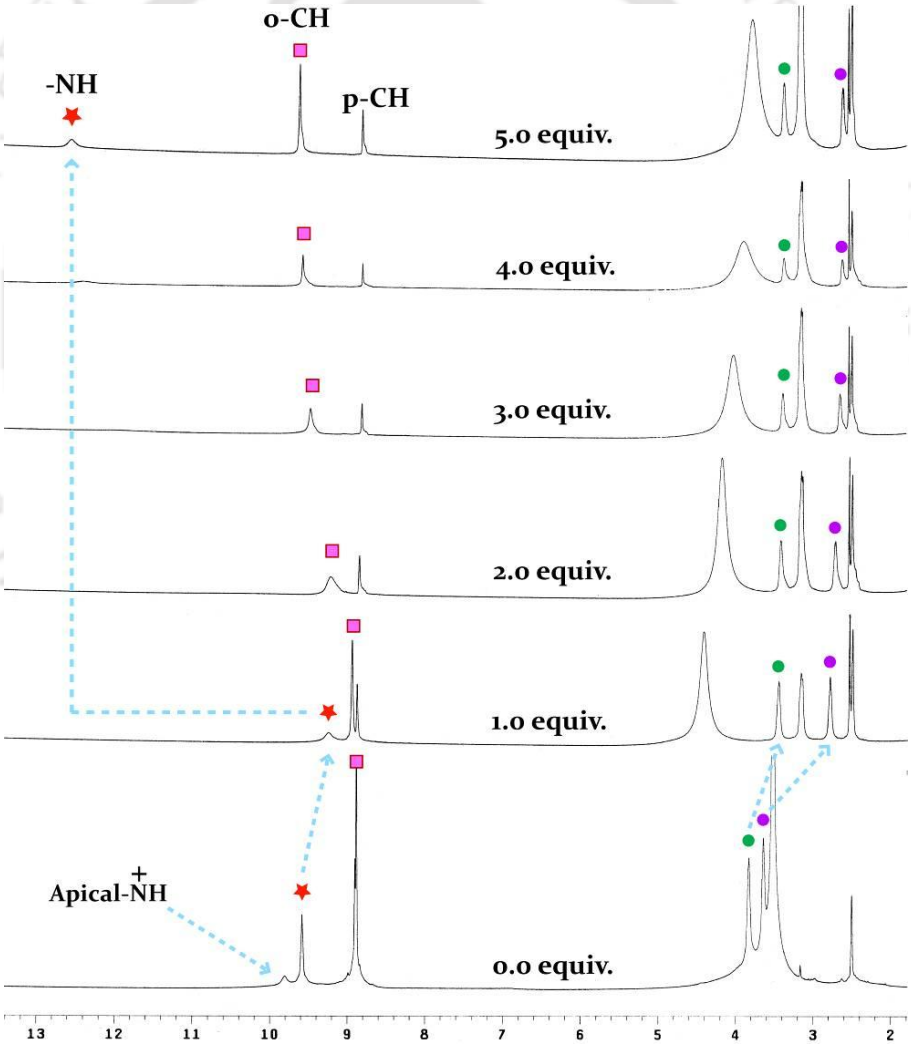

Figure 4.12 Partial ^{1}H-NMR spectra showing the titration of complex **3f** with increasing equivalents of TBAF in DMSO-d_6, which demonstrates the transformation of a charged anion complex into an F^-–encapsulated complex upon addition of 5 equivalents of TBAF.

Table 4.3 Crystallographic parameters and refinement details of complexes **3b-3f**.

Parameter	**3b**	**3c**	**3d**	**3e**	**3f**
Formula	$C_{27}H_{24}FKN_{10}O_{17}$	$C_{27}H_{25}ClN_{10}O_{15}$	$C_{54}H_{52}Br_2N_{20}O_{32}$	$C_{29}H_{33}ClN_{10}O_{22}S$	$C_{29}H_{31}N_{10}O_{21}S_2$
Fw	1858.21	765.02	1652.96	1201.21	919.78
System	Triclinic	Triclinic	Monoclinic	Triclinic	Monoclinic
Group	*P*-1	*P*-1	$P2_1/c$	*P*-1	*Cc*
a/Å	11.2710(12)	12.3254(4)	15.1066(6)	11.2376(9)	22.249(2)
b/Å	12.4543(13)	13.5063(5)	20.5781(8)	11.5873(10)	11.9035(11)
c/Å	12.8718(14)	20.0938(7)	22.9600(8)	16.4312(12)	15.5067(13)
α/°	84.825(6)	93.146(3)	90.00	100.305(4)	90.00
β/°	79.744(6)	95.493(2)	102.365(2)	106.260(4)	112.327(5)
γ/°	88.329(6)	92.688(2)	90.00	94.657(5)	90.00
V/Å^3	1770.6(3)	3320.1(2)	6971.9(5)	2001.2(3)	3799.0(6)
Z	2	4	4	2	4
D_c/g cm^{-3}	1.536	1.531	1.575	1.562	1.608
μ (mm^{-1})	0.246	0.203	1.267	0.247	0.242
T/°K	298(2)	298(2)	298(2)	298(2)	298(2)
θ max.	27.140	28.530	28.36	28.39	28.28
Tot. reflns	26731	30898	90986	25763	22691
Ind. reflns	7784	16876	17344	9585	4706
Obs. reflns	6870	13623	14087	6198	3954
Parameters	505	987	1013	594	576
R_1,$I > 2\sigma(I)$	0.0838	0.0565	0.0555	0.0919	0.0605
wR_2	0.2728	0.1584	0.1666	0.2428	0.1578
GOF (F^2)	1.035	0.951	0.901	0.919	0.998

4.9 Conclusion

In summary, the dinitrophenyl functionalized tris(amide) receptor has been established as a selective chemosensor for fluoride over other anions because of strong anion—π CT interactions in organic solvents. F^-—π CT interaction has been identified and fully characterized by a set of experimental results in solution-states and validated by single-crystal X-ray crystallography as well. Binding and encapsulation of F^- within the receptor cavity result in better orbital interactions between the encapsulated anion and the π-acidic aryl functions, which eventually promote an unprecedented electron transfer process from the F^- ion to electron deficient triamide receptor. F^-—π CT interactions demonstrated a strong solvent dependence (solvatomorphism) due to different extent of solute–solvent

interactions in various aprotic solvents, as confirmed with the X-ray structures of solvatomorphs of F^-–encapsulated complexes (**3a**, **I-IV**). Solution-state participation of the –NH and aryl–CH protons in F^- binding has been confirmed by ^1H NMR spectroscopy whereas encapsulation of the anion was confirmed by 2D-NOESY NMR spectroscopy.

Furthermore, the structural insights of coordination of halides (spherical) and oxyanions (tetrahedral) with the protonated form of the receptor has been investigated in detail, and transformation of these charged anion complexes into F^-–bound pseudo-molecular capsule of the receptor has been accomplished in the presence of excess fluoride ion (5 equiv.). ^1H NMR titration experiments revealed that fluoride ion encourages deprotonation of the protonated apical nitrogen with 1 equiv. of TBAF, followed by formation of the capsular assembly with 5 equiv. of fluoride addition. Thus, receptor $\mathbf{L_3}$ provides an excellent case of understanding the anion coordination chemistry with high selectivity towards F^-.

Table 4.4 Characteristic hydrogen bonding contacts of halides (Cl^- and Br^-) and oxoanions (ClO_4^- and HSO_4^-) with multiple receptor cations in complexes **3c-3f**.

Complexes	D-H···A	*d*(H···A)/Å	*d*(D···A)/Å	∠D-H···A/°
3c	N8-H···Cl1	2.53(3)	3.228(2)	154(2)
	N12-H···Cl1	2.66(3)	3.389(2)	155(2)
	N18-H···Cl1	2.28(3)	3.136(2)	153(2)
	C23-H···Cl1	2.75(7)	3.673(3)	168(2)
	C36-H···Cl1	2.79(7)	3.671(3)	157(2)
	N2-H···Cl2	2.64(3)	3.408(3)	162(2)
	N5-H···Cl2	2.42(4)	3.197(3)	158(3)
	N15-H···Cl2	2.43(3)	3.252(2)	170(2)
	C5-H···Cl2	2.70(7)	3.630(3)	173(2)
	C41-H···Cl2	2.87(7)	3.384(3)	115(2)
3d	N12-H···Br1	2.69(4)	3.375(4)	155(4)
	N15-H···Br1	2.95(3)	3.663(4)	178(3)
	N18-H···Br1	2.65(3)	3.463(4)	165(3)
	C32-H···Br1	2.80(4)	3.734(4)	173(3)
	C41-H···Br1	2.98(5)	3.386(4)	108(2)
	N2-H···Br2	2.48(4)	3.335(4)	165(4)
	N5-H···Br2	2.72(4)	3.437(4)	167(4)

	C5-H···Br2	2.90(6)	3.807(4)	164(3)
	C18-H···Br2	2.98(5)	3.449(4)	112(3)
	O31-H(B)···Br2	2.42(2)	3.314(8)	172(2)
	N8-H···O31	2.01(4)	2.952(7)	171(4)
3e	N2-H···O17	2.54(5)	3.122(1)	125(4)
	N2-H···O18	2.38(5)	3.183(1)	153(4)
	C5-H···O18	2.48(9)	3.340(1)	154(3)
	C1-H(B)···O17	2.69(1)	3.495(1)	140(3)
	C2-H(A)···O17	2.69(7)	3.354(9)	126(3)
	C28-H(A)···O16	2.63(2)	3.450(2)	144(7)
3f	N2-H···O16	2.59(6)	3.264(9)	155(6)
	N2-H···O18	2.43(6)	3.077(9)	149(6)
	N5-H···O17	1.86(5)	2.732(7)	156(4)
	C1-H(B)···O18	2.48(6)	3.318(8)	143(3)
	C9-H···O16	2.64(8)	2.990(1)	103(3)
	C23-H···O16	2.49(6)	3.361(7)	155(3)
	C28-H(C)···O17	2.51(5)	3.391(1)	151(5)

References

1. (a) B. L. Schottel, H. T. Chifotides and K. R. Dunbar, *Chem. Soc. Rev.*, 2008, **37**, 68; (b) O. B. Berryman and D. W. Johnson, *Chem. Commun*., 2009, 3143; (c) P. Gamez, T. J. Mooibroek, S. J. Teat and Jan Reedijk, *Acc. Chem. Res*., 2007**, 40**, 435; (d) V. Gorteau, G. Bollot, J. Mareda, A. Perez-Velasco and S. Matile, *J. Am. Chem. Soc*., 2006, **128**, 14788; (e) B. P. Hay and V. S. Bryantsev, *Chem. Commun*., 2008, 2417; (f) M. Albrecht, C. Wessel, M. de Groot, K. Rissanen, and A Luchow, *J. Am. Chem. Soc*., 2008, **130**, 4600.
2. H. T. Chifotides, B. L. Schottel, and K. R. Dunbar, *Angew. Chem., Int. Ed*., 2010, **49**, 7202.
3. S. Guha and S. Saha, *J. Am. Chem. Soc*., 2010, **132**, 17674.
4. (a) K. L. Kirk, *Biochemistry of the Halogens and Inorganic Halides*; Plenum: New York, 1991; (b) S. Ayoob and A. K. Gupta, *Crit. Rev. Environ. Sci. Technol*., 2006, **36**, 433; (c) E. B. Bassin, D. Wypij, R. B. Davis, M. A. Mittleman, *Cancer Causes and Control*, 2006, **17**, 421.
5. J. M. Kauffman, *J. Am. Phys. Surg*., 2005, **10**, 38.
6. (a) M. Takeuchi, T. Shioya and T. M. Swager, *Angew. Chem., Int. Ed*., 2001, **40**, 3372; (b) S. O. Kang, J. M. Llinares, D. Powell, D. VanderVelde and K. Bowman-James, *J. Am. Chem. Soc*., 2003, **125**, 10152; (c) S. V. Bhosale, M. B. Kalyankar and S. J. Langford, *Org. Lett*., 2009, **11**, 5418; (d) P. A. Gale, *Chem. Commun*., 2008, 4525.
7. M. Cametti and K. Rissanen, *Chem. Commun.*, 2009, 2809.
8. S. K. Dey and G. Das, *Chem. Commun.*, 2011, **47**, 4983.
9. S. K. Dey and G. Das, *Cryst. Eng. Comm.*, DOI: 10.1039/C2CE25592H.
10. S. K. Dey and G. Das, *Cryst. Growth Des*., 2011, **11**, 4463.

Chapter 5

Efficient Fixation of Atmospheric CO_2 by a Tris(urea) receptor

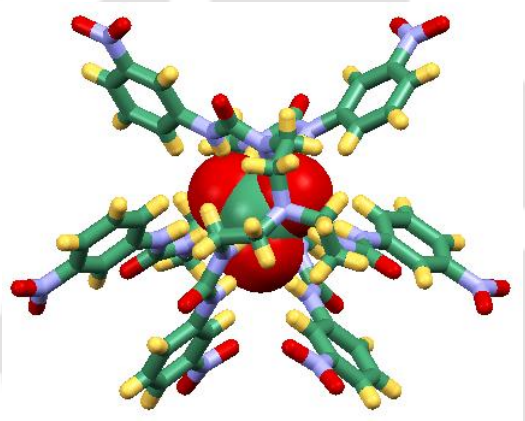

5.1 Background and Focus of the Chapter

A major environmental issue of utmost concern is the significant rise in CO_2 concentration in the atmosphere caused by increased consumption of fossil fuels and the overgrowing number of industries, automobiles, etc., which eventually demands the efficient fixation and activation of atmospheric CO_2 into green chemicals.[1] There is a well-established correlation, initially proposed by Arrhenius in the late 19th century, between atmospheric CO_2 content and global temperature.[2] It is obvious that humankind's excessive burning of fossil fuels is producing large amounts of excess CO_2 contributing to the increase in global temperature.[3] Natural warming cycles by themselves may also increase CO_2 concentrations. Therefore, to significantly reduce emissions, recovery of CO_2 from industrial and natural sources is clearly becoming necessary and new technologies must be developed and enforced.

Nature captures and recycles atmospheric CO_2 efficiently in its photosynthetic cycle. Capturing CO_2, although not generally employed on a large scale, is a well-studied process. The separation of CO_2 from gas streams can be achieved by diverse separation techniques based on different physical and chemical processes, including absorption into a liquid solution, adsorption onto suitable solids, cryogenic separation, and permeation through membranes.[4] Additionally, microporous aluminosilicates, silica gel, activated carbons, and metal−organic frameworks (MOFs) have widely been employed to capture and store CO_2 among other approaches, which utilize the effective conversion of CO_2 into green chemicals for the synthesis of specific chemical intermediates.[5] However, in light of supramolecular chemistry, fixation of aerial carbon dioxide as carbonate/bicarbonate can been achieved with artificial hydrogen bonding receptors mostly in the presence of hydroxide and fluoride ions.[6] Furthermore, Gale et al. have also demonstrated CO_2 capture as carbamates (alkylammonium/alkylcarbamate) by a series of urea-based receptors in the presence of aliphatic amines (CO_2 scrubbers) bubbled with CO_2 in dimethyl sulfoxide (DMSO) solution.[7]

This chapter highlights the rare evidence of hydroxide- and fluoride-ion-induced fixation of atmospheric CO_2 as air-stable crystals of CO_3^{2-}–encapsulated complex of a nitro functionalized tris(urea) receptor, **L_4** (Scheme 5.1).[8] Furthermore, the structural evidence of an optimally coordinated divalent sulfate anion (SO_4^{2-}) encapsulated within a dimeric capsular assembly of the receptor and detailed solution-state anion binding studies of **L_4** are also presented in this chapter. Scheme 5.1 represents a comprehensive representation of the research work included in this chapter.

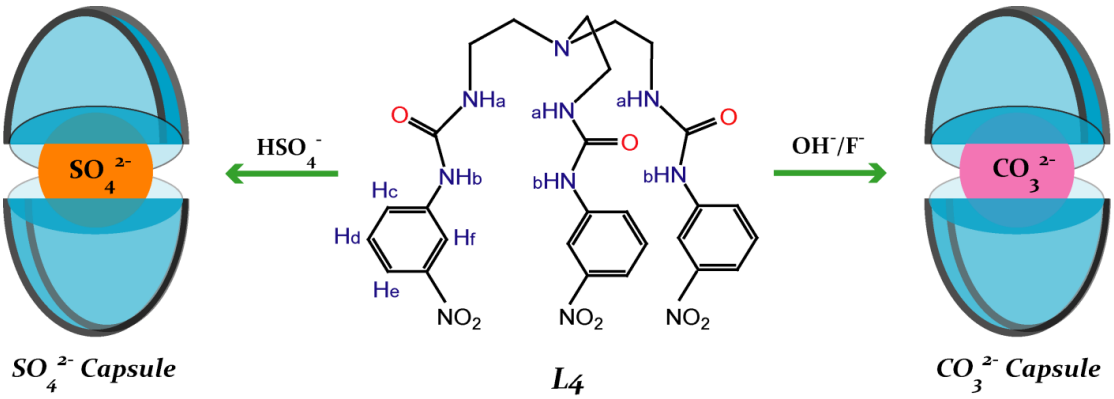

Scheme 5.1 Molecular structure of tris(urea) receptor, $\mathbf{L_4}$ and schematic representation depicting the anion induced capsular assembly formation.

5.2 Crystal structure of receptor $\mathbf{L_4}$

Single crystals of $\mathbf{L_4}$ suitable for XRD analysis were obtained from DMSO, which crystallizes in triclinic space group *P*-1 with Z=4. The asymmetric unit contains two symmetry-independent receptor molecules ($Z' = 2$), which differ considerably in their torsions involving the aliphatic urea nitrogen and carbonyl carbon of each tripodal side arm, i.e., $CH_2{-}CH_2{-}NH{-}(C{=}O)$. In supramolecular chemistry, the existence of more than one molecular conformer in the same crystal structure has been described by the term 'conformational isomorphism' and their occurrence enlighten concepts like kinetic and thermodynamic crystal stability because these are considered to be consequences of interrupted crystallization, as exemplified by Desiraju et al.[9] Structural elucidation revealed that both conformational isomorphs (**C1** and **C2**) are involved in intramolecular N–H···O hydrogen bonding between two arms of the receptor, which assist one of the aryl functions of hydrogen bonded side arms to be in closer proximity with the aryl function of the third side arm, that is not involved in any intramolecular hydrogen bonding. The urea protons N2H and N3H of conformer **C1** and N12H and N13H of conformer **C2** are hydrogen bonded to the amide oxygen atoms O7 and O16 in the respective conformers with a donor-to-acceptor distance of < 3.0 Å, whereas the distances between the centroids of π-stacked phenyl rings are 3.882 Å (C2g···C3g) in conformer **C1** and 3.689 Å (C5g···C6g) in conformer **C2** (Figure 5.1a) Thus, the combined effect of intramolecular N–H···O hydrogen bonding and aromatic π···π stacking resists the opening of the tripodal side arms. Furthermore, each receptor unit is linked to two adjacent units of identical symmetry and of opposite orientation by intermolecular N–H···O hydrogen bonding, donated from the urea functions of π-stacked receptor side arms to the amide oxygen of adjacent inversion-symmetric molecules. The packing diagram as viewed down the crystallographic *b*-axis, shows bilayer assembly formation among conformers of identical symmetry (Figure 5.1b),

which are further linked to the molecules of adjacent bilayers (of different symmetry) through multiple C−H···O-(nitro) hydrogen bonds and C−H···π interactions (Figure 5.1c). The details of the intra- and intermolecular hydrogen bonding interactions involved in the crystal structure of **L_4** are provided in Annexure 5.

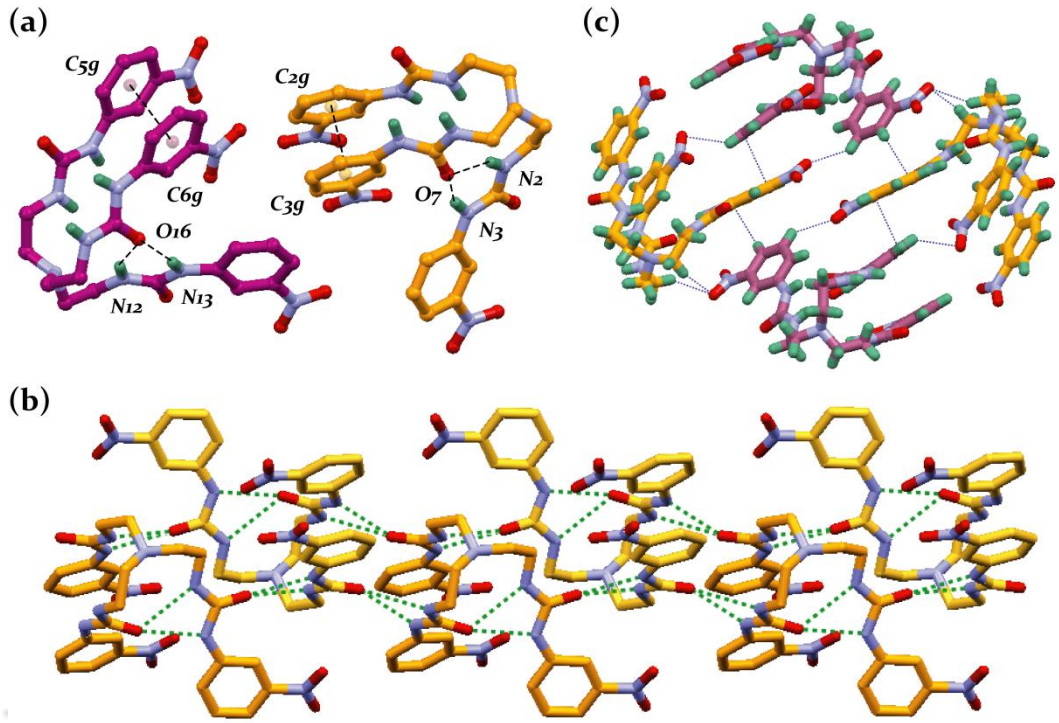

Figure 5.1 (a) X-ray structure of **L_4** depicting the intramolecular hydrogen bonding between the receptor side arms; (b) Complementary hydrogen bonding of the urea moieties forming a 1D bilayer network among molecules of identical symmetry in **L_4**; (c) Intermolecular C-H···O(nitro) and C-H···π interactions formed between the symmetry independent molecules in **L_4**.

5.3 Fixation of atmospheric CO_2 as CO_3^{2-}-encapsulated molecular capsule (4a)

It is interesting to note that, attempted crystallization of fluoride complex from a DMSO solution mixture of **L_4** and excess TBAF yielded single crystals of CO_3^{2-}-encapsulated complex 2TBA[2**L_4**(CO_3)], **4a** where the source of CO_3^{2-} is from the atmospheric CO_2 that has been efficiently fixed by the in situ generated OH^- ions. Structural information obtained from single crystal XRD analysis provides insight into the proper binding topology of the entrapped oxyanion with the neutral receptor molecule and anion-induced capsular assembly formation. Structural elucidation revealed that the in situ generated complex, **4a** crystallizes in the monoclinic system with centrosymmetric space group *C*2/c. Two symmetry-identical receptor molecules with opposite orientation form a capsular nanocavity that encapsulates a carbonate anion in its centre *via* 12 N−H···O hydrogen bonds to the six urea functions and two aryl C−H···O interactions (Figure 5.2a). The inversion-symmetric molecules are flipped inward toward each other in a face-to-face fashion with a distance measuring 9.058(3) Å

between the apical nitrogen atoms (Figure 5.2b) and thereby, generate a centrosymmetric dimeric capsule assembled by aliphatic C−H···O-(nitro) hydrogen bonds between each capsular unit. The carbonate oxygen atoms accept four N−H···O hydrogen bonds each, resulting in 12 hydrogen bonding contacts with an average donor-to-acceptor distance of 2.862 Å (Table 5.2). In addition, an aryl proton from each coordinating unit of the dimeric capsule makes contact with the symmetry related carbonate oxygen atoms (O11 and O11′) via weak C−H···O interactions with a donor-to-acceptor distance of 3.344(4) Å. Thus, multiple (14) hydrogen bonding interactions involving the urea −NH and aryl −CH protons provide high stability to the carbonate-encapsulated molecular capsule and serve as the foundation for efficient crystallization of the in situ formed complex. A correlation of the D−H···O angle versus the D−H···O (D = donor atom, N/C) distance shows that 10 out of 14 hydrogen bonds are in the strong hydrogen bonding interaction regions of d(H···O) < 2.5 Å and d(D···O) < 3.2 Å (Table 5.2). Thermo gravimetric analysis (TGA) of the isolated crystals of **4a** showed that the complex is stable up to 185°C (Annexure 5). Furthermore, the dimeric cages are interlinked with one another via weak aliphatic C−H···O-(nitro) interactions to form a one-dimensional (1D) chain of capsular assemblies along the crystallographic *a*-axis (C19···O3 = 3.442(4) Å, ∠C19−H(A)···O3 = 134^{o}(2)). The packing diagram of **4a** as viewed down the crystallographic *c*-axis shows that the TBA cations are located between the 1D chains of hydrogen bonding capsules via multiple aliphatic C−H···O-(nitro) interactions (Figure 5.2c).

In order to validate the induction of hydroxide ions toward aerial CO_2 fixation, we attempted to grow crystals from an equimolar solution of $\mathbf{L_4}$ and (TBA)OH in DMSO. Slow evaporation of solvent in an unmodified atmosphere (RT) yielded colourless crystals in a bulk amount within 1 or 2 days that have proven to be complex **4a**, as confirmed by PXRD, FT-IR, and ^{1}H NMR analyses of the isolated crystals. The PXRD patterns of isolated bulk crystals from the receptor-OH^- solution matches perfectly with the diffraction patterns of crystals of **4a** obtained from the receptor-F^- solution, indicating the homogeneity of the isolated crystals of the carbonate complex (Annexure 5). It is remarkable to note that almost quantitative yield of **4a** (above 90% based on $\mathbf{L_4}$) can be obtained upon simple filtration/decantation of the crystals from the basic solution mixture ($\mathbf{L_4}$/OH^- solution) after 3 days of exposure to an unmodified atmosphere, which indeed indicates the high affinity of $\mathbf{L_4}$ toward CO_2 fixation by encapsulation of the in situ generated CO_3^{2-} guest within the dimeric assembly of the receptor via multiple hydrogen bonds. A comparatively longer time duration required for the crystallization of **4a** from a receptor-F^- solution is presumably due

to the slow generation of OH^- ions in a moist DMSO solution induced by excess F^- ions, which eventually fix atmospheric CO_2 at the air/solvent interface.

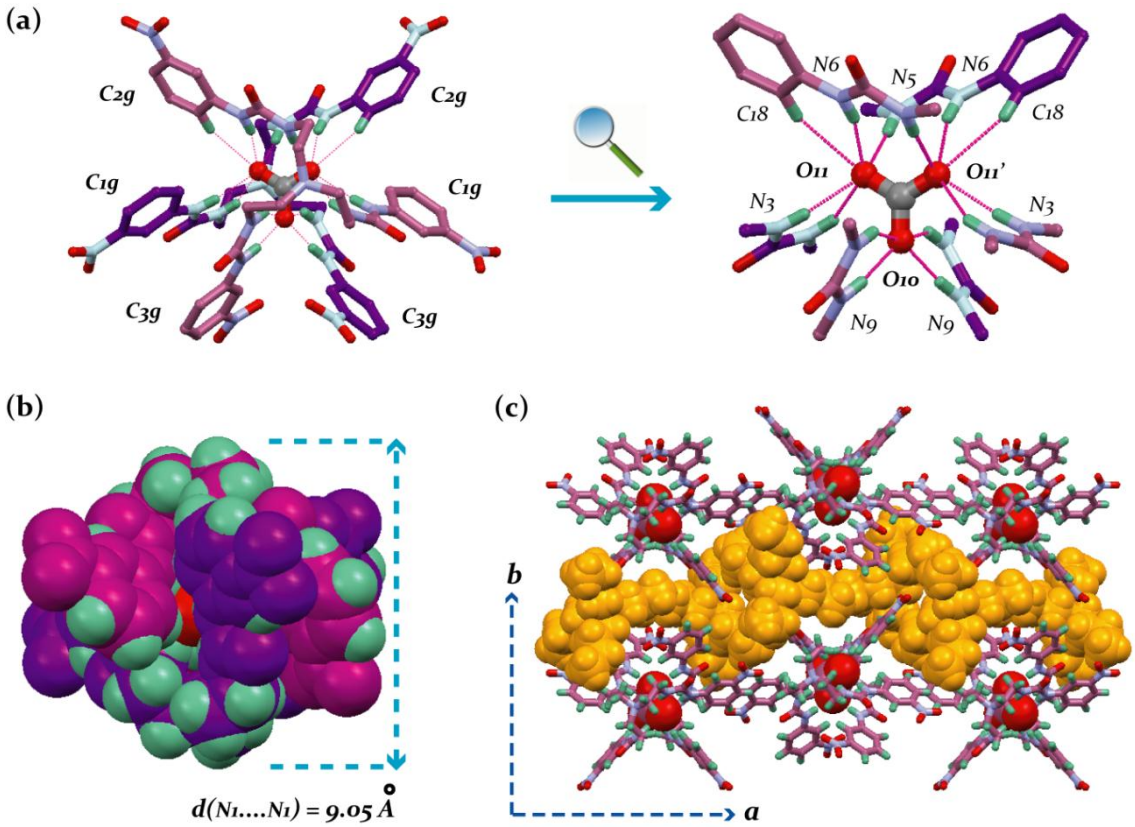

Figure 5.2 (a) X-ray structure of complex **4a** depicts the 14 hydrogen bonding contacts on encapsulated CO_3^{2-} anion within the dimeric capsule of $\mathbf{L_4}$; (b) Spacefill representation depicting the full encapsulation of CO_3^{2-} anion; (c) Crystal packing in complex **4a** as viewed down the crystallographic *c*-axis.

5.4 SO_4^{2-}-encapsulated molecular capsule (4b)

The sulfate-encapsulated complex 2TBA[2$\mathbf{L_4}$(SO_4)], **4b** was obtained as suitable crystals for XRD analysis upon slow evaporation of a DMSO solution of $\mathbf{L_4}$ and excess (TBA)HSO_4, which crystallizes in the monoclinic system with centrosymmetric space group *C*2/c. Crystal structure elucidation revealed that a hydrogensulfate anion has deprotonated and is bound in the form of SO_4^{2-} (divalent sulfate) by two inversion-symmetric molecules of $\mathbf{L_4}$ and thereby, creating a caged supramolecular structure assembled by aliphatic C–H···O-(nitro) hydrogen bonds [C2···O2 = 3.625(7) Å, ∠C2–H(B···O2 = 150(3)° and C20···O5 = 3.522(7) Å, ∠C20–H(B)···O5 = 135(3)°] and aromatic π-stacking interactions between the receptor molecules [C13···C22 = 3.486(6) Å or C2g···C3g = 4.190 Å] (Figure 5.3a). Similar deprotonation of HSO_4^- has previously been observed by Ghosh et al. with a pentafluorophenyl-based tris(urea) receptor, which under identical crystallization conditions encapsulates SO_4^{2-} in a 2:1 (host/guest) ratio.[10] Such a solution-state deprotonation of the

protonated state of an anion, *viz.*, $H_2PO_4^-$, HCO_3^-, and HSO_4^-, is not uncommon and results due to the formation of multiple hydrogen bonding interactions with the receptor that lower the p*K*a of the bound guest to the extent that it is deprotonated by the free guest species in solution, and we presume the same process to occur here, as suggested by Gale et al.[11] Two inversion-symmetric molecules of **L_4** are flipped inward toward each other in a face-to-face fashion with a distance measuring 9.602(4) Å between the apical nitrogen atoms (Figure 5.3b) and forms a centrosymmetric molecular cage that encapsulates a sulfate anion in its centre *via* 12 N−H···O hydrogen bonds to the six urea functions with an average donor-to-acceptor distance of 2.862 Å (Table 5.2). Each sulfate oxygen atom behaves as a trifurcated hydrogen bond acceptor and each −NH group donates one N−H···O bond (Figure 5.3c) resulting in 12 hydrogen bonds, which is consistent with the electronic structure calculations by Hay et al. suggesting that each oxyanion oxygen atom could be involved in a maximum of three hydrogen bonds.[12] Thus, the structure represents the optimal coordination number for the sulfate anion. A correlation of the N−H···O angle versus the N−H···O distance shows that 10 out of 12 hydrogen bonds are in the strong hydrogen-bonding interaction regions of *d*(H···O) < 2.5 Å and *d*(N···O) < 3.2 Å, which perhaps contributes to the high stability of **4b** (m.p. = 242 °C), as is evident from TGA of the isolated crystals of **4b** (Annexure 5). Furthermore, the sulfate-encapsulated dimeric cages are interlinked with one another via weak aromatic C−H···π interactions (C8···C3g = 3.897 Å; ∠C8−H···C3g = 138°) to form a 1D chain of capsular assemblies along the crystallographic b-axis. Two such 1D arrays of capsular assemblies are further interconnected with one another by weak aliphatic C−H···O-(nitro) interactions (C19···O3 = 3.155(7) Å; ∠C19−H···O3 = 107(3)°), generating hexagonal networks of sulfate-encapsulated dimeric cages around each capsular unit (Figure 5.3d). In addition, multiple C−H···O-(nitro) interactions formed between the TBA cations and nitro groups of the receptor side arms provide increased stability to the caged supramolecular assembly formation.

It is important to mention here that attempted crystallization of a DMSO or MeCN solution of **L_4** in the presence of excess $(TBA)_2SO_4^{2-}$ (50 wt % solution in water) was not fruitful, presumably because of the high moisture content of the receptor-anion solution and the capability of protic solvents to compete for SO_4^{2-} along with urea −NH functions of **L_4**, disfavouring the formation of a SO_4^{2-}-encapsulated molecular capsule (**4b**). However, encapsulation of a sulfate–$(H_2O)_3$–sulfate adduct within the pseudomolecular capsule of a positional isomer of **L_4** (*p*-nitrophenyl derivative) has been reported from identical crystallization conditions (MeCN/water) with a 1:1 receptor to anion binding.[13]

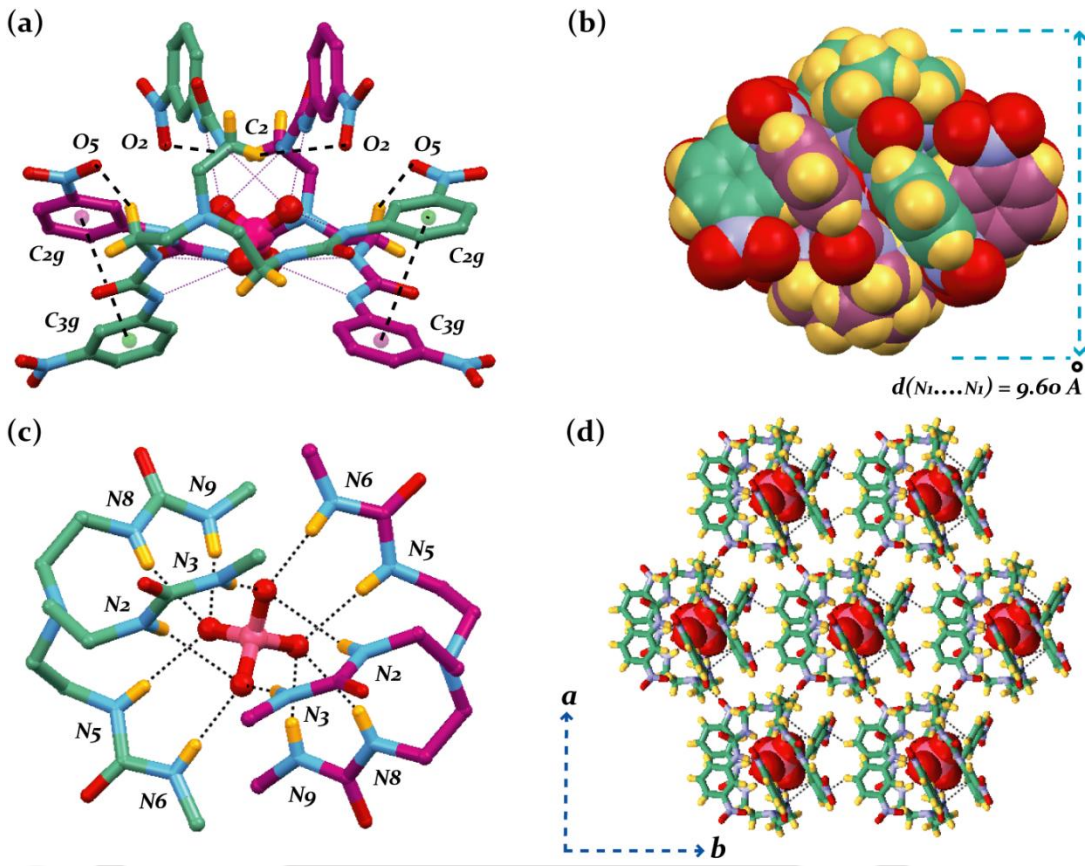

Figure 5.3 (a) X-ray structure of complex **4b** depicting the intermolecular hydrogen bonding interactions between the two receptor molecules of SO_4^{2-}–entrapped dimeric capsule of $\mathbf{L_4}$; (b) Spacefill representation depicting the full encapsulation of SO_4^{2-} anion; (c) Coordination of SO_4^{2-} by twelve N-H···O hydrogen bonds within the dimeric capsule; (d) Crystal packing in complex **4b** as viewed down the crystallographic *c*-axis (TBA cations are omitted for clarity).

5.5 Auxiliary evidence of CO_3^{2-} and SO_4^{2-} encapsulation

The presence of CO_3^{2-} and existence of strong N−H···O hydrogen bonds in complex **4a** have also been established by solid-state FT-IR analysis. In the case of receptor $\mathbf{L_4}$, the carbonyl (−C=O) stretching frequency is observed at 1655 cm^{-1}, whereas in complex **4a**, it is observed at 1699 cm^{-1}, showing a huge shift of 44 cm^{-1} for the −C=O stretching relative to free $\mathbf{L_4}$ due to the formation of strong N−H···O hydrogen bonds with the carbonate oxygen atoms. The N–H stretching frequency of complex **4a** (ν 3390 cm^{-1}) shows a considerable shift of 62 cm^{-1} with concomitant broadening of the peak in comparison to $\mathbf{L_4}$ (ν 3328 cm^{-1}), further establish the existence of strong N−H···O hydrogen bonds between $\mathbf{L_4}$ and the entrapped CO_3^{2-} anion. Furthermore, the intense and strong peak at 2965 cm^{-1} may be attributed to C−H stretching of the TBA groups in complex **4a** (Annexure 5).

In complex **4b**, the carbonyl (−C=O) stretching frequency is observed at 1695 cm^{-1}, showing a considerable shift of 40 cm^{-1} relative to free $\mathbf{L_4}$ due to the formation of strong N-H···O hydrogen bonds with the sulfate oxygen atoms. Additional information regarding the existence of strong N−H···O hydrogen bonds between $\mathbf{L_4}$ and SO_4^{2-} can be obtained by examining the N–H peak of the spectrum, which gets broadened in **4b** relative to $\mathbf{L_4}$. Furthermore, the intense and strong peak at 2963 cm^{-1} may be attributed to C−H stretching of the TBA groups in complex **4b**. In addition, a new peak is observed at 1089 cm^{-1} which can be attributed to the symmetric stretching frequency of the sulfate anion. Typically, the symmetric absorption (ν 1089 cm^{-1}) is intense and broad and most often does exists as multiple band structure as observed for **4b**, and this may be used to characterize the presence of sulfate in individual compounds/complexes (Annexure 5).

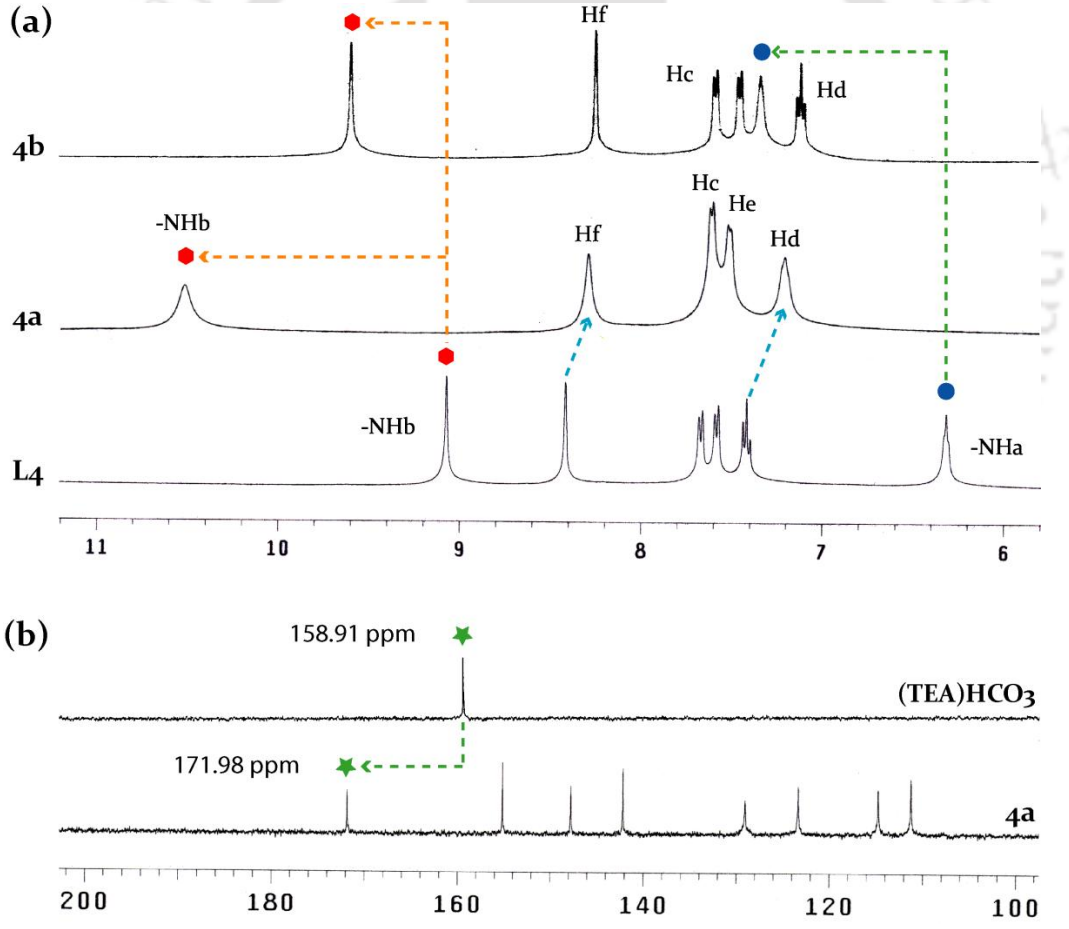

Figure 5.4 (a) Partial ^{1}H NMR spectra of complexes **4a** and **4b**, showing the spectral changes relative to receptor $\mathbf{L_4}$; (b) Partial ^{13}C NMR spectrum of complex **4a** showing the huge downfield shift of the encapsulated CO_3^{2-} resonance relative to the free resonance of $(TEA)HCO_3$ salt.

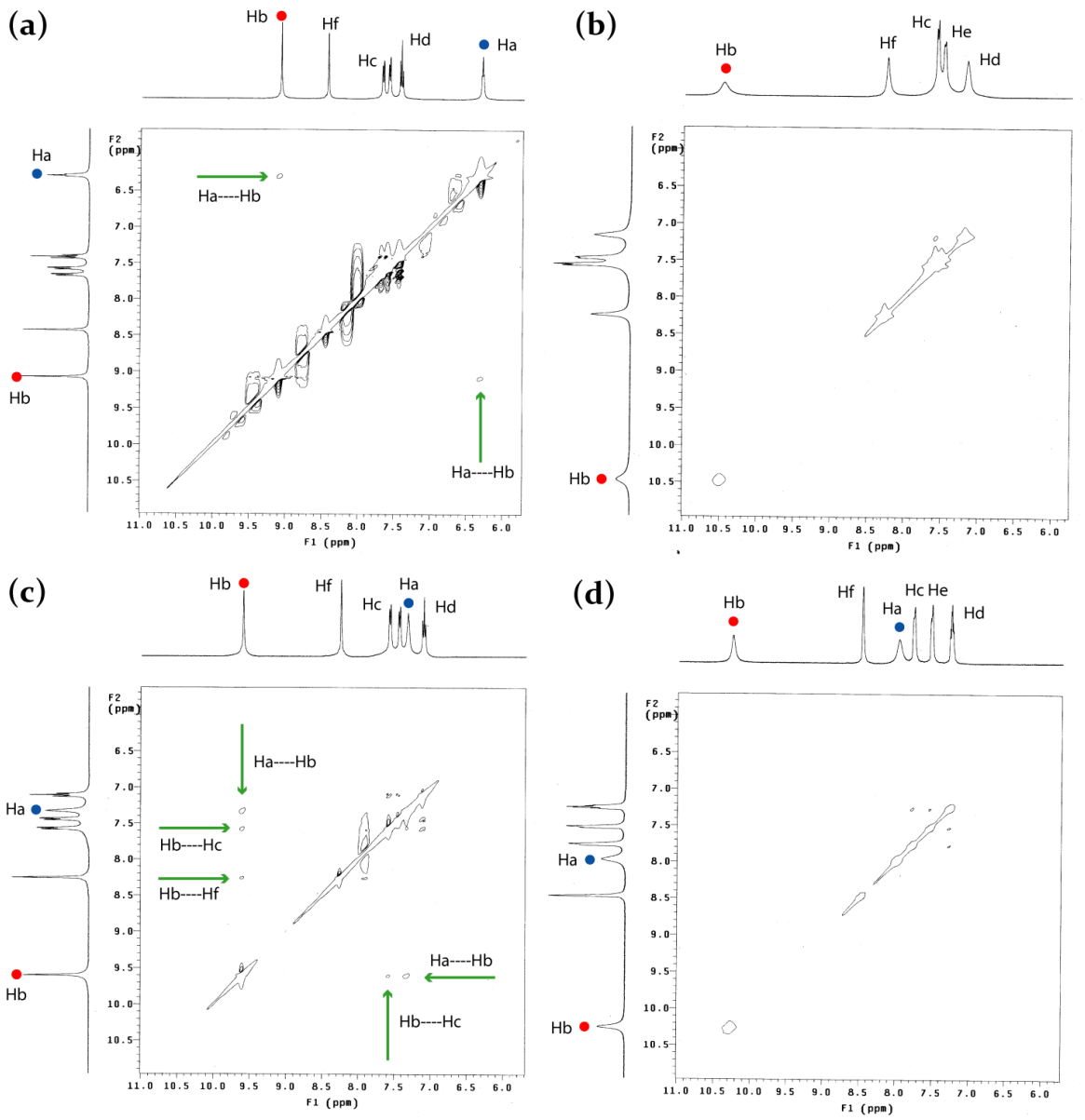

Figure 5.5 2D NOESY NMR experiments of (a) receptor, **L_4**; (b) CO_3^{2-}–encapsulated complex, **4a**; (c) SO_4^{2-}–encapsulated complex, **4b** and (d) **L_4** in presence of excess sulfate anion (5 equiv.) in DMSO-d_6.

The ^{1}H NMR spectrum of complex **4a** (DMSO-d_6) showed an appreciable downfield shift and concomitant broadening of the urea $-NH_b$ resonance with a $\Delta\delta$ shift of 1.44 ppm, indicative of a strong solution-state binding of CO_3^{2-} with the urea functions of **L_4** (Figure 5.4a). However, the resonance for the $-NH_a$ proton could not be observed presumably because of binding induced broadening of the signals, as observed in the case of $-NH_b$ proton. Whereas, the ^{1}H NMR spectrum of complex **4b** (DMSO-d_6) showed a significant downfield shift of both the $-$NH resonances with a $\Delta\delta$ value of 1.02 and 0.51 ppm for $-NH_a$ and $-NH_b$ protons respectively (Figure 5.4a), suggesting a strong solution-state binding of SO_4^{2-} with **L_4**. In addition, spectral changes have also been observed for the aliphatic

(−NCH_2) and aromatic (Ar−CH) protons, which undergo a notable upfield shift in the oxyanion complexes, suggesting a solution-state structural alteration of receptor side arms in presence of anionic guest species. Binding and encapsulation of CO_3^{2-} has also been confirmed by monitoring the changes in the chemical shift of ^{13}C NMR signal of $TEAHCO_3$ and complex **4a**. Tetraethyl ammonium bicarbonate in DMSO-d_6 showed a sharp ^{13}C NMR signal at 158.91 ppm, whereas in complex **4a** the carbonate resonance occurs at 171.98 ppm ($\Delta\delta$ = 13.07 ppm), that may be attributed to the encapsulated CO_3^{2-} anion (Figure 5.4b).

Table 5.1 Crystallographic parameters and refinement details of receptor $\mathbf{L_4}$ and oxyanion-encapsulated complexes **4a** and **4b.**

Parameters	$\mathbf{L_4}$	**4a**	**4b**
Formula	$C_{27}H_{30}N_{10}O_9$	$C_{87}H_{132}N_{22}O_{21}$	$C_{86}H_{132}N_{22}O_{22}S$
Fw	638.61	1822.15	1858.21
Crystal system	Triclinic	Monoclinic	Monoclinic
Space group	*P*-1	*C*2/*c*	*C*2/*c*
a/Å	13.0495(4)	33.4669(13)	22.9827(10)
b/Å	13.4255(4)	15.1439(5)	13.3103(6)
c/Å	19.0544(9)	22.8357(10)	33.5349(15)
α/°	99.512(2)	90.00	90.00
β/°	98.195(2)	120.928(3)	98.705(2)
γ/°	109.665(1)	90.00	90.00
V/Å^3	3029.0(2)	9928.0(7)	10140.4(8)
Z	4	4	4
D_c/g cm^{-3}	1.400	1.219	1.217
μ Mo K_α/mm^{-1}	0.108	0.088	0.108
T/K	298(2)	298(2)	298(2)
θ max.	27.860	21.630	19.600
Total no. of reflections	37783	48123	41939
Independent reflections	11778	5776	4384
Observed reflections	10284	4045	3646
Parameters refined	830	592	595
R_1, $I > 2\sigma(I)$	0.0461	0.0496	0.0486
wR_2 (all data)	0.1691	0.1831	0.1467
GOF (F^2)	0.964	1.030	0.983

Table 5.2 Hydrogen bonding contacts on CO_3^{2-} and SO_4^{2-} anion within the centrosymmetric dimeric capsule of $\mathbf{L_4}$ in complexes **4a** and **4b.**

Complexes	D-H···O	*d*(H···O)/Å	*d*(D···O)/Å	∠D-H···O/°
4a	N2-H···O11	2.38(2)	3.151(4)	148(2)
	N3-H···O11	2.07(2)	2.912(4)	164(2)
	N5-H···O11	2.06(2)	2.926(3)	177(2)
	N6-H···O11	1.99(2)	2.831(3)	164(2)
	N9-H···O10	1.92(2)	2.781(3)	172(2)
	N8-H···O10	2.64(3)	3.358(2)	141(2)
	C18-H···O11	2.60(2)	3.344(4)	137(2)
4b	N5-H···O10	2.17(4)	3.022(5)	168(2)
	N8-H···O10	2.25(4)	3.049(5)	153(3)
	N9-H···O10	2.15(4)	2.974(5)	159(2)
	N3-H···O11	2.02(3)	2.882(4)	172(2)
	N6-H···O11	1.99(3)	2.849(4)	174(2)
	N2-H···O11	2.69(3)	3.464(5)	150(3)

The solution-state encapsulation of CO_3^{2-} and SO_4^{2-} has further been confirmed by 2D NOESY NMR experiments of the isolated complexes (**4a** and **4b**) and free receptor ($\mathbf{L_4}$) in DMSO-d_6. The free receptor molecule showed a strong NOE signal between the urea protons $-NH_a$ and $-NH_b$ (Figure 5.5a), whereas such $H_a\cdots H_b$ interaction was found to be absent in complex **4a** (Figure 5.5b), indicating the binding and encapsulation of carbonate within the receptor scaffold in a 2:1 host-guest stoichiometry, an observation that is also supported by the X-ray structure of the CO_3^{2-}–encapsulated molecular capsule (**4a**). In contrast, two strong NOE signals between $H_a\cdots H_b$ and $H_b\cdots H_c$ protons have been observed in complex **4b** (Figure 5.5c), which indeed suggests that the 2:1 host-guest stoichiometry is not the prevalent mode of sulfate binding in solution. However, upon further addition of sulfate ions to the solution of **4b** in DMSO-d_6, the NOE signals between $H_a\cdots H_b$ and $H_b\cdots H_c$ disappeared, indicating a conformational change of the receptor side arms due to encapsulation of sulfate anion in a 1:1 host-guest ratio (Figure 5.5d).

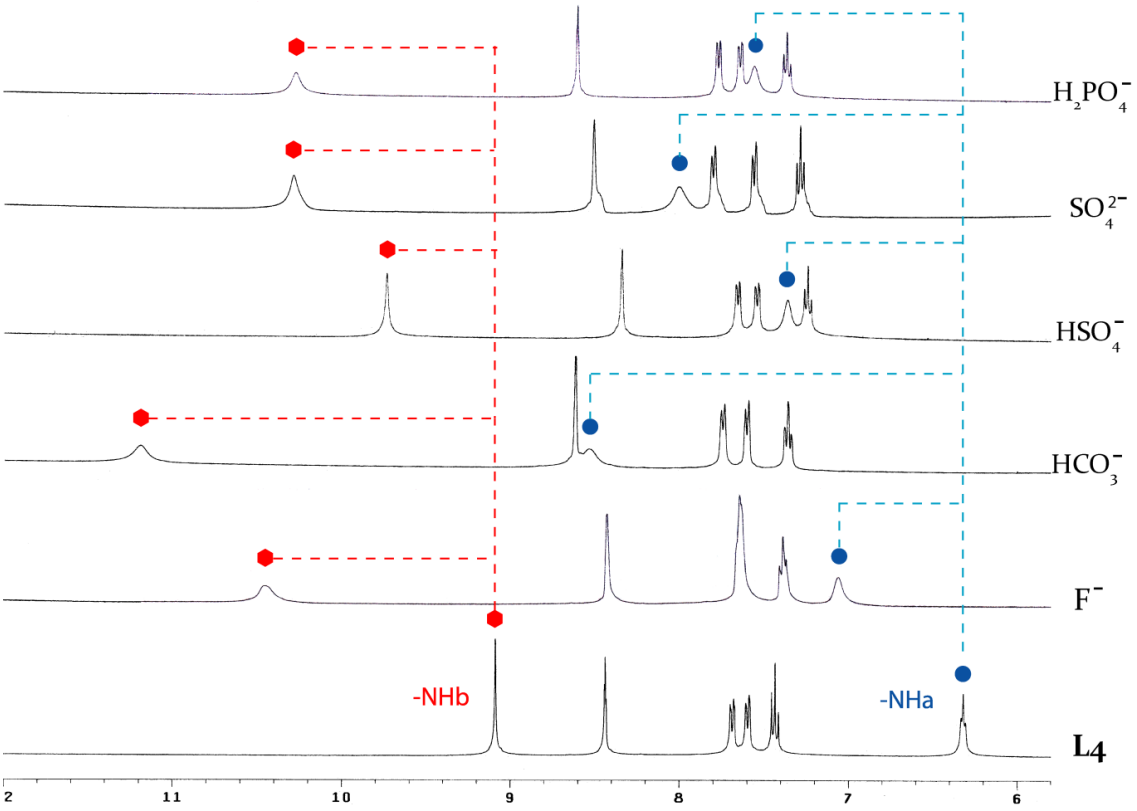

Figure 5.6 Partial ^{1}H NMR spectra (400 MHz, DMSO-d_6) of **L$_4$** and maximum observable shift of urea -NH resonances upon excess (5 equiv.) addition of F^-, HCO_3^-, HSO_4^-, SO_4^{2-}, $H_2PO_4^-$ and AcO^- as their TEA/TBA salts. The quaternary ammonium salts were added at once to the individual solutions of **L$_4$**.

5.6 Anion-binding studies by ^{1}H NMR spectroscopy

Solution-state anion binding properties of **L$_4$** were examined by qualitative as well as quantitative ^{1}H NMR experiments in DMSO-d_6 , with quaternary ammonium (TEA/TBA) salts of different anions such as HCO_3^-, F^-, $H_2PO_4^-$, HSO_4^-, and SO_4^{2-}. Figure 5.6 represents the qualitative test of anions, which shows the chemical shift changes of receptor protons observed upon the excess addition of different anions to the receptor **L$_4$**. The most significant changes have been observed for the urea protons (−NH$_a$ and −NH$_b$), indicating that the −NH functions provide the primary sites of interaction between the receptor and anions. In the quantitative ^{1}H NMR titration of **L$_4$** with a standard HCO_3^- solution, a large downfield shift of −NH resonances with an average Δδ value of 1.48 ppm (Δδ −NH$_a$ = 1.51 ppm; Δδ −NH$_b$ = 1.45 ppm) were observed. Following the shift of the −NH signal, the association constant (log *K*) for HCO_3^- was calculated to be 4.14 with a 1:1 host-guest stoichiometry, in agreement with Job's plot analysis (Figure 5.7). The titration data for F^- as well gave the best fit for 1:1 stoichiometry with a log *K* value of 3.87 (Figure 5.8). The considerably larger shift of −NH$_b$ (Δδ = 1.44 ppm) relative to −NH$_a$ signals (Δδ = 0.89 ppm) suggests that F^- is bound more strongly to −NH$_b$ than −NH$_a$ protons of the receptor. However, in a proof-of-

concept experiment, when the titrated receptor-F^- solution (1:10 host/guest) was bubbled with CO_2 for about 5 min (100 mL min^{-1}), and immediate ^1H NMR analysis showed a further downfield shift of the $-NH_a$ resonance ($\Delta\delta$ = 1.42 ppm with respect to **L_4**), indicating the in situ formation of carbonate/bicarbonate in the presence of excess F^- ions.

^1H NMR titration of **L_4** with standard HSO_4^- and SO_4^{2-} solutions led to the best fit for 1:1 stoichiometry of host to guest, in agreement with Job's plot analyses (Figures 5.9 and 5.10), whereas the single-crystal XRD analysis of complex **4b** showed a 2:1 host-guest binding for the divalent sulfate anion. Such a binding discrepancy in the solid and solution states is not uncommon. In the solid state, the receptor is more organized and prefers binding and encapsulation of the oxyanion within the dimeric cage structure of the receptor stabilized by several hydrogen bonding interactions, whereas binding of a single anion inside the receptor cavity has been observed in solution. The association constants (log *K*) for SO_4^{2-} and HSO_4^- were calculated to be 4.78 and 4.52. The identical modes of binding (1:1 host-guest) and association constants of $K > 10^4$ M^{-1} calculated using both sulfate and bisulfate indicate that in solution-state bisulfate gets converted to sulfate in our experimental conditions, which indeed supports the solid-state formation of the SO_4^{2-}-encapsulated complex **4b** when **L_4** is treated with excess TBA salt of HSO_4^- in DMSO. Additionally, the changes in chemical shift of the urea −NH signals in the presence of 1 equivalent of SO_4^{2-} and HSO_4^- have been found to be almost the same (in the case of SO_4^{2-}, $\Delta\delta$ $-NH_a$ = 1.18 ppm and $-NH_b$ = 0.72 ppm, and in the case of HSO_4^-, $\Delta\delta$ $-NH_a$ = 1.13 ppm and $-NH_b$ = 0.71 ppm) and closely resemble those in the ^1H NMR spectrum of the isolated crystals of **4b**. A comparatively larger downfield shift of the aliphatic $-NH_a$ signal relative to the aryl $-NH_b$ signal suggests that in solution SO_4^{2-}/HSO_4^- is bound more strongly to $-NH_a$ than $-NH_b$ protons of the receptor, which is in contrast to the X-ray structure of **4b** that shows equal participation from both the urea protons toward SO_4^{2-} binding within the dimeric cage of **L_4**.

Similar to the HCO_3^- titration experiment, increasing the addition of a standard $H_2PO_4^{2-}$ solution results in an identical downfield shift of both the −NH signals with an average $\Delta\delta$ value of 1.42 ppm ($\Delta\delta$ $-NH_a$ = 1.43 ppm and $\Delta\delta$ $-NH_b$ = 1.42 ppm), indicative of equal and active participation of both the urea protons toward binding of this anion in a 1:1 stoichiometry (**L_4**/$H_2PO_4^{2-}$) with an association constant (log *K*) of 4.38 (Figure 5.11). However, in the presence of other oxyanions such as nitrate and perchlorate, no appreciable changes in the chemical shift values of the −NH resonances were observed, suggesting the non-interacting nature or very weak interactions with **L_4**. The association constants (log *K*) calculated by following the shift of the most deshielded urea proton ($-NH_a$ or $-NH_b$) in the ^1H NMR titration experiments of **L_4** with different anions, are comparable to those observed

for the pentafluorophenyl[10], *p*-nitrophenyl,[13] or *p*-cyanophenyl[14] substituted tris(urea) receptors.

5.7 Conclusion

In summary, we have demonstrated the efficient fixation of aerial CO_2 in the form of air-stable crystals of CO_3^{2-}-encapsulated molecular capsule of a simple tris(urea) receptor, **L_4**. The fixation process can reproducibly be accomplished from a DMSO solution of the receptor charged either with an equivalent amount of hydroxide ions or an excess of fluoride ions. It is remarkable to note that almost quantitative conversion of **L_4** to the carbonate-encapsulated complex (**4a**) can be obtained from the basic receptor-OH^- solution, which establishes **L_4** as a potential hydrogen bonding scaffold for the effective fixation of atmospheric CO_2. The in situ generated carbonate anion is bound within a centrosymmetric dimeric cage of the receptor with an array of twelve N−H···O and two C−H···O hydrogen bonds. In addition, we have also shown the structural evidence for encapsulation of a deprotonated hydrogensulfate anion (SO_4^{2-}) within a fully complementary centrosymmetric dimeric assembly of the receptor via 12 N−H···O hydrogen bonds (**4b**). Thus, receptor **L_4** provides an excellent case of understanding the significance of hydrogen bonding tripodal scaffolds toward the formation of oxyanion-encapsulated caged supramolecular frameworks by in situ generation of the bound anionic species.

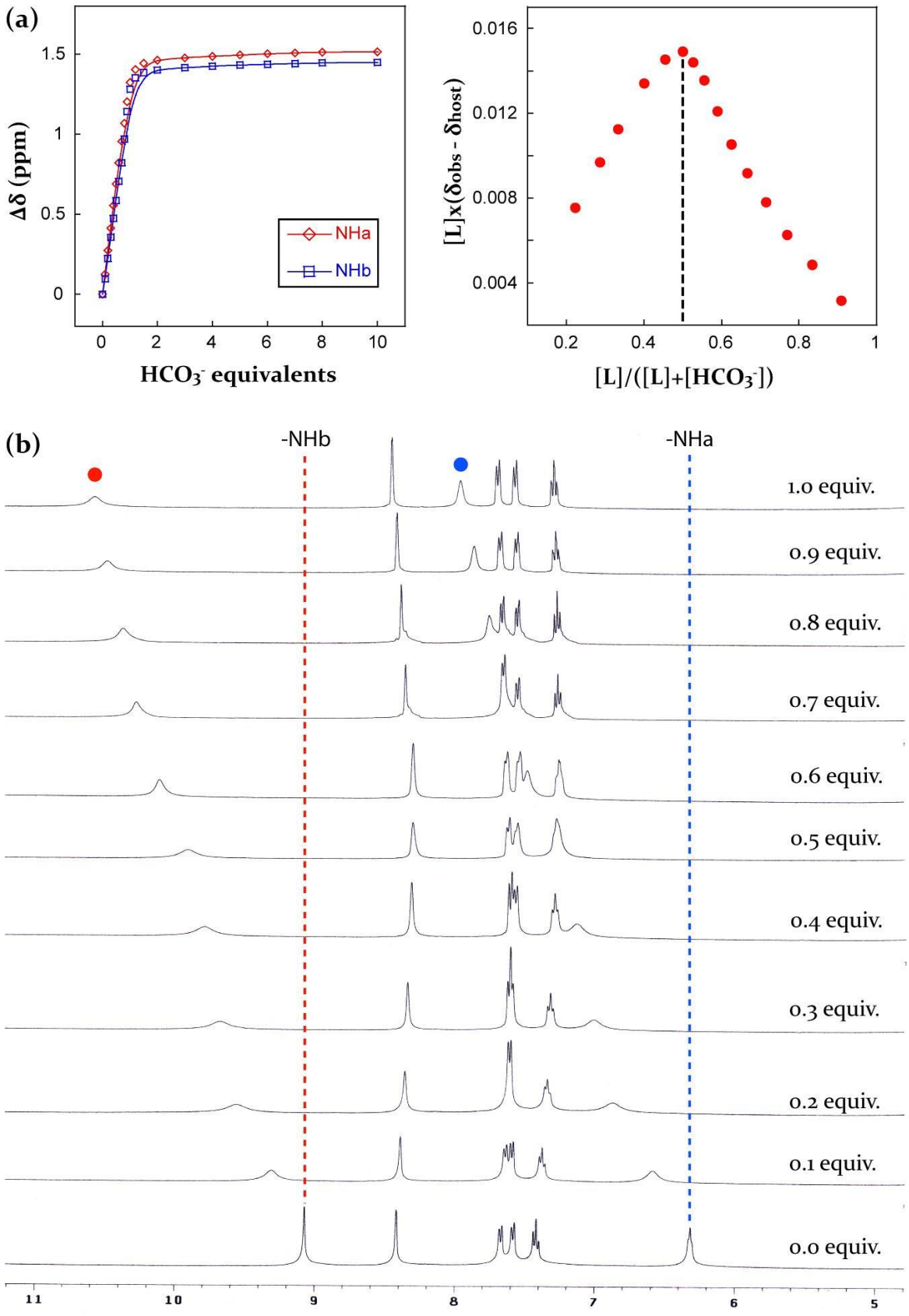

Figure 5.7 (a) Change in chemical shift of –NH resonances of $\mathbf{L_4}$ (5 mM) with increasing conc. of standard HCO_3^- solution (50 mM) in DMSO-d_6 and the corresponding Job's plot suggesting the formation of 1:1 host/guest complex; (b) Partial ^{1}H NMR titration spectra of $\mathbf{L_4}$ with (TBA)HCO_3.

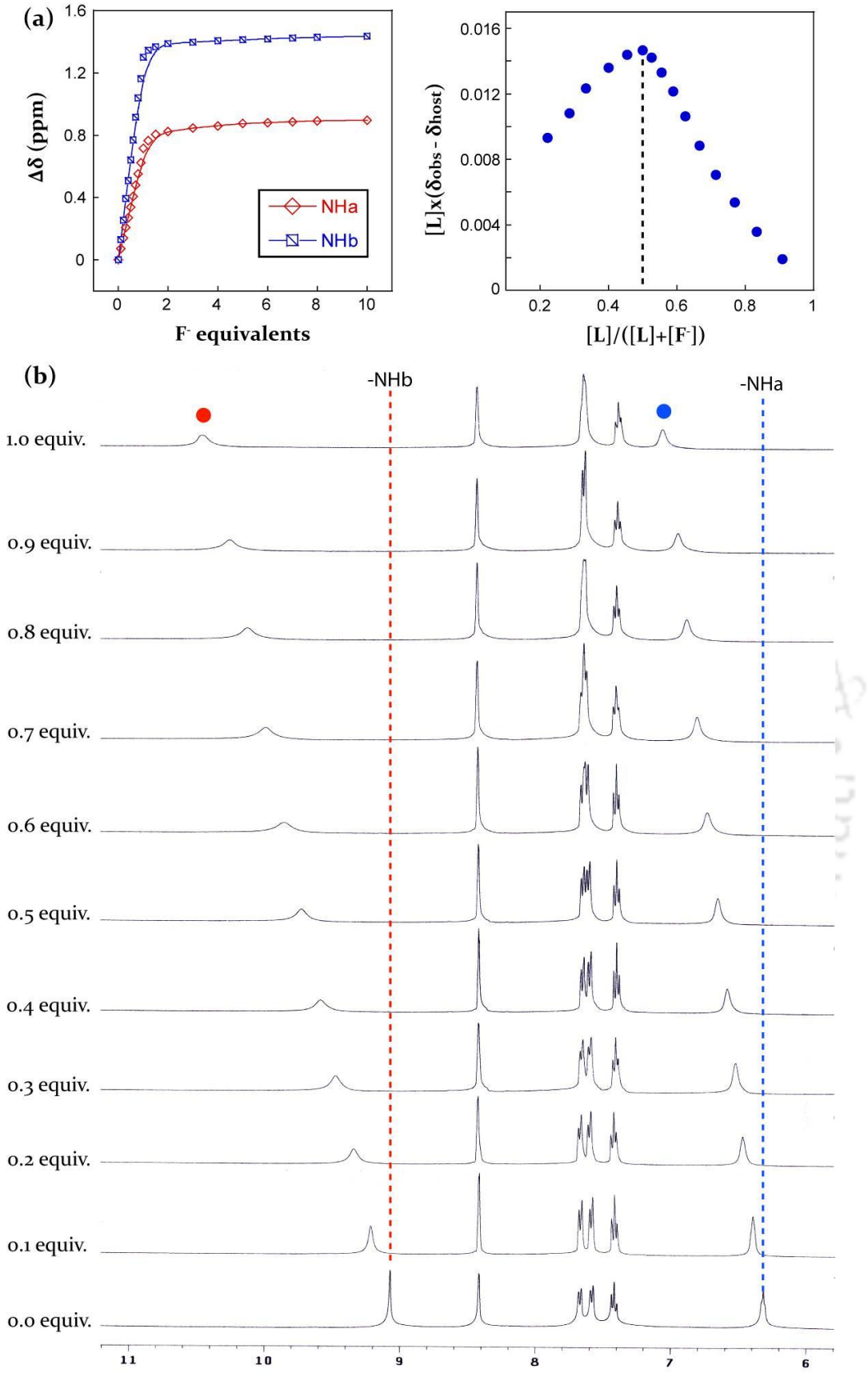

Figure 5.8 (a) Change in chemical shift of –NH resonances of $\mathbf{L_4}$ (5 mM) with increasing conc. of standard F^- solution (50 mM) in DMSO-d_6 at 298 K and the corresponding Job's plot suggesting the formation of 1:1 host/guest complex in solution; (b) Partial ^{1}H NMR titration spectra of $\mathbf{L_4}$ with TBAF.

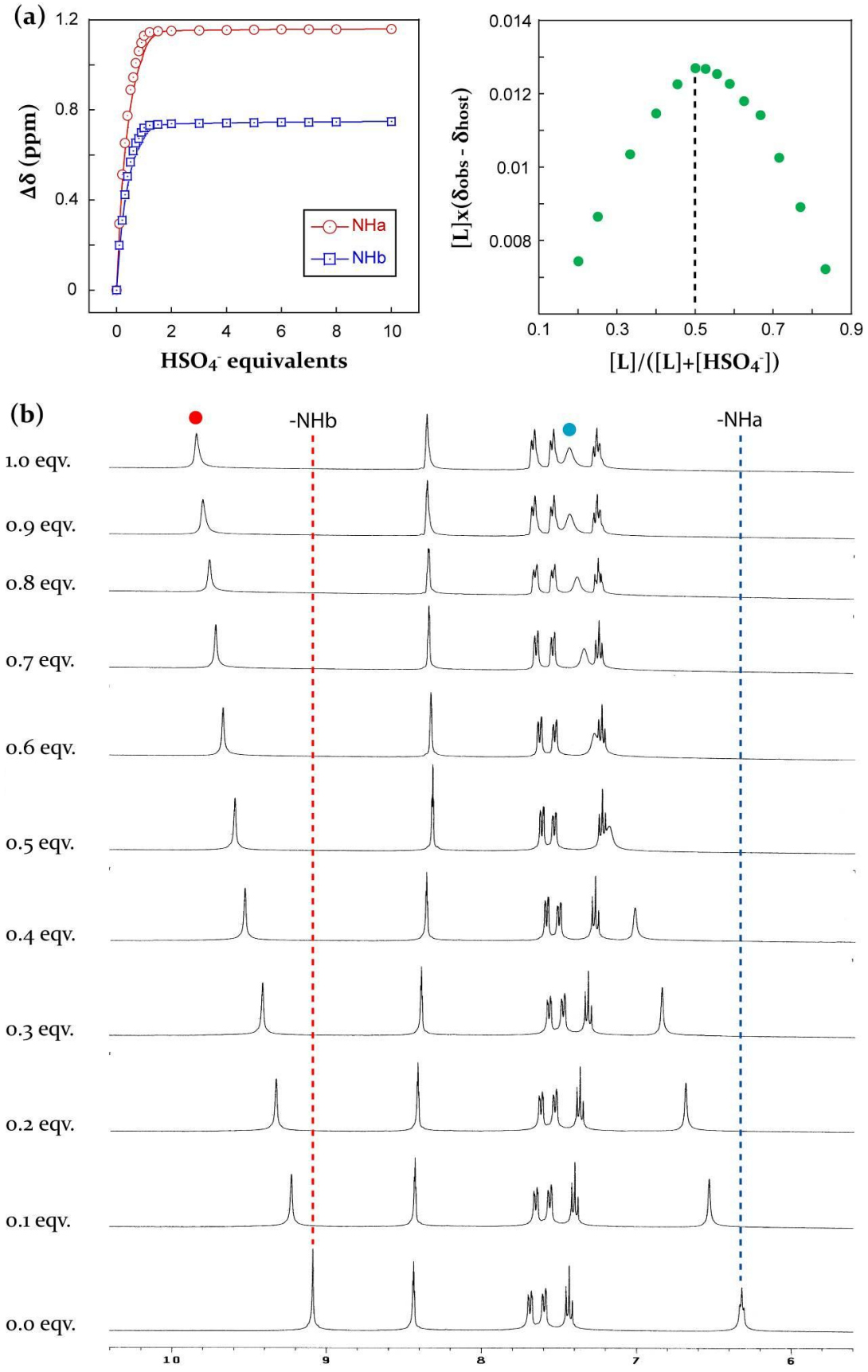

Figure 5.9 (a) Change in chemical shift of –NH resonances of **L_4** (5 mM) with increasing conc. of standard HSO_4^- solution (50 mM) in DMSO-d_6 and the corresponding Job's plot suggesting the formation of 1:1 host/guest complex; (b) Partial ^{1}H NMR titration spectra of **L_4** with (TBA)HSO_4.

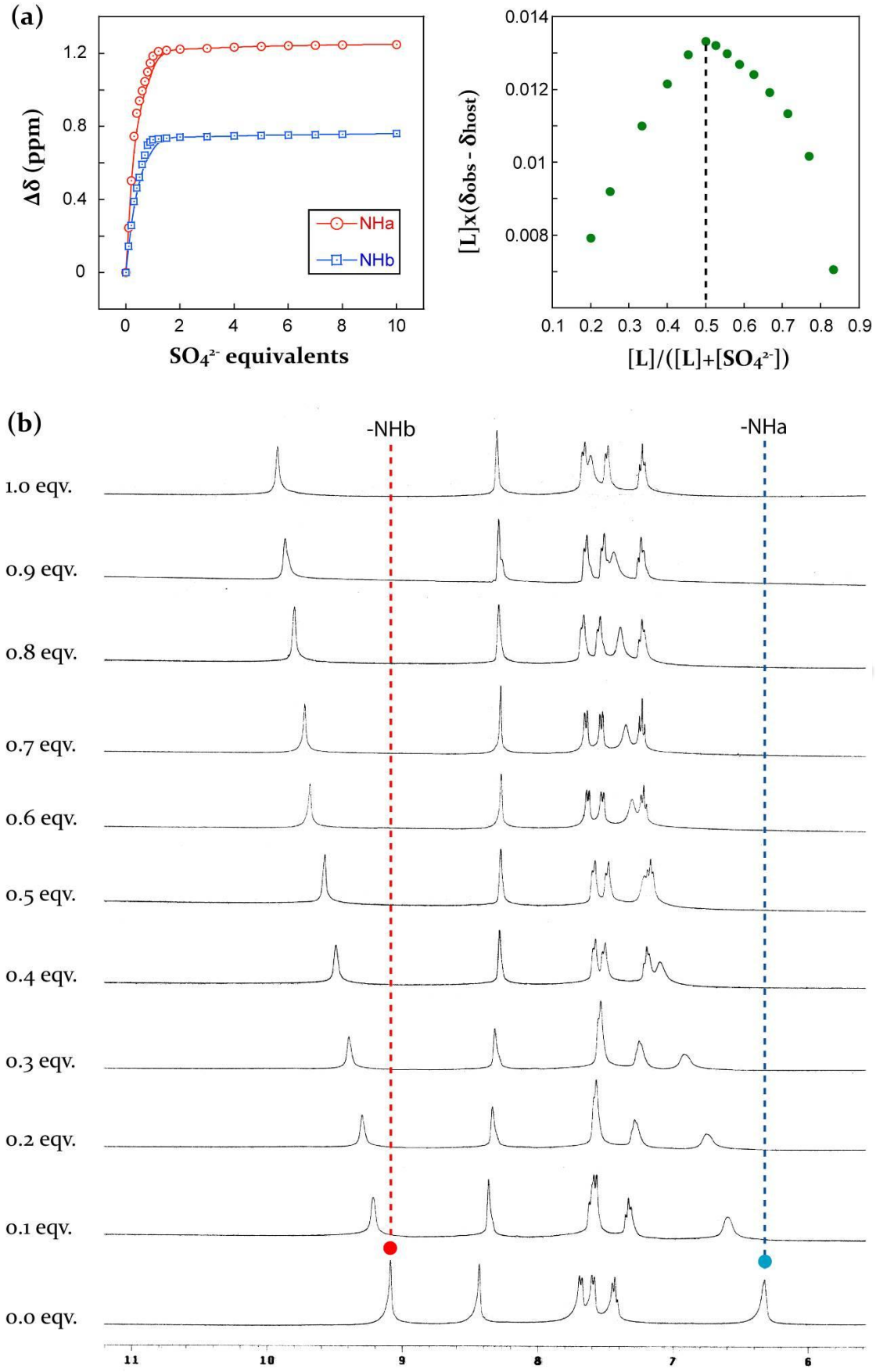

Figure 5.10 (a) Change in chemical shift of –NH resonances of **L_4** (5 mM) with increasing conc. of standard SO_4^{2-} solution (50 mM) in DMSO-d_6 and the corresponding Job's plot suggesting the formation of 1:1 host/guest complex; (b) Partial ^{1}H NMR titration spectra of **L_4** with $(TBA)_2SO_4$.

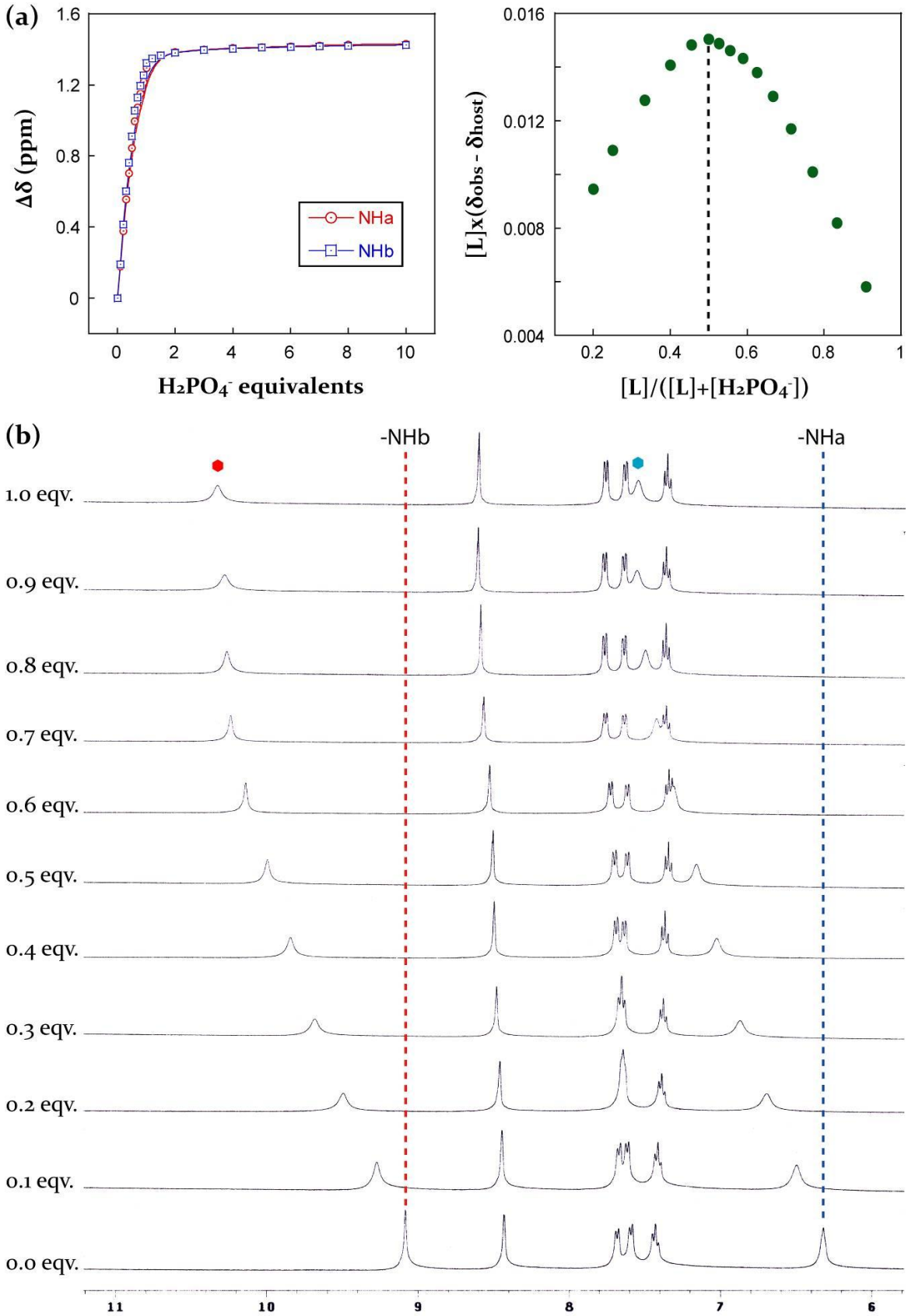

Figure 5.11 (a) Change in chemical shift of –NH resonances of **L_4** (5 mM) with increasing conc. of standard $H_2PO_4^-$ solution (50 mM) in DMSO-d_6 and the corresponding Job's plot suggesting the formation of 1:1 host/guest complex; (b) Partial ^{1}H NMR titration spectra of **L_4** with (TBA)H_2PO_4.

References

1. (a) D. S. Jenkinson, D. E. Adams and A. Wild, *Nature*, 1991, **351**, 304; (b) K. Caldeira, A. K. Jain and M. I. Hoffert, *Science*, 2003, **299**, 2052.

2. *IPCC Third Assessment Report: Climate Change 2001: The Scientific Basis*; Cambridge University Press: Cambridge, U.K., 2001.

3. (a) R. H. Essenhigh, *Chemical Innovation*, 2001, *May*, 44; (b) *Kyoto Protocol*; United Nations Framework Convention on Climate Change, 1998.

4. (a) A. Kohl and R. Nielsen, *Gas Purification*, 5th ed.; Gulf Publishing Co.; Houston, 1997; (b) G. A. Olah, A. Goeppert, and G. K. S. Prakash, *J. Org. Chem.*, 2009, **74**, 487.

5. (a) R. Banerjee, A. Phan, B. Wang, C. Knobler, H. Furukawa, M. O'Keeffe and O. M. Yaghi, *Science*, 2008, **319**, 939; (b) J. L. C. Rowsell, E. C. Spencer, J. Eckert, A. K. Howard, and O. M. Yaghi, *Science*, 2005, **309**, 1350; (c) C. M. Momming, E. Otten, G. Kehr, R. Frohlich, S. Grimme, D. W. Stephan and G. Erker, *Angew. Chem., Int. Ed*., 2009, **48**, 6643. (d) G. A. Olah, *Angew. Chem., Int. Ed*., 2005, **44**, 2636; (e) L.-Y. Kong, Z.-H. Zhang, H.-F. Zhu, H. Kawaguchi, T.-A. Okamura, M. Doi, Q. Chu, W.-Y. Sun and N. Ueyama, *Angew. Chem., Int. Ed.*, 2005, **44**, 4352; (f) E. Garcia-Espana, P. Gavina, J. Latorre, C. Soriano and B. Verdejo, *J. Am. Chem. Soc*., 2004, **126**, 5082; (g) Z. W. Mao, G. Liehr and R. Van Eldik, *J. Am. Chem. Soc*., 2000, **122**, 4839.

6. (a) S. J. Brooks, S. E. Garcia-Garrido, M. E. Light, P. A. Cole and P. A. Gale, *Chem. -Eur. J*., 2007, **13**, 3320; (b) I. Ravikumar and P. Ghosh, *Chem. Commun*., 2010, **46**, 1082; (c) T. Gunnlaugsson, P. E. Kruger, P. Jensen, F. M. Pfeffer and G. M. Hussey, *Tet. Lett*., 2003, **44**, 8909.

7. (a) P. R. Edwards, J. R. Hiscock and P. A. Gale, *Tetrahedron Lett.*, 2009, **50**, 4922; (b) P. R. Edwards, J. R. Hiscock, P. A. Gale and M. E. Light, *Org. Biomol. Chem.*, 2010, **8**, 100.

8. S. K. Dey, R. Chutia and G. Das, *Inorg. Chem*., 2012.

9. G. R. Desiraju, *Angew. Chem., Int. Ed.*, 2007, **46**, 8342.

10. I. Ravikumar, P. S. Lakshminarayanan, M. Arunachalam, E. Suresh and P. Ghosh, *Dalton Trans*., 2009, 4160.

11. (a) C. Caltagirone, J. R. Hiscock, M. B. Hursthouse, M. E. Light and P. A. Gale, *Chem. –Eur. J*., 2008, **14**, 10236; (b) P. A. Gale, J. R. Hiscock, S. J. Moore, C. Caltagirone, M. B. Hursthouse and M. E. Light, *Chem. –Asian J.*, 2010, **5**, 555; (c) C. Jia, B. Wu, S. Li, Z. Yang, Q. Zhao, J. Liang, Q. -S. Li and X. -J. Yang, *Chem. Commun.*, 2010, **46**, 5376.

12. B. P. Hay, T. K. Firman and B. A. Moyer, *J. Am. Chem. Soc*., 2005, **127**, 1810.

13. D. A. Jose, D. K. Kumar, B. Ganguly and A. Das, *Inorg. Chem.*, 2007, **46**, 5817.

14. A. Pramanik, B. Thompson, T. Hayes, K. Tucker, D. R. Powell, P. V. Bonnesen, E. D. Ellis, K. S. Lee, H. Yu and M. A. Hossain, *Org. Biomol. Chem*., 2011**, 9,** 4444.

Chapter 6

Selective Inclusion of PO_4^{3-} within Persistent Dimeric Capsules of a Tris(thiourea) receptor

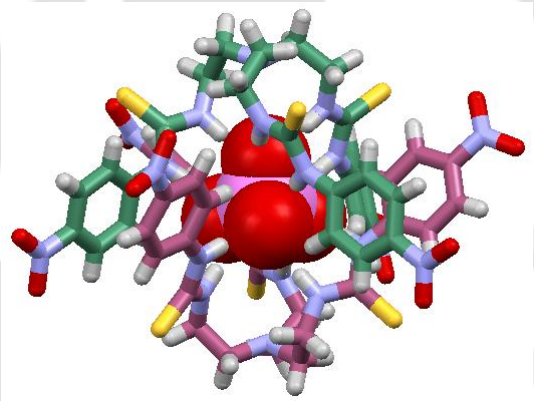

6.1 Background and Focus of the Chapter

Although Nature exemplify how proteins can selectively and efficiently bind anions by weak intermolecular forces,[1] the development of artificial receptors for the selective recognition of anions still remains a challenging task. In particular, inorganic phosphates ($H_2PO_4^-$, HPO_4^{2-} and PO_4^{3-}) and phosphate containing metabolites such as AMP^{2-}, ADP^{3-} and ATP^{4-} are among the most targeted anionic species on account of their vital role in many biological processes.[2] Besides hydrogen bonding and electrostatic contacts with the phosphate moiety, proteins often use other types of noncovalent interactions such as π-stacking and C-H···π interactions involving the organic part of the substrate in order to achieve selectivity and high binding affinity.[3] In the active site of phosphate binding protein (PBP) from *E. coli* bacteria, the anion is encapsulated between the two lobes of protein with an array of twelve hydrogen bonds where the carboxylate from an aspartate residue (Asp-56) is specifically coordinated to orthophosphate.[1a] Furthermore, it has been shown that much of the inorganic phosphates released in soil as fertilizers eventually make their way to surface water and leads to euthrophication of aquatic ecosystems.[4] Thus, development of artificial receptors capable of selective binding and encapsulation of inorganic phosphates using noncovalent interactions are crucial due to their diverse biological and environmental relevance. Over the last decade, many researchers have devoted themselves in developing artificial receptors for the selective and preferential binding of phosphates via noncovalent interactions, featuring different topological complementarities for the anion and are capable of mimicking enzymatic functions in some cases.[5]

This chapter describes the anion recognition properties of a nitro-functionalized tris(thiourea) receptor, $\mathbf{L_5}$ (Scheme 6.1) which has been established as a competent hydrogen bonding scaffold that can selectively encapsulate PO_4^{3-} within persistent and rigidified dimeric capsules, assembled by aromatic *π*-stacking interactions between the receptor side arms. The receptor in presence of excess TBA(H_2PO_4) has been found to encapsulate a PO_4^{3-} anion within a rigidified dimeric capsule of the receptor with twelve strong hydrogen bonds (**5b-I**) *via* hydrogen bond activated deprotonation of bound $H_2PO_4^-$, as evident from the origin of a new set of signals in the ^{1}H NMR titration experiments.[6] Furthermore, quaternary ammonium salt (TBA/TEA) of PO_4^{3-}–encapsulated complexes (**5b-I** and **5b-II**, 2:1 host-guest) can reproducibly be obtained in quantitative yield by a solution-state deprotonation of $[H\mathbf{L_5}]^+$ moieties and bound HPO_4^{2-} anion of HPO_4^{2-} complex of protonated $\mathbf{L_5}$ (**5a**, 2:1 host-guest), induced by the presence of large excess of anions such as HCO_3^-, CH_3COO^-, and F^-.[7] Competitive crystallization experiments performed in presence of excess anions such as HCO_3^-, HSO_4^-, $CH_3CO_2^-$, NO_3^- and halides (F^- and Cl^-) further establish the phenomenon of

selective PO_4^{3-} encapsulation as confirmed by ^1H NMR, ^{31}P NMR, FT-IR and powder X-ray diffraction patterns of the isolated crystals. X-ray structural analyses and ^{31}P NMR studies of the isolated crystals of phosphate complexes (**5a**, **5b-I** and **5b-II**) provide evidences of binding discrepancy of inorganic phosphates with protonated and neutral form of $\mathbf{L_5}$.[7] Furthermore, extensive studies have been carried out with other anions of different sizes and dimensions in solid- as well as in solution-states. Scheme 6.1 depicts the different types of molecular capsules of $\mathbf{L_5}$ obtained in presence of anions of different dimensionality.

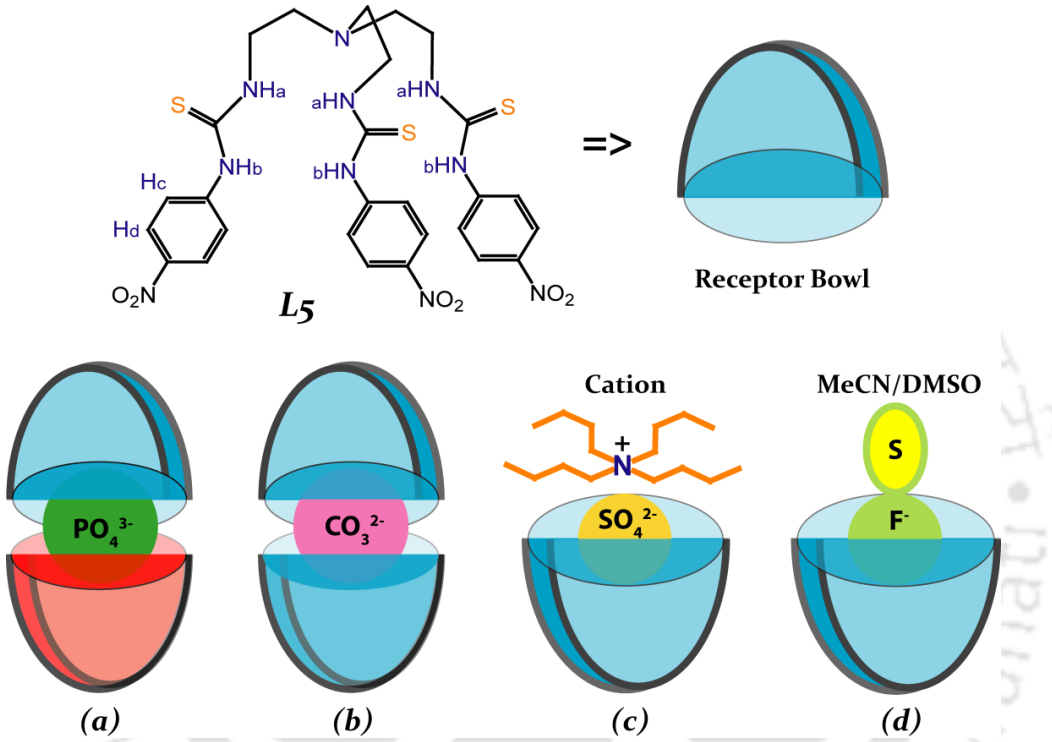

Scheme 6.1 Molecular structure of tris(thiourea) receptor $\mathbf{L_5}$ and schematic representation depicting the anion induced capsular and pseudocapsular assemblies of $\mathbf{L_5}$: (a) PO_4^{3-}–encapsulated dimeric capsule of $\mathbf{L_5}$ having independent symmetry (2:1 host/guest); (b) CO_3^{2-}–encapsulated dimeric capsule of $\mathbf{L_5}$ having identical symmetry (2:1 host/guest); (c) cation sealed SO_4^{2-}–encapsulated unimolecular capsule of $\mathbf{L_5}$ (1:1 host/guest), and (d) solvent (MeCN/DMSO) sealed F^-–encapsulated unimolecular capsule of $\mathbf{L_5}$ (1:1 host/guest).

6.2 Crystal structure of receptor $\mathbf{L_5}$, [$\mathbf{L_5}$•DMF]

Single crystals of $\mathbf{L_5}$ suitable for X-ray diffraction analysis were obtained from a dimethylformamide (DMF) solution, upon slow evaporation at room temperature. The receptor molecule crystallizes in the triclinic space group *P*-1 with a DMF molecule as solvent of crystallization. Structural elucidation of [$\mathbf{L_5}$•DMF] (Figure 6.1a) revealed that one of the thiourea functions from a receptor side arm is hydrogen bonded to lattice solvents *via* N-H···O and C-H···S interactions (N2···O7 = 2.875(6) Å; N3···O7 = 2.755(7) Å and C29···S1 = 3.536(1) Å) resulting in 1D association of the receptor molecules bridged by DMF, with

two additional C-H···O-(nitro) interactions (C29···O6 = 3.633(1) Å and C30···O6 = 3.553(1) Å) along crystallographic *a*-axis (Figure 6.1b). Two such 1D chains of receptor molecules are further associated with one another by N-H···S interactions between identical receptor side arms (N6···S2 = 3.479(5) Å and N9···S3 = 3.430(4) Å) along crystallographic *c*-axis (Figure 6.1b).

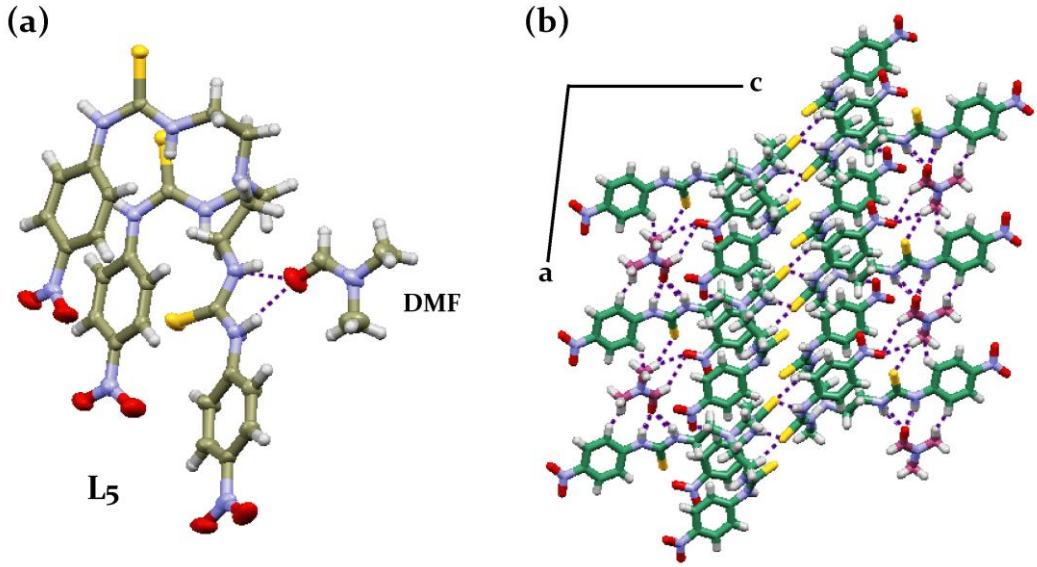

Figure 6.1 (a) Thermal ellipsoid plot (30% probability) of crystal structure of $\mathbf{L_5}$•DMF; (b) Crystal packing motif of $\mathbf{L_5}$•DMF as viewed down the *b*-axis (carbon atoms of receptor and solvent molecules are shown in different colours).

6.3 Structural aspects of anion binding with neutral and protonated $\mathbf{L_5}$

Structural information obtained from single crystal X-ray analyses of the anion complexes can provide insight into the proper binding topology of different anions with the cationic and neutral $\mathbf{L_5}$. From the perspective of anion receptor chemistry, crystallization has traditionally been a route to understand the structural insights of the anion complexes, which are then related to the observed selectivity in solution. Efforts were made to examine the solid-state binding of different anions with protonated and neutral form of receptor $\mathbf{L_5}$, by charging an excess of different mineral acids (HF, HCl, CH_3COOH, H_2SO_4, H_3PO_4) or a large excess of quaternary ammonium (TBA/TEA) salt of different anions (F^-, Cl^-, CH_3COO^-, HCO_3^-, HSO_4^-, $H_2PO_4^-$) to the individual solutions of $\mathbf{L_5}$ in polar aprotic solvents (MeCN and DMSO). However, we were able to isolate only six complexes (**5a-5f**), as single crystals suitable for X-ray crystallography analysis from individual solutions of $\mathbf{L_5}$ in presence of H_3PO_4, TBA(H_2PO_4), TEA(HCO_3), TBA(HSO_4), TBAF and HCl respectively. Interestingly, single crystals of $(TEA)_3PO_4^{3-}$ complex of $\mathbf{L_5}$ (**5b-II**) was obtained from a MeCN solution of **5a** charged with an excess (10 equiv) TEA(HCO_3) or TEA(CH_3CO_2). Furthermore, single

crystals of $(TBA)_3PO_4^{3-}$ complex of $\mathbf{L_5}$ (**5b-I**) were also obtained in quantitative yield from individual MeCN solution of **5a** in presence of excess $TBA(CH_3CO_2)$ and TBAF.

Table 6.1 Crystallographic parameters and refinement details of receptor $\mathbf{L_5}$ and phosphate complexes **5a, 5b-I** and **5b-II.**

Parameters	$\mathbf{L_5}$•DMF	**5a**	**5b-I**	**5b-II**
Formula	$C_{30}H_{37}N_{11}O_7S_3$	$C_{54}H_{69}N_{20}O_{19}PS_6$	$C_{106}H_{174}N_{25}O_{16}PS_6$	$C_{78}H_{120}N_{23}O_{16}PS_6$
Fw	759.92	1518.63	2278.09	1859.36
Cry. system	Triclinic	Triclinic	Triclinic	Rhombohedral
Space group	*P*-1	*P*-1	*P*-1	$P3_1c$
a/Å	9.3675(5)	14.2058(8)	13.5840(7)	19.957(3)
b/Å	10.4400(6)	15.0756(9)	16.0821(8)	19.957(3)
c/Å	19.5297(11)	19.4881(11)	28.9547(15)	14.7921(18)
α/°	94.671(4)	100.526(4)	103.421(4)	90.00
β/°	92.962(4)	109.789(4)	93.523(4)	90.00
γ/°	110.626(3)	100.260(4)	92.808(4)	120.00
V/Å^3	1774.95(18)	3728.9(4)	6128.0(6)	5102.1(12)
Z	2	2	2	2
D_c/g cm^{-3}	1.422	1.353	1.235	1.210
μ (mm^{-1})	0.271	0.283	0.194	0.217
T/°K	298(2)	298(2)	298(2)	298(2)
θ max.	28.340	28.460	28.460	24.780
Total reflns	24704	69613	92714	57085
Ind. reflns	8599	18459	29779	2865
Obs. reflns	6935	14268	24513	2633
Parameters	463	903	1401	376
R_1, $I > 2\sigma(I)$	0.0890	0.0956	0.0860	0.0796
wR_2(all data)	0.2071	0.2413	0.2158	0.2391
GOF (F^2)	0.972	0.972	1.067	1.011

6.3.1 Hydrogenphosphate complex, $[2(HL_5)^+ \bullet HPO_4^{2-}] \bullet 3H_2O$ (5a)

Complex **5a** crystallizes in triclinic space group *P*-1 with three water molecules as solvent of crystallization and the asymmetric unit contains two symmetry independent receptor cations (Z = 2 and Z′ = 2) where the tertiary nitrogen of $\mathbf{L_5}$ is protonated by H_3PO_4. Due to disorder, it was not possible to locate the hydrogen on HPO_4^{2-} anion, in order to unambiguously determine the degree of protonation and charge upon the anion. However, structural elucidation reveals a 2**:**1 receptor-anion stoichiometric salt formation confirming the HPO_4^{2-}

complex of protonated $\mathbf{L_5}$. Both the conformers (**C1** and **C2**) of protonated $\mathbf{L_5}$ are conformationally locked due to intramolecular $(N\text{-}H)^{+}\cdots S$ hydrogen bonding (N1···S1 = 3.250(1) Å and N11···S5 = 3.261(9) Å) between the *endo*-oriented proton of bridgehead nitrogen with a thiourea-sulphur atom from a single receptor side arm and complementary N-H···S hydrogen bonding (N8···S2 = 3.409(8) Å and N18···S4 = 3.329(7) Å) between the other two arms of individual receptor cations (Figure 6.2a). Additionally, intramolecular C-H···π and π···π interactions have also been observed in conformers **C1** and **C2** (Figure 6.2a). Examining the coordination environment of HPO_4^{2-} suggests that, it is involved in side-cleft binding with four receptor cations via eleven hydrogen bonding interactions comprised of ten N-H···O and one C-H···O bonds having an average donor-to-acceptor distance of 3.071 Å (Table 6.3). A correlation of N-H···O angle *vs.* N-H···O distance shows that eight out of ten N-H hydrogen bonds are in the strong hydrogen bonding interaction region of d(H···O) < 2.5 Å, d(N···O) < 3.2 Å and <N-H···O > 140° whereas the C-H···O bond operates in the weak hydrogen bonding interaction region (C28···O15 = 3.405(2) Å). The coordination environment of the anion is shown in Figure. 1b which shows that, two adjacent receptor cations with dissimilar conformation provides a three-point attachment to O13 whereas two adjacent receptors with similar conformation (conformer **C2**) provide a two-point attachment each to O14 and O15. Finally, the eleven-point coordination on HPO_4^{2-} is satisfied by a four-point attachment to O16 donated from the –NH functions of two adjacent receptors with similar conformation (conformer **C1**).

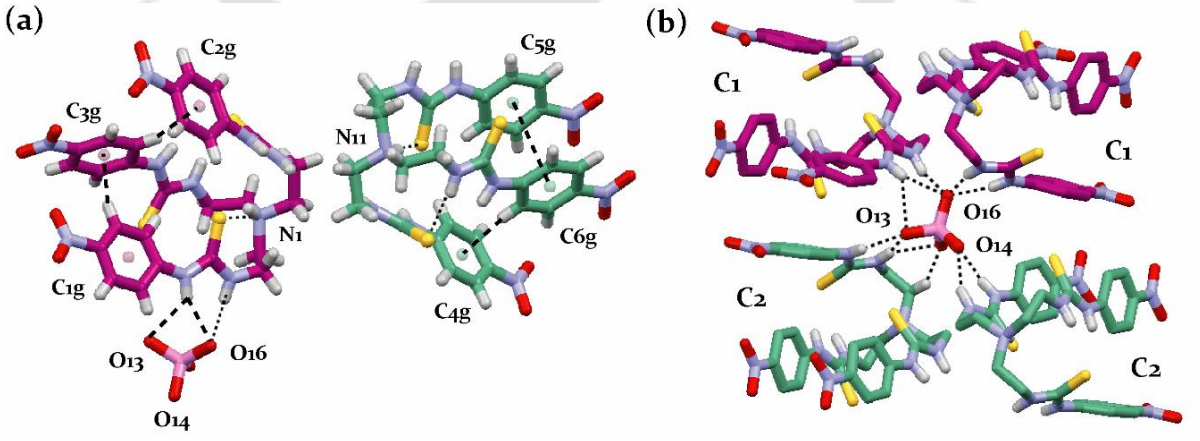

Figure 6.2 (a) X-ray structure of complex **5a** depicting the intramolecular noncovalent interactions between the receptor side arms of two symmetry independent molecules; (b) 11-point coordination of HPO_4^{2-} anion in **5a** with four encircling cationic receptor molecules. The symmetry independent molecules are shown in different colours.

6.3.2-I Phosphate-encapsulated complex, 3TBA[2L_5(PO_4)]•2MeCN (5b-I)

The phosphate complex, **5b-I** was obtained as suitable crystals for XRD analysis upon slow evaporation of a solution mixture of $\mathbf{L_5}$ and excess TBA dihydrogen phosphate in MeCN or by charging an excess TBA(CH_3CO_2) and TBAF to the individual solutions **5a** in MeCN. Structural elucidation revealed that, added $H_2PO_4^-$ anion or bound HPO_4^{2-} anion of **5a** has deprotonated in solution-state and is bound in the form of PO_4^{3-} by two units of receptor $\mathbf{L_5}$ which are flipped inward toward each other in a face-to-face fashion ($d_{N1\cdots N11}$ = 9.535 Å) with one ligand coordinating in the axial mode and the other in facial mode (Figure 6.3a) and thereby, creating a caged supramolecular structure assembled by $\pi\cdots\pi$ interactions of the phenyl rings (C2g···C6g = 3.968 Å and C3g···C4g = 3.872 Å) (Figure 6.3b). Similar deprotonation of $H_2PO_4^-$ has also been observed by Gale et al. and Wu et al. with tris(urea) receptors, which can be explained due to the formation of multiple hydrogen bonding interactions that lowers the pK_a of the bound guest to the extent that it is deprotonated by free dihydrogen phosphate in solution. Two symmetry independent molecules of $\mathbf{L_5}$ with opposite orientation form a capsular nanocavity that encapsulates a trivalent phosphate anion in its centre *via* twelve strong hydrogen bonds to the six thiourea groups (d(D···A) < 3.00 Å). Each phosphate oxygen atom behaves as trifurcated hydrogen bond acceptor and each -NH group donates one N-H···O bond, resulting in twelve hydrogen bonds with an average d(N···O) of 2.798 Å (Table 6.3 and Figure 6.3c). Interestingly, in the phosphate-binding protein, bound hydrogen phosphate anion accepts eleven hydrogen bonds from the protein and donates one to it making a total of twelve hydrogen bonds. Thus, the structure reported here represents the optimal coordination number for phosphate. Moreover, several weaker interactions involving the –NH and aryl –CH protons could be added to the encapsulated phosphate anion when the d(D···A) is restricted to < 3.5 Å for hydrogen bonding, which provide additional stability for phosphate binding within the capsular assembly. Notably, aryl –CH protons C9H and C27H from the axial coordinating ligand and C45H and C50H from the facial ligand make contacts with the phosphate anion with an average d(C···O) of 3.301 Å (Table 6.3).

6.3.2-II Phosphate-encapsulated complex, 3TEA[2L_5(PO_4)] (5b-II)

Good quality crystals of **5b-II** suitable for X-ray diffraction analysis were obtained upon slow evaporation of a MeCN solution of **5a** in presence of excess (10 equiv) tetraethylammonium acetate/bicarbonate, which crystallizes in the trigonal system with centrosymmetric space group $P3_1c$. Structural elucidation revealed that, the protonated receptor molecules and bound HPO_4^{2-} anion of complex **5a** has deprotonated in presence of

excess acetate/bicarbonate ions and forms a PO_4^{3-}–encapsulated rigidified dimeric assembly of the neutral receptor. Two symmetry-independent receptor molecules are flipped inward toward each other in a face-to-face fashion ($d_{N1\cdots N11}$ = 9.605 Å) with one ligand coordinating to PO_4^{3-} in the axial mode and other in the facial mode (Figure 6.3d) and thereby, creating a caged supramolecular structure assembled by $\pi\cdots\pi$ interactions of the terminal aryl functions (C1g···C2g = 3.680 Å) and aromatic C-H···N interactions (C14···N2 = 3.582(7) Å) (Figure 6.3e). Hydrogen bonding interactions (d(D···A) < 3.20 Å) on PO_4^{3-} shows that, the anion is completely engulfed within a highly symmetrical π-stacked dimeric assembly of $\mathbf{L_5}$ with an array of 12 strong hydrogen bonds to the six thiourea groups (Figure 6.3f). Each phosphate oxygen atom behaves as trifurcated hydrogen bond acceptor and each -NH group donates one N-H···O bond, resulting in twelve hydrogen bonds with an average donor-to-acceptor distance of 2.811 Å (Table 6.3). Moreover, several weaker interactions involving the –NH and aryl –CH protons could be added to the encapsulated PO_4^{3-} anion when the donor-to-acceptor distance is restricted to < 3.5 Å for hydrogen bonding, which provide additional and increased stability for phosphate binding within the capsular assembly. Notably the aryl proton -C9H and thiourea proton -N6H from the facial coordinating unit make contacts with phosphate oxygen O6 with distances of 3.349(6) Å and 3.285(7) Å respectively. The phosphate oxygen O5 is coordinated only with the axial receptor unit by three N-H···O hydrogen bonds whereas each symmetry-related oxygen atoms O6 is coordinated to both the units of the dimeric capsule by 4 N-H···O and one C-H···O hydrogen bonds.

Thus, by a mere change of countercation (tetraethyl ammonium), we have been able to isolate and structurally authenticate a highly symmetric and robust PO_4^{3-}–encapsulated molecular capsule, **5b-II** as compared to the structure of tetrabutylammonium salt of PO_4^{3-}–encapsulated molecular capsule, **5b-I** where the dimeric cage is self-assembled by two π-stacking pairing between the aryl functions upon coordination to a PO_4^{3-} anion. It is worth to mention here that, the solution-state deprotonation of $[H\mathbf{L_5}]^+$ moieties in **5a** can be attributed to the high basicity of crystallization medium induced by the presence of excess fluoride/acetate/bicarbonate ions whereas, deprotonation of bound HPO_4^{2-} can be explained due to the formation of multiple hydrogen bonding interactions with the in situ generated $\mathbf{L_5}$ that lowers the pK_a of the bound HPO_4^{2-} to the extent that it is deprotonated by free (excess) fluoride/acetate/bicarbonate in solution. Such a solution-state deprotonation of the protonated state of an anion *viz*. $H_2PO_4^-$, HCO_3^- and HSO_4^- is not uncommon.

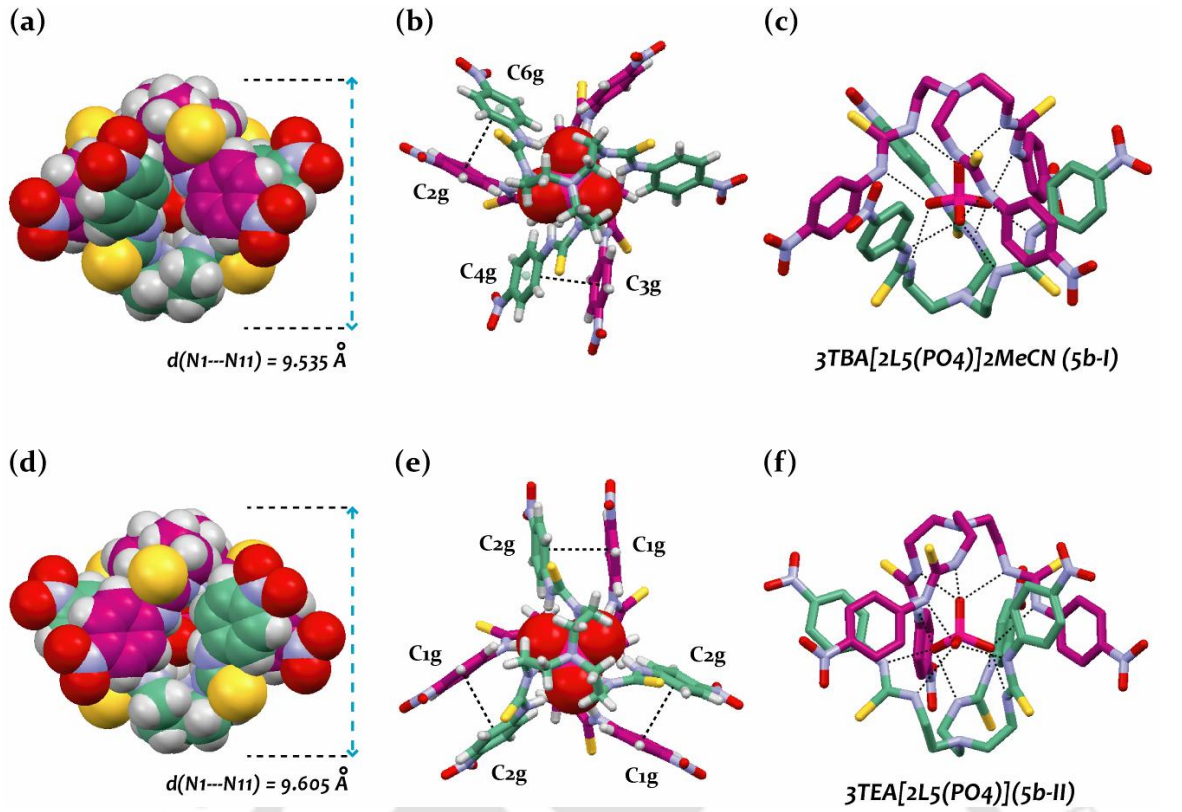

Figure 6.3 (a) X-ray structure (spacefill model) of **5b-I** depicting the encapsulation of PO_4^{3-} within a dimeric assembly of two symmetry-independent molecules of $\mathbf{L_5}$; (b) Aromatic π•••π stacking between the receptor side arms of the dimeric capsule in **5b-I**; (c) 12 strong hydrogen-bonding contacts on PO_4^{3-} within the dimeric capsule in **5b-I**; (c) X-ray structure (spacefill model) of **5b-II** depicting the encapsulation of PO_4^{3-} within a dimeric assembly of two symmetry-independent molecules of $\mathbf{L_5}$; (b) Aromatic π•••π stacking between the receptor side arms of the dimeric capsule in **5b-II**; (c) 12 strong hydrogen-bonding contacts on PO_4^{3-} within the dimeric capsule in **5b-II**.

6.3.3 Carbonate-encapsulated complex, 2TEA[2L$_5$(CO$_3$)] (5c)

Complex **5c** was obtained as suitable crystals for X-ray diffraction analysis upon slow evaporation of a DMSO solution of $\mathbf{L_5}$ and excess tetraethyl ammonium bicarbonate, which crystallizes in the monoclinic system with centrosymmetric space group *C*2/c. Crystal structure elucidation revealed a 2:1 complex stoichiometry (host-guest), where two symmetry-identical receptor molecules with opposite orientation encapsulates a in situ generated CO_3^{2-} in its centre *via* multiple N-H···O hydrogen bonds to the six thiourea functions. Similar deprotonation of HCO_3^- has recently been observed by Gale et al. with indole, carbazole and tripodal based receptors, which were attributed to the hydrogen bonding activated proton transfer between the free and bound anions.[8] The inversion-symmetric molecules are flipped inward toward each other in a face-to-face fashion with a distance of 7.925(5) Å between the apical nitrogen atoms (Figure 6.4a) and thereby, generate a centrosymmetric molecular capsule assembled by C-H···O-(nitro) and C-H···S hydrogen

bonds between each capsular unit. The carbonate oxygen O7 accepts four N-H···O hydrogen bonds whereas symmetry-identical O8 and O8′ accepts five N-H···O hydrogen bonds each (Figure 6.4b), resulting in a total of 14 hydrogen bonding contacts on CO_3^{2-} with an average donor-to-acceptor (N···O) distance of 2.862 Å (Table 6.3). The urea protons N2H, N5H, N6H, N8H and N9H from the individual coordinating units of the dimeric capsule donate one N-H···O bond each to the carbonate oxygen O8 and O8′ whereas N2H and N3H from each coordinating unit are hydrogen bonded to carbonate oxygen O7. A correlation of N-H···O angle *vs*. N-H···O distance shows that eight out of fourteen hydrogen bonds are in the strong hydrogen bonding interaction region of *d*(H···O) < 2.5 A and *d*(D···O) < 3.2 A (Table 6.3).

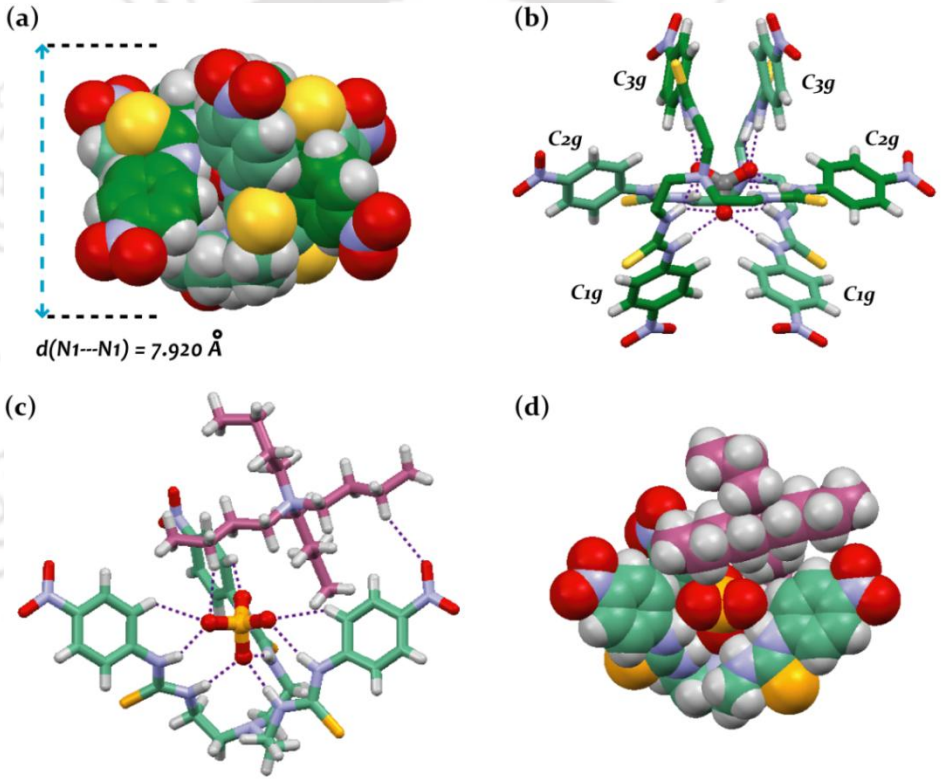

Figure 6.4 (a) X-ray structure (spacefill model) of complex **5c** depicting the encapsulation of CO_3^{2-} within a dimeric capsular assembly of two symmetry-identical molecules of $\mathbf{L_5}$; (b) Ball and stick representation depicting the 14 hydrogen-bonding contacts on CO_3^{2-} within the dimeric capsule of $\mathbf{L_5}$; (c) X-ray structure of complex **5d** depicting the 10 hydrogen bonding contacts on SO_4^{2-} with **L** and a tetrabutylammonium (TBA) cation; (d) Spacefill model of **5d** showing the formation of TBA cation sealed SO_4^{2-} encapsulated unimolecular capsule.

6.3.4 Sulfate-encapsulated complex 2TBA[$L_5(SO_4)$] (5d)

Complex **5d** was obtained as suitable crystals for X-ray diffraction analysis upon slow evaporation of a DMSO solution of $\mathbf{L_5}$ and excess tetrabutylammonium hydrogensulfate, which crystallizes in the monoclinic system with $P2_1/c$ space group. Crystal structure

elucidation revealed a 1:1 complex stoichiometry, where three arms of the receptor form a cavity that encapsulates a divalent sulfate anion (SO_4^{2-}) in its centre *via* six N-H···O hydrogen bonds to the three thiourea functions of **L_5**. The sulfate oxygen O7 accepts three N-H···O hydrogen bonds from the aliphatic $–NH_a$ protons whereas O8, O9 and O10 accepts one N-H···O bond each from the aromatic $–NH_b$ protons of **L_5** (Figure 6.4c), with an average donor-to-acceptor distance of 2.861 Å. Additionally, an *ortho*-aryl proton from each receptor side arm is C-H···O hydrogen bonded to sulfate oxygen O8, O9 and O10 with an average donor-to-acceptor distance of 3.298 Å (Table 6.3). Furthermore, one of the TBA cations is held in close contact with the encapsulated SO_4^{2-} by a C-H···O hydrogen bond to O8 and also interacts with the receptor moiety by another C-H···O interaction donated to a nitro oxygen O3 (Figure 6.5a). Thus, the encapsulated sulfate is involved in nine hydrogen bonding interactions with the receptor molecule and a C-H···O interaction from a TBA cation which acts as a seal to the anion entrapped unimolecular capsule (Figure 6.4d).

6.3.5-I Fluoride-encapsulated complex, TBA[L_5(F)]•2DMSO (5e-I)

DMSO solvate of F^-–encapsulated complex, **5e-I** crystallize in the monoclinic space group *C*2/c with two DMSO molecules as solvent of crystallization. Structural elucidation revealed that, a F^- anion is encapsulated inside the tripodal scaffold with an array of six strong N-H···F^- hydrogen bonds involving all three thiourea functions and a lattice DMSO molecule is hydrogen bonded to the peripheral nitro-aromatic functions by four C-H···O interactions demonstrating the ditopic binding of a negatively charged species (F^-) and a neutral molecule (DMSO) by receptor **L_5** (Figure 6.5a). The encapsulated F^- anion is bound more strongly to the aryl $–NH_b$ protons than the aliphatic $–NH_a$ protons of the receptor with an average donor-to-acceptor distance of 2.927 and 2.733 Å for $–NH_a$ and $–NH_b$ respectively [average d(N···F^-) = 2.830 Å] (Table 6.3). The interactions of a DMSO molecule with the aryl functions of a F^-–encapsulated receptor by four C-H···O hydrogen bonds [average *d*(C···O) = 3.396 Å] seals the fluoride bound unimolecular capsule of **L_5**. Furthermore, two solvent sealed receptor capsules are interlinked with each other by a C-H···O interaction [C45···O1 = 3.306(1) Å] donated from a DMSO methyl proton to a nitro oxygen of the subsequent fluoride bound receptor resulting in a solvent-bridged pseudodimeric capsular assembly (Figure 6.5b).

6.3.5-II Fluoride-encapsulated complex, TBA[L_5(F)]•MeCN (5e-II)

MeCN solvate of F^-–encapsulated complex, **5e-II** crystallize in the triclinic space group *P*-1 with Z=4. Structural elucidation revealed that, the asymmetric unit contains two F^-–encapsulated receptor molecules ($Z^{/}$= 2) wherein F^- is bound individually within the tripodal

scaffold of two symmetry independent receptor units by six N-H···F^- hydrogen bonds involving all three thiourea functions (Figure 6.5c). As observed in **5e-I**, the encapsulated F^- anions are bound more strongly to the aryl $–NH_b$ protons than the aliphatic $–NH_a$ protons of the receptor with an average donor-to-acceptor distance of 2.908 and 2.737 Å for $–NH_a$ and $–NH_b$ respectively [average d(N···F^-) = 2.822 Å] (Table 6.3). Furthermore, each MeCN molecule is hydrogen bonded to the peripheral nitro-functions of individual F^-–encapsulated receptor by three C-H···O interactions [average d(C···O) = 3.706 Å] and thereby, seals the F^- bound receptor capsule identical to **5e-I**. Additionally, the F^-–encapsulated receptor units are held together by weak intermolecular C-H···π and π···π interactions (C23···C6g = 4.097 Å; C45···C1g = 3.993 Å and C3g···C5g = 4.149 Å). To the best our knowledge, MeCN and DMSO solvates of F^-–encapsulated $\mathbf{L_5}$ (**5e-I** and **5e-II**) represents the first structural evidences on solvent sealed encapsulation of anion inside a tripodal scaffold.

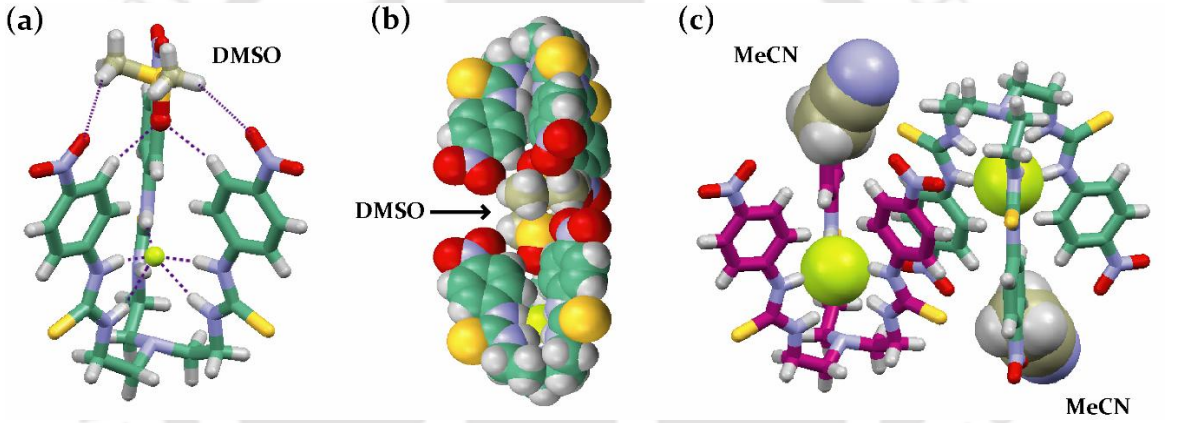

Figure 6.5 (a) X-ray structure of **5e-I** depicting the encapsulation of F^- within the receptor cavity by six N-H•••F^- hydrogen bonds and peripheral binding of a DMSO molecule by four C-H•••O hydrogen bonds; (b) Space fill model showing the formation of solvent-sealed pseudocapsular dimeric assembly in **5e-I**; (c) X-ray structure of **5e-II** depicting the formation of solvent (MeCN) sealed unimolecular capsule of $\mathbf{L_5}$ identical to **5e-I.**

6.3.6 Chloride complex, $[(HL_5)^+ \bullet Cl^-]\bullet$DMF (5f)

Complex **5f** crystallizes in triclinic space group *P*1 with a DMF molecule as solvent of crystallization, where the tertiary nitrogen of the receptor is found to be protonated. The hydrogen of the protonated bridgehead nitrogen is *endo*-oriented towards the receptor cavity and is hydrogen bonded with a thiourea-sulphur atom from a single receptor side arm [N1···Cl^- = 3.315(3) Å]. Due to intramolecular (N-H)$^+$···S hydrogen bonding and π–stacking interaction between two receptor side arms [C2g···C3g = 3.731(3) Å], the receptor cavity is conformationally restricted for chloride encapsulation. However, chloride anion is coordinated via side-cleft binding to two adjacent receptor cations with an array of six N-

H···Cl^- hydrogen bonds (Figure 6.6a). An average donor-to-acceptor distance of 3.303 Å demonstrates the weak binding of Cl^- as compared to HPO_4^{2-} by cationic form of the receptor in solid-state (Table 6.3). Examining the coordination environment of Cl^- revealed that, one of the coordinating receptor cations donates four N-H hydrogen bonds while the other donates two N-H bonds satisfying the optimal coordination number of chloride in complex **5f**. Furthermore, the lattice DMF molecule is in interaction with the chloride bound receptor cations by two strong N-H···O and three weak C-H···O hydrogen bonds (Table 6.3) demonstrating the ditopic binding of a negatively charged species (Cl^-) and a neutral molecule (DMF) by cationic $\mathbf{L_5}$ (Figure 6.6b).

Table 6.2 Crystallographic parameters and refinement details of anion complexes **5c-5f.**

Parameters	**5c**	**5d**	**5e-I**	**5e-II**	**5f**
Formula	$C_{71}H_{100}N_{22}O_{15}S_6$	$C_{59}H_{102}N_{12}O_{10}S_4$	$C_{47}H_{78}FN_{11}O_8S_5$	$C_{45}H_{69}FN_{12}O_6S_3$	$C_{30}H_{38}ClN_{11}O_7S_3$
Fw	1694.15	1267.81	1104.55	989.33	796.37
Cry. system	Monoclinic	Monoclinic	Monoclinic	Triclinic	Triclinic
Space group	C_2/c	$P2_1/c$	C_2/c	P-1	$P1$
a/Å	19.2809(7)	20.0884(19)	35.832(3)	13.0874(4)	8.2973(3)
b/Å	19.0630(7)	14.6094(13)	13.5139(14)	13.1320(4)	9.0007(4)
c/Å	24.6347(9)	24.4952(19)	27.699(3)	35.7500(11)	12.7365(5)
α/°	90.00	90.00	90.00	79.965(2)	98.535(3)
β/°	108.323(3)	101.722(5)	117.856(7)	86.542(3)	98.527(2)
γ/°	90.00	90.00	90.00	60.285(2)	97.221(2)
V/Å^3	8595.5(6)	7038.9(11)	11859(2)	5252.1(3)	919.58(6)
Z	4	4	8	4	1
D_c/g cm^{-3}	1.309	1.196	1.237	1.251	1.438
μ (mm^{-1})	0.232	0.195	0.255	0.201	0.336
T/°K	298(2)	298(2)	298(2)	298(2)	298(2)
θ *max.*	24.780	19.220	28.420	28.360	28.380
Total reflns	61244	35275	47212	49038	13809
Ind. reflns	7338	5664	14739	25528	4525
Obs. reflns	3976	4857	12704	21878	3422
Parameters	519	774	681	1217	499
R_1, $I > 2\sigma(I)$	0.0962	0.0535	0.0988	0.0875	0.0481
wR_2	0.2487	0.1741	0.2458	0.2076	0.1201
GOF (F^2)	1.030	1.026	0.943	1.0061	0.972

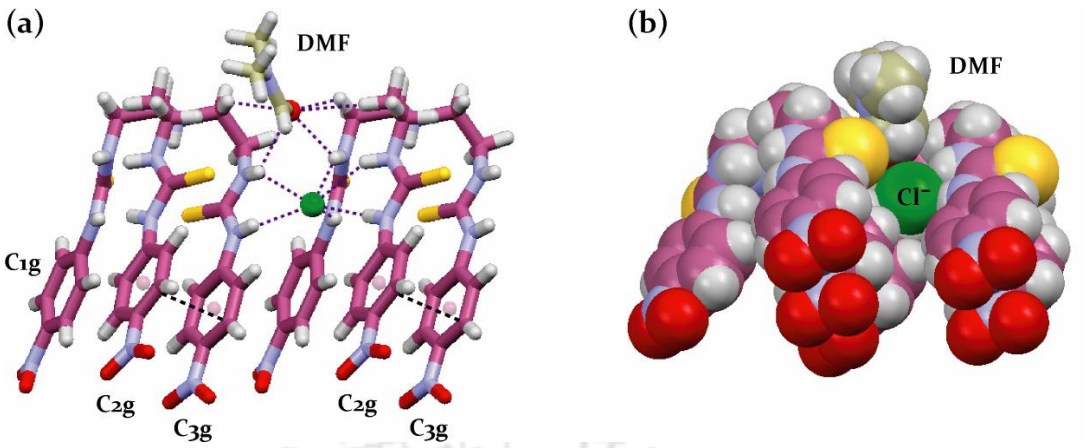

Figure 6.6 (a) X-ray structure of complex **5f** depicting the ditopic binding of Cl^- and a DMF molecule with two cationic receptor molecules outside the receptor cavity; (b) Spacefill model of the ditopic binding in complex **5f**.

6.4 Solution-state anion binding studies

Solution-state complexation of anions and binding stoichiometry (1:1/2:1, host: guest) of the isolated complexes were monitored by ^1H, ^{31}P (for complexes **5a**, **5b-I** and **5b-II** only) and 2D-NOESY NMR experiments in DMSO-d_6. Analysis of the ^1H NMR spectrum of HPO_4^{2-} complex, **5a** showed a slight spectral change in the resonances of aliphatic $-NCH_2$ ($\Delta\delta$ = 0.11 ppm) and thiourea –NH protons ($\Delta\delta$, $-NH_a$ = 0.17 ppm and $\Delta\delta$, $-NH_b$ = 0.33 ppm) as compared to PO_4^{3-}–encapsulated complexes **5b-I** and **5b-II**, which showed a huge downfield shift of –NH resonances (*w.r.t* $\mathbf{L_5}$) with an average $\Delta\delta$ value of 3.55 and 2.65 ppm for $-NH_a$ and $-NH_b$ protons respectively (Figure 6.7). The huge deshielding of –NH protons in PO_4^{3-}–complexes, **5b-I** and **5b-II** can be attributed to the strong solution-state binding and encapsulation of trivalent phosphate (PO_4^{3-}) within the receptor cavity. Whereas marginal spectral changes rules out the possibility of divalent phosphate (HPO_4^{2-}) encapsulation in **5a**, presumably due to protonation (at bridgehead N) induced conformational locking of the receptor in solution as well. In addition, the two doublets of aromatic –CH protons (H_c and H_d in $\mathbf{L_5}$) get merged into a single triplet with a concomitant upfield shift in PO_4^{3-}–complexes (**5b-I** and **5b-II**), which indeed indicates a solution-state structural alteration of the receptor side arms that could facilitate the formation of multiple N–H···O hydrogen bonds to encapsulate PO_4^{3-} within the receptor cavity.

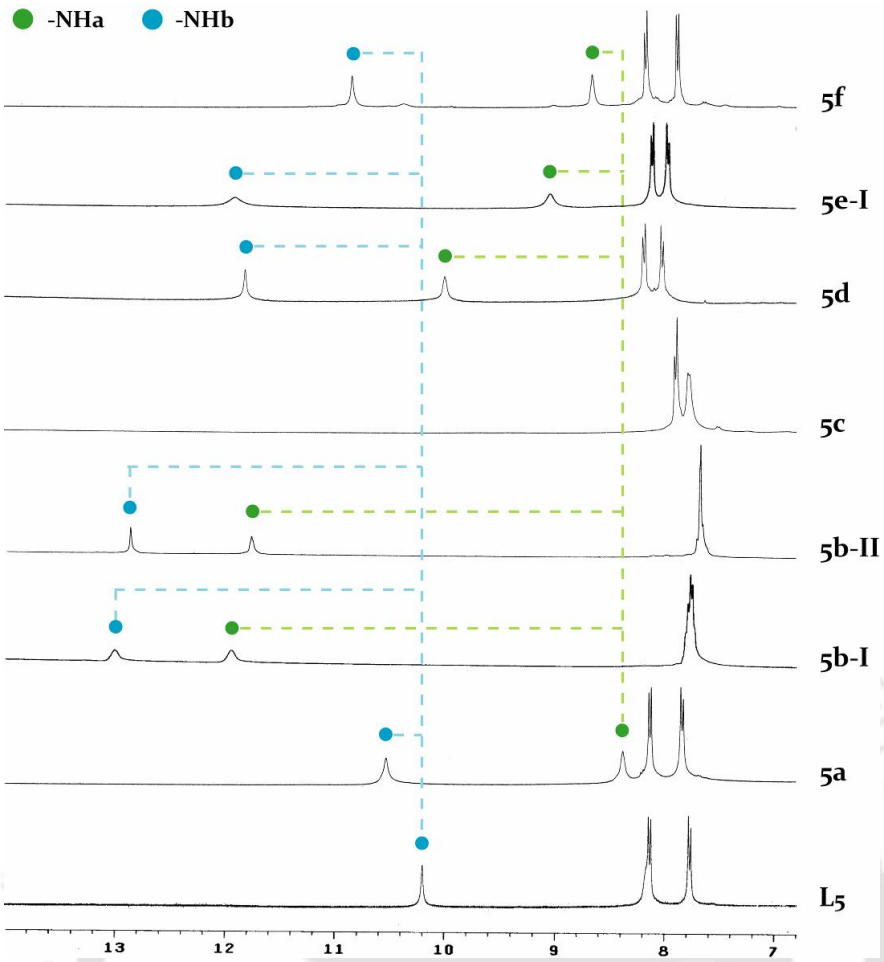

Figure 6.7 Partial ^{1}H NMR spectra (aromatic region) of isolated anion complexes (**5a-5f**) showing the downfield shift of thiourea –NH resonances relative to receptor $\mathbf{L_5}$.

^{31}P NMR analyses carried out on complexes **5a**, **5b-I** and **5b-II** further provide evidences of binding discrepancy of inorganic phosphates with protonated and neutral form of receptor $\mathbf{L_5}$. In **5a**, the ^{31}P resonance of HPO_4^{2-} originates at 0.555 ppm whereas in capsular complexes **5b-I** and **5b-II**, the ^{31}P resonances of encapsulated PO_4^{3-} occur at 10.338 and 10.157 ppm respectively. Comparison with the free resonance of TBA($H_2PO_4^-$) revealed a substantial upfield shift of 1.85 ppm in the ^{31}P resonance of **5a** whereas a huge downfield shift of 7.93 and 7.75 ppm has been observed in the ^{31}P resonances of **5b-I** and **5b-II** respectively (Figure 6.8). Thus, ^{31}P NMR studies also establish the variable mode of phosphate binding with protonated and neutral $\mathbf{L_5}$ in solution-state.

In the ^{1}H NMR spectrum of CO_3^{2-}–encapsulated complex, **5c** the resonances for the –NH protons could not be observed presumably because of significant binding-induced broadening of the –NH signals. Similar to PO_4^{3-}–encapsulated complexes, the SO_4^{2-}–encapsulated complex **5d** showed a significant deshielding of thiourea –NH protons with a $\Delta\delta$ (*w.r.t* $\mathbf{L_5}$) value of 1.70 and 1.47 ppm for $-NH_a$ and $-NH_b$ respectively (Figure 6.7). Additionally, an observable downfield shift of 0.21 ppm for the *ortho*-CH resonances further

confirms the solution-state participation of these protons towards SO_4^{2-} binding via weak C−H···O interactions in association with strong N−H···O hydrogen bonds as observed in the solid-state structure of **5d**. Comparatively larger downfield shift of the aliphatic $-NH_a$ signal relative to the aryl $-NH_b$ signal suggests that, in solution-state tetrahedral anions such as PO_4^{3-} and SO_4^{2-} is bound more strongly to $-NH_a$ than $-NH_b$ protons of the neutral receptor, which is in contrast to the X-ray structures of oxyanion complexes that show equal participation from both the –NH protons toward anion binding within the receptor cavity (Table 6.3). On the other hand, the ^{1}H NMR spectra of F^-–encapsulated complexes, **5e-I** and **5e-II** showed an appreciable downfield shift [average $\Delta\delta$ (ppm)] of 0.85 and 1.67 ppm for thiourea $-NH_a$ and $-NH_b$ signals respectively (Figure 6.7), suggesting that F^- is bound more strongly by the $-NH_b$ protons of the receptor in solution as well in solid-state (Table 6.3). In contrast to the X-ray structures, chloride complex (**5f**) showed a comparatively larger downfield shift of aliphatic $-CH_2$ and thiourea –NH resonances *w.r.t* the hydrogenphosphate complex (**5a**) suggesting that, in solution-state Cl^- is bound more strongly to the –NH functions of protonated $\mathbf{L_5}$ in **5f** than HPO_4^{2-} in **5a**. The aliphatic protons experience a downfield shift of 0.69 and 0.34 ppm for $-NCH_2$ and $-NCH_2CH_2$ respectively, that indicate the influence of protonation at the apical nitrogen on the neighbouring methylene protons whereas the thiourea protons experience a downfield shift of 0.45 and 0.64 ppm for $-NH_a$ and $-NH_b$ respectively (Figure 6.7), suggesting hydrogen bonding interactions between –NH functions of protonated $\mathbf{L_5}$ with Cl^- anion.

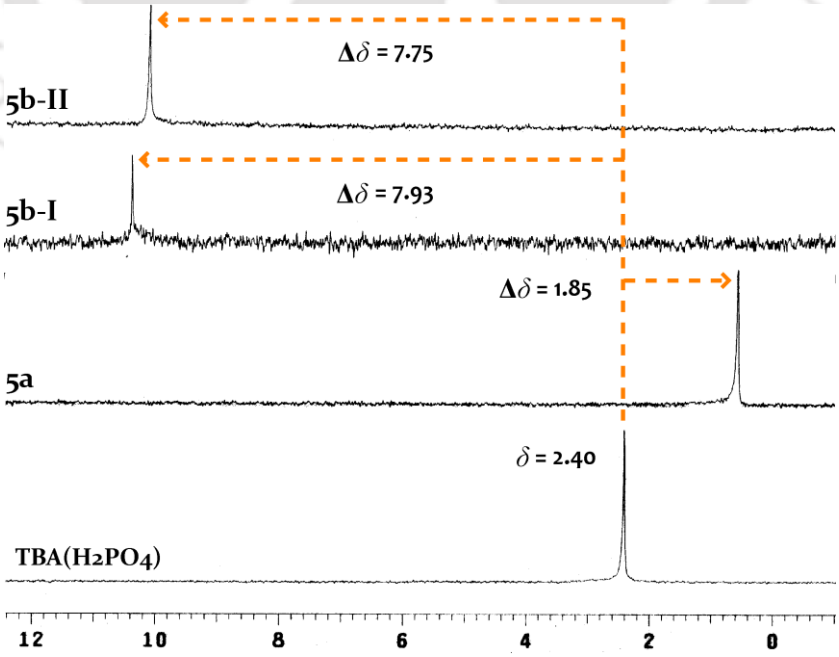

Figure 6.8 Partial ^{31}P NMR spectra of complexes **5a, 5b-I** and **5b-II** showing the significant spectral changes relative to the free ^{31}P resonance of TBA(H_2PO_4).

The solution-state encapsulation of anions and their binding stoichiometry with **L_5** has further been confirmed by 2D-NOESY NMR experiments of the isolated capsular complexes (**5b-5e**) in DMSO-d_6. 2D-NOESY NMR of the free receptor molecule (**L_5**) showed a strong NOE coupling between the thiourea –NH_a protons and water (H_a···H-O-H) present in highly moisture sensitive DMSO-*d_6* whereas no H_b···H-O-H signal was observed in the 2D spectrum (Figure 6.9a). This implies that a water molecule is encapsulated within the receptor cavity where the oxygen of water is hydrogen bonded to the more acidic aromatic –NH_b protons whereas the hydrogens of encapsulated water are involved in through-space NOE coupling with the less acidic aliphatic –NH_a protons of **L_5**. A schematic representation of the water capsule and 1:1 encapsulation of anions by **L_5** is depicted in Scheme 6.2 based on the 2D NOESY NMR experiments.

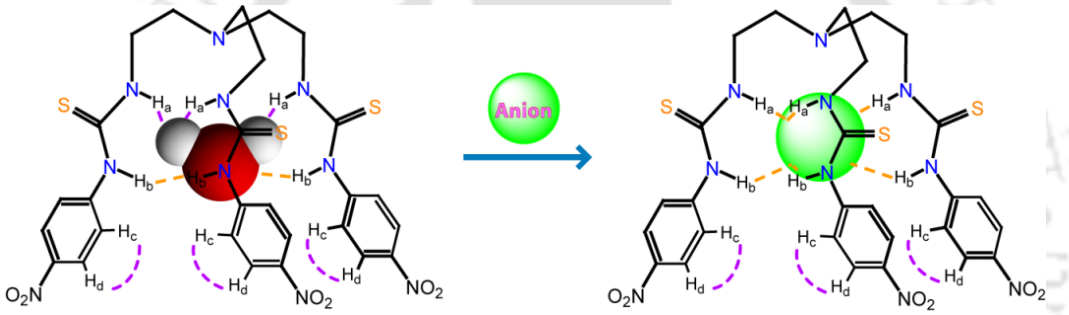

Scheme 6.2 Schematic representation depicting the formation of water capsule in a DMSO-*d_6* solution of **L_5**, and observed binding mode of anions with **L_5** as confirmed by 2D NOESY NMR spectroscopy.

Analysis of the 2D-NOESY NMR spectrum of complex **5b-I**, showed some significant NOE couplings between the –NH protons (H_a···H_b), between –NH and aromatic –CH protons (H_a/H_b···H_c/H_d) and between –NH and water (H_a/H_b···H-O-H) of DMSO-*d_6* (Figure 6.9b). These observations suggest that, 2:1 host-guest stoichiometry is not the prevalent mode of phosphate binding in solution. However, upon addition of 0.5 equiv. of a 2:1 mixture of TBA(OH) and TBA(H_2PO_4) to the solution of **5b-I** in DMSO-*d_6*, the NOE signals due to H_a···H_b, H_a/H_b···H_c/H_d and H_a/H_b···H-O-H couplings were found to be absent or considerably weakened, indicating the binding and encapsulation of PO_4^{3-} in a 1:1 host-guest ratio (Annexure 6). In contrast, complex **5c** showed the only NOE coupling between the aromatic protons of the receptor (H_c···H_d) whereas no other couplings including H_a···H_b, H_a/H_b···H_c/H_d or H_a/H_b···H-O-H were observed, indicating the binding and encapsulation of carbonate in a 2:1 host-guest stoichiometry (Figure 6.9c), an observation that is also supported by the X-ray structure of carbonate capsule (**5c**). 2D-NOESY NMR experiments further confirm the 1:1

binding stoichiometry of SO_4^{2-} and F^- in solution-state, as observed in the solid-state structures of complexes **5d** and **5e** respectively. In complexes **5d** and **5e**, the through-space $H_a \cdots H_b$ coupling has significantly weakened and couplings due to $H_a/H_b \cdots H_c/H_d$ and $H_a/H_b \cdots$H-O-H were found to be absent, suggesting the encapsulation of sulfate and fluoride in a 1:1 host-guest stoichiometry (Figure 6.9d).

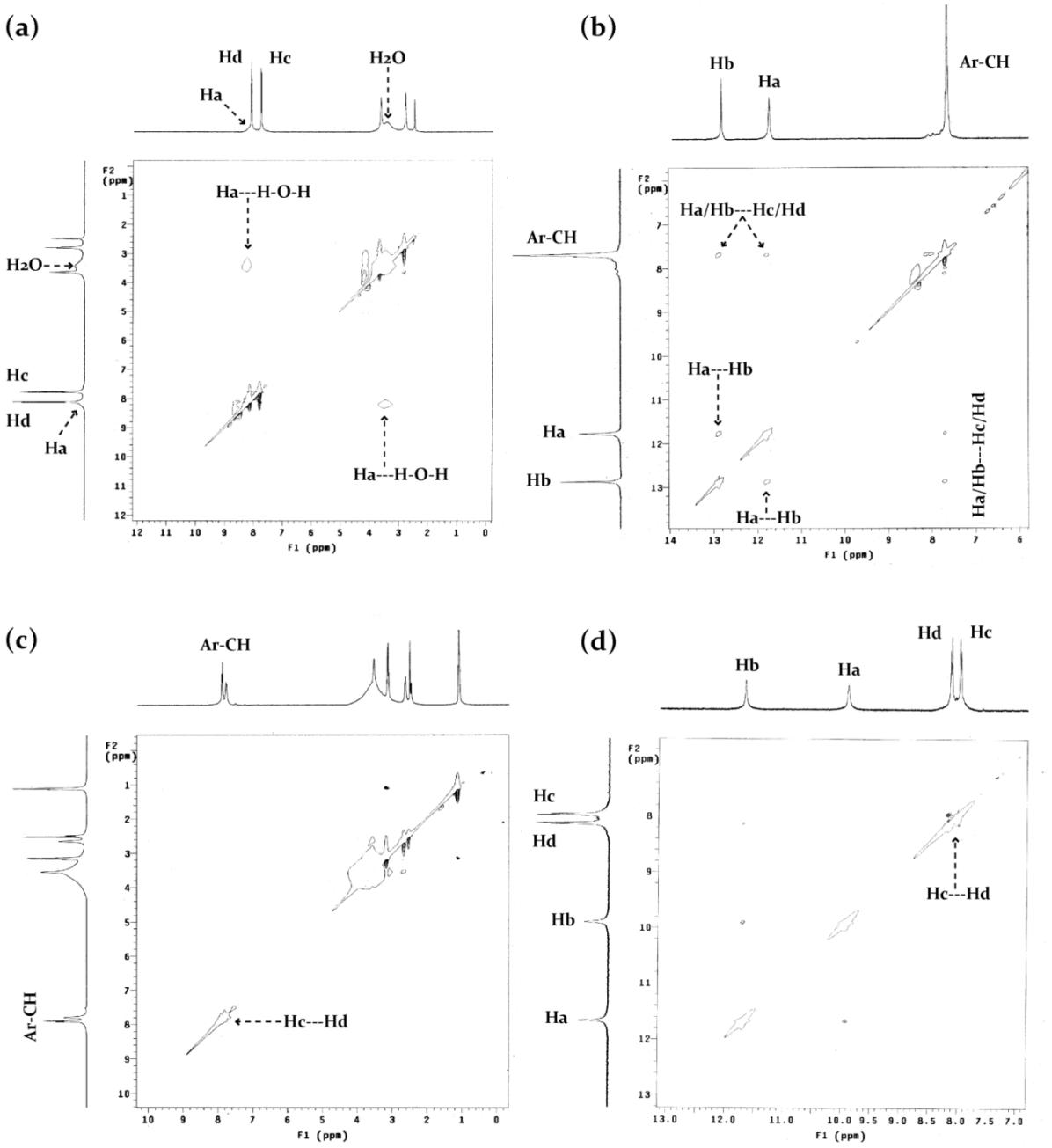

Figure 6.9 2D-NOESY NMR spectra (DMSO-d_6) of (a) $\mathbf{L_5}$ depicting the formation of water capsule in solution; (b) PO_4^{3-} encapsulated complex, **5b-I**; (c) CO_3^{2-} encapsulated complex, **5c** and (d) SO_4^{2-} encapsulated complex **5d**.

6.5 Evidence on selective inclusion of PO_4^{3-} anion

In the quantitative ^{1}H NMR titration of **L$_5$** with $TBAH_2PO_4^-$, two sets of signals were observed for the –NH and aryl –CH protons, which corresponds to the slow formation of PO_4^{3-}–encapsulated complex (between the *in situ* generated PO_4^{3-} anion and receptor **L$_5$**) from the complex that is initially formed between added $H_2PO_4^-$ and **L$_5$** (Figure 6.10). Initially, addition of up to 1.0 equivalent of $H_2PO_4^-$, both the $-NH_a$ and $-NH_b$ signals experienced a considerable downfield shifts of 0.63 and 1.13 ppm respectively, indicating the cooperative binding of $H_2PO_4^-$ by the -NH groups. Beyond 1.0 equivalent of $H_2PO_4^-$ addition, a new set of signals for the –NH and aryl –CH protons appeared and intensified with increasing anion concentration (NH_a* = 11.78 ppm, NH_b* = 12.88 ppm and ArH* = 7.71 ppm). This result may be attributed to the formation of a 1:1 host-guest complex *via* deprotonation of monovalent phosphate ($H_2PO_4^-$) to trivalent phosphate (PO_4^{3-}) by excess $H_2PO_4^-$ in solution. Moreover, beyond addition of 1.0 equivalent of $H_2PO_4^-$, the initial $-NH_a$ and $-NH_b$ resonances get shifted further downfield ($\Delta\delta$ = 1.13 and 1.57 ppm respectively *w.r.t* **L**) and at 2.0 equivalents of $H_2PO_4^-$, the $-NH_b$ signal gets merged with the new $-NH_a$* signal of the PO_4^{3-}–encapsulated complex. Such a process involving slow exchange of complexes has also been reported in the $H_2PO_4^-$ binding behaviour of a tris(urea)-functionalized receptor, which can be attributed to the hydrogen-bonding activated proton transfer between the free and bound anions. The slow formation of PO_4^{3-}–encapsulated complex, was finally confirmed by ^{1}H NMR analysis of the titrated sample charged with an excess of $H_2PO_4^-$ (5 equiv.), which after 12 h (overnight equilibration) showed a dominance of the new set of –NH* and ArH* resonances closely resembling the spectrum observed for the isolated crystals of **5b-I** (Figure 6.10). It is important to mention here that at equimolar concentration of $H_2PO_4^-$ (1:1 host-guest; DMSO-d_6) no new signals were observed, even after overnight equilibration of the sample, validating the fact that PO_4^{3-}–encapsulated complex does not form at lower stoichiometry of $H_2PO_4^-$ (Annexure 6). However, in presence of 3 equivalent of $H_2PO_4^-$ (1:3 host-guest; DMSO-d_6), the solution mixture after overnight equilibration showed in situ generation of PO_4^{3-}–encapsulated complex in a considerably greater proportion than the complex formed between added $H_2PO_4^-$ and **L$_5$**, as evident from the integration data of the spectrum (Annexure 6). Monitoring the gradual downfield shift of –NH resonances, the association constant (log *K*) for $H_2PO_4^-$ was calculated to be approx. 5.87 M^{-1} with a 1:2 host-guest stoichiometry in agreement with the Job's plot analysis (Annexure 6). However, due to the deprotonation of some $H_2PO_4^-$ anions, the association constant could not be calculated accurately and have some definite errors. Additionally, the binding affinity of **L$_5$** with PO_4^{3-} is invariably influenced by the protonated

state of the anion, as $H_2PO_4^-$ induced comparatively smaller downfield shifts ($\Delta\delta$ ppm; $-NH_a$ 1.13 and $-NH_b$ 1.57 ppm) of the thiourea protons than PO_4^{3-} ($\Delta\delta$ ppm; $-NH_a$ 3.76 and $-NH_b$ 2.80 ppm), while H_3PO_4 induced marginal spectral changes of the –NH resonances with $\Delta\delta \sim$ 0.30 ppm (**5a**).

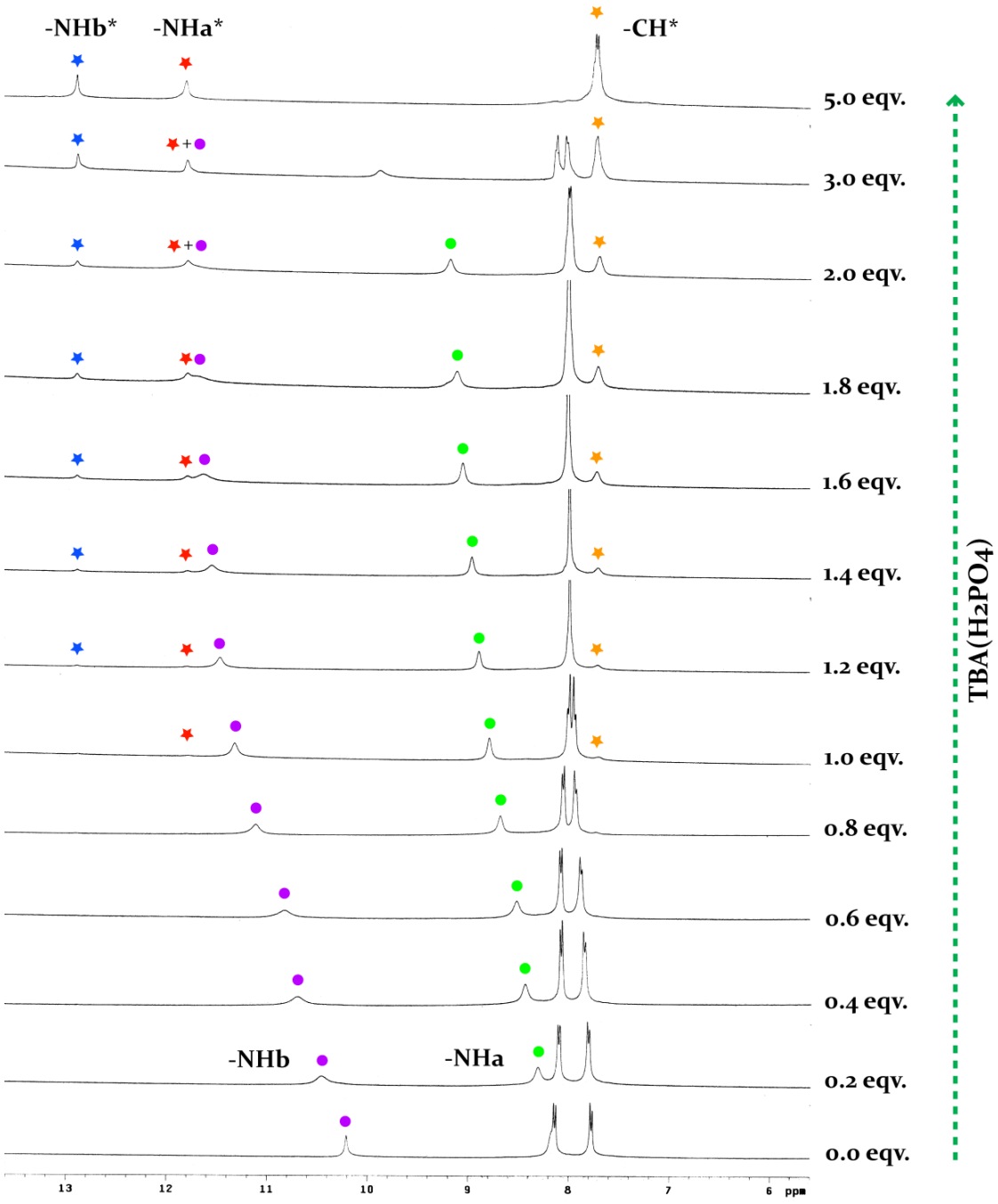

Figure 6.10 Partial ^{1}H NMR titration spectra of $\mathbf{L_5}$ (10 mM) recorded with increasing concentration of TBA(H_2PO_4) salt in DMSO-d_6.

Encouraged by the high affinity of $\mathbf{L_5}$ towards trivalent phosphate encapsulation in solid and solution-states, we have monitored a set of two competitive crystallization experiments by charging an excess (10 equiv.) of tetrabutylammonium (set-I) and tetraethylammonium (set-

II) salts of various anions (F^-, Cl^-, AcO^-, NO_3^-, HCO_3^-, and HSO_4^-) to the individual solutions of **5a** in MeCN, where at least one of the competitive anions used should be basic enough to induce neutralization of protonated $\mathbf{L_5}$ in complex **5a**. In set-I, tetrabutylammonium salts of F^-, AcO^- and HSO_4^- were used whereas in set-II, tetraethylammonium salts of HCO_3^-, NO_3^- and Cl^- were employed as per the commercial availability. Slow evaporation (at RT) of the individual solution mixtures has resulted in the exclusive crystallization of phosphate capsules **5b-I** and **5b-II** from set-I and II respectively (within 10-12 days), which were confirmed by FT-IR, $^1H/^{31}P$ NMR and PXRD analyses of the isolated crystals. The selective crystallization of phosphate capsules in a highly competitive environment of F^-, Cl^-, AcO^-, NO_3^-, HCO_3^-, and HSO_4^- can be attributed to the formation of rigid capsular assembly guided by aromatic π···π stacking between the receptor side arms and multiple hydrogen bonding interactions on PO_4^{3-} which provide high organizational rigidity and thereby, preventing the accommodation of undesired competing anions through structural distortions and rearrangement of the host framework.

In our effort to further validate the selective inclusion of PO_4^{3-} within the receptor cavity, we have carried out quantitative ^1H NMR and ^{31}P NMR titration experiments of **5a** with increasing equivalents of TEA(HCO_3) in DMSO-d_6. Interestingly, in the ^1H NMR titration with TEA(HCO_3), two sets of signals were observed for –NH and aryl –CH protons which corresponds to the formation of PO_4^{3-}-encapsulated complex from the in situ generated HPO_4^{2-} complex of $\mathbf{L_5}$ via –NH hydrogen bond activated deprotonation of bound HPO_4^{2-} anions by titrated HCO_3^- anions. Initially, up to 2 equivalent of HCO_3^- addition, the aliphatic $–CH_2$ resonances experienced a notable upfield shift of 0.24 and 0.14 ppm for $–NCH_2$ and $–NCH_2CH_2$ respectively, which indeed indicates the formation of charge neutral $\mathbf{L_5}$ in solution. Furthermore, the –NH resonances experienced a considerable downfield shift of 0.48 and 0.86 ppm for $–NH_a$ and $–NH_b$ respectively, indicating the cooperative binding of HPO_4^{2-} by the -NH functions of $\mathbf{L_5}$. Upon 3 equivalent of HCO_3^- addition, a new set of signals for the –NH and aryl –CH protons appeared (NH_a* = 11.79 ppm, NH_b* = 12.89 ppm and ArH* = 7.72 ppm) which intensified with increasing equivalents of HCO_3^- (Figure 6.11). Finally, at 6 equivalent of HCO_3^-, the new set of signals (-NH* and –CH*) dominate over the old set of signals (-NH and –CH) which get much suppressed and the observed spectrum closely resembles the ^1H NMR spectrum of the isolated crystals of **5b-II** (Figure 6.11). Similar spectral changes have also been observed during the course of titration of **5a** with increasing equivalents of TBAF (Annexure 6). Furthermore, as a proof of experiment performed, addition of 6 equivalents of TEA(CH_3CO_2) to a solution of **5a** in DMSO-d_6

induce an identical spectral behaviour as observed for 6 equivalents of HCO_3^- addition to **5a** (Annexure 6).

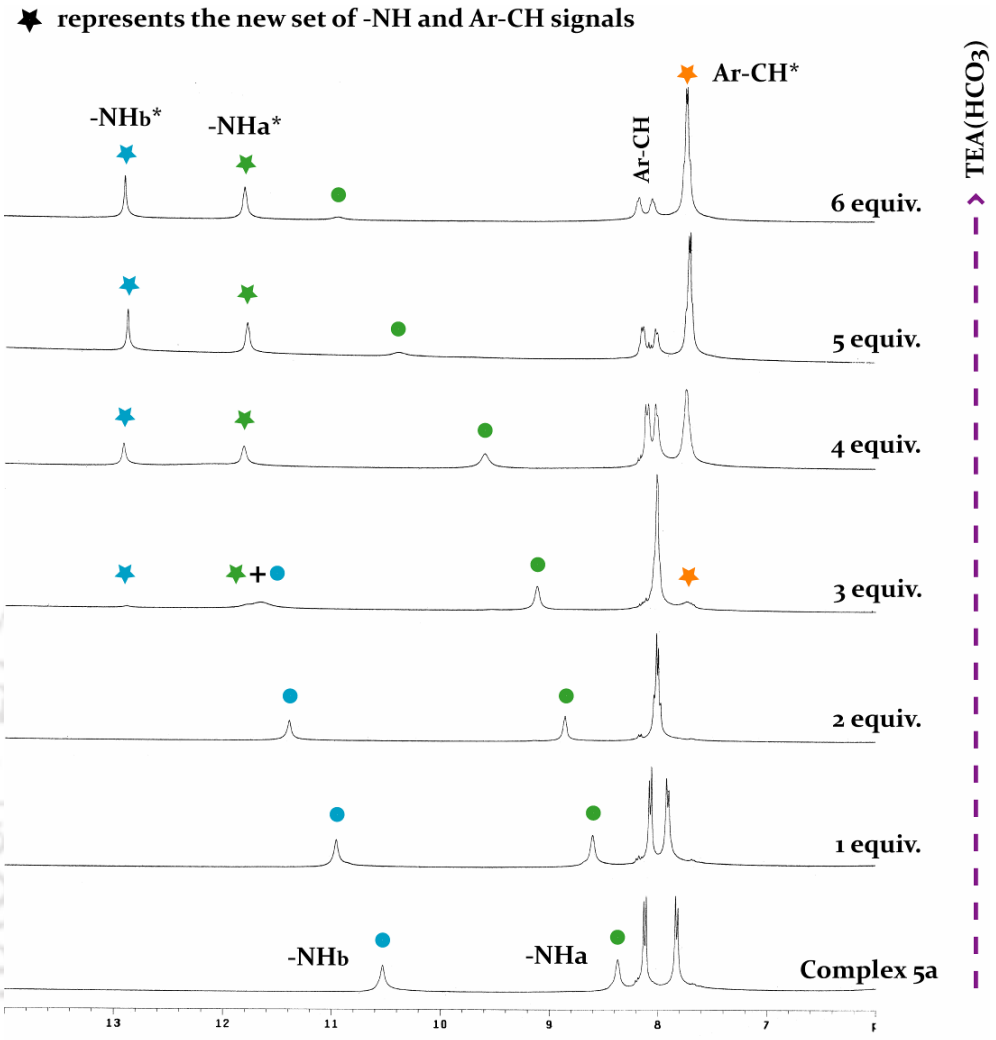

Figure 6.11 Partial ^{1}H NMR titration spectra of **5a** (10 mM) recorded with increasing equivalents of TEA(HCO_3) salt.

^{31}P NMR titration of **5a** with increasing equivalents of TEA(HCO_3) provide further insight into the phenomena of selective PO_4^{3-} encapsulation and equilibrium of –NH coordinated PO_4^{3-}/HPO_4^{2-} in DMSO-d_6. The ^{31}P resonance of HPO_4^{2-} experienced a significant downfield shift of 1.52 ppm (*w.r.t.* **5a**) up to 3 equivalent of HCO_3^- addition to **5a**, suggesting the coordinative encapsulation of divalent phosphate by neutral $\mathbf{L_5}$ (Figure 6.12). However, upon further addition of HCO_3^- ions, the ^{31}P resonance of HPO_4^{2-} was more deshielded and a new ^{31}P resonance originated at 10.17 ppm which corresponds to the in situ generated PO_4^{3-} capsule. Finally, at 6 equivalent of HCO_3^-, the resonance of HPO_4^{2-} gets much suppressed and the spectrum thus obtained closely resembles the ^{31}P NMR spectrum of the isolated crystals of **5b-II** (Figure 6.12). Thus, the insitu formation of PO_4^{3-}-encapsulated complex via

hydrogen bond induced deprotonation of bound HPO_4^{2-} can nicely be captured in solution by quantitative ^1H NMR and ^{31}P NMR titration experiments.

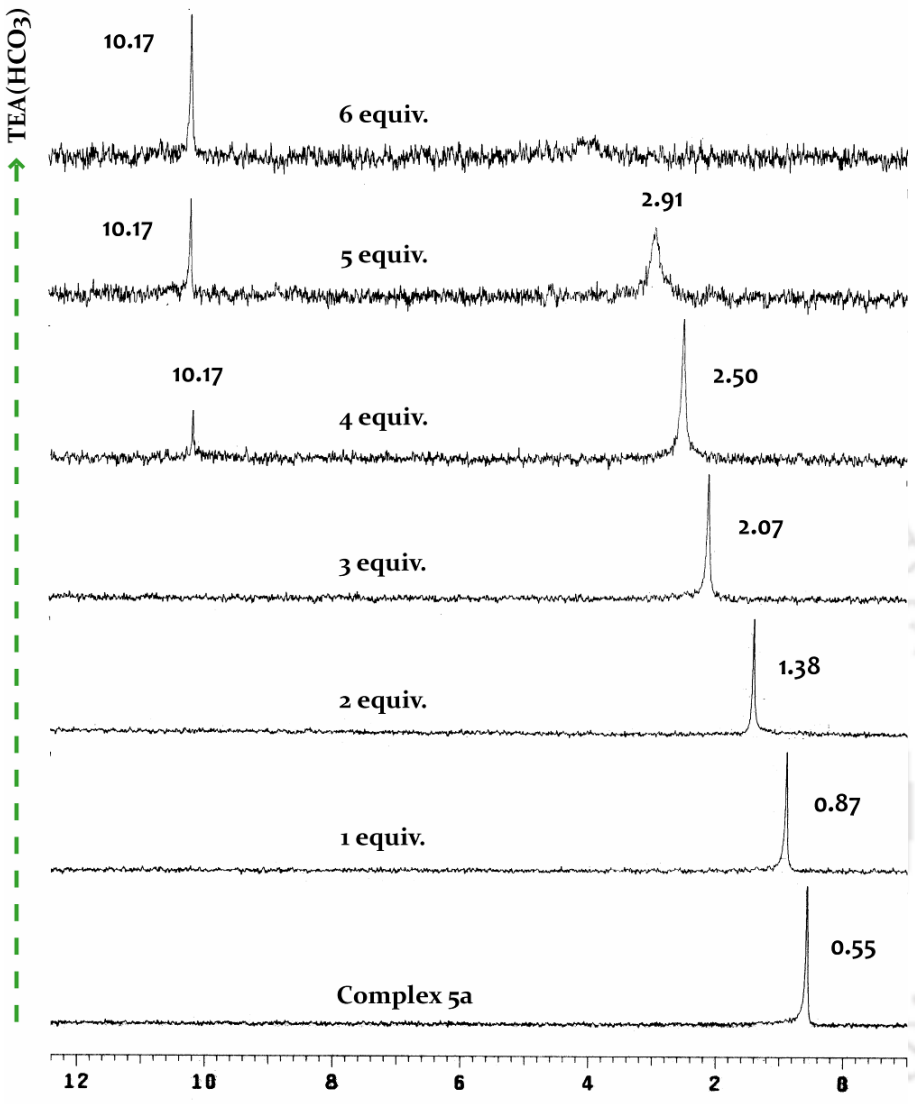

Figure 6.12 Partial ^{31}P NMR titration spectra of **5a** (10 mM) recorded with increasing equivalents of TEA(HCO_3) salt.

Quantitative ^1H NMR titration experiments (DMSO-d_6) have also been performed with TBA/TEA salts of other anions to assess the binding constants of different anions with $\mathbf{L_5}$. The titration data for F^- and Cl^- gave the best fit for 1:1 stoichiometry with an association constant (log *K*) of 4.47 and 3.54 M^{-1} (Figure 6.13 and 6.14). The considerably larger shift of $-NH_b$ (1.68 and 0.85 ppm for F^- and Cl^- respectively) relative to $-NH_a$ signals (0.82 and 0.47 ppm for F^- and Cl^- respectively) suggests that the halides bind more strongly by $-NH_b$ than $-NH_a$ protons of the receptor, as established in the X-ray structures of complexes **5e** and **5f**. The titration data for HSO_4^- gave the best fit for 2:1 host-guest stoichiometry with an association constant (log *K*) of 3.75 M^{-1} and results in an ultimate $\Delta\delta$ shift of 0.96 and 0.84

ppm for $-NH_a$ and $-NH_b$ protons respectively (Figure 6.15). However, in the ^1H NMR titration of $\mathbf{L_5}$ with HCO_3^-, the resonances for the thiourea –NH protons could not be observed consistently and therefore, the association constant could not be calculated. However, in cases of other oxyanions (NO_3^- and ClO_4^-) no appreciable change in chemical shift values of the -NH resonances were observed, suggesting the non-interacting nature or very weak interactions with $\mathbf{L_5}$.

6.6 Conclusion

In summary, we have demonstrated the selective and preferential inclusion of trivalent phosphate anion (PO_4^{3-}) within two independent dimeric capsular assembly (**5b-I** and **5b-II**) of a tris(thiourea) receptor $\mathbf{L_5}$, assembled by aromatic π···π stacking (and aryl C-H···N interactions in **5b-II**) between the receptor side-arms. The quaternary ammonium salts (TBA and TEA) of PO_4^{3-} capsule can reproducibly be obtained in quantitative yield, by a solution-state deprotonation of $[H\mathbf{L}]^+$ moieties and bound HPO_4^{2-} anion of **5a** (HPO_4^{2-} complex of protonated $\mathbf{L_5}$), in presence of large excess of highly competitive anions such as HCO_3^- /CO_3^{2-}, CH_3COO^-, and F^- having invariably similar basicity to those of inorganic phosphates. The phenomenon of selective PO_4^{3-} encapsulation has also been demonstrated in solution-state by quantitative ^1H NMR and ^{31}P NMR titration experiments whereas 2D-NOESY NMR experiment established the 1:1 binding stoichiometry of PO_4^{3-} by $\mathbf{L_5}$. Furthermore, ^1H and ^{31}P NMR analyses of isolated phosphate complexes showed evidences of binding discrepancy of phosphate with cationic and neutral $\mathbf{L_5}$ as observed in the X-ray structures of complexes **5a** and **5b** respectively. Overall, receptor $\mathbf{L_5}$ provides an ideal example of hydrogen bonding scaffold that can be efficiently employed for selective separation of inorganic phosphates via encapsulation within a dimeric capsular assembly.

We have also provided the first structural evidence on solvent sealed encapsulation of anion inside a receptor scaffold as observed in the F^--encapsulated complexes, **5e-I** and **5e-II** and the rare example of cation sealed unimolecular capsule as observed in SO_4^{2-}-encapsulated complex, **5d**.

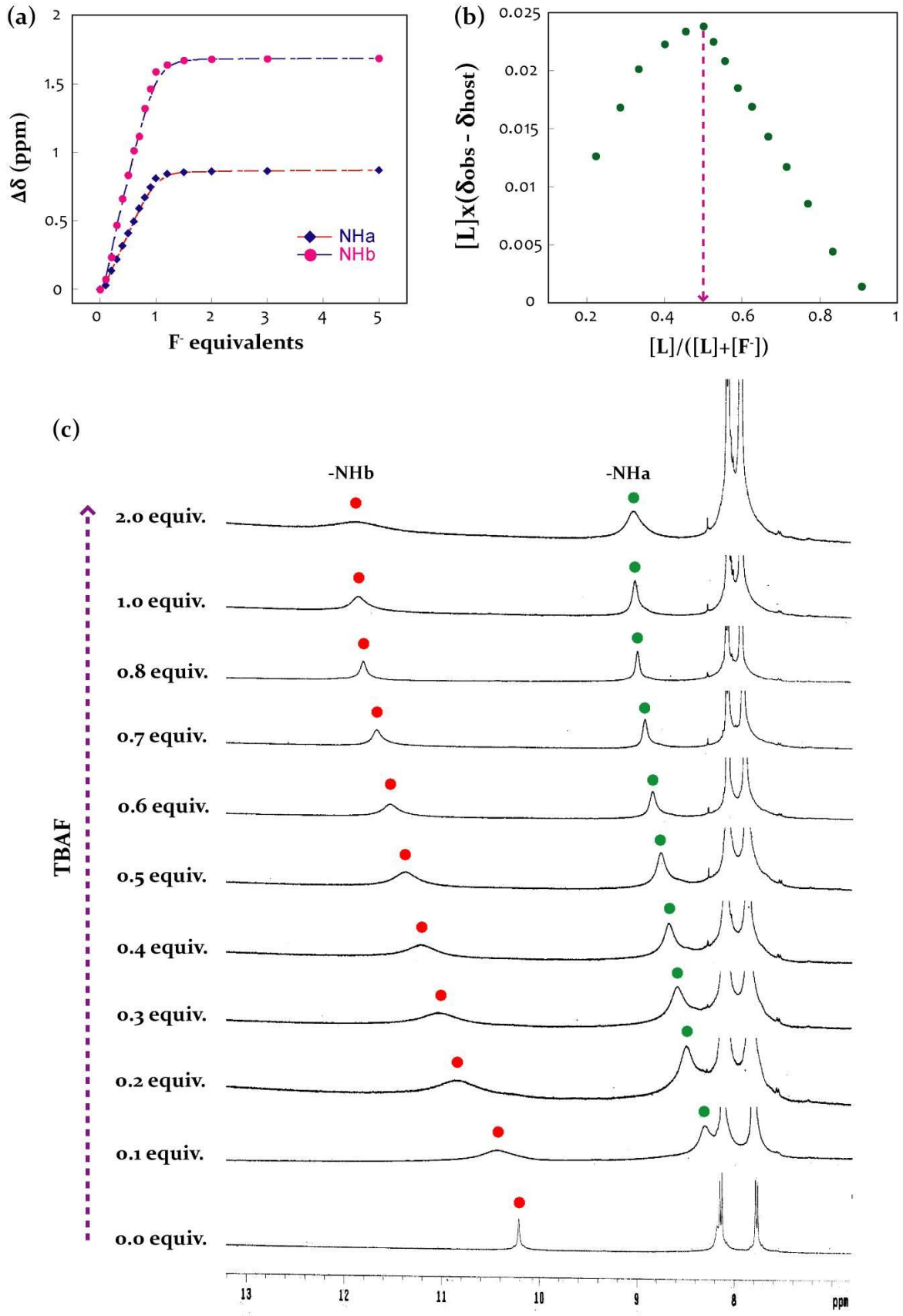

Figure 6.13 (a) Change in chemical shift of –NH resonances of $\mathbf{L_5}$ (10 mM) with increasing conc. of standard F^- solution (50 mM) in DMSO-d_6; (b) Job's plot suggesting the formation of 1:1 host-guest complex in solution; (c) Partial ^{1}H NMR titration spectra of $\mathbf{L_5}$ with TBAF.

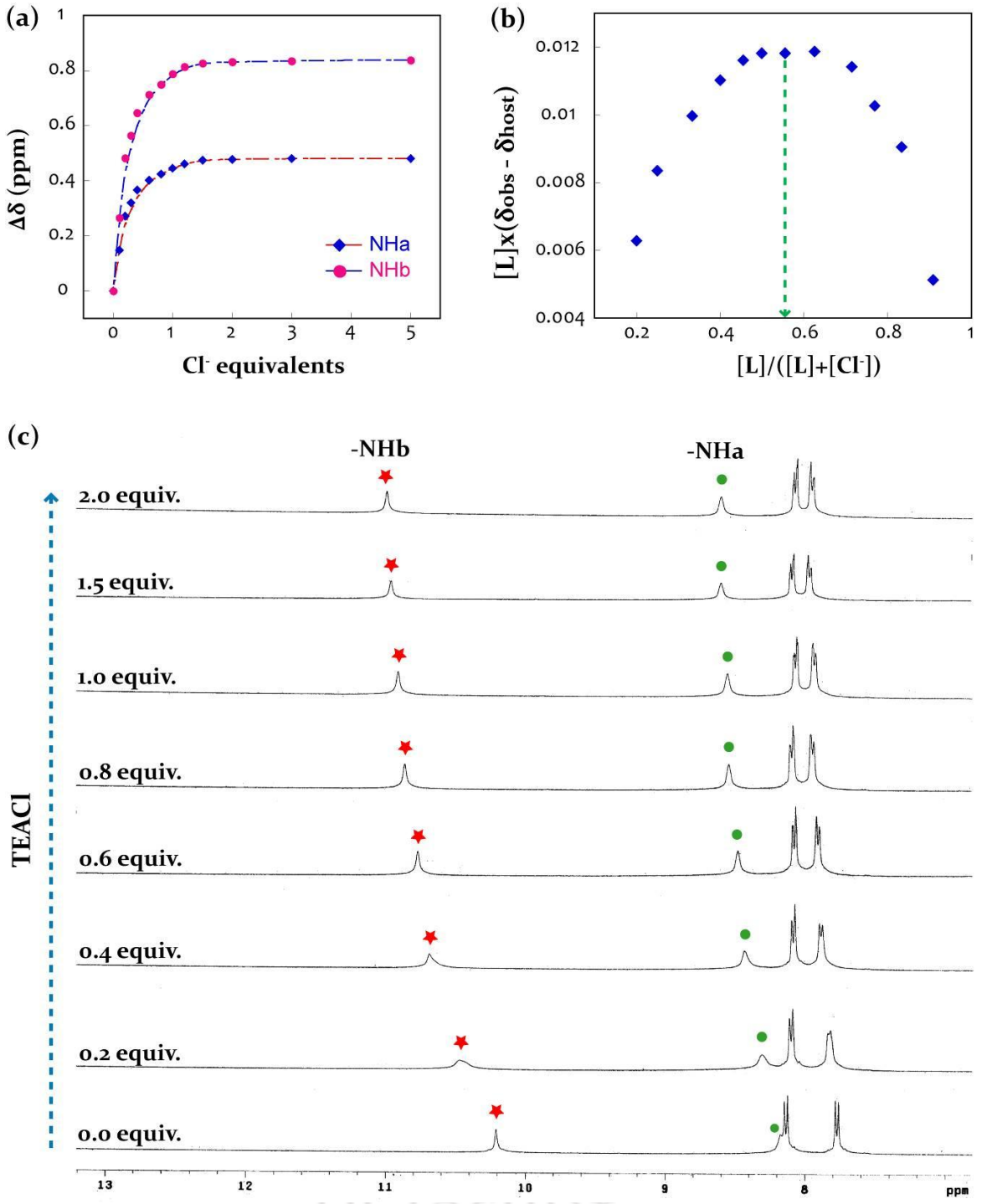

Figure 6.14 (a) Change in chemical shift of –NH resonances of $\mathbf{L_5}$ (10 mM) with increasing conc. of standard Cl^- solution (50 mM) in DMSO-d_6; (b) Job's plot suggesting the formation of 1:1 host-guest complex in solution; (c) Partial ^{1}H NMR titration spectra of $\mathbf{L_5}$ with TEACl.

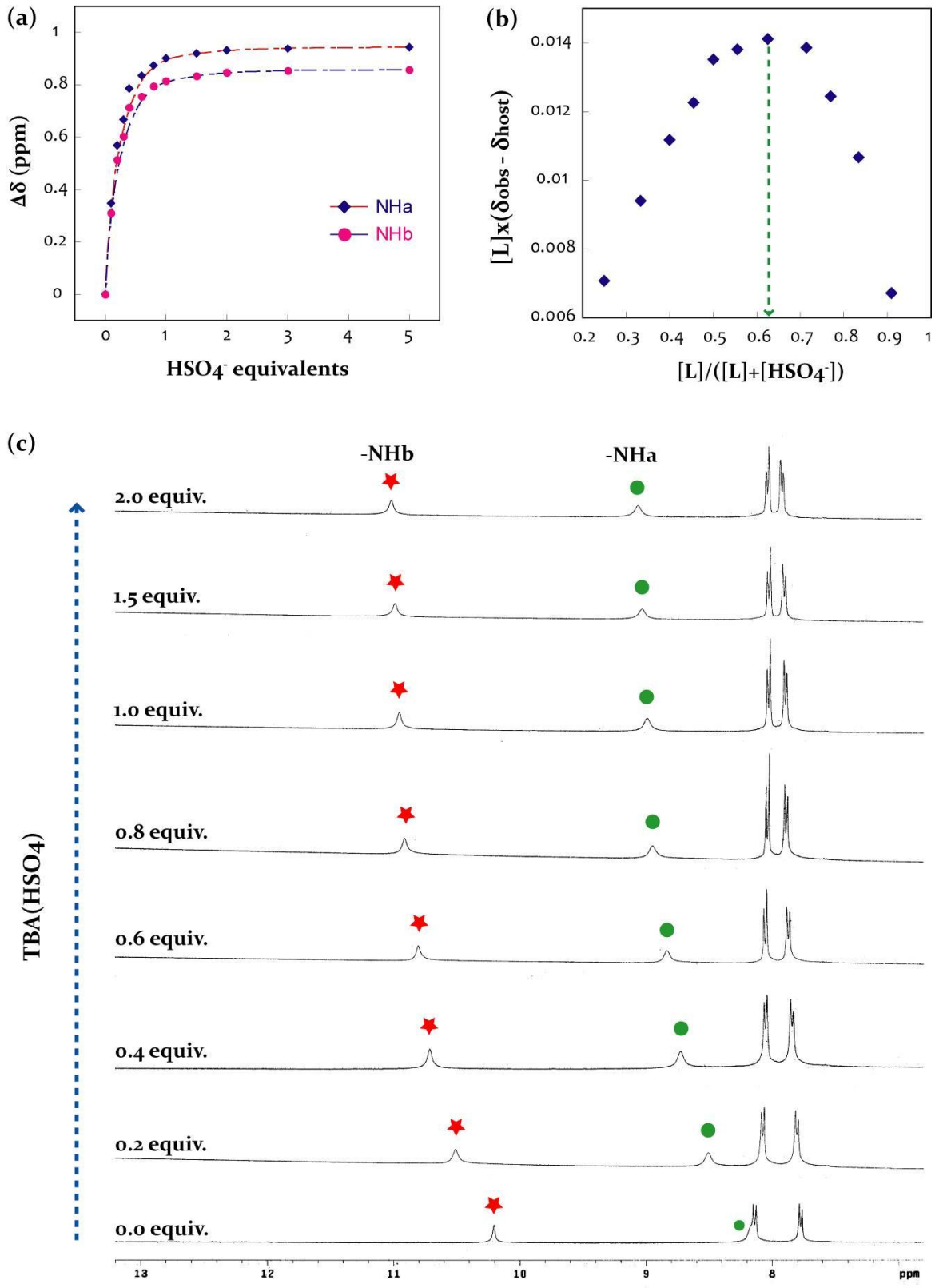

Figure 6.15 (a) Change in chemical shift of –NH resonances of $\mathbf{L_5}$ (10 mM) with increasing conc. of standard HSO_4^- solution (50 mM) in DMSO-d_6; (b) Job's plot suggesting the formation of 2:1 host-guest complex in solution; (c) Partial ^{1}H NMR titration spectra of $\mathbf{L_5}$ with TBA(HSO_4).

Table 6.3 Hydrogen bonding contacts on anions with receptor $\mathbf{L_5}$ in complexes **5a-5f.**

Complexes	D-H···A	*d*(H···A)/Å	*d*(D···A)/Å	∠D-H···A/°
5a	N3-H···O13	2.62(1)	3.270(1)	134(6)
	N12-H···O13	2.54(1)	3.301(1)	148(6)
	N13-H···O13	2.18(8)	2.922(1)	146(7)
	N15-H···O14	2.30(7)	3.083(1)	151(6)
	N16-H···O14	2.03(8)	2.860(1)	159(5)
	N12-H···O15	2.40(9)	3.174(1)	149(6)
	C28-H···O15	2.55(1)	3.405(2)	147(6)
	N2-H···O16	2.13(6)	2.916(8)	150(6)
	N3-H···O16	2.26(7)	3.078(1)	157(6)
	N5-H···O16	2.04(7)	2.877(1)	162(5)
	N6-H···O16	2.09(7)	2.916(1)	158(6)
5b-I	N2-H···O13	1.92(2)	2.781(4)	178(2)
	N5-H···O13	1.93(3)	2.730(5)	154(3)
	N8-H···O13	1.90(2)	2.733(4)	161(3)
	N9-H···O14	2.05(2)	2.862(5)	156(3)
	N12-H···O14	2.06(3)	2.908(4)	166(2)
	N19-H···O14	1.86(2)	2.721(4)	170(2)
	N3-H···O15	1.97(2)	2.776(4)	153(2)
	N13-H···O15	1.89(3)	2.749(5)	174(2)
	N15-H···O15	1.96(2)	2.792(4)	162(2)
	N6-H···O16	2.02(3)	2.872(4)	167(3)
	N16-H···O16	2.00(2)	2.823(4)	158(3)
	N18-H···O16	2.01(2)	2.844(4)	160(2)
	N3-H···O13	2.69(2)	3.403(4)	141(2)
	N9-H···O13	2.71(3)	3.393(4)	137(3)
	N18-H···O14	2.71(3)	3.339(4)	131(2)
	C27-H···O14	2.62(3)	3.333(5)	133(3)
	C50-H···O14	2.56(2)	3.284(5)	134(3)
	C9-H···O15	2.54(2)	3.164(5)	124(3)
	C45-H···O16	2.69(3)	3.423(6)	135(4)
5b-II	N2-H···O5	1.89(2)	2.748(6)	172(3)
	N3-H···O6	1.95(3)	2.802(6)	168(3)
	N6-H···O6	2.10(2)	2.933(4)	162(3)
	N7-H···O6	1.91(3)	2.764(6)	171(3)
	N6-H···O6	2.66(2)	3.285(4)	128(3)
	C9-H···O6	2.70(3)	3.349(7)	127(3)
5c	N2-H···O6	2.57(5)	3.288(3)	141(3)
	N3-H···O6	1.93(3)	2.798(5)	178(3)
	N2-H···O5	2.55(4)	3.330(6)	150(3)
	N5-H···O5	2.67(4)	3.364(6)	138(3)
	N6-H···O5	1.94(5)	2.783(6)	165(3)
	N8-H···O5	2.40(4)	3.141(5)	144(3)
	N9-H···O5	1.94(4)	2.803(5)	172(3)
5d	N2-H···O7	2.00(4)	2.831(7)	160(5)
	N5-H···O7	2.00(4)	2.792(8)	152(5)
	N8-H···O7	2.07(4)	2.905(9)	162(5)
	N9-H···O8	2.03(4)	2.822(8)	152(6)
	C23-H···O8	2.61(4)	3.241(1)	125(8)
	C42-H···O8	2.57(5)	3.462(1)	152(5)
	N3-H···O9	2.00(4)	2.859(8)	171(5)
	C9-H···O9	2.63(4)	3.343(1)	134(6)
	N6-H···O10	2.12(4)	2.962(8)	165(5)
	C14-H···O10	2.60(4)	3.312(1)	134(6)

5e-I	N2-H···F1	2.04(6)	2.927(7)	159(5)
	N3-H···F1	1.84(3)	2.735(4)	167(3)
	N5-H···F1	2.11(4)	2.941(6)	151(3)
	N6-H···F1	1.86(1)	2.757(6)	169(3)
	N8-H···F1	2.17(3)	2.913(4)	152(4)
	N9-H···F1	1.84(3)	2.709(5)	159(3)
	C15-H···O7	2.35(4)	3.234(8)	157(4)
	C24-H···O7	2.34(4)	3.211(6)	156(4)
	C44-H···O3	2.61(6)	3.470(1)	148(6)
	C45-H···O5	2.75(5)	3.670(1)	158(6)
5e-II	N2-H···F1	2.15(2)	2.910(4)	146(2)
	N3-H···F1	1.88(2)	2.729(4)	166(2)
	N5-H···F1	2.19(2)	2.937(5)	145(3)
	N6-H···F1	1.88(3)	2.730(5)	169(3)
	N8-H···F1	2.10(2)	2.874(4)	148(3)
	N9-H···F1	1.91(2)	2.749(3)	163(3)
	N12-H···F2	2.12(2)	2.882(4)	147(2)
	N13-H···F2	1.90(3)	2.743(5)	164(2)
	N15-H···F2	2.21(2)	2.956(4)	145(2)
	N16-H···F2	1.88(2)	2.731(3)	168(2)
	N18-H···F2	2.13(2)	2.894(4)	148(3)
	N19-H···F2	1.90(2)	2.744(5)	166(3)
5f	N2-H···Cl1	2.77(4)	3.448(2)	150(4)
	N3-H···Cl1	2.41(6)	3.164(3)	151(5)
	N5-H···Cl1	2.46(4)	3.302(3)	150(3)
	N6-H···Cl1	2.33(6)	3.161(3)	169(5)
	N8-H···Cl1	2.82(5)	3.529(3)	148(4)
	N9-H···Cl1	2.43(3)	3.219(3)	167(3)
	N2-H···O7	2.58(4)	3.100(4)	128(4)
	N8-H···O7	2.54(5)	3.119(4)	130(4)
	C2-H(A)···O7	2.49(2)	3.206(4)	130(2)
	C10-H(A)···O7	2.61(2)	3.584(4)	178(2)
	C19-H(B)···O7	2.60(3)	3.325(4)	131(2)

References

1. (a) Z. Wang, H. Luecke, N. Yao and F. A. Quiocho, *Nat. Struct. Biol*., 1997, 4, 519; (b) J. W. Pflugrath and F. A. Quiocho, *Nature*, 1985, **314**, 257; (c) C. J. Avers, *Molecular Cell Biology*., Addison-Wesley: Reading, 1986.

2. (a) C. Bazzicalupi, A. Bencini and V. Lippolis, *Chem. Soc. Rev.*, 2010, **39**, 3709; (*b*) A. Bencini, A. Bianchi, E. Garcia-Espana, M. Micheloni and J. A. Ramirez, *Coord. Chem. Rev*., 1999, **188**, 97; (c) C. Bazzicalupi, A. Bencini, A. Bianchi, E. Faggi, C. Giorgi, S. Santarelli and B. Valtancoli, *J. Am. Chem. Soc*., 2008, **130**, 2440; (*d*) C. Bazzicalupi, A. Bencini, S. Biagini, E. Faggi, S. Meini, C. Giorgi, A. Spepi and B. Valtancoli, *J. Org. Chem*., 2009, **74**, 7349; (*e*) C. Bazzicalupi, A. Bencini, A. Bianchi, A. Danesi, C. Giorgi and B. Valtancoli, *Inorg. Chem*., 2009, **48**, 2391.

3. A. K. H. Hirsch, F. R. Fischer and F. Diederich, *Angew. Chem. Int. Ed*., 2007, **46**, 338.

4. (a) K. E. Havens and C. L. Schelske, *Environ. Pollut*., 2001, **113**, 1; (b) M. F. Coveney, E. F. Lowe, L. E. Battoe, E. R. Marzolf and R. Conrow, *Freshwater Biol.*, 2005, **50**, 1718; (c) C. L. Schelske, E. F. Stoermer and W. F. Kenney, *Limnol. Oceanogr.*, 2006, **51**, 728.

5. (*a*) P. D. Beer and P. A. Gale, *Angew. Chem. Int. Ed*., 2001, **40**, 486; (*b*) R. Martinez-Manez and F. Sancenon, *Chem. Rev*., 2003, **103**, 4419; (*c*) P. A. Gale, S. E. Garcia-Garrido and J. Garric, *Chem. Soc. Rev*., 2008, **37**, 151; (*d*) H. -J. Schneider, *Angew. Chem. Int. Ed*., 2009, **48**, 3924; (*e*) S. O. Kang, V. W. Day and K. Bowman-James, *Org. Lett*., 2008, **10**, 2677; (*f*) S. O. Kang, V. W. Day and K. Bowman-James, *Org. Lett*., 2009, **11**, 3654; (*g*) E. A. Katayev, J. L. Sessler, V. N. Khrustalev and Y. A. Ustynyuk, *J. Org. Chem*., 2007, **72**, 7244.

6. S. K. Dey and G. Das, *Dalton Trans*., 2011, **40**, 12048.

7. S. K. Dey and G. Das, *Dalton Trans*., 2012, DOI: 10.1039/C2DT30687E.

8. (a) N. Busschaert, M. Wenzel, M. E. Light, P. Iglesias-Hernandez, R. Perez-Tomas and P. A. Gale, *J. Am. Chem. Soc*., 2011, **133**, 14136; (b) C. Caltagirone, J. R. Hiscock, M. B. Hursthouse, M. E. Light and P. A. Gale, *Chem. –Eur. J*., 2008, **14**, 10236; (c) P. A. Gale, J. R. Hiscock, S. J. Moore, C. Caltagirone, M. B. Hursthouse and M. E. Light, *Chem. –Asian J*., 2010, **5**, 555.

To conclude, this thesis provides some significant results in the arena of 'supramolecular chemistry of anions', where the anion binding capability of some newly synthesized hydrogen bonding tripodal scaffolds (**L_1-L_5**) were explored in the solid-state and in solution as well. In general, the present findings provide evidence of anion induced formation of capsular and pseudo-capsular assembly of the neutral receptor molecules and non-capsular aggregation of the receptor units, when protonated in presence of different anions. Each podand receptor has shown an interesting property in presence of a specific anion or a set of anionic guest species.

The inorganic anion assisted conformational adaptation of podand **L_1** into an extended/open conformation and of podand **L_2** into a locked/closed conformation is remarkable. A mere variation of the terminal aryl substitution in tripodal ether receptors, **L_1** (*p*-nitrophenyl) and **L_2** (*p*-tolyl) showed a marked difference in their conformational adaptability when protonated in presence of the same inorganic anion. Such a conformational movement can prove to be helpful in the development of hosts for switchable binding of guests.

In recent times, the synthesis and evaluation of π–acidic, shape persistent receptors that can transport (synport/antiport) anions across lipid bilayer membranes *via* conventional hydrogen bonding or anion–π interaction has evolved as an emerging theme in the growing field of 'anion receptor chemistry', considering the importance of anions in diseases like cystic fibrosis or channelopathesis. Furthermore, the low level of fluoride tolerance in human body and progressive increase in concentration of anions such as, sulphate and phosphate in the natural ecosystem, demands for the strategic development of receptors for selective anion recognition. In such a situation, recognition and separation of the targeted anionic species *via* encapsulation within a receptor cage or cavity could be a superior approach. Capsular assembly of a receptor creates a distinct microenvironment that isolates the encapsulated guest from the bulk of the solvent media. Additionally, to overcome the Hofmeister bias, which disfavours the complexation and separation of the extremely hydrophilic anions (such as F^-, CO_3^{2-}, SO_4^{2-} and PO_4^{3-}), the receptor must have both excellent affinity and selectivity for the target anion.

Understanding the importance of anionic analytes and anion induced molecular capsules, we have synthesized three π–acidic tripodal receptors **L_3** (amide) **L_4** (urea) and **L_5** (thiourea) for the selective and/or preferential encapsulation of a specific anion over other competitive

anions. The amide receptor, **L_3** has been shown to selectively detect F^- ion by anion–π interaction *via* encapsulation of the anion within the tripodal scaffold with an array of six strong hydrogen bonds. In contrast, the urea receptor, **L_4** in presence of F^- or OH^- ion has been shown to efficiently fix atmospheric CO_2 as CO_3^{2-}–encapsulated molecular capsule. Finally, the thiourea receptor, **L_5** has been established as a competent hydrogen bonding scaffold that can selectively encapsulate PO_4^{3-} within persistent and rigidified molecular capsules, assembled by aromatic π-stacking interactions between the receptor side arms. All these results are important to address some of the problems related to environment clean-up effort.

Thus, the thesis demonstrates some of the core and erratic concepts of supramolecular chemistry and versatility of the podand receptors as efficient building block for the generation of molecular capsules. The recognition and binding of anions in molecular capsules is definitely a field which can expand considerably and bring immense advances in specialised applications such as drug delivery, transmembrane anion transport and stabilizing the anionic reactive intermediates inside the capsular assembly. However, for these applications to reach their prospective, basic work in tuning anion binding inside the molecular capsules is highly appreciated. Although the results included in this thesis are extremely useful from a fundamental viewpoint, there are other challenging aspects in supramolecular chemistry that need to be developed, primarily from an applicative viewpoint. Research in these areas with a focus on technological and biomedical applications, based upon the remarkable anion binding molecular capsules appear to be forthcoming.

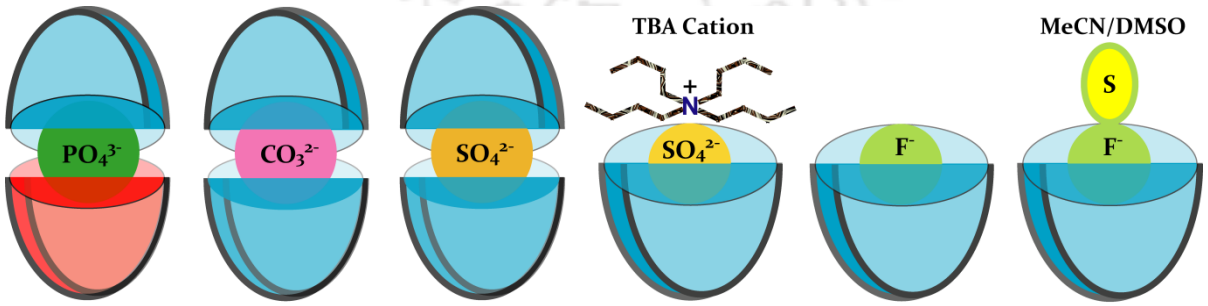

Anion coordination induced capsular and pseudocapsular assemblies

Scheme representing the capsular and pseudo-capsular assemblies of receptors **L_3**, **L_4** and **L_5** upon complexation with anions of varied size, charge and dimensions.

List of Publications

(1) Oxyanion-encapsulated caged supramolecular frameworks of a tris(urea) receptor: Evidences of hydroxide- and fluoride-ion-induced fixation of atmospheric CO_2 as a trapped CO_3^{2-} anion.

S. K. Dey, R. Chutia and G. Das, ***Inorg. Chem.*, 2012**, 51, 1727–1738.

(2) Selective inclusion of PO_4^{3-} within persistent dimeric capsules of a tris(thiourea) receptor and evidence of cation/solvent sealed unimolecular capsules.

S. K. Dey and G. Das, ***Dalton. Trans.*, 2012**, DOI: 10.1039/C2DT30687E

(3) Binding discrepancy of fluoride in quaternary ammonium and alkali salts by a tris(amide) receptor in solid and solution-states.

S. K. Dey, B. Datta and G. Das, ***Cryst. Eng. Comm*., 2012**, DOI: 10.1039/C2CE25592H

(4) A selective fluoride encapsulated neutral tripodal receptor capsule: solvatochromism and solvatomorphism.

S. K. Dey and G. Das, ***Chem. Commun*., 2011**, 11, 4463–4473.

(5) Encapsulation of trivalent phosphate anion within a rigidified π-stacked dimeric capsular assembly of tripodal receptor.

S. K. Dey and G. Das, ***Dalton. Trans*., 2011**, 40, 12048-12051.

(6) Fluoride selectivity induced transformation of charged anion complexes into unimolecular capsule of a π-acidic triamide receptor stabilized by strong N-H•••F^- and C-H•••F^- hydrogen-bonds.

S. K. Dey and G. Das, ***Cryst. Growth and Des*., 2011**, 11, 4463–4473.

(7) Anion specificity induced conformational changes in cresol-based tripodal podands controlled by weak interactions: structural and Hirshfeld surface analysis.

S. K. Dey, A. Pramanik and G. Das, ***Cryst. Eng. Comm*., 2011**, 13, 1664-1675.

(8) A subtle interplay of C–H hydrogen bonds in complexation of anions of varied dimensionality by a nitro functionalized tripodal podand.

S. K. Dey, B. Ojha and G. Das, ***Cryst. Eng. Comm*., 2011**, 13, 269-278.

(9) Binding of $HgCl_2$ by a nitro functionalized tripodal receptor and its decomplexation controlled by anion complexation.

S. K. Dey and G. Das, ***Euro. J. Inorg. Chem*., 2011**, 3, 429–438.

(10) Crystal to Calcite: Fabrication of pure calcium carbonate polymorphs in the solid-state.

B. M. Borah, **S. K. Dey** and G. Das, ***Cryst. Growth and Des*., 2011**, 11, 2773–2779.

(11) Excited-state intermolecular proton transfer induced "TURN ON" fluorescent chemosensor for selective detection of PO_4^{3-} anion.

C. Kar, **S. K. Dey** and G. Das, ***Sensor Letters*., 2011**, 9, 1430-1434.

(12) Conformational polymorphism of a simple tripodal podand bearing nitro functionality.

S. K. Dey and G. Das, ***Cryst. Growth and Des*., 2010**, 10, 754–760.

(13) Surface-modification-directed controlled adsorption of serum albumin onto magnetite nanocuboids synthesized in a gel-diffusion technique.

B. M. Borah, B. Saha, **S. K. Dey** and G. Das, ***J. Colloid Interface Sci*., 2010**, 349, 114-121.

(14) Positional isomeric effect in nitro-phenyl functionalized tripodal urea receptors towards binding and encapsulation of divalent anions.

R. Chutia, **S. K. Dey** and G. Das, Manuscript under communication.